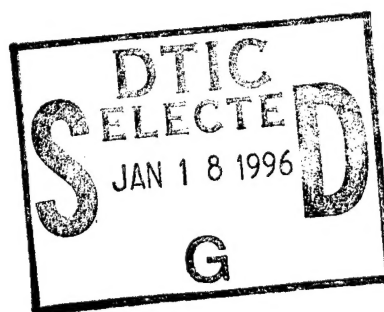


AFIT/DS/ENY/96-1



NON-LINEAR FINITE ELEMENT ANALYSES OF COMPOSITE
SHELLS BY TOTAL LAGRANGIAN DECOMPOSITION
WITH APPLICATION TO THE AIRCRAFT TIRE

DISSERTATION
James McKay Greer, Jr.
Major, USAF

AFIT/DS/ENY/96-1

19960116 006

19960116 006

Approved for public release; distribution unlimited

NON-LINEAR FINITE ELEMENT ANALYSES OF COMPOSITE
SHELLS BY TOTAL LAGRANGIAN DECOMPOSITION
WITH APPLICATION TO THE AIRCRAFT TIRE

DISSERTATION

Presented to the Faculty of the Graduate School of Engineering

of the Air Force Institute of Technology

Air Education and Training Command

In Partial Fulfillment of the

Requirements for the Degree of

Doctor of Philosophy

James McKay Greer, Jr., B.S., M.S.

Major, USAF

March, 1996

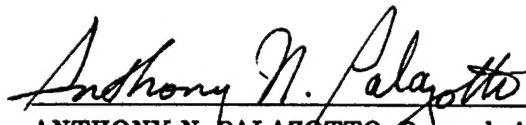
Accession For	
NTIS CRA&I	<input checked="checked" type="checkbox"/>
DTIC TAB	<input type="checkbox"/>
Unannounced	<input type="checkbox"/>
Justification	
By	
Distribution /	
Availability Codes	
Dist	Avail and/or Special
A-1	

NON-LINEAR FINITE ELEMENT ANALYSES OF COMPOSITE
SHELLS BY TOTAL LAGRANGIAN DECOMPOSITION
WITH APPLICATION TO THE AIRCRAFT TIRE

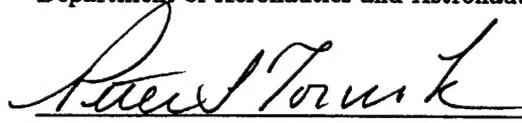
James McKay Greer, Jr., B.S., M.S.

Major, USAF

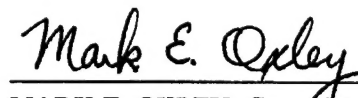
Approved:


ANTHONY N. PALAZOTTO, Research Advisor
Professor of Aerospace Engineering
Department of Aeronautics and Astronautics


22 Dec 1995


PETER J. TORVIK, Committee Member
Professor of Aerospace Engineering and Engineering Mechanics
Department of Aeronautics and Astronautics

22 Dec 1995


MARK E. OXLEY, Committee Member
Associate Professor of Mathematics
Department of Mathematics and Statistics

20 Dec 95


WON B. ROH, Dean's Representative
Professor of Engineering Physics
Department of Engineering Physics

22 Dec 95



ROBERT A. CALICO, JR., Dean
Graduate School of Engineering

Table of Contents

	Page
List of Figures	viii
List of Tables	xii
Dedication and Acknowledgements	xiii
Abstract	xv
 I. Introduction	 1-1
1.1 Objective	1-1
1.2 Overview	1-1
1.3 Novelty of Research	1-2
1.4 Overview	1-2
 II. Background	 2-1
2.1 Development of Shell Theory.	2-1
2.1.1 Finite Rotations and Polar Decomposition Theory.	2-6
2.2 Finite Element Modeling	2-7
2.2.1 Previous Shell Work.	2-7
2.3 Solution Techniques	2-11
2.3.1 Static Problems.	2-11
2.3.2 Dynamic Problems.	2-12
2.4 Vector/Concurrent Processing.	2-12
2.5 Tire (and related) Modeling by Finite Elements.	2-13
2.6 Summary	2-16

	Page
III. Theory	3-1
3.1 Stress and Strain Theories	3-1
3.1.1 Jaumann Stress and Strain Measures.	3-1
3.2 Kinematics in Curvilinear Coordinates	3-13
3.3 Characterization of Reference Surface Behavior	3-24
3.4 Strain-Displacement Relations	3-40
3.5 Constitutive Relations	3-51
3.6 Shear Warping Functions	3-54
3.7 Thickness Stretching Functions	3-58
3.8 Summary	3-62
IV. Finite Element Formulation	4-1
4.1 Element Independent Formulation	4-3
4.2 Element-Independent Stiffnesses and Coupling	4-26
4.2.1 Flat Plate.	4-28
4.2.2 Cylindrical Shell.	4-28
4.2.3 Bi-Curved Shell (Spherical/Toroidal).	4-30
4.2.4 Shell with All Curvatures Present.	4-30
4.3 Element-Dependent Formulation	4-32
4.4 External Loads	4-42
4.5 Solution to Incremental Equations	4-43
4.6 Summary	4-45
V. Linear Results	5-1
5.1 Patch Test for 44-DOF Element	5-1
5.2 The Square Isotropic Plate Subjected to Uniform Transverse Pressure	5-3
5.3 The Isotropic Pinched Cylinder	5-6
5.4 Elasticity Solutions of Pagano and the Flat Plate Strip	5-8

	Page
5.5 The Toroidal Shell	5-13
5.6 Summary	5-14
VI. Nonlinear Results	6-1
6.1 The Composite Beam	6-1
6.2 The Shallow Cylindrical Panel	6-2
6.3 The Composite Cylindrical Shell	6-4
6.4 The Isotropic Deep Arch	6-8
6.5 Summary	6-15
VII. Application to the Aircraft Tire	7-1
7.1 Tire Geometry	7-3
7.2 Connected Meshes	7-10
7.2.1 The x -connected mesh.	7-12
7.2.2 The y -connected mesh.	7-12
7.2.3 Connecting in both directions.	7-13
7.3 The Shuttle Tire	7-14
7.3.1 Inflation	7-15
7.3.2 Static Contact.	7-27
7.4 Summary	7-40
VIII. Summary and Conclusions	8-1
8.1 Summary	8-1
8.2 Conclusions	8-1
Bibliography	BIB-1
Appendix A. Elements of $[\Psi]$	A-1

	Page
Appendix B. <i>Mathematica</i> ¹ Source Files	B-1
B.1 Development of the Matrix $[\Phi]$	B-1
B.2 Development of the Matrix $[\Psi]$	B-2
B.3 Development of Shear Wapring Functions	B-5
B.4 Thickness Stretch Function Development	B-16
B.5 Development of the Stiffness Matrices	B-20
Appendix C. The Computer Program	C-1
C.1 Using the <i>JAGS</i> Program.	C-2
C.2 Program Output	C-9
C.3 Sample Input Files	C-9
C.3.1 The Composite Beam.	C-10
C.3.2 The Cylindrical Arch	C-12
C.3.3 The Torus of Spline Cross Section	C-13
C.3.4 The Spline-Torus with Contact	C-20
Appendix D. The Steadily Rotating Shell of Revolution	D-1
D.1 Kinetic Energy.	D-1
D.1.1 Incremental Equations.	D-9
D.2 Shell Rotation	D-10
D.3 Inertial Effects of Rotation	D-16
D.3.1 Kinetic Energy Relative to j -Frame.	D-16
D.3.2 Kinetic Energy Associated with Angular Acceleration.	D-17
D.3.3 Kinetic Energy Associated with Coriolis Acceleration.	D-18
D.3.4 Kinetic Energy Associated with Centripetal Acceleration.	D-18
D.3.5 Incremental Equations	D-23
D.4 Solution Techniques.	D-24
D.5 Summary	D-26

¹*Mathematica* is a registered trademark of Wolfram Research, Inc.

	Page
Appendix E. Elements of $[\hat{\Psi}]$	E-1
Appendix F. Material Properties	F-1
F.1 Inflation of Shuttle Nose Wheel Tire (Section 7.3.1)	F-1
F.2 Whole Tire Contact Problem	F-5
Vita	VITA-1

List of Figures

Figure	Page
3.1. Deformation of an infinitesimal volume element	3-2
3.2. Comparison of Jaumann and Second-Piola/Green measures	3-6
3.3. Step-wise application of the polar decomposition method	3-8
3.4. Geometric interpretation of the Jaumann shear strain	3-12
3.5. Coordinate system for the circular torus	3-14
3.6. Change in orientation of unit vectors along a coordinate curve (axis)	3-20
3.7. Infinitesimal element undergoing deformation (after Pai and Palazotto 1995a) .	3-25
3.8. Superimposition of deformed element $A'B'C'$ onto undeformed element ABC .	3-29
3.9. Transformation of infinitesimal shell element	3-33
3.10. Deformation associated with displacement field of Eqns (3.96)	3-35
3.11. Displacement field in the vicinity of point A	3-41
3.12. A layered composite of N layers indicating ply numbering scheme and interface coordinates, z_i	3-41
3.13. Shear warping in a layered composite	3-42
3.14. Rigid rotations and shear rotations in an originally undeformed parallelogram .	3-43
3.15. Trapezoidal cross-section effect	3-45
3.16. In-plane deformations relating to derivatives of displacement components	3-46
3.17. Change in orientation of fibers during deformation	3-52
3.18. The three-ply laminate	3-56
4.1. The variation of unit vector \mathbf{i}_3 , shown as the sum of two infinitesimal rotations	4-12
4.2. (a) Rigid-body movement associated with small v displacements, (b) Deformation associated with finite v displacements	4-28
4.3. Element independent stiffness matrix for flat plate, undeformed configuration .	4-29
4.4. Element independent stiffness matrix for cylindrical shell, undeformed configura- tion	4-29

Figure	Page
4.5. (a) Rigid body motion associated with small w displacement; (b) deformation caused by small w displacement when initial curvature is present	4-30
4.6. Element independent stiffness matrix for shell with two curvatures, undeformed configuration	4-31
4.7. Element independent stiffness matrix for shell with all curvatures, undeformed configuration	4-31
4.8. The 36-DOF shell element	4-34
4.9. The 44-DOF shell element	4-35
4.10. Load \mathbf{R} acting at a node and its components along the Lagrangian coordinate axes	4-43
5.1. In-plane patch test of the 44-DOF shell element	5-2
5.2. Isotropic square flat plate problem indicating 2×2 mesh of square elements modeling one fourth of plate	5-4
5.3. Isotropic cylinder pinched by transverse point loads at mid-length	5-7
5.4. Half plate strip in circular bending	5-8
5.5. Displacement u_1 at plate strip end, $S = 6$	5-11
5.6. Membrane stress J_{11} at plate strip center, $S = 6$	5-12
5.7. Transverse shear stress J_{13} at plate strip end, $S = 6$	5-12
5.8. Transverse normal stress J_{33} at plate strip center, $S = 6$	5-13
5.9. Isotropic toroidal shell segment subjected to a pressure load over a portion of its surface	5-15
5.10. Displacement along outer circumference of toroidal shell section	5-16
5.11. Displacement along meridional line 45 degrees to shell free ends	5-16
6.1. Composite cantilever beam subjected to an end-load	6-2
6.2. Load versus displacement for composite cantilever beam; experimental results are from (Minguet and Dugundji 1990)	6-3
6.3. Shallow circular cylindrical panel subjected to a transverse point load	6-4
6.4. Shallow circular cylindrical panel subjected to a transverse point load, $h = 25.4$ mm	6-5

Figure	Page
6.5. Shallow circular cylindrical panel subjected to a transverse point load, $h = 12.7$ mm	6-5
6.6. Shallow circular cylindrical panel subjected to a transverse point load, $h = 6.35$ mm	6-6
6.7. Composite circular cylindrical shell subjected to a transverse point load	6-7
6.8. Load versus displacement for composite cylindrical shell at point of load application	6-8
6.9. Isotropic deep circular arch with asymmetric boundary conditions subjected to transverse point load	6-9
6.10. Load versus displacement for crown of deep arch	6-11
6.11. Deformed geometry of deep arch indicating maximum deflection achieved for 36 and 44 degree-of-freedom elements	6-11
6.12. Load versus displacement for crown of deep arch, 44 degree-of-freedom element	6-14
6.13. Load versus displacement for crown of deep arch indicating response with different numbers of equal size elements	6-14
6.14. Load versus displacement for crown of deep arch indicating maximum displacement step size	6-15
7.1. Typical bias-ply aircraft tire indicating complexity of construction	7-2
7.2. Shell of revolution with irregular cross section	7-3
7.3. Piece-wise continuity of second derivative associated with classical cubic spline	7-7
7.4. Connecting a mesh to itself to form a continuous shell	7-10
7.5. Unconnected 2×5 mesh indicating degrees-of-freedom associated with element 10	7-11
7.6. Mesh joined along constant x coordinate curves	7-13
7.7. Mesh joined along constant y coordinate curves	7-14
7.8. Mesh joined along both constant x and constant y coordinate curves	7-15
7.9. Estimating the effect of tire deflection on tire pressure	7-17
7.10. Conservative estimate of increase in shuttle nose wheel tire pressure due to inflation	7-19
7.11. Finite element mesh vs. actual tire cross-section	7-20
7.12. Three views of the shuttle nose wheel tire mesh	7-21

Figure	Page
7.13. Tire cross section indicating coordinate system and boundary conditions	7-22
7.14. Finite element calculations compared to experimental (measured) values for space shuttle nose-wheel tire. See text for discussion of error bars.	7-22
7.15. Finite element stress resultants compared to finite element calculations of Kim and Noor (1990)	7-24
7.16. Discontinuity introduced by adjacent elements of different ply lay-up	7-25
7.17. Geometry of deformed tire for contact algorithm	7-28
7.18. Configuration of axisymmetric loading case for contact study	7-31
7.19. Displacements of opposing nodes on full tire model during inflation; displacements exaggerated—actual in-plane displacement is < 0.5 mm	7-32
7.20. Surface-normal loads (Newtons) vs. nondimensionalized meridional coordinate (ζ) at nodes on axisymmetric tire slice without update of pressure direction	7-33
7.21. Surface-normal loads (Newtons) vs. nondimensionalized meridional coordinate (ζ) at nodes on axisymmetric tire slice with updated pressure vector directions	7-35
7.22. Four deformed geometries of axisymmetric tire model with updated pressure vectors	7-36
7.23. Full tire undergoing contact at 28.5 % deflection; lower right is view of mesh	7-38
7.24. Surface-normal nodal loads and deformed geometry associated with the five nodes in contact; angle ply tire at 28.5 % deflection	7-39
D.1. The absolute displacement vector	D-2
D.2. Geometry of rotating shell	D-11

List of Tables

Table	Page
5.1. Nondimensionalized displacement, \bar{w} , at center of simply supported plate transversely loaded with uniform pressure	5-5
5.2. Comparison of Gauss integration order to nondimensionalized displacement at center of simply supported plate	5-6
5.3. Comparison of displacements at six points on the pinched isotropic cylinder; displacements in millimeters	5-8
5.4. Finite element results as compared to Pagano (1969) for the [0/90/0] laminated plate strip of various thickness ratios S	5-9
7.1. Effect of different mesh connection schemes	7-14
7.2. Maximum stresses and strains due to inflation of the shuttle tire model without pressure direction updates	7-26
7.3. Maximum stresses and strains due to inflation of the shuttle tire model without pressure direction updates indicating differences caused by updating warping functions in constitutive matrix	7-27
7.4. Maximum stresses and strains due to inflation of the axisymmetric tire model without pressure direction updates	7-31
7.5. Maximum stresses and strains due to inflation of the axisymmetric tire model with pressure direction updates	7-34
C.1. Differences in AFIT shell analysis codes	C-2

Dedication and Acknowledgements

Dedication

This work is dedicated to my father and my mother, James and Mary Way Greer. Now having the vantage point of parenthood myself, I have begun in the past few years to understand the enormity of their sacrifice in terms of love, time, and energy. In lovingly raising four children through the tumultuous and "socially experimental" 1960's and 70's, they chose to stay married during a time of disposable marriages. They chose family over expediency—love for others over love of self. May I model to my children their selflessness and, in doing so, repay some of what they have given me.

Acknowledgments

This research was sponsored by Dr. Arje Nachman of the Air Force Office of Scientific Research, and by Dr. Arnold Mayer of the Vehicle Subsystems Division of the Flight Dynamics Laboratory, Wright Laboratories (WL/FIV). Their support and sponsorship is very much appreciated. Also, Mr. John Medzorian (WL/FIVMA) was very helpful in providing tire data and valuable insights into tire analysis.

I owe a great debt to my research advisor, Prof. Anthony Palazotto, who has helped me grow both professionally and personally. His support, direction, advice, and friendship steered me through the course of this effort. I thank my committee members, Prof. Peter Torvik, Prof. Mark Oxley, and, representing the Dean, Prof. Won Roh. Their time spent in evaluating, critiquing, and suggesting improvements to this work is appreciated. Several AFIT faculty members were always willing to let me bend their ears at a moment's notice (or with no notice at all!). Maj. Robert Canfield, Maj. David Robertson, and Prof. William Baker made themselves available to me for spontaneous brain-storming sessions, and I appreciate their taking the time out of their schedules for that.

This work is built upon the research of many others who laid the ground work for it. Most notably, Prof. P. Frank Pai from the Mechanical Engineering Department, North Carolina A&T State University. Aside from developing the baseline theory for this effort, he was very gracious in promptly and thoroughly answering many, many questions regarding his work. Dr. Nagesh Gummadi, who is pursuing efforts somewhat related to this research, proffered numerous helpful suggestions regarding the theory and its finite element implementation. His help is gratefully acknowledged, as is that of Capt. Eric Herup, a fellow student who responded at lightning speed to my questions and requests for sometimes obscure data. His resourcefulness and friendship were a boon to my work. Thanks also go to fellow students and great friends (Captains) Jim Solti and Richard Cobb who, over several hundred lunch-times, encouraged me and gave me many helpful ideas. During the tougher times, when no progress was apparent, their friendship spurred me on.

None of this work would have been possible without the excellent computer resources of AFIT. Foremost among these resources are the people who maintain and trouble-shoot the systems, while patiently helping and answering the questions of students. Mr. Anthony Schooler, Mr. Robert Forbes, and Ms. Kristin Larsen are all credits to their respective organizations in this regard. Their professional skills keep the computers up and running virtually continually, and their personal help to me was invaluable in conducting my research.

My wife made many, many sacrifices of her own time and energy during the course of this effort, and "thank you" hardly seems enough. Denise cheerfully supported me as I spend many evenings and weekends away, with never a complaint, and I'm so grateful for her. I'm also grateful for my wonderful children, Drew, Joshua, and Lisa, who always (well, nearly always) showed understanding when hearing those fateful words: "Daddy has to go to school."

Finally, and mostly, I thank the One who gives me my next breath. (Ephesians 3:14-21)

James McKay Greer, Jr.

Abstract

A total Lagrangian finite element scheme for arbitrarily large displacements and rotations is applied to a wide range of shell geometries. The scheme decomposes the deformation into stretches and rigid-body rotations, examining the deformed state with respect to an orthogonal, rigidly translated and rotated triad located at the point of interest on the deformed structure. The Jaumann stresses and strains, which are resolved along the axes of this triad, are employed in the algorithm. Local and layer-wise thickness stretching and shear warping functions are used to model the three-dimensional behavior of the shell. These functions are developed through the use of the constitutive equations, certain stress and displacement continuity requirements at ply interfaces and laminate surfaces, and the behavior of the shell reference surface. Two finite elements are employed in the analyses: an eight-noded, 36 degree-of-freedom (DOF) element, and a four-noded, 44 DOF element. The 36 DOF element, which is not a compatible element with respect to the derivatives of in-plane deformations (i.e., $u_{,x}$, $u_{,y}$, $v_{,x}$, and $v_{,y}$ are not forced to be continuous along interelement boundaries) proves adequate for moderate rotation problems, but fails in modeling very large rotation problems. The use of the 44 DOF element provides dramatically improved results in the large rotation problem. The scheme is used to analyze isotropic and anisotropic beams, plates, arches, and shells. As a special application, a detailed finite element model of an aircraft tire is analyzed with regard to deformations resulting from inflation pressure. Finally, the feasibility of static contact analysis is also demonstrated.

NON-LINEAR FINITE ELEMENT ANALYSES OF COMPOSITE SHELLS BY TOTAL LAGRANGIAN DECOMPOSITION WITH APPLICATION TO THE AIRCRAFT TIRE

I. Introduction

1.1 Objective

The objective of this research is to investigate the nonlinear static behavior of anisotropic shells of compound curvature via the finite element method. The code developed for this research is capable of handling large displacements and rotations, and easily includes special cases of general shells, such as flat plates, cylindrical shells, and toroidal shells. Though the current research effort is limited to static analyses, equations are developed for dynamical analysis of rotating shells by modifying the equations of Pai and Palazotto (1995a) to include the inertial effects of steady rotation.

1.2 Overview

The finite element approach for the current work involves applying a "corotational" total-Lagrangian method that does not suffer from some of the problems inherent in attempting to approximate finite rotations with trigonometric functions (or series expansions thereof). The present research uses two-dimensional finite elements and warping/thickness-stretch functions to provide a quasi-three-dimensional result. This includes the through-the-thickness direct strains and stresses. A local deformation scheme (Pai and Nayfeh 1994a, Pai and Palazotto 1995a), which is essentially a polar decomposition method, is used as the basis for the theory. The analysis employs the Jaumann (or Biot-Cauchy-Jaumann) stresses and strains. These stresses and strains are objective, work-conjugate, and geometric.

1.3 Novelty of Research

The novelty in this research lies less in theoretical development (though the extensions of the dynamics equations of motion are certainly that) than in application of recent theoretical advances to the finite element method. Theoretical advances were made in the area of shear-warping functions, as singularities possible in the baseline formulation were revealed. New warping functions were subsequently used in the analyses. The concepts of (1) a layer-wise local displacement field (Pai and Nayfeh 1994b), (2) Jaumann stress and strain measures, and (3) a new interpretation and manipulation of orthogonal virtual rotations (Pai and Nayfeh 1991, 1992) are applied, and modified where necessary, to the finite element method for the analysis of anisotropic shells. Also, for application to the tire, the finite element code incorporates the features of tension spline curve fitting, force-follower loading, mesh connection, and a static contact algorithm. No experimental work was conducted under this effort, though experimental and other analytical data available were used for comparison purposes.

1.4 Overview

Chapter II provides the background for the current work, namely the use of two-dimensional finite element techniques incorporating transverse shear (and, in a few cases, thickness stretching) models to extract quasi-three-dimensional response of anisotropic materials undergoing geometrically nonlinear deformations. Some of the literature on recent applications of the polar decomposition method is presented, as is some of the literature on concurrent and vector processing. Though not fully exploited in this research, this area offers potentially high pay-offs, as the transformations involved in the decomposition scheme are computationally expensive. At the time of this writing, significant progress in the area of concurrent processing for finite element modeling is being made at the Air Force Institute of Technology.

Chapter III presents the theory of Pai and Nayfeh (1994a), largely as presented by Pai and Palazotto (1995a), but expanded and modified for the sake of completeness, clarity, and its application to the current research. The shear warping and thickness stretch functions are developed as suggested by Pai and Palazotto (1995a), examined, and then found wanting. The formulation of Pai (1995) is applied as well, but an additional modification is made resulting in significant improvement in representing the transverse behavior. A summary concludes the chapter.

The theory is taken into the finite element domain in Chapter IV. The procedure suggested by Pai and Palazotto (1995a) is found to be adequate by-and-large, but some modification is required. The implementation of the decomposition scheme is found to be computationally expensive, largely due to the linearization scheme used to discretize the equations for solution.

The results of some geometrically linear (small deformation) analyses are presented in Chapter V, including comparisons of finite element results with those of Pagano (1969) for flat plates. The pinched cylinder problem is solved with the current method, and the results of an isotropic toroidal shell analysis are also presented in this chapter.

Geometrically nonlinear results are the topic of Chapter VI, where several geometries and material configurations are examined. A deep arch having asymmetric boundary conditions is analyzed, revealing a shortcoming in the 36-degree-of-freedom (DOF) element. This leads to development of a new, 44-DOF element.

This finite element technique is applied to the aircraft tire in Chapter VII. Automated mesh connection, tension spline curve-fitting, force follower pressure loading, and a contact algorithm are added to the code for these analyses. The space shuttle nose wheel tire is analyzed in inflation and contact scenarios.

A summary and some conclusions are presented in Chapter VIII.

Several appendices are included. *Mathematica* source code used in the development of the *JAGS*¹ program, as well as instructions for use of the program and sample input files are included (Appendix C). Appendix D presents the dynamical equations associated with the current theory, then extends them to model a steadily rotating shell of revolution. This appendix is provided for the benefit of future researchers who may wish to extend the current work to dynamic analyses; no dynamics problems are solved in the current research. In addition, material of importance that was thought to be distracting in the main body of the text has been relegated to the appendices.

¹*JAGS* is an acronym for "Jaumann Analysis of General Shells"

II. Background

A review of the literature related to the current research is presented here. An overview of shell theory with some recent developments is presented, then the developments leading to the current state-of-the-art in finite element shell analysis are shown. A survey of numerical solution techniques, as well as some recent developments in vector/concurrent processing are then presented. Finally, because a goal of this research is to apply the theory to the analysis of tire-like structures, recent progress in the finite element analysis of tires is presented.

2.1 Development of Shell Theory.

If the flat plate is considered to be a special case of a shell (a shell with infinite radii of curvature), then classical shell theory could be said to have its roots in Lagrange's equation

$$D \nabla^4 w + \rho h \frac{\partial^2 w}{\partial t^2} = q(x, y, t) \quad (2.1)$$

for the two-dimensional theory of flexural motions of flat plates. Rayleigh (1889), Lamb (1917), and Timoshenko (1922) found exact solutions to the linear equations of elasticity for the problem, confirming Lagrange's result for the cases in which the flexural wavelengths are long in comparison to the plates thickness (i.e., thin plates, lower modes of vibration). In cases of thicker plates and higher modes, the classical solution quickly diverges from the three-dimensional elasticity solution. In a manner analogous to Timoshenko's (1921) introduction of transverse shear deformation into Bernoulli-Euler beam theory, Mindlin (1951) examined the effect of including rotatory inertia and through-the-thickness shear on the flat plate, bringing the classical solution dramatically close to the exact three-dimensional linear solution. His work follows closely that of Reissner (1945, 1947) and hence the theory is often referred to as "Reissner-Mindlin" plate theory.

As in plate theory, the foundational classical thin shell theory (see, e.g., Love 1891) neglected through-the-thickness shear by applying Kirchhoff's hypotheses to the cross-section deformation.

While adequate for thin isotropic shells (see also Sanders 1962), Love's theory does not model thick or layered (composite) shells well. Applying Kirchhoff's hypothesis to the cross-section deformation of laminated composites is often inadequate owing to the high ratio of the in-plane Young's moduli to the transverse shear moduli. This is particularly true in the case of anisotropic lay-ups (as opposed to orthotropic or transversely orthotropic) as shown by Gulati and Essenburg (1967). In addition, normal strains and stresses, often neglected in all but very thick isotropic shells, can be very significant for laminated anisotropic shells due to the anisotropy, high transverse thermal expansion coefficients (in the case of thermal loads), and non-uniformity of Poisson's ratios through the thickness (Noor and Burton 1990; Whitney 1971; Whitney and Sun 1974; Sivakumaran and Chia 1985; Doxsee and Springer 1991). Because of these factors, applying the classical shell theory typically results in an artificially stiff structure; underpredicting deflections (see, e.g., John 1965) and overpredicting stiffness (and hence overpredicting natural frequencies of vibration).

Reissner (1950), in possibly the first work on the influence of thickness stretching in the bending of laminated composite shells, stressed the importance of (and the difficulty knowing when to account for) effects of shearing and thickness stretching:

"The results of this investigation indicate the necessity of taking account of transverse shear and normal stress in sandwich-type shells, as soon as there is an order-of-magnitude difference between the elastic constants of the core layer and of the face layers of the composite shell. . . . The actual magnitude of the changes [in stress deformation] is greatly dependent on the geometry and loading condition of the structure under consideration so that *no general rules may be given* which indicate for which elastic modulus ratio the changes begin to be significant." (emphasis added)

Accounting for transverse shear deformations in shells has been done in several ways, but the majority fall into three classes: (1) first-order (Mindlin) theories, (2) third-order theories (Bhimaraddi 1984; Reddy and Liu 1985; Dennis and Palazotto 1989), and (3) higher-order theories (Mirsky and Herrmann 1957; Zukas and Vinson 1971; Whitney and Sun 1974; Voyiadjis and Shi 1991; Smith and Palazotto 1993).

First-order shear deformation theories, in which transverse normal stresses are neglected and the transverse shear stresses are assumed to be constant, are typified by the work of Chandrasekhara (1988), which must use shear correction factors to account for the parabolic distribution of shear stresses through the thickness (though parabolic for the isotropic flat plate, this distribution is, in general, not parabolic for the shell). According to Di Sciuva (1987), first order theories for multi-layered anisotropic plates and shells were first developed by Whitney and Pagano (1970) and Dong and Tso (1972) respectively. The degenerated shell element of Ahmad et al. (1970) also uses shear correction factors, due to the assumption that normals may rotate, but not warp or stretch. His element uses a five DOF node having three rectilinear and orthogonal displacements and two rotations about two in-plane orthogonal axes.

A piecewise linear assumed displacement field in conjunction with the principle of virtual work was used by Di Sciuva (1987) for modeling moderately thick multi-layered anisotropic shells and plates. His assumed displacement field fulfills continuity of interlaminar displacements. In this paper, Di Sciuva gives a thorough overview of the history of attempts to adequately model through-the-thickness shear effects in plates and shells (see also the review by Reddy 1989.) Plate kinematics are described in terms of the warping and rotation of the midsurface normal by Hodges et al. (1993). This approach avoids expanding the kinematic relations in the thickness coordinate, but assumes that rigid body rotations are large in comparison to the warping.

Smith and Palazotto (1993) (see also Smith 1991) applied eight higher order transverse shear theories to the nonlinear finite element analysis of composite cylindrical shells. The formulation used the Green-Lagrange strains and second Piola-Kirchhoff stresses. The shell displacement functions were expressed in cubic and quartic expansions of the thickness variable. The cubic expansions led to the parabolic through-the-thickness shear distribution, while the quartic expansions contained correction terms that yield the shear-stress-free conditions at the top and bottom of the curved shell surface. Both linear and nonlinear transverse shear strain expressions were used. Smith

and Palazotto showed that, for cylindrical shells of thickness h and radius R , a transverse shear deformation theory that uses only linear terms was improved little by including nonlinear terms for cases where $h^2/R^2 \ll 1$. In cases of collapse, however, the use of nonlinear strain-displacement terms for transverse shear produced a more flexible response. In a similar vein, Bařar et al. (1993) used a cubic series expansion in thickness coordinates for displacements to generate parabolic through-the-thickness shear strains. After casting the theory in a finite element formulation, they give examples of their applicability to finite rotation phenomena.

Belytschko and Glaum (1979) used a corotational approach (for a discussion of this approach, the reader is referred to the works of Oden 1972, Bathe et al. 1975, Bathe 1982, and Crisfield 1991, p. 211) for static nonlinear finite element analysis of clamped arches using a curved beam element. Their corotational formulation performs the additive decomposition, associated with infinitesimal strains, of the infinitesimal displacement at a point in the undeformed body $\{d\mathbf{u}\}$, having components $\{du_1, du_2, du_3\}$ along three mutually perpendicular directions $\{x_1, x_2, x_3\}$, into rigid body displacements and deformation displacements (see, e.g., Saada 1989):

$$\begin{Bmatrix} du_1 \\ du_2 \\ du_3 \end{Bmatrix} = \begin{bmatrix} e_{11} & e_{12} & e_{13} \\ e_{12} & e_{22} & e_{23} \\ e_{13} & e_{23} & e_{33} \end{bmatrix} \begin{Bmatrix} dx_1 \\ dx_2 \\ dx_3 \end{Bmatrix} + \begin{bmatrix} 0 & -\omega_{21} & \omega_{13} \\ \omega_{21} & 0 & -\omega_{32} \\ -\omega_{13} & \omega_{32} & 0 \end{bmatrix} \begin{Bmatrix} dx_1 \\ dx_2 \\ dx_3 \end{Bmatrix}. \quad (2.2)$$

The infinitesimal strains are represented by the e_{ij} , which have the form $e_{ij} = \partial u_i / \partial x_j + \partial u_j / \partial x_i$, and the infinitesimal rotations are represented by the $\omega_{ij} = \partial u_i / \partial x_j - \partial u_j / \partial x_i$. In contrast, the current research uses finite displacement theory, in which the final orientation and length, $\{d\mathbf{y}\}$, of an undeformed infinitesimal fiber $\{d\mathbf{x}\}$, is written in terms of the gradient of the finite displacements, $u_i = y_i - x_i$, as

$$\{d\mathbf{y}\} = [\mathbf{F}]\{d\mathbf{x}\}, \quad (2.3)$$

where $[\mathbf{F}] = \partial y_i / \partial x_j$. This displacement gradient tensor is multiplicatively decomposed as

$$\begin{bmatrix} \partial y_1 / \partial x_1 & \partial y_1 / \partial x_2 & \partial y_1 / \partial x_3 \\ \partial y_2 / \partial x_1 & \partial y_2 / \partial x_2 & \partial y_2 / \partial x_3 \\ \partial y_3 / \partial x_1 & \partial y_3 / \partial x_2 & \partial y_3 / \partial x_3 \end{bmatrix} = \begin{bmatrix} R_{11} & R_{12} & R_{13} \\ R_{21} & R_{22} & R_{23} \\ R_{31} & R_{32} & R_{33} \end{bmatrix} \begin{bmatrix} U_{11} & U_{12} & U_{13} \\ U_{12} & U_{22} & U_{23} \\ U_{13} & U_{23} & U_{33} \end{bmatrix}, \quad (2.4)$$

where the U_{ij} comprise a symmetric matrix representing the finite stretches and the R_{ij} form an orthogonal rotation matrix describing the rigid-body rotation of an orthogonal triad originally in the undeformed material axis orientation. Chapter III will describe how these stretches and rotations are formulated. Where the theory of Belytschko and Glaum (1979) is limited to moderate variations of rotation within an element, the current theory is not. Though not explicitly stated in their paper, from the geometry and deflection data presented one can deduce that the largest rotations evaluated were on the order of 10–20 degrees.

By using the concept of a local displacement field, Pai and Nayfeh (1994b) (see also Pai and Palazotto 1994) develop a shear deformation theory for laminated anisotropic shells that has the desirable attributes of: (1) continuity of interlaminar shear stresses (see also Librescu and Schmidt 1991) and (2) shear-stress-free conditions on the bounding surfaces. Third order theory, while meeting (2), does not meet (1).

Palmerio et al. (1990a) develop a moderate rotation theory for laminated anisotropic shells. The moderate rotations are of the order of the strains, and small strain theory is used. Equations of motion are developed through the use of Hamilton's principle. This theory is applied to several static problems (plates/shells) by Palmerio et al. (1990b).

An energy and momentum conserving algorithm for shell analysis is developed by Simo and Tarnow (1994) and applied to shells experiencing large rigid-body motions (e.g., tumbling freely in space) as well as elastic motions. The nonlinear shell model incorporates transverse shear deformation as well as thickness stretch. The mathematical development uses director theory, treating

the shell midsurface as a Riemann (two-dimensional) space with an associated director field (the director field describes the transverse dimension of the shell). A Galerkin finite element projection is utilized to discretize the equations of motion, which are then applied to the dynamics of an isotropic tumbling cylinder and the dynamics of three intersection isotropic plates. For these problems, an inextensible director (no thickness stretch) version of the theory is applied.

Theories based upon layer-wise 2-D assumed displacement fields provide background for the present work (Epstein and Glockner 1977, Epstein and Huttelmaier 1983, Murakami 1984, Heinrichsen and Palazotto 1986, Reddy 1989). While polynomial expressions are most often used to describe the transverse variation in displacements, Reddy's layer-wise theory (Reddy 1987, Barbero and Reddy 1990) requires only that the functions be continuous. The current work is similar to Reddy's in that the displacement functions are continuous at ply interfaces while their derivatives with respect to z , the thickness coordinate, are not. This leads to discontinuous transverse strains at interfaces. In the case of Reddy, this allows, but does not require, the stresses to be continuous across interlaminar boundaries (Reddy 1989). It also maintains a purely displacement-based scheme. In contrast, the current approach *enforces* the continuity of stresses at the interlaminar boundaries, thereby yielding the unknown coefficients of the cubic (in the case of in-plane displacements u and v) or quadratic (in the case of the thickness displacement w) displacement functions. The other significant difference is the inclusion of the transverse normal strain in the current work.

2.1.1 Finite Rotations and Polar Decomposition Theory. Polar decomposition theory (see Malvern 1969) has been applied to many fields, including solid mechanics (Simo et al. 1992, Souchet 1993, Pai and Palazotto 1995b, Griffin et al. 1993), stochastics (Tsuchiya 1992), physics (Rembielinski and Tybor 1992), and others. Many algorithms have been developed for its implementation (see e.g., Gander 1990 and Higham and Schreiber 1990).

Fraeijns de Veubeke (1972) derived a new set of variational principles through the application of polar decomposition theory, noting that the Piola stress tensor, "...however interesting from a

theoretical standpoint, does not appear suitable for practical applications." (The Piola stresses are not associated with physical body axes.)

Pai and Nayfeh (1991) introduced the concept of virtual orthogonal rotations. They point out that since finite rotations are sequence-dependent quantities, the use of Euler-like angles to describe the finite rotations in a structure is inappropriate. These virtual orthogonal rotations are infinitesimal (and therefore vector) rotations about the axes associated with the displaced, undeformed reference surface (Pai and Palazotto 1995a). Their local displacement field theory uses the cubic local displacement field of the form suggested by Reddy for laminated plates (1984b) and shells (1985). This assumed displacement field is applied to an orthogonal curvilinear coordinate axis system that rigidly translates and rotates with an infinitesimal element of the body as it deforms.

Pai and Palazotto (1995a) employed the objective, work-conjugate and geometric Jaumann stresses and strains (Fraeijs de Veubeke 1972, Atluri and Murakawa 1977, Atluri 1984, Danielson and Hodges 1987) in their development of a new total Lagrangian finite element formulation. These stress/strain measures employ polar decomposition theory and have the advantages of being geometric (rather than energy) measures of strain, and having directions aligned along the axes of the deformed structure (Pai and Palazotto 1995b; Pai and Nayfeh 1994a).

2.2 Finite Element Modeling

2.2.1 Previous Shell Work. In analyses of fiber-reinforced composite materials, as in most other areas of engineering, the modeler must trade between the level of complexity of the model and fidelity of results. Criticality of application, cost (and time) to benefit ratio, and other factors may play a role in the trade-off. In the modeling of composite plates and shells, the smallness of the thickness dimension (relative to the other dimensions) is exploited to avoid fully three-dimensional analyses (Antman 1989). Classical plate and shell theory assumptions, in which it is assumed that

normals to the reference surface remain straight, normal, and of unchanged length after deformation have proven inadequate for composites owing to the large ratios of elastic modulus to shear modulus of these materials. An adequate theory must account for transverse shear strains (Reddy 1984b) and, in some cases, for thickness stretching.

The current research depends upon decomposing the displacement field into a stretch and a rigid body rotation. As will be seen, classical eigenvalue decomposition techniques are not employed, but an identical result is achieved by following the deformation of two mutually perpendicular differential elements on the shell reference surface.

Horrigmoe and Bergan (1978) investigated the geometric nonlinearity of thin shell structures using very simple flat finite elements. Their approach used an updated Lagrangian, corotational method. They point out that the dominant factors in the geometric nonlinearities of thin shells are the product of finite rotations, with strains remaining small. Where some investigators have approached the shell problem through the use of very complex elements with higher order shape functions and many degrees of freedom, Horrigmoe and Bergan have gone the other route—choosing instead to trade element complexity for mesh refinement, when needed. They compare their results to curved element work by Sabir and Lock (1972) and others.

In his Ph.D. dissertation, Dennis (1988) developed a two-dimensional geometrically nonlinear shell theory applicable to arbitrary geometries. His theory encompasses large displacement and moderately large rotation deformation cases in which the strain is “small.” The theory utilizes a parabolic transverse shear stress distribution through the shell’s thickness. He develops a finite element code for the static analysis of composite shells. The theory is included in the book on nonlinear shell theory by Palazotto and Dennis (1992). Their finite element code was called *SHELL*.

Silva (1989) used *SHELL* to investigate the snapping (static) phenomena associated with transversely load composite cylindrical shells as did Tsai and Palazotto (1991a) in their comparison of displacement control and the Riks method.

Taylor Jr. (1990), Tsai and Palazotto (1991b), and Palazotto et al. (1992) extended the work to dynamic analyses of snapping composite shells using a modified version of *SHELL* called *DSHELL*. The *DSHELL* code used an implicit version of the beta-*m* numerical integration scheme (Katona and Zienkiewicz 1985). Some of their analyses, in which transversely loaded cylindrical shells were loaded beyond the dynamic snapping load, exhibited a type of erratic post-snapping behavior later shown by Greer and Palazotto (1994) to be numerical instability resulting from choosing too large an integration time step for the analysis. Later work by Greer and Palazotto (1995) and Forral and Palazotto (1994) indicated that, with the choice of an appropriate time step, the erratic behavior persists, but takes on characteristics associated with chaotic vibration rather than numerical instability.

Wagner (1990) developed a total Lagrangian finite element to analyze the static behavior of nonlinearly deforming elastic shells. His method formulates the fully nonlinear strains in the axisymmetric case, and he applied his model to the transversely (point) loaded spherical shell, the torus subjected to an axisymmetric ring load (for the tire, this would be equivalent to pinching the tire side-walls around the entire circumference), and a spherical rubber shell under point load. As Wagner's analysis deals with isotropic materials with thin cross-sections, he invokes the "Reissner-Mindlin-kinematic", in that transverse shear strains occur without cross-section warping. That is, the undeformed surface normal need not remain normal, but planar cross sections remain planar.

Sacco and Reddy (1992) compared their first- and second-order moderate rotation theories and the von Kármán plate theory with shear deformation to 2-D finite elasticity theory. They found their second-order theory to be closest to the elasticity theory.

Wriggers and Gruttmann (1993) developed a finite element formulation using polar decomposition for the static analysis of thin shells using the Reissner-Mindlin theory (no cross-sectional deformation). They use order-dependent Euler angles to describe the finite rotations. The method is applied to an end-loaded cantilever beam, an end-loaded and clamped *L*-shaped beam, a ring-

plate loaded at the free edge, and a hyperbolic paraboloid shell subjected to couples at the hinged supports.

A large strain theory was used by Schimmels and Palazotto (1994) in investigating the elastic-plastic response of layered composites. The shell model incorporates through-the-thickness shear (parabolic) and transformation of the Cauchy stress-strain relations into Lagrangian coordinates. These static analyses showed the more flexible response generated by allowing in-plane extensibility.

Pai and Palazotto (1995a) developed the approach upon which the current work is based. A polar decomposition method is applied to the large deformation problem with the rotations being described by the order-independent orthogonal virtual rotations. The total Lagrangian theory allows for through-the-thickness shear by including shear warping functions. These functions enforce continuity of interlaminar stresses and stress-free conditions at the free surfaces.

With the goal of developing a finite element theory more closely related to classical shell theory than that of Ahmad et al. (1970) and many other related formulations (including the current one), Simo et al. (1989) (see also Simo et al. 1990) developed a geometrically exact stress resultant shell model for isotropic shells. The single director theory allows for transverse shearing and thickness stretch, though the director is by definition straight and may not "warp" (as is permitted by the current theory). An example of a transversely loaded rubber sphere is used to demonstrate dramatic (52 %) thickness change, though in the example transverse shearing is not allowed. Simo et al. (1992) describes the application of this theory to nonlinear dynamics. The following problems are solved: (1) an isotropic tumbling cylindrical panel, (2) free motion of an isotropic spherical panel, (3) the pinched cylinder, and (4) the "pencil toss" problem of free motion of a flexible pencil and its subsequent motion after forces are removed. Simo's work differs from the current work in several respects: (1) Simo uses extensible director theory, in which a two-dimensional reference surface (the so-called Cosserat surface) and its associated director field describe the material deformation, (2) the theory is expressed entirely in stress resultants, so

numerical integration through-the-thickness of constitutive relations is not done (i.e., the *resultant* is the unknown, not a *stress* (derived from displacements) as a function of the thickness coordinate that must be integrated to *get* the resultant), (3) the method involves updating the orientation of the coordinate system (though Simo et al. 1990 shows that this is not necessary for “thick” shells) incrementally, and (4) warping in the thickness direction is not permitted, though piecewise-linear (as opposed to piecewise cubic in the current work) variation in displacement could arise in a multiple director scheme in which each layer has its own director.

2.3 Solution Techniques

Rheinboldt and Riks (1983) have provided an overview of solution techniques for nonlinear finite element problems. Such nonlinear problems are, by their nature, iterative, and the authors discuss solution methods for several types of nonlinearities: material, geometric, force, and kinematic boundary.

2.3.1 Static Problems. Many analyses of shell structures involve phenomena such as snap-through, collapse, and/or buckling. These responses are characterized by limit points, bifurcation points, and unstable regions of the force-displacement curve (i.e., greater displacement is not accompanied by increased resistance by the structure). In such analyses, conventional Newton-Raphson techniques fail, and methods such as those by Riks (1979) (and modifications thereof; see, e.g., Crisfield 1981) are often used. These methods establish a search region to determine the equilibrium solution. The search region may be delineated by an arc, a sphere, an ellipse, or some other constraining geometric construct. These methods facilitate the tracing of very convoluted (if physically unrealizable) load-displacement curves, finding all possible equilibrium states: stable and unstable.

2.3.2 Dynamic Problems. Finite element problems in nonlinear analysis frequently take the form of

$$\mathbf{M}\ddot{\mathbf{x}}(t) + \mathbf{C}\dot{\mathbf{x}}(t) + \mathbf{K}(\mathbf{x}(t))\mathbf{x}(t) = \mathbf{f}(t). \quad (2.5)$$

The beta- m family of integration methods (Katona and Zienkiewicz 1985) are commonly used to integrate such equations. These are single-step methods applicable to any set of initial value problems. Many other single-step methods (Newmark, Wilson, Houbolt, etc.) are special cases of the beta- m method.

2.4 Vector/Concurrent Processing.

As mesh sizes increase and/or shape functions become higher order, computational burden increases. Nonlinear problems, in which the stiffness matrices frequently depend upon the displacement vector, use large amounts of computational time performing the integrations necessary to formulate the elemental stiffness matrices (this is by far the biggest computational burden for a current in-house dynamic finite element model, *DSHELL*). Application of vector/concurrent processing appear to fall into three broad categories. These categories, along with some appropriate references, are described below.

2.4.0.1 "Smart" Compilers. A smart compiler on a vector/concurrent computer is able to recognize independent tasks and attempt to optimize the code for execution. Among other parameters, the compiler can optimize the code for the number of internal processors (usually < 10). Even programs written with little forethought as to vector/concurrent processing can be optimized (to varying degrees) by such compilers. Obviously, prudent coding can maximize the advantage offered by the compiler. Such code can generally be run as easily (though perhaps not as efficiently) on a one-processor machine; a big advantage of this method. The coding performed in the current research effort was geared toward this approach. Domain decomposition, a technique having its roots in the work of Przemieniecki (1963), is frequently employed in concert with smart

compilers, as exemplified in the work of Beran (1994), Moran and Beran (1994), Lutton and Beran (1994), Gilbertsen and Belytschko (1990), Luo and Friedman (1990), Farhat and Roux, (1991, 1992), Navon and Cai (1993), Babuška et al. (1992), and Johan et al. (1992).

2.4.0.2 Networking. In this approach, separate workstations are networked together using commercially available networking software. Unlike the smart compiler, the programmer must decide which workstations will do which tasks and when, and the code is not generally portable to other machines (Bertrand and Tanguy 1992).

2.4.0.3 Massively Parallel Processing. Computers having hundreds or even thousands of processors, such as the Connection Machine CM-2 system, have demonstrated extremely fast processing speeds. For example, Johnsson and Mathur (1990) used one CM-2 processor for each of 32,000 elements (400,000 degrees of freedom) in a linear finite element analysis, and achieved a peak performance of $2.5 \text{ G flops s}^{-1}$. (See also Belytschko and Plaskacz 1992; Law and Mackay 1993; Malone and Johnson 1994a, 1994b.)

2.5 Tire (and related) Modeling by Finite Elements.

In dynamic analyses, the inertias produced by rigid-body rotation have frequently been handled by the Galilean transformation (Sve and Herrmann 1974; Padovan et al. 1984; Padovan and Kazempour 1989) in which a moving reference frame is attached to the rolling object eliminating the time-dependency of the problem. Through the use of this technique, the problem becomes a static analysis, obviating the need for time integration.

The static contact problem was attacked using flat triangular finite elements by DeEskinazi et al. (1978). A meridional strip of a passenger-car tire cross-section was analyzed in inflation and contact. The geometry was somewhat artificial in that curvature in the circumferential direction was not included.

Rolling contact may be modeled in a number of ways. Kennedy and Padovan (1987) mention five ways rolling contact has been introduced into finite element formulations: (1) directly via boundary conditions, (2) the Hughes-type scheme, (3) the method of influence coefficients, (4) use of constraint equations, and (5) using "gap" elements. In his three-dimensional finite element formulation, Kennedy uses of the gap element method.

A three dimensional finite element model is used by Kulkarni et al. (1990, 1991) to model repeated, frictionless rolling contact. Likewise, Faria et al. (1992) used a 3-D finite element model including the effects of viscoelasticity, rolling contact, applied torque, and constant pressure volume. Their analysis investigated static and steady-state rolling problems. Their results showed qualitative agreement with experimental and theoretical results.

Noor and others have been responsible for much of the research performed through numerical modeling of tires. An excellent survey paper (Noor and Tanner 1985) outlines advancements made in tire modeling both outside and within the National Tire Modeling Program (NTMP). Semi-analytic finite elements, in which the shell variables are represented by Fourier series in the circumferential direction and piecewise polynomials in the meridional direction were used by Noor et al. (1990) in investigating nonlinear tire response. Noor et al. (1987) examined the types of symmetries often present in tire problems and how these symmetries may be exploited. Mixed finite element models are used having independent shape functions for stress resultants, strain components, and generalized displacements. A reduced basis technique is described in the work of Noor et al. (1993) for reducing the computational requirements for finite element analysis. In this technique, the vector describing the structural response (in this case the strain parameters, stress-resultant parameters, and nodal displacements) is examined with respect to changes in design variables (ply orientation, fiber diameters, material properties, etc.). These vector derivatives, called sensitivity coefficients (which are themselves vectors), are written as linear combinations of (initially unknown) basis, or approximation, vectors. Then, using a Bubnov-Galerkin technique described in the reference, finite

element equations are developed representing the response and sensitivity coefficients by a small number of algebraic equations written in terms of the amplitudes of these approximation vectors. This "reduced basis" of approximation vectors significantly reduces the computational expense of calculating the sensitivity coefficients, which can be very high in a complex model having many degrees of freedom.

Padovan et al. at the University of Akron have attacked the tire problem from many directions. The tire has been modeled using the classical ring on foundation model (1976) to examine the standing wave phenomenon seen behind the contact patch in rolling tires. These waves, under certain conditions (at critical tire speed, or resonance), can initiate catastrophic tire failure. Padovan (1977) employed a Lindstedt-Poincaré perturbation method to study the nonlinear effects of circumferentially traveling loads on rings and cylinders, where the road contact patch is modeled as the traveling load. Zeid and Padovan (1981) developed a new static/rolling contact element for applications to tires, rail-car wheels, roller bearings, and similar structures. The contact element has application to both linear and nonlinear problems. Again the classical ring on foundation model is used with two-dimensional finite elements. In 1982, Padovan used a family of generalized Rayleigh quotients and 3-D non-polar elasticity theory to investigate the spectral and critical speed characteristics of a structure subject to moving loads. The finite element method with an updated Lagrangian method was then applied to the problem by Padovan et al. in 1984. This method attaches a moving Lagrangian observer to the wheel axle to make the solution entirely spatially dependent, eliminating the need for time integration (see also Kazempour and Padovan 1989). In addition, the gap element method of Stadter and Weiss (1979) and the Hughes type contact strategy of Padovan and Paramadilok (1985) are used to handle the rolling contact problem. Padovan (1987) developed a theory to handle the steady-state and transient response of a moving/rolling nonlinear viscoelastic structure. Fractional integrodifferential representations (Grunwald 1867; Bagley and Torvik 1983 & 1985, Eldred et al. 1995) are used to model the viscoelastic response of the tire. Kennedy and Padovan (1987) use three-dimensional brick and their associated degenerate thick

shell element counterparts (see Ahmad et al. 1970, Surana 1983) to model the steadily rolling tire. Direct time integration is avoided using the Galilean transform. The gap element method is used to model rolling contact.

Lindsley and Cusumano (1993) modeled the tire as a nonlinear, viscoelastic, shearable and extensible ring on a viscoelastic foundation. They compared their model to the finite element results of Medzorian (1992). The simple ring model is much simpler than the finite element model, can be run on a PC, and showed good correlation to the finite element model in calculating critical speeds. The ring model incorporated the full complement of inertial forces and due to rotation, and included stiffening due to inflation.

Transient contact/impact problems are analyzed by Nakajima and Padovan (1987) using the theory developed by Padovan (1987). Rolling/sliding impact of tires with road obstructions is considered.

Another impact-contact method, the so-called "pinball" method, is the subject of a paper by Belytschko and Neal (1991). This method requires less conditional branching than other methods and thus lends itself to vectorization.

2.6 Summary

So where does the current work "fit" into the extensive body of literature on finite element analysis of shells? The theory described herein is a *geometrically exact* theory as defined by Simo et al. (1989), in that no restriction is placed on the allowable deformation or rotation of the shell. In keeping with this, finite deformation theory, rather than infinitesimal strain theory, is employed. Thus *geometrically nonlinear* problems may be examined.

This work uses a *materially linear* formulation, in that the material response is assumed to be linear throughout the range of deformation. So while the theory is not kinematically limited to small strains, results must always be interpreted in view of the known material response characteristics.

The current work employs a layerwise and continuous polynomial field throughout the thickness of a composite laminate to describe the transverse shearing and thickness stretching. This is similar in principle to the layerwise theory of Reddy, but differs in that continuity of interlaminar stresses is *enforced* in generating the displacement polynomials. It differs from director-type methods in that while a director may stretch, it does not warp. The layerwise polynomials permit warping of the cross section. Furthermore, the layerwise displacement field, while continuous at a ply interface, may abruptly change direction at the interface—the so-called “zig-zag” displacement field. This leads to discontinuous transverse shear strains, allowing for the (physically correct) continuous transverse shear stresses. This is in contrast to the approach of Palazotto and Dennis (1992) and many others who have used a single cubic polynomial to represent displacement through the entire thickness of the laminate. This leads to continuous transverse shear strains but discontinuous stresses.

In the current formulation, all kinematic behavior is related to the original, undeformed coordinate system. Even though the approach utilizes decomposition of the deformation gradient tensor, yielding the rigid-body rotation matrix, the members of that matrix are, *at each and every increment*, described in terms of the *global* displacements and their derivatives, and the initial curvatures. Though not unique in this regard, it stands in contrast to the almost universal use of updated-Lagrangian corotational techniques of large displacement/finite rotation analyses, in which the original undeformed coordinate system is discarded.

III. Theory

The theory presented in this chapter is chiefly that of Pai and Palazotto (1995a). The theory makes use of the polar decomposition method to facilitate the use of a local (and linear) displacement field at an infinitesimal region of interest in the nonlinearly deforming body. In this chapter, the theory is presented in the context of static (as opposed to dynamic) analysis¹. The finite element implementation of the theory, presented in Chapter IV, is limited to static analyses.

3.1 Stress and Strain Theories

It is desirable to be able to use experimentally determined (via tensile tests of coupons, etc.) material properties in constitutive equations. Unfortunately, not all measures of stress and strain lend themselves to this. Useful measures in this regard are (Pai and Nayfeh 1994a): (1) *work-conjugate*, i.e., the stress and strain measures are mathematically related in such a way that the elastic energy of the solid can be entirely accounted for, (2) *objective*, i.e., the stress and strain measures are invariant with respect to coordinate system (a by-product of this property is that pure rigid body rotations produce no strains), (3) *directional*, in that the stress and strain measures have identifiable directions, and (4) *geometric*, or the directions of the stress and strain measures are associated with the deformed body axes so that they may be matched with the natural boundary conditions of a structural system without having to transform the measures to another coordinate system. The Jaumann stresses and strains, which are equivalent to local engineering measures, meet these criteria.

3.1.1 Jaumann Stress and Strain Measures. The major differences between the Jaumann, Cauchy, and Second Piola-Kirchhoff Stress/Strain measures are outlined in this section (refer to Figure 3.1). The rectangular Cartesian case (rather than curvilinear) is used for illustrative pur-

¹In Appendix D, the dynamic equations associated with this general shell theory are presented, then modified for application to a special case: the rotating toroidal shell. The formulation accounts for the inertia generated by rigid body rotation of the tire.

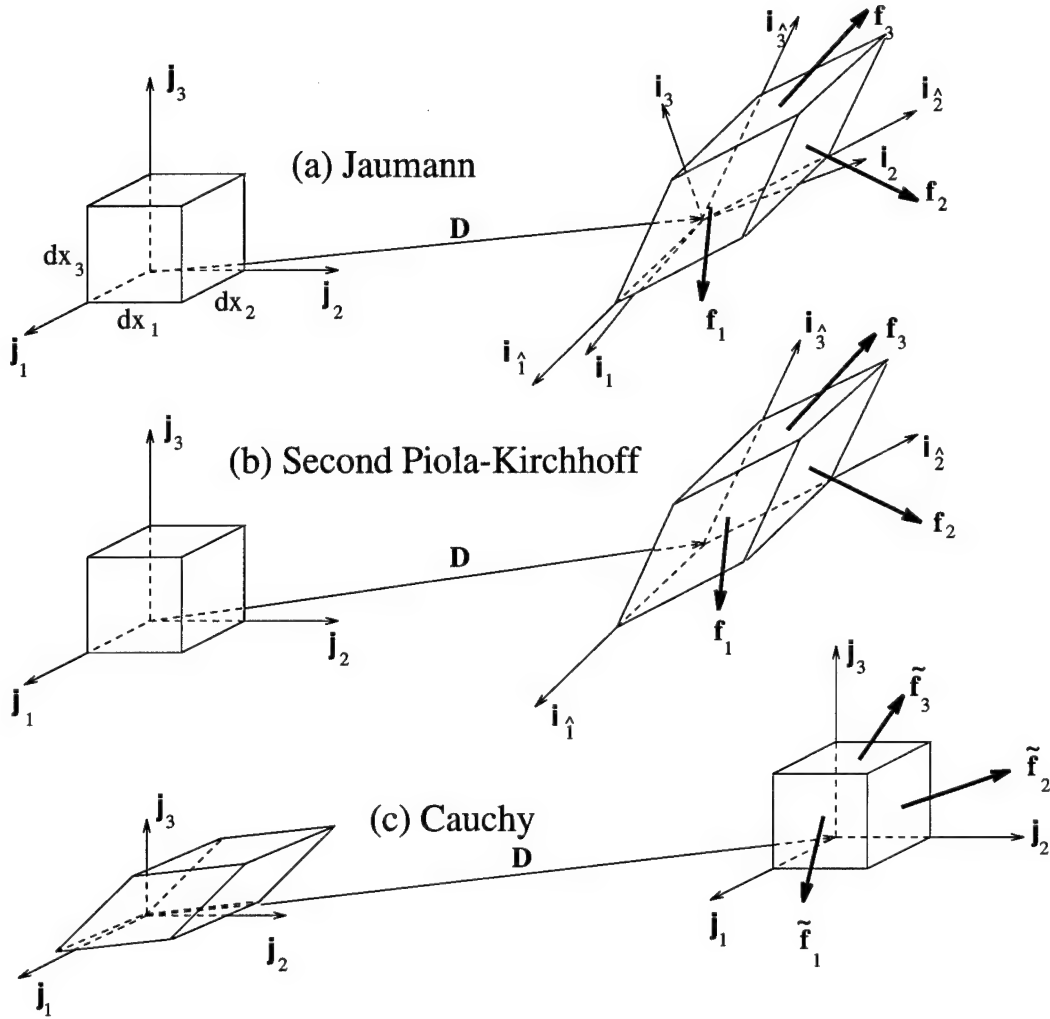


Figure 3.1 Deformation of an infinitesimal volume element

poses. The Jaumann stress J_{mn} and strain B_{mn} are given by Pai and Palazotto (1995a)

$$J_{mn} = \frac{1}{2 dx_1 dx_2 dx_3} (dx_m \mathbf{f}_m \cdot \mathbf{i}_n + dx_n \mathbf{f}_n \cdot \mathbf{i}_m) \quad (3.1a)$$

$$B_{mn} = \frac{1}{2} \left(\frac{\partial \mathbf{u}}{\partial x^m} \cdot \mathbf{i}_n + \frac{\partial \mathbf{u}}{\partial x^n} \cdot \mathbf{i}_m \right) \quad (3.1b)$$

where the \mathbf{f}_m are the force resultants on the faces of the deformed parallelepiped (Figure 3.1). For example, \mathbf{f}_1 acts on the deformed $dx_2 dx_3$ plane. The local displacement vector \mathbf{u} is measured with respect to the *displaced* location of a material point, hence at any given point on the reference

surface, $\mathbf{u} = \mathbf{0}$, though its derivatives (which will give rise to the strains) are non-zero. As can be seen from Eq (3.1b), the Jaumann stresses and strains are defined with respect to the orthogonal directions, denoted by unit vectors \mathbf{i}_k , associated with the stretched and rigidly rotated volume element (Figure 3.1(a)). Note that the stress measures are associated with *undeformed* cross-sectional areas.

On the other hand, the second Piola-Kirchhoff stresses S_{mn} and Green's strain L_{mn} are defined by Pai and Palazotto (1995a)

$$\frac{1}{dx_1 dx_2 dx_3} dx_{(m)} \mathbf{f}_{(m)} = \sum_{n=1}^3 (S_{m(n)} \lambda_{(n)} \mathbf{i}_{(\hat{n})}) \quad (3.2a)$$

$$L_{mn} = \frac{1}{2} (\lambda_{(m)} \mathbf{i}_{(\hat{m})} \cdot \lambda_{(n)} \mathbf{i}_{(\hat{n})} - \delta_{mn}) \quad (3.2b)$$

where $\lambda_n = \|\mathbf{E}_n\|$, the magnitude of the lattice vector (Washizu 1982), and the parenthesis suspend the tensor summing convention. In the figure, it is seen that the second-Piola/Green measures are associated with the directions along the deformed (and, in general, not orthogonal) edges of the element, as shown in Figure 3.1(b). The directions of the lattice vectors correspond to the directions of the unit vectors \mathbf{i}_k (note the circumflex on the subscript). So, in general, the components of the second-Piola stresses are along neither the undeformed coordinate system, as are the Cauchy measures depicted in Figure 3.1(c), nor its rigidly translated and rotated counterpart in the deformed body (as are the Jaumann measures). This is a consequence of the Green's strains being energy-related measures (dealing with the change in *squared* length of a fiber) rather than strictly geometric measures, like Jaumann or engineering strains. To use the Jaumann measures, which are local, the effect of rigid body translation and rotation must be removed so that only the effect of stretching (the source of elastic strain energy) is seen. The means to perform this are now shown in an example using the *polar decomposition method*, which explicitly performs this

separation of rigid body and stretching movements, allowing Eq (3.1b) to be formed very quickly.

According to Malvern (1969, p. 173):

“The fact that the deformation at a point may be considered as the result of a translation followed by a rotation of the principal axes of strain, and stretches along the principal axes, was apparently recognized by Thomson and Tait in 1867, but first explicitly stated by Love in 1892.”

By way of the polar decomposition, the Green and Jaumann strain measures are now compared and contrasted using the following (two-dimensional) global displacement field (Torvik 1992):

$$u_1 = a t x_1 x_2, \quad u_2 = b t x_2 \quad (3.3)$$

where the u_i are components of displacement, the x_i are the global coordinates of an undeformed point in the body, a and b are constants, and t represents time. The coordinates (y_1, y_2) for a material point, originally located at (x_1, x_2) , may then be written as

$$y_1 = x_1 + u_1, \quad y_2 = x_2 + u_2 \quad (3.4)$$

The deformation gradient tensor $[\mathbf{F}]$ is given by

$$[\mathbf{F}] = \mathbf{i}_k \cdot \frac{\partial \vec{\mathbf{r}}_\alpha}{\partial x_m} = \frac{\partial y_k}{\partial x_m} = \begin{bmatrix} 1 + a t x_2 & a t x_1 \\ 0 & 1 + b t \end{bmatrix}, \quad (3.5)$$

where \mathbf{r}_α is the position vector to a displaced point (y_1, y_2) . The polar decomposition² is now employed: The deformation gradient tensor may be decomposed into the product of two tensors, $[\mathbf{R}]$ and $[\mathbf{U}]$, where $[\mathbf{R}]$ describes the rigid rotation of the body at a material point, and $[\mathbf{U}]$ describes

²Here the decomposition is discussed in the context of rectangular Cartesian coordinates. But the decomposition may be performed in curvilinear coordinates as well (see, e.g., Pai and Palazotto 1995b)

the material deformation (stretching) at that point:

$$[\mathbf{F}] = [\mathbf{R}][\mathbf{U}]. \quad (3.6)$$

These matrices have some special properties. The matrix $[\mathbf{R}]$ is an orthogonal rotation matrix, that is

$$[\mathbf{R}]^T[\mathbf{R}] = [\mathbf{I}], \quad (3.7)$$

where $[\mathbf{I}]$ is the identity matrix and the stretch tensor $[\mathbf{U}]$ is symmetric:

$$[\mathbf{U}]^T = [\mathbf{U}]. \quad (3.8)$$

The Green deformation tensor $[\mathbf{C}]$, is defined as (Malvern 1969, p. 159) $[\mathbf{F}]^T[\mathbf{F}] = [\mathbf{U}]^2$. For any admissible (i.e., one-to-one) transformation between the x_i and the y_i , $[\mathbf{C}]$ is a positive definite symmetric matrix, and hence may be decomposed as (see, e.g., Strang 1988)

$$[\mathbf{C}] = [\mathbf{U}]^2 = [\mathbf{Q}][\mathbf{\Lambda}][\mathbf{Q}]^{-1} \quad (3.9)$$

where $[\mathbf{Q}]$ is the matrix of eigenvectors of $[\mathbf{C}]$ and $[\mathbf{\Lambda}]$ is a diagonal matrix having the eigenvalues of $[\mathbf{C}]$ as its members. The matrix $[\mathbf{U}]$ may then be written as

$$[\mathbf{U}] = [\mathbf{Q}][\mathbf{\Lambda}]^{-1/2}[\mathbf{Q}]^{-1}. \quad (3.10)$$

As a numerical example, consider the material point originally at $(x_1, x_2) = (1, 1)$ at time $t = 1$ sec, with $a = 1 \text{ m}^{-1} \text{ s}^{-1}$ and $b = 1 \text{ sec}^{-1}$. The deformation of an infinitesimal region near the point of interest is illustrated in Figure 3.2. In the figure, the candidate point is A , and the undeformed region is described by the square $ABCD$. This square deforms to $\tilde{A}\tilde{B}\tilde{C}\tilde{D}$ through the relationships of Eqns (3.3) and (3.4). Given the above parameters, the displacement gradient tensor $[\mathbf{F}]$ is given

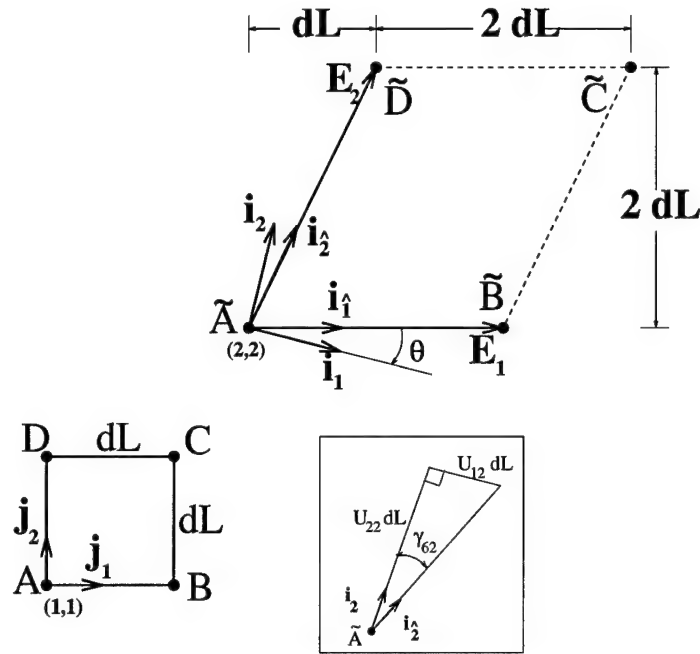


Figure 3.2 Comparison of Jaumann and Second-Piola/Green measures

by

$$[\mathbf{F}] = \begin{bmatrix} 2 & 1 \\ 0 & 2 \end{bmatrix}, \quad (3.11)$$

whose eigenvalues Λ_i and eigenvectors \mathbf{Q}_i are

$$\Lambda_1 = 2.43845, \quad \mathbf{Q}_1 = \begin{bmatrix} -0.788205 \\ 0.625412 \end{bmatrix} \quad \text{and} \quad \Lambda_2 = 6.56155, \quad \mathbf{Q}_2 = \begin{bmatrix} -0.615412 \\ -0.788205 \end{bmatrix}. \quad (3.12)$$

Hence $[\mathbf{\Lambda}]$ and $[\mathbf{Q}]$ are given by

$$[\mathbf{\Lambda}] = \begin{bmatrix} 2.43845 & 0 \\ 0 & 6.56155 \end{bmatrix}, \quad [\mathbf{Q}] = \begin{bmatrix} -0.788205 & -0.615412 \\ 0.615412 & -0.788205 \end{bmatrix}, \quad (3.13)$$

and from Eq (3.10) one obtains

$$[\mathbf{U}] = [\mathbf{Q}][\Lambda]^{-1/2}[\mathbf{Q}]^{-1} = \begin{bmatrix} 1.94029 & 0.485071 \\ 0.485071 & 2.18282 \end{bmatrix}, \quad (3.14)$$

and the rotation tensor is

$$[\mathbf{R}] = \begin{bmatrix} \cos \theta & \sin \theta \\ -\sin \theta & \cos \theta \end{bmatrix} = \begin{bmatrix} 0.970143 & 0.242536 \\ -0.242536 & 0.970143 \end{bmatrix}, \quad (3.15)$$

where $\theta = \cos^{-1} 0.970143 = 14.0362^\circ$ indicates the clockwise rotation of the \mathbf{j} -frame to the \mathbf{i} -frame.

A more intuitive view of the polar decomposition may be seen by recognizing its application as (Malvern 1969, p. 174)

1. a stretch by the operator \mathbf{U}
2. a rigid-body rotation by the operator \mathbf{R}
3. and finally a translation³ to \tilde{A}

Consider vector \mathbf{AB} of Figure 3.2 as these are applied (Figure 3.3(a)). First, the stretch tensor of Eq (3.14) is applied to vector $\mathbf{AB} = \{dL, 0\}$:

$$\begin{bmatrix} 1.94029 & 0.485071 \\ 0.485071 & 2.18282 \end{bmatrix} \begin{Bmatrix} dL \\ 0 \end{Bmatrix} = \begin{Bmatrix} 1.94029 dL \\ 0.485071 dL \end{Bmatrix}. \quad (3.16)$$

³As Malvern (1969, p. 174) points out, in this Cartesian example, the translation changes neither the vector nor its rectangular components. These would change in curvilinear components, however, and the curvature matrices of Eqns (3.66) will be used to describe these changes, which arise from taking derivatives with respect to curvilinear coordinates.

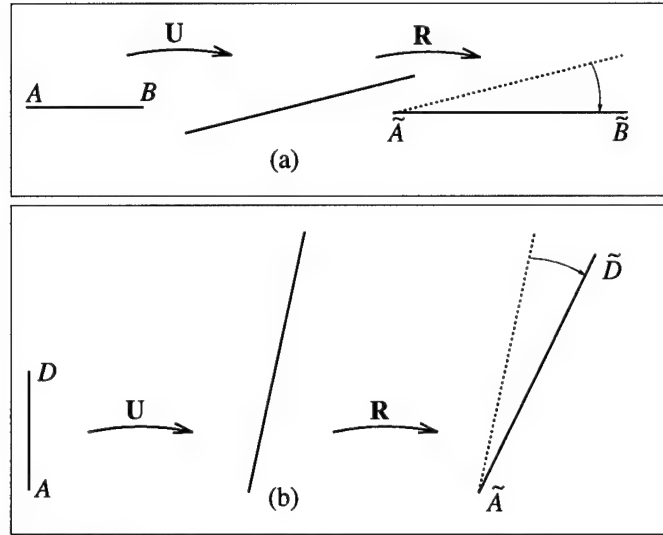


Figure 3.3 Step-wise application of the polar decomposition method

Then this stretched fiber is rotated by $[\mathbf{R}]$ of Eq (3.15):

$$\begin{bmatrix} 0.970143 & 0.242536 \\ -0.242536 & 0.970143 \end{bmatrix} \begin{Bmatrix} 1.94029 \, dL \\ 0.485071 \, dL \end{Bmatrix} = \begin{Bmatrix} 2 \, dL \\ 0 \end{Bmatrix}. \quad (3.17)$$

Likewise, applying the stretch tensor to vector $\mathbf{AD} = \{0, dL\}$ of Figure 3.2 (see Figure 3.3(b))

results in

$$\begin{bmatrix} 1.94029 & 0.485071 \\ 0.485071 & 2.18282 \end{bmatrix} \begin{Bmatrix} 0 \\ dL \end{Bmatrix} = \begin{Bmatrix} 0.485071 \, dL \\ 2.18282 \, dL \end{Bmatrix}. \quad (3.18)$$

Again, this stretched fiber is rotated by $[\mathbf{R}]$ of Eq (3.15):

$$\begin{bmatrix} 0.970143 & 0.242536 \\ -0.242536 & 0.970143 \end{bmatrix} \begin{Bmatrix} 0.485071 \, dL \\ 2.18282 \, dL \end{Bmatrix} = \begin{Bmatrix} dL \\ 2 \, dL \end{Bmatrix}. \quad (3.19)$$

The Jaumann strain⁴, is given by

$$[\mathbf{B}] = [\mathbf{U}] - [\mathbf{I}] = \begin{bmatrix} 0.94029 & 0.485071 \\ 0.485071 & 1.18282 \end{bmatrix} \quad (3.20)$$

Note that Eq (3.20) includes only the elastic stretches at a material point (the rotation tensor is not present). In comparing this to Eq (3.1b), it is seen that the stretch tensor is equivalent to the gradient of the *local* displacement vector (given by \mathbf{u} in Eq 3.1b) in the *rigidly rotated* coordinate system denoted by the $\{\mathbf{i}_{123}\}$ -basis. The Green-Lagrange strain is given by (Malvern 1969, p. 158)

$$[\mathbf{L}] = \frac{1}{2} ([\mathbf{U}]^2 - [\mathbf{I}]) = \begin{bmatrix} 1.5 & 1 \\ 1 & 2 \end{bmatrix} \quad (3.21)$$

As an aside, while the tensors $[\mathbf{B}]$ and $[\mathbf{L}]$ above have different eigenvalues (principal strains), they have identical principal directions, as they should. The *values* of the principle strains are determined by the choice of measure (Jaumann vs. Green), while the principle *directions* are not. Also note that the transformation between Green-Lagrange and Jaumann strains is given by (Pai and Palazotto 1995b)

$$[\mathbf{L}] = \frac{1}{2} [\mathbf{B}] ([\mathbf{U}] + [\mathbf{I}]), \quad (3.22)$$

and substituting the results into the above equation will verify the transformation.

A significant disparity between the two strain measures is seen. But the disparity is not only in magnitude, but direction as well.

First consider the direct strains. The Jaumann strain B_{22} has the direction illustrated in Figure 3.2 by the unit vector \mathbf{i}_2 , while the Green strain L_{22} is along \mathbf{i}_2 . Now consider the strain

⁴While not naming this strain "Jaumann" *per se*, Malvern (1969, p. 164) refers to the components of $[\mathbf{B}]$ as "unit extensions" (for direct strains referred to herein as B_{11} and B_{22}) and "angle change" (for the shear strain B_{12}). He notes that, in the finite deformation case, the so-called "angle change" is not the geometric angle change, but is dependent upon the stretches, as will be shown. He attributes his derivation to the works of Truesdell and Toupin (1960) and Eringen (1967).

magnitudes as they relate to the “fibers” forming the edges of the infinitesimal area $ABCD$. In particular, consider fiber AD which deforms to become $\tilde{A}\tilde{D}$. In deforming, the fiber has rotated $\arctan(dL/2 dL) = 26.565^\circ$ clockwise, and has stretched to a new length of $\left[(2 dL)^2 + dL^2\right]^{1/2} = \sqrt{5} dL$, a physical stretch of 123.6%. Neither the Jaumann strain, $B_{22} = 1.18282$ (from Eq 3.20), nor the Green strain of $L_{22} = 2$ (from Eq 3.21) are representing this physical stretch. The Green strain represents half the change in the squared length of the fiber, i.e., $\frac{1}{2}(\sqrt{5}^2 - 1^2) = 2$. The Jaumann strain $B_{22} = 1.18282$ represents the *projection* of the actual physical stretching of fiber AD onto the direction \mathbf{i}_2 . This geometric meaning is shown as follows. Let the physical straining of fiber AD in the engineering strain sense be denoted by e_2 as:

$$e_2 = \frac{\|\tilde{A}\tilde{D}\| - \|AD\|}{\|AD\|} = \frac{\sqrt{5} dL - dL}{dL} = 1.23607. \quad (3.23)$$

Let the “stretch” of the fiber be defined as the ratio of the deformed length to the original length, or

$$U_{AD} = \|\tilde{A}\tilde{D}\|/\|AD\| = \sqrt{5} dx/dx = \sqrt{5} = 1 + e_2 = 2.23607. \quad (3.24)$$

Now note the “shear” (rotation) angle associated with the ‘2’ direction, denoted γ_{62} in Figure 3.2. This angle may be used to find the projection of the stretch U_{AD} onto the \mathbf{i}_2 direction, U_{22} as

$$U_{22} = U_{AD} \cos \gamma_{62} = (1 + e_2) \cos \gamma_{62} = 2.18282, \quad (3.25)$$

where γ_{62} is given by (the geometric interpretation of the angle may be seen in the inset of Figure 3.2)

$$\gamma_{62} = \tan^{-1} U_{12}/U_{22}. \quad (3.26)$$

Note that the values of U_{12} and U_{22} of the right stretch tensor describe the stretching and rotation *due to deformation* of the infinitesimal fiber of length dL originally located along the \mathbf{j}_2 direction. Likewise, U_{11} and U_{12} describe the deformation of the fiber originally located along the \mathbf{j}_1 direction.

Finally, the Jaumann strain, B_{22} is seen to be

$$B_{22} = (1 + e_2) \cos \gamma_{62} - 1 = 1.18282. \quad (3.27)$$

In the same manner, B_{11} describes the physical stretching of fiber AB projected onto the \mathbf{i}_1 direction. Notice that for small shear ($\cos \gamma_{62} \rightarrow 1$) the result yields the engineering strain result:

$$B_{22} = (1 + e_2) - 1 = e_2 = 1.23607. \quad (3.28)$$

If the additional constraint of small direct strain is enforced, i.e., $e_2 \ll 1$ it is found that the Green strain approaches the engineering strain result as well. This may be shown as follows (Torvik 1992). The Green strain may be written as⁵

$$2L_{22} = \frac{\mathbf{E}_2 \cdot \mathbf{E}_2 - dx^2}{dx^2} = \frac{(\sqrt{\mathbf{E}_2 \cdot \mathbf{E}_2} + dx)(\sqrt{\mathbf{E}_2 \cdot \mathbf{E}_2} - dx)}{dx^2}. \quad (3.29)$$

But for small strain, $\sqrt{\mathbf{E}_2 \cdot \mathbf{E}_2} \approx dx$, leading to

$$2L_{22} \approx \frac{2dx(\sqrt{\mathbf{E}_2 \cdot \mathbf{E}_2} - dx)}{dx^2} \approx 2 \frac{(\sqrt{\mathbf{E}_2 \cdot \mathbf{E}_2} - dx)}{dx} \approx 2e_2. \quad (3.30)$$

Examining the shear strains, from Eq (3.2b) it is seen that the shear strain L_{12} is simply the dot product of the lattice vectors.

$$L_{12} = \frac{1}{2} (\mathbf{E}_1 \cdot \mathbf{E}_2) = 1. \quad (3.31)$$

In general, the lattice vectors are not of unit magnitude, so this strain is *not* the change in angle between two originally perpendicular fibers, which for this example is found from the geometry in

⁵Note that \mathbf{E}_2 is the lattice vector related to the deformation of $dL\mathbf{j}_2$ (Washizu 1982).

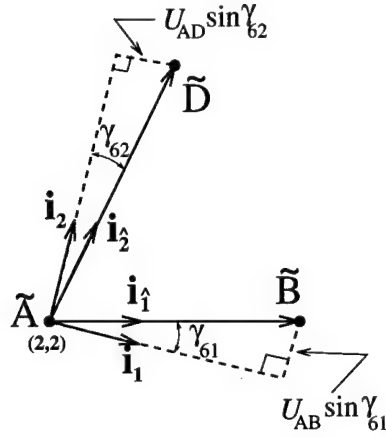


Figure 3.4 Geometric interpretation of the Jaumann shear strain

Figure 3.2 as

$$\tan \gamma_6 = \frac{dL}{2dL} = 0.5, \quad \text{or} \quad \gamma_6 = 26.565^\circ = 0.46365 \text{ radians} \quad (3.32)$$

From Eq (3.20) and the inset of Figure 3.2, the Jaumann shear strain B_{12} is given by:

$$B_{12} = U_{12} = U_{22} \tan \gamma_{62} = 0.485071. \quad (3.33)$$

The first thing noticed is that $B_{12} = 0.485071$ radians is much closer to representing the actual angle change of $\gamma_6 = 0.46365$ radians than is $L_{12} = 1$. But why is it different at all? Consider Figure 3.4, which describes the geometry of the problem. In terms of the geometry shown⁶, the shear strain is given by

$$2B_{12} = U_{AB} \sin \gamma_{61} + U_{AD} \sin \gamma_{62} = (1 + e_1) \sin \gamma_{61} + (1 + e_2) \sin \gamma_{62}. \quad (3.34)$$

From this equation, it is seen that the tensorial strain, $2B_{12}$, approaches the physical angle change, γ_6 , as both of the following are approached: (1) the stretch becomes negligible ($U_{AB} \rightarrow 1, U_{AD} \rightarrow 1$) and (2) the shearing angle is small ($\sin \gamma_{61} \rightarrow \gamma_{61}, \sin \gamma_{62} \rightarrow \gamma_{62}$). Under these conditions, the

⁶The origin of Eq (3.34) covered in Section 3.3.

engineering strain result is obtained (see also Malvern 1969, p. 165)

$$2B_{12} = \gamma_6 = \gamma_{61} + \gamma_{62}. \quad (3.35)$$

To summarize, while both strain measures asymptotically approach the engineering strain values as strains become infinitesimal, the Jaumann measures are closely related to the engineering strains, even for (small) finite strains. This is an important feature, as it allows constitutive data from experiments (engineering measures) to be used in the numerical analysis without transformation⁷.

In the following section, the Jaumann measures are generalized to curvilinear coordinates.

3.2 Kinematics in Curvilinear Coordinates

A guiding assumption in the following theoretical development is that a vector-oriented derivation can be readily related to the physical problem at hand and hence is more easily understood by the engineer. Furthermore, such an approach is more easily implemented numerically (on the computer). For these reasons, the derivations of this chapter and the next use a vector approach, rather than tensorial notation, wherever possible.

The kinematic relationships for the shell of revolution are now developed. This geometry is chosen for its generality, in that many other geometries (plate, cylindrical shell, spherical shell) are special cases of this shell. Furthermore, as one of the applications for the current research is the aircraft tire, the torus represents a good starting point⁸. Consider Figure 3.5, a circular torus. The body-fixed Cartesian coordinate system

⁷A caveat is in order here: The lack of a need for transformation between stress measures reflects the use of the *nominal* or *engineering stress* which is referred to the undeformed cross-sectional area of the test specimen. This would reflect the use of test data at load levels below the ultimate load of the specimen (where necking of the specimen begins to occur). Beyond this load level, by assuming such plastic deformation occurs at constant volume, a corrected measure may be employed as shown by Malvern (1969, p. 332).

⁸Of course the actual tire is not of circular cross section, but this affects mainly the curvature terms. Hence the new curvature terms associated with non-circular shells of revolution are developed in Chapter VII

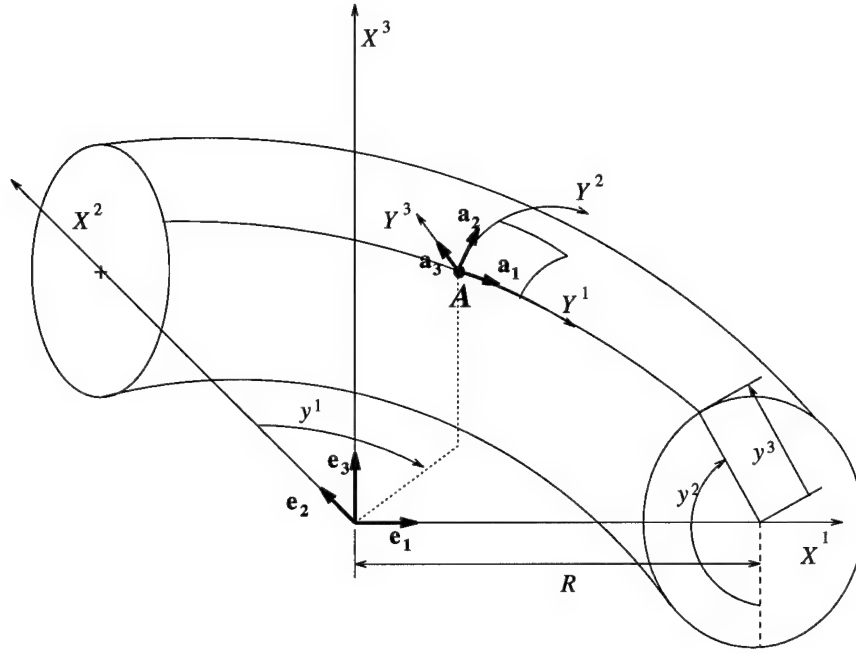


Figure 3.5 Coordinate system for the circular torus

$$x^i = x^i(x^1, x^2, x^3) \quad (3.36)$$

has unit basis vectors of orthogonal Cartesian system \mathbf{e}_i (the superscripts indicate contravariance of the tensor components, they are not exponents). The orthogonal curvilinear coordinate system

$$Y^i = Y^i(y^1, y^2, y^3) \quad (3.37)$$

has basis vectors \mathbf{a}_i (in general not of unit length). The surface has radius of revolution R . The directions of these "toroidal" coordinates are chosen as shown to correspond to the reference surface being described, namely the circular torus. Referring again to Figure 3.5, the y^1 coordinate describes the circumferential location, y^2 the meridional location, and y^3 the radial location. Furthermore, the position of a point A on the shell can be described in terms of the X^i or Y^i through

the transformation

$$X^1 = (R - y^3 \sin y^2) \sin y^1 \quad (3.38a)$$

$$X^2 = (R - y^3 \sin y^2) \cos y^1 \quad (3.38b)$$

$$X^3 = -y^3 \cos y^2. \quad (3.38c)$$

The basis vectors for the curvilinear system, \mathbf{a}_i , may now be found by $\mathbf{a}_i = \frac{\partial X^j}{\partial y^i} \mathbf{e}_j$. That is

$$\mathbf{a}_1 = \frac{\partial X^1}{\partial y^1} \mathbf{e}_1 + \frac{\partial X^2}{\partial y^1} \mathbf{e}_2 + \frac{\partial X^3}{\partial y^1} \mathbf{e}_3 \quad (3.39a)$$

$$\mathbf{a}_2 = \frac{\partial X^1}{\partial y^2} \mathbf{e}_1 + \frac{\partial X^2}{\partial y^2} \mathbf{e}_2 + \frac{\partial X^3}{\partial y^2} \mathbf{e}_3 \quad (3.39b)$$

$$\mathbf{a}_3 = \frac{\partial X^1}{\partial y^3} \mathbf{e}_1 + \frac{\partial X^2}{\partial y^3} \mathbf{e}_2 + \frac{\partial X^3}{\partial y^3} \mathbf{e}_3 \quad (3.39c)$$

which yields, from Eqns (3.38),

$$\mathbf{a}_1 = (R - y^3 \sin y^2) \cos y^1 \mathbf{e}_1 - (R - y^3 \sin y^2) \sin y^1 \mathbf{e}_2 \quad (3.40a)$$

$$\mathbf{a}_2 = -y^3 \cos y^2 \sin y^1 \mathbf{e}_1 - y^3 \cos y^2 \cos y^1 \mathbf{e}_2 + y^3 \sin y^2 \mathbf{e}_3 \quad (3.40b)$$

$$\mathbf{a}_3 = -\sin y^2 \sin y^1 \mathbf{e}_1 - \sin y^2 \cos y^1 \mathbf{e}_2 - \cos y^2 \mathbf{e}_3. \quad (3.40c)$$

The basis vectors \mathbf{a}_i are not, in general, of unit magnitude, but the corresponding unit vectors are easily found by dividing each vector by its magnitude.

$$\mathbf{j}_1 = \cos y^1 \mathbf{e}_1 - \sin y^1 \mathbf{e}_2 \quad (3.41a)$$

$$\mathbf{j}_2 = -\cos y^2 \sin y^1 \mathbf{e}_1 - \cos y^2 \cos y^1 \mathbf{e}_2 + \sin y^2 \mathbf{e}_3 \quad (3.41b)$$

$$\mathbf{j}_3 = -\sin y^2 \sin y^1 \mathbf{e}_1 - \sin y^2 \cos y^1 \mathbf{e}_2 - \cos y^2 \mathbf{e}_3, \quad (3.41c)$$

where $\mathbf{j}_i = \mathbf{a}_i / \|\mathbf{a}_i\|$, and $\|\mathbf{a}_i\|$ is simply $\sqrt{\mathbf{a}_i \cdot \mathbf{a}_i}$.

The basis vectors, \mathbf{e}_i , of the Cartesian coordinate system are of fixed orientation throughout the space they describe. That is, if the triad described by \mathbf{e}_1 , \mathbf{e}_2 , and \mathbf{e}_3 is translated from the origin to any point in three-space, their directions do not change. This is not the case with the new basis vectors, \mathbf{j}_i . The directions of these vectors are uniquely determined by the coordinates (y^1, y^2, y^3) at which they reside. This becomes important in taking derivatives of any vector quantity measured with these unit vectors. Subsequently, all of this is to be used in defining strain-displacement relationships. For example, if there exists some vector \mathbf{V} , given by $\mathbf{V} = V^1\mathbf{e}_1 + V^2\mathbf{e}_2 + V^3\mathbf{e}_3$, its derivative with respect to a direction associated with the Cartesian coordinates, x^k , may be taken as

$$\frac{\partial \mathbf{V}}{\partial x^k} = \frac{\partial V^1}{\partial x^k} \mathbf{e}_1 + \frac{\partial V^2}{\partial x^k} \mathbf{e}_2 + \frac{\partial V^3}{\partial x^k} \mathbf{e}_3. \quad (3.42)$$

Note that there are no terms involving the derivatives of the unit vectors themselves. This is because they do not change direction when moving along a coordinate curve (or Cartesian axis). This is not the case with the curvilinear system. Because the directions of the unit vectors change along a coordinate curve (curvilinear axis), expressions must be formulated that describe the derivatives of these unit vectors. One way to describe these derivatives is through the use of Christoffel symbols. But these are cumbersome and do not lend themselves well to numerical implementation. Instead, in keeping with the desire to develop a vectorial approach to the equations, the derivatives of the unit vectors will be written using “curvature matrices”. The use of this term reflects the fact that the numbers populating these matrices will reflect how “curved” the coordinates are. For example, a unit vector moving along a curvilinear axis having a small radius (large curvature) changes direction rapidly, while a unit vector moving along an axis having an infinite radius (a straight line) does not change direction at all. Thus entries in the curvature matrix will reflect how “curved” the axes are at a particular point.

To begin the development of the curvature matrices, it is noted that the expressions of Eq (3.39) may be written in matrix form as

$$\begin{Bmatrix} \mathbf{a}_1 \\ \mathbf{a}_2 \\ \mathbf{a}_3 \end{Bmatrix} = \begin{bmatrix} \frac{\partial X^1}{\partial y^1} & \frac{\partial X^2}{\partial y^1} & \frac{\partial X^3}{\partial y^1} \\ \frac{\partial X^1}{\partial y^2} & \frac{\partial X^2}{\partial y^2} & \frac{\partial X^3}{\partial y^2} \\ \frac{\partial X^1}{\partial y^3} & \frac{\partial X^2}{\partial y^3} & \frac{\partial X^3}{\partial y^3} \end{bmatrix} \begin{Bmatrix} \mathbf{e}_1 \\ \mathbf{e}_2 \\ \mathbf{e}_3 \end{Bmatrix}, \quad (3.43)$$

or

$$\{\mathbf{a}\} = [\mathbf{J}]^T \{\mathbf{e}\}, \quad (3.44)$$

where

$$[\mathbf{J}] = \begin{bmatrix} \frac{\partial X^1}{\partial y^1} & \frac{\partial X^1}{\partial y^2} & \frac{\partial X^1}{\partial y^3} \\ \frac{\partial X^2}{\partial y^1} & \frac{\partial X^2}{\partial y^2} & \frac{\partial X^2}{\partial y^3} \\ \frac{\partial X^3}{\partial y^1} & \frac{\partial X^3}{\partial y^2} & \frac{\partial X^3}{\partial y^3} \end{bmatrix}, \quad (3.45)$$

the Jacobian of the transformation. From Eqns (3.38), $[\mathbf{J}]$ is found to be

$$[\mathbf{J}] = \begin{bmatrix} (R - y^3 \sin y^2) \cos y^1 & -y^3 \cos y^2 \sin y^1 & -\sin y^2 \sin y^1 \\ -(R - y^3 \sin y^2) \sin y^1 & -y^3 \cos y^2 \cos y^1 & -\sin y^2 \cos y^1 \\ 0 & y^3 \sin y^2 & -\cos y^2 \end{bmatrix}, \quad (3.46)$$

Similarly, an equation for the *unit* vectors \mathbf{e}_i may be written. First, note that a diagonal matrix $[\mathbf{g}]$, consisting of the squares of magnitudes of the vectors \mathbf{a}_i is generated by $[\mathbf{J}]^T[\mathbf{J}]$:

$$[\mathbf{g}] = [\mathbf{J}]^T[\mathbf{J}] = \begin{bmatrix} (R - y^3 \sin y^2)^2 & 0 & 0 \\ 0 & (y^3)^2 & 0 \\ 0 & 0 & 1 \end{bmatrix}. \quad (3.47)$$

This is the so-called “metric tensor,” as it describes how distances are measured in the curvilinear coordinate system. The measurement issue will be discussed more later. For now, recall that these

are the *squares* of the magnitudes of the vectors \mathbf{a}_i . For example, $g_{11} = \mathbf{a}_1 \cdot \mathbf{a}_1$. Furthermore, $[\mathbf{g}]$ is a diagonal matrix because the vectors \mathbf{a}_i , are always mutually perpendicular. That is, $\mathbf{a}_i \cdot \mathbf{a}_j = 0$ for $i \neq j$. A diagonal matrix consisting of the magnitudes of the basis vectors is found by simply taking the square roots of the elements of $[\mathbf{g}]$, calling this new matrix⁹ $[\mathbf{g}]^{(1/2)}$:

$$[\mathbf{g}]^{(1/2)} = \begin{bmatrix} R - y^3 \sin y^2 & 0 & 0 \\ 0 & y^3 & 0 \\ 0 & 0 & 1 \end{bmatrix} = \begin{bmatrix} \|\mathbf{a}_1\| & 0 & 0 \\ 0 & \|\mathbf{a}_2\| & 0 \\ 0 & 0 & \|\mathbf{a}_3\| \end{bmatrix}. \quad (3.48)$$

The inverse of this matrix is given by

$$[\mathbf{g}]^{-(1/2)} = \begin{bmatrix} 1/(R - y^3 \sin y^2) & 0 & 0 \\ 0 & 1/y^3 & 0 \\ 0 & 0 & 1 \end{bmatrix} = \begin{bmatrix} 1/\|\mathbf{a}_1\| & 0 & 0 \\ 0 & 1/\|\mathbf{a}_2\| & 0 \\ 0 & 0 & 1/\|\mathbf{a}_3\| \end{bmatrix}. \quad (3.49)$$

Since, $\mathbf{j}_i = \mathbf{a}_i/\|\mathbf{a}_i\|$, it is apparent that

$$\begin{Bmatrix} \mathbf{j}_1 \\ \mathbf{j}_2 \\ \mathbf{j}_3 \end{Bmatrix} = \begin{bmatrix} 1/(R - y^3 \sin y^2) & 0 & 0 \\ 0 & 1/y^3 & 0 \\ 0 & 0 & 1 \end{bmatrix} \begin{Bmatrix} \mathbf{a}_1 \\ \mathbf{a}_2 \\ \mathbf{a}_3 \end{Bmatrix} \quad (3.50)$$

Substituting the expression for $\{\mathbf{a}\}$ given by Eq (3.44) into the above yields

$$\{\mathbf{j}\} = [\mathbf{g}]^{-(1/2)}[\mathbf{J}]^T\{\mathbf{e}\}, \quad (3.51)$$

or, defining a new matrix

$$[\tilde{\mathbf{J}}]^T = [\mathbf{g}]^{-(1/2)}[\mathbf{J}]^T \quad (3.52a)$$

⁹The elements of this matrix are called "scale factors" (see, e.g., Saada 1989, p. 118).

$$= \begin{bmatrix} 1/(R - y^3 \sin y^2) & 0 & 0 \\ 0 & 1/y^3 & 0 \\ 0 & 0 & 1 \end{bmatrix} \begin{bmatrix} (R - y^3 \sin y^2) \cos y^1 & -(R - y^3 \sin y^2) \sin y^1 & 0 \\ -y^3 \cos y^2 \sin y^1 & -y^3 \cos y^2 \cos y^1 & y^3 \sin y^2 \\ -\sin y^2 \sin y^1 & -\sin y^2 \cos y^1 & -\cos y^2 \end{bmatrix} \quad (3.52b)$$

$$= \begin{bmatrix} \cos y^1 & -\sin y^1 & 0 \\ -\cos y^2 \sin y^1 & -\cos y^2 \cos y^1 & \sin y^2 \\ -\sin y^2 \sin y^1 & -\sin y^2 \cos y^1 & -\cos y^2 \end{bmatrix}, \quad (3.52c)$$

one may write

$$\{\mathbf{j}\} = [\tilde{\mathbf{J}}]^T \{\mathbf{e}\}. \quad (3.53)$$

The matrix $[\tilde{\mathbf{J}}]$ has a very useful property: it is orthonormal. That is, the transpose of the matrix is also its inverse. This allows the inverse transform of Eq (3.53) to be written as

$$\{\mathbf{e}\} = [\tilde{\mathbf{J}}] \{\mathbf{j}\}, \quad (3.54)$$

where

$$[\tilde{\mathbf{J}}] = \begin{bmatrix} \cos y^1 & -\cos y^2 \sin y^1 & -\sin y^2 \sin y^1 \\ -\sin y^1 & -\cos y^2 \cos y^1 & -\sin y^2 \cos y^1 \\ 0 & \sin y^2 & -\cos y^2 \end{bmatrix}, \quad (3.55)$$

since $[\tilde{\mathbf{J}}]^T = [\tilde{\mathbf{J}}]^{-1}$ from the orthonormality condition.

Now that the transformation between unit vectors has been cast in matrix form, the expressions for taking derivatives of these unit vectors in curvilinear space may be formed. Again, the curvatures to be derived describe how the orientation of a unit vector changes as it moves along a coordinate curve (curvilinear axis). Furthermore, since vector's direction may change arbitrarily, the change in direction will be described in terms of its three orthogonal components resolved along the \mathbf{j} -basis. An example is in order.

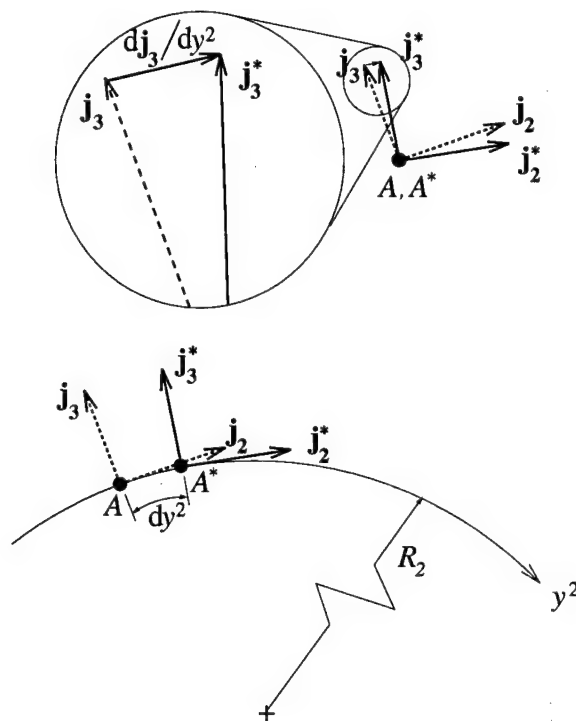


Figure 3.6 Change in orientation of unit vectors along a coordinate curve (axis)

Consider Figure 3.6, illustrating in a two-dimensional example how the unit vectors change orientation along a coordinate curve (axis). In this simple example, the point A , and a point A^* located an infinitesimal distance dy^2 away are examined. At the bottom of the figure, it is shown that the effect of moving along the y^2 axis is to rotate the unit vectors slightly clockwise. This infinitesimal rotation is a vector quantity, denoted in the top portion of the figure as $\partial \mathbf{j}_3 / \partial y^2$. Note that because the rotation is infinitesimal, the direction of $\partial \mathbf{j}_3 / \partial y^2$ is parallel to the \mathbf{j}_2 unit vector. Hence the magnitude of its component in the \mathbf{j}_2 direction is simply $\partial \mathbf{j}_3 / \partial y^2 \cdot \mathbf{j}_2$. This particular curvature is called $k_2 = 1/R_2$, and its geometric meaning is clear: the curvature is simply the reciprocal of the radius of curvature and so will have units of length^{-1} . Note that \mathbf{j}_3 could also rotate *into or out of the page* (the $-\mathbf{j}_1$ or \mathbf{j}_1 directions respectively) if the plane defined by \mathbf{j}_1 and \mathbf{j}_2 were to rotate about the y^2 axis when moved in the y^2 direction. This would connote twisting, and the associated curvature, $\partial \mathbf{j}_3 / \partial y^2 \cdot \mathbf{j}_1$ is denoted k_{62} .

These curvatures are now formally developed. The initial curvatures of the shell reference surface describe its undeformed shape and so are of immediate interest. As seen in the example, they may be found by taking the derivatives of the $\{\mathbf{j}\}$ basis vectors with respect to each coordinant direction, y^k . In addition, these curvatures are used to take the derivatives necessary to develop the strains. Using the relationships expressed by Eqns (3.53) and (3.54), one obtains

$$\frac{\partial \{\mathbf{j}\}}{\partial y^k} = \frac{\partial}{\partial y^k} \left([\tilde{\mathbf{J}}]^T \{\mathbf{e}\} \right) = \frac{\partial [\tilde{\mathbf{J}}]^T}{\partial y^k} \{\mathbf{e}\} = \frac{\partial [\tilde{\mathbf{J}}]^T}{\partial y^k} [\tilde{\mathbf{J}}] \{\mathbf{j}\} = [\mathbf{K}_k^0] \{\mathbf{j}\}, \quad (3.56)$$

where

$$[\mathbf{K}_k^0] = \frac{\partial [\tilde{\mathbf{J}}]^T}{\partial y^k} [\tilde{\mathbf{J}}]. \quad (3.57)$$

This is the *initial curvature matrix* following the notation of Pai and Nayfeh (1994b) and Pai and Palazotto (1995a). Note that since the directions of the \mathbf{e} -bases do not change, their derivatives are identically zero. The entries in this matrix have the following physical meaning: the n^{th} row of $[\mathbf{K}_k^0]$ represents the components (in the \mathbf{j} -basis) of $\partial \{\mathbf{j}_n\} / \partial y^k$.

$$[\mathbf{K}_k^0] = \begin{bmatrix} \frac{\partial \mathbf{j}_1}{\partial y^k} \cdot \mathbf{j}_1 & \frac{\partial \mathbf{j}_1}{\partial y^k} \cdot \mathbf{j}_2 & \frac{\partial \mathbf{j}_1}{\partial y^k} \cdot \mathbf{j}_3 \\ \frac{\partial \mathbf{j}_2}{\partial y^k} \cdot \mathbf{j}_1 & \frac{\partial \mathbf{j}_2}{\partial y^k} \cdot \mathbf{j}_2 & \frac{\partial \mathbf{j}_2}{\partial y^k} \cdot \mathbf{j}_3 \\ \frac{\partial \mathbf{j}_3}{\partial y^k} \cdot \mathbf{j}_1 & \frac{\partial \mathbf{j}_3}{\partial y^k} \cdot \mathbf{j}_2 & \frac{\partial \mathbf{j}_3}{\partial y^k} \cdot \mathbf{j}_3 \end{bmatrix} \quad (3.58)$$

Using the identities (see, e.g., Saada 1989, pp. 126–127)

$$\frac{\partial \mathbf{j}_n}{\partial y^k} \cdot \mathbf{j}_m = -\frac{\partial \mathbf{j}_m}{\partial y^k} \cdot \mathbf{j}_n, \quad \frac{\partial \mathbf{j}_{(m)}}{\partial y^k} \cdot \mathbf{j}_{(m)} = 0, \quad (3.59)$$

where the parentheses suspend the summing convention, the curvature matrix of Eq (3.58) may be written as

$$[\mathbf{K}_k^0] = \begin{bmatrix} 0 & -\frac{\partial \mathbf{j}_2}{\partial y^k} \cdot \mathbf{j}_1 & -\frac{\partial \mathbf{j}_3}{\partial y^k} \cdot \mathbf{j}_1 \\ \frac{\partial \mathbf{j}_2}{\partial y^k} \cdot \mathbf{j}_1 & 0 & -\frac{\partial \mathbf{j}_3}{\partial y^k} \cdot \mathbf{j}_2 \\ \frac{\partial \mathbf{j}_3}{\partial y^k} \cdot \mathbf{j}_1 & \frac{\partial \mathbf{j}_3}{\partial y^k} \cdot \mathbf{j}_2 & 0 \end{bmatrix}. \quad (3.60)$$

For the present curvilinear coordinate system (the circular torus) has the following curvature matrices.

$$[\mathbf{K}_1^0] = \begin{bmatrix} 0 & \cos y^2 & \sin y^2 \\ -\cos y^2 & 0 & 0 \\ -\sin y^2 & 0 & 0 \end{bmatrix}, \quad (3.61a)$$

and

$$[\mathbf{K}_2^0] = \begin{bmatrix} 0 & 0 & 0 \\ 0 & 0 & -1 \\ 0 & 1 & 0 \end{bmatrix}. \quad (3.61b)$$

The matrix $[\mathbf{K}_3^0]$ is identically zero, since \mathbf{j}_3 is rectilinear and normal to the undeformed shell surface. These curvatures correspond to the “rate of change of unit vectors” described by Saada (1989) on pages 128 and 129. But because of the particular choice of curvilinear coordinates, these “curvatures” do not have the units expected (length^{-1}). While each of the three Cartesian coordinates x_1 , x_2 , and x_3 expresses a length, two of the curvilinear coordinates, y_1 and y_2 , are *angles*. This has led to the inconsistent units. The “rates of change” described by Eqns (3.61) are mathematically correct, but are not useful in their current form. Recall the *metric tensor* of Eq (3.47). This tensor will now be used to make the units dimensionally consistent, thus making the curvature quantities physically meaningful.

This is done by multiplying the curvatures by the reciprocals of their appropriate *scale factor*.

The scale factors, h_i , are the elements of the matrix $[\mathbf{g}]^{(1/2)}$ of Eq (3.48). That is

$$[\mathbf{g}]^{(1/2)} = [\mathbf{J}]^T [\mathbf{J}] = \begin{bmatrix} h_1 & 0 & 0 \\ 0 & h_2 & 0 \\ 0 & 0 & h_3 \end{bmatrix} = \begin{bmatrix} \|\mathbf{a}_1\| & 0 & 0 \\ 0 & \|\mathbf{a}_2\| & 0 \\ 0 & 0 & \|\mathbf{a}_3\| \end{bmatrix}. \quad (3.62)$$

So to get the dimensionally consistent, or "physical," curvature matrices, $[\mathbf{K}_k^0]_{(P)}$, each of the curvature matrices is multiplied by the reciprocal of its scale factor:

$$[\mathbf{K}_k^0]_{(P)} = (1/h_{(k)}) [\mathbf{K}_k^0]. \quad (3.63)$$

The means are now available to write the derivatives of the unit bases vectors in a very concise matrix form:

$$\frac{\partial}{\partial y^k} \begin{Bmatrix} \mathbf{j}_1 \\ \mathbf{j}_2 \\ \mathbf{j}_3 \end{Bmatrix} = [\mathbf{K}_k^0]_{(P)} \begin{Bmatrix} \mathbf{j}_1 \\ \mathbf{j}_2 \\ \mathbf{j}_3 \end{Bmatrix} \quad (3.64)$$

Following the notation of Pai et al. (1993), the entries of these matrices are given by

$$[\mathbf{K}_1^0]_{(P)} \equiv \begin{bmatrix} 0 & k_5^0 & -k_1^0 \\ -k_5^0 & 0 & -k_{61}^0 \\ k_1^0 & k_{61}^0 & 0 \end{bmatrix}, \quad [\mathbf{K}_2^0]_{(P)} \equiv \begin{bmatrix} 0 & k_4^0 & -k_{62}^0 \\ -k_4^0 & 0 & -k_2^0 \\ k_{62}^0 & k_2^0 & 0 \end{bmatrix}, \quad (3.65)$$

For the circular torus, the curvature matrices are

$$[\mathbf{K}_1^0] = \begin{bmatrix} 0 & \frac{\cos y^2}{(R - y^3 \sin y^2)} & \frac{\sin y^2}{(R - y^3 \sin y^2)} \\ -\frac{\cos y^2}{(R - y^3 \sin y^2)} & 0 & 0 \\ -\frac{\sin y^2}{(R - y^3 \sin y^2)} & 0 & 0 \end{bmatrix}, \quad (3.66a)$$

and

$$[\mathbf{K}_2^0] = \begin{bmatrix} 0 & 0 & 0 \\ 0 & 0 & -\frac{1}{y^3} \\ 0 & \frac{1}{y^3} & 0 \end{bmatrix}. \quad (3.66b)$$

For example, the derivative of \mathbf{j}_1 with respect to y^1 is given by $\partial \mathbf{j}_1 / \partial y^1 = \kappa_5^0 \mathbf{j}_2 - \kappa_1^0 \mathbf{j}_3$. In future calculations using the curvature matrices, the (P) subscript is dropped.

3.3 Characterization of Reference Surface Behavior

The kinematics of an infinitesimal element of area on the reference surface may now be described in terms of the curvilinear coordinate system. For ease of notation, the superscript notation of the previous section will be dropped. Furthermore, the notation

$$\{y^1, y^2, y^3\} = \{x, y, z\} \quad (3.67)$$

shall be used.

Consider Figure 3.7, showing an element of the reference surface before and after its movement, which consists of both rigid body translation/rotation and deformation. The xyz system is the curvilinear coordinate system, and the displacements u , v , and w are the orthogonal (and rectilinear) displacements in the \mathbf{j}_1 , \mathbf{j}_2 , and \mathbf{j}_3 directions, respectively. The axes $\hat{\xi}$ and $\hat{\eta}$ represent the deformed x and y axes, respectively; and $\gamma_6 = \gamma_{61} + \gamma_{62}$ is the in-plane shear deformation.

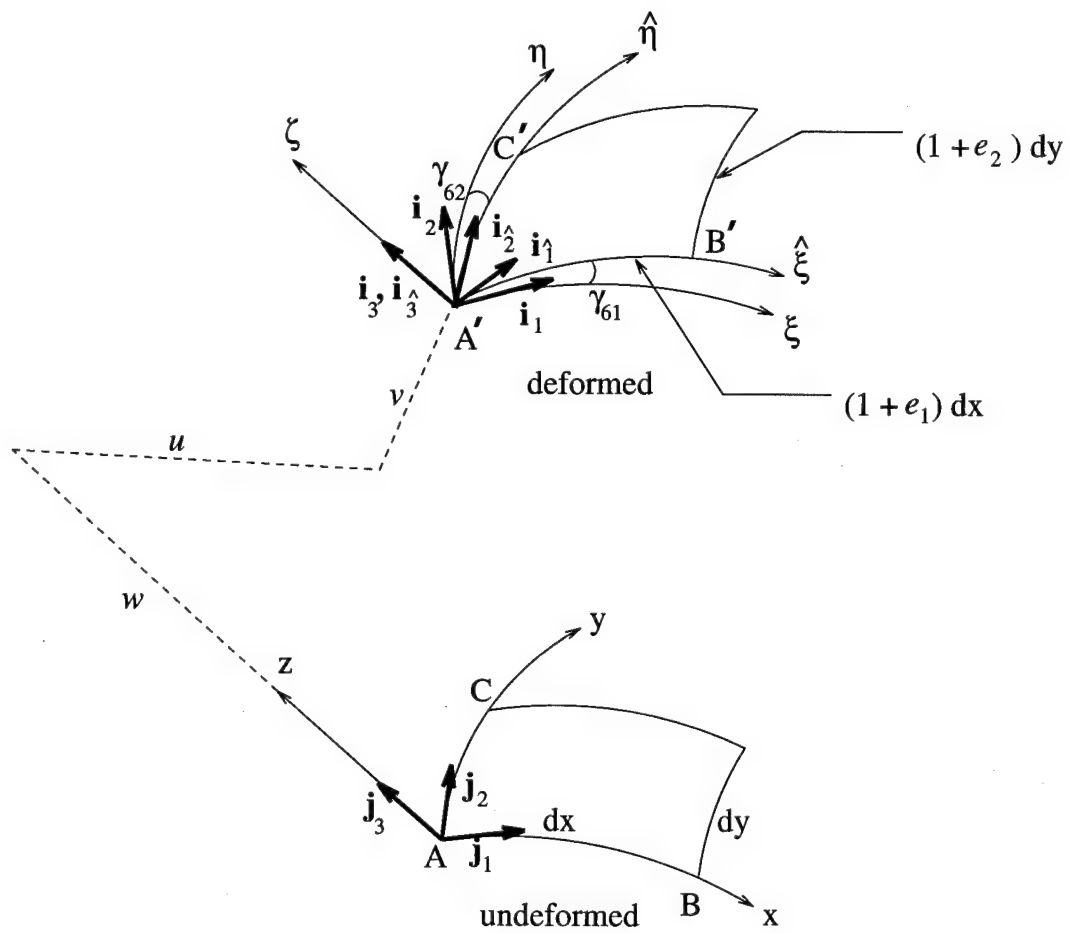


Figure 3.7 Infinitesimal element undergoing deformation (after Pai and Palazotto 1995a)

(More precisely, this "shear" is the change in angle between two originally mutually perpendicular infinitesimal lengths.) The unit vectors \mathbf{i}_1 and \mathbf{i}_2 are along the $\hat{\xi}$ and $\hat{\eta}$ axes, respectively. Axes ξ and η coincide with the axes $\hat{\xi}$ and $\hat{\eta}$ only if the in-plane shear deformation γ_6 is zero. Note that a significant simplification would occur if the interest were in beams rather than shells. In the beam, in-plane shear would be neglected, and the following development would be significantly simpler: one would not have to be concerned with finding the $\{\mathbf{i}_{123}\}$ basis from the $\{\mathbf{i}_{123}\}$ basis, where $\{\mathbf{i}_{123}\} = \{\mathbf{i}_1, \mathbf{i}_2, \mathbf{i}_3\}$.

In Figure 3.7, the right angle formed by CAB is (in the general case) changed as the infinitesimal region deforms to $C'A'B'$. The displacement vector associated with point A is denoted \mathbf{D} , where $\mathbf{D} \equiv u\mathbf{j}_1 + v\mathbf{j}_2 + w\mathbf{j}_3$. Treating the sides of the undeformed infinitesimal area as vectors, they may be written as \mathbf{AB} and \mathbf{AC} . Then the displacement vector \mathbf{D} is used to generate the sides of the area after movement as

$$\mathbf{A'B'} = \mathbf{AB} + \frac{\partial \mathbf{D}}{\partial x} dx, \quad \mathbf{A'C'} = \mathbf{AC} + \frac{\partial \mathbf{D}}{\partial y} dy. \quad (3.68)$$

But since $\mathbf{AB} = dx\mathbf{j}_1$ and $\mathbf{AC} = dy\mathbf{j}_2$, one obtains

$$\mathbf{A'B'} = dx\mathbf{j}_1 + \frac{\partial \mathbf{D}}{\partial x} dx, \quad \mathbf{A'C'} = dy\mathbf{j}_2 + \frac{\partial \mathbf{D}}{\partial y} dy. \quad (3.69)$$

Using the curvature matrices of Eq (3.65), one obtains

$$\begin{aligned} \mathbf{A'B'} &= dx\mathbf{j}_1 + \left[u_{,x}\mathbf{j}_1 + v_{,x}\mathbf{j}_2 + w_{,x}\mathbf{j}_3 + u\frac{\partial \mathbf{j}_1}{\partial x} + v\frac{\partial \mathbf{j}_2}{\partial x} + w\frac{\partial \mathbf{j}_3}{\partial x} \right] dx \\ &= dx\mathbf{j}_1 + [u_{,x}\mathbf{j}_1 + v_{,x}\mathbf{j}_2 + w_{,x}\mathbf{j}_3 + u(k_5^0\mathbf{j}_2 - k_1^0\mathbf{j}_3) + v(-k_5^0\mathbf{j}_1 - k_{61}^0\mathbf{j}_3) \\ &\quad + w(k_1^0\mathbf{j}_1 + k_{61}^0\mathbf{j}_2)] dx \\ &= [(1 + u_{,x} - v k_5^0 + w k_1^0)\mathbf{j}_1 + (v_{,x} + u k_5^0 + w k_{61}^0)\mathbf{j}_2 + (w_{,x} - u k_1^0 - v k_{61}^0)\mathbf{j}_3] dx \end{aligned} \quad (3.70)$$

In the same way,

$$\begin{aligned}
\mathbf{A}'\mathbf{C}' &= dy \mathbf{j}_2 + \left[u_{,y} \mathbf{j}_1 + v_{,y} \mathbf{j}_2 + w_{,y} \mathbf{j}_3 + u \frac{\partial \mathbf{j}_1}{\partial y} + v \frac{\partial \mathbf{j}_2}{\partial y} + w \frac{\partial \mathbf{j}_3}{\partial y} \right] dy \\
&= dy \mathbf{j}_1 + [u_{,y} \mathbf{j}_1 + v_{,y} \mathbf{j}_2 + w_{,y} \mathbf{j}_3 + u (k_4^0 \mathbf{j}_2 - k_{62}^0 \mathbf{j}_3) + v (-k_4^0 \mathbf{j}_1 - k_2^0 \mathbf{j}_3) \\
&\quad + w (k_{62}^0 \mathbf{j}_1 + k_2^0 \mathbf{j}_2)] dy \\
&= [(u_{,y} - v k_4^0 + w k_{62}^0) \mathbf{j}_1 + (1 + v_{,y} + u k_4^0 + w k_2^0) \mathbf{j}_2 + (w_{,y} - u k_{62}^0 - v k_2^0) \mathbf{j}_3] dy \quad (3.71)
\end{aligned}$$

Note that these two vectors $\mathbf{A}'\mathbf{B}'$ and $\mathbf{A}'\mathbf{C}'$ are the *lattice vectors* described in Section 3.1.1. The axial stretching e_1 and e_2 (along $\hat{\xi}$ and $\hat{\eta}$) is defined by using the familiar concept of the fiber length change divided by its original length.

$$e_1 = \frac{\|\mathbf{A}'\mathbf{B}'\| - dx}{dx}, \quad e_2 = \frac{\|\mathbf{A}'\mathbf{C}'\| - dy}{dy}, \quad (3.72)$$

where

$$\|\mathbf{A}'\mathbf{B}'\| = \sqrt{\mathbf{A}'\mathbf{B}' \cdot \mathbf{A}'\mathbf{B}'}, \quad \|\mathbf{A}'\mathbf{C}'\| = \sqrt{\mathbf{A}'\mathbf{C}' \cdot \mathbf{A}'\mathbf{C}'}, \quad (3.73)$$

such that

$$e_1 = \sqrt{(1 + u_{,x} - v k_5^0 + w k_1^0)^2 + (v_{,x} + u k_5^0 + w k_{61}^0)^2 + (w_{,x} - u k_1^0 - v k_{61}^0)^2} - 1 \quad (3.74a)$$

$$e_2 = \sqrt{(u_{,y} - v k_4^0 + w k_{62}^0)^2 + (1 + v_{,y} + u k_4^0 + w k_2^0)^2 + (w_{,y} - u k_{62}^0 - v k_2^0)^2} - 1. \quad (3.74b)$$

These quantities e_1 and e_2 represent the stretching of the lattice vectors. As an aside, these quantities are related to the Green strain measure, L_{mn} , as

$$2L_{11} = \frac{\|\mathbf{A}'\mathbf{B}'\|^2 - dx^2}{dx^2}, \quad 2L_{22} = \frac{\|\mathbf{A}'\mathbf{C}'\|^2 - dy^2}{dy^2}, \quad (3.75)$$

The unit vectors along the $\hat{\xi}$ and $\hat{\eta}$ directions are given by:

$$\mathbf{i}_1 = \frac{\mathbf{A}'\mathbf{B}'}{(1+e_1)dx} = \hat{T}_{11}\mathbf{j}_1 + \hat{T}_{12}\mathbf{j}_2 + \hat{T}_{13}\mathbf{j}_3, \quad \mathbf{i}_2 = \frac{\mathbf{A}'\mathbf{C}'}{(1+e_2)dy} = \hat{T}_{21}\mathbf{j}_1 + \hat{T}_{22}\mathbf{j}_2 + \hat{T}_{23}\mathbf{j}_3, \quad (3.76)$$

where the \hat{T}_{ij} are given by

$$\hat{T}_{11} = \frac{1 + u_{,x} - vk_5^0 + wk_1^0}{1 + e_1}, \quad \hat{T}_{12} = \frac{v_{,x} + uk_5^0 + wk_{61}^0}{1 + e_1}, \quad \hat{T}_{13} = \frac{w_{,x} - uk_1^0 - vk_{61}^0}{1 + e_1} \quad (3.77a)$$

$$\hat{T}_{21} = \frac{u_{,y} - vk_4^0 + wk_{62}^0}{1 + e_2}, \quad \hat{T}_{22} = \frac{1 + v_{,y} + uk_4^0 + wk_2^0}{1 + e_2}, \quad \hat{T}_{23} = \frac{w_{,y} - uk_{62}^0 - vk_2^0}{1 + e_2} \quad (3.77b)$$

Careful inspection of Eqns (3.74) and (3.77) reveals a physical insight into the meaning of the \hat{T}_{ij} : they represent the derivatives of the two stretches, e_1 and e_2 , with respect to the derivatives of the components of displacement. That is,

$$\hat{T}_{11} = \frac{\partial e_1}{\partial u_{,x}}, \quad \hat{T}_{12} = \frac{\partial e_1}{\partial v_{,x}}, \quad \hat{T}_{13} = \frac{\partial e_1}{\partial w_{,x}}, \quad \hat{T}_{21} = \frac{\partial e_2}{\partial u_{,y}}, \quad \hat{T}_{22} = \frac{\partial e_2}{\partial v_{,y}}, \quad \hat{T}_{23} = \frac{\partial e_2}{\partial w_{,y}} \quad (3.78)$$

Since $\mathbf{i}_1 \cdot \mathbf{i}_2 = \cos(\mathbf{i}_1, \mathbf{i}_2)$, one finds

$$\gamma_6 = \frac{\pi}{2} - \cos^{-1}(\mathbf{i}_1 \cdot \mathbf{i}_2) = \sin^{-1}(\mathbf{i}_1 \cdot \mathbf{i}_2). \quad (3.79)$$

So, using Eqns (3.76) and (3.79), an expression for the total in-plane change in angle between two originally perpendicular infinitesimal lengths is obtained:

$$\gamma_6 = \gamma_{61} + \gamma_{62} = \sin^{-1}(\hat{T}_{11}\hat{T}_{21} + \hat{T}_{12}\hat{T}_{22} + \hat{T}_{13}\hat{T}_{23}) \quad (3.80)$$

Thus, γ_6 is expressed in terms of u , v , w , and the initial curvatures, which arise from taking derivatives of \mathbf{D} with respect to the curvilinear coordinate system. A theorem from the polar decomposition technique allows unique expressions for γ_{61} and γ_{62} to be determined. Recall from

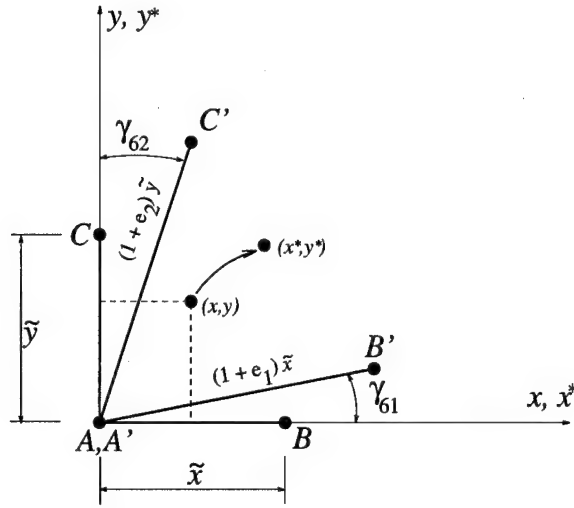


Figure 3.8 Superimposition of deformed element $A'B'C'$ onto undeformed element ABC

Section 3.1.1 that the deformation gradient tensor, $[\mathbf{F}]$, to be written as $[\mathbf{F}] = [\mathbf{R}][\mathbf{U}]$, where $[\mathbf{R}]$ is an orthogonal rotation matrix, and $[\mathbf{U}]$ is a symmetric stretch tensor. For the current formulation, $[\mathbf{U}]$ is given by:

$$[\mathbf{U}] = \begin{bmatrix} (1 + e_1) \cos \gamma_{61} & (1 + e_2) \sin \gamma_{62} & 0 \\ (1 + e_1) \sin \gamma_{61} & (1 + e_2) \cos \gamma_{62} & 0 \\ 0 & 0 & 1 \end{bmatrix}. \quad (3.81)$$

The derivation of Eq (3.81) is the subject of an entire paper (Pai and Palazotto 1995b), but a simple illustration gives some insight into the origin of this tensor. Figure 3.8 shows the deformed element superimposed over its undeformed counterpart. This is equivalent to removing the effects of rigid body rotation and translation. Consider the displacement of a point originally located at (x, y) . From the geometrical relationships depicted in Figure 3.8, one finds the final location of the point (x^*, y^*) as

$$x^* = (x/\tilde{x})(1 + e_1)\tilde{x} \cos \gamma_{61} + (y/\tilde{y})(1 + e_2)\tilde{y} \sin \gamma_{62} \quad (3.82a)$$

$$y^* = (x/\tilde{x})(1 + e_1)\tilde{x} \sin \gamma_{61} + (y/\tilde{y})(1 + e_2)\tilde{y} \cos \gamma_{62}. \quad (3.82b)$$

The deformation gradient tensor of this transformation is given by

$$[\mathbf{F}] = \begin{bmatrix} \partial x^*/\partial x & \partial x^*/\partial y \\ \partial y^*/\partial x & \partial y^*/\partial y \end{bmatrix} = \begin{bmatrix} (1+e_1)\cos\gamma_{61} & (1+e_2)\sin\gamma_{62} \\ (1+e_1)\sin\gamma_{61} & (1+e_2)\cos\gamma_{62} \end{bmatrix} \quad (3.83)$$

Since rigid body rotation has been removed in the illustration, the rotation matrix is simply the identity matrix:

$$[\mathbf{R}] = \begin{bmatrix} 1 & 0 \\ 0 & 1 \end{bmatrix}. \quad (3.84)$$

So one obtains

$$[\mathbf{F}] = [\mathbf{R}][\mathbf{U}] = [\mathbf{U}]. \quad (3.85)$$

As stated earlier, a fundamental principle of singular value decomposition (of which polar decomposition is a special case) is that the tensor $[\mathbf{U}]$ is symmetric¹⁰ So, by enforcing the symmetry of Eq (3.81), one finds

$$(1+e_1)\sin\gamma_{61} = (1+e_2)\sin\gamma_{62}. \quad (3.86)$$

As an aside, the Jaumann strain associated with in-plane shear (at the reference surface), B_{12} , will be developed later and shown to be

$$2B_{12} = (1+e_1)\sin\gamma_{61} + (1+e_2)\sin\gamma_{62}. \quad (3.87)$$

As an aside, this equation may be developed from Eq (3.81) purely from the geometric considerations of Figure 3.8 without knowledge of the symmetry of $[\mathbf{U}]$. This may be done in the manner presented by Atluri (1984), where the symmetry of a new tensor, $[\mathbf{r}]$, is *forced* from the Biot-Lur ¹¹

¹⁰Furthermore, if $[\mathbf{F}]$ is invertible (which it is for an admissible transformation) then $[\mathbf{U}]$ is positive definite (see Strang 1988, p. 445).

¹¹The Biot-Lur  stress tensor is defined as $[\mathbf{r}^*] = [\mathbf{S}][\mathbf{U}]$, where $[\mathbf{S}]$ is the second-Piola Kirchhoff stress tensor and $[\mathbf{U}]$ is the right stretch tensor (Atluri 1984). In general, the Biot-Lur  stress tensor is unsymmetric.

stress tensor, $[\mathbf{r}^*]$, through:

$$[\mathbf{r}] = \frac{1}{2} ([\mathbf{r}^*] + [\mathbf{r}^*]^T), \quad (3.88)$$

where $[\mathbf{r}]$ will, by construction, be symmetric¹². This method could likewise be applied to Eq (3.83) (with rigid rotations removed), yielding Eq (3.87).

Now getting back to the original goal of finding unique expressions for the two values of in-plane shear rotation, Eq (3.80) and Eq (3.86) are simultaneously solved, yielding the values for γ_{61} and γ_{62} as follows.

$$(1 + e_1) \sin \gamma_{61} = (1 + e_2) \sin \gamma_{62} \quad (3.89a)$$

$$(1 + e_1) \sin \gamma_{61} = (1 + e_2) \sin(\gamma_6 - \gamma_{61}). \quad (3.89b)$$

But since $\sin(\alpha - \beta) = \sin \alpha \cos \beta - \cos \alpha \sin \beta$, one finds

$$(1 + e_1) \sin \gamma_{61} = (1 + e_2)(\sin \gamma_6 \cos \gamma_{61} - \cos \gamma_6 \sin \gamma_{61}) \quad (3.89c)$$

$$(1 + e_1) \sin \gamma_{61} + (1 + e_2) \cos \gamma_6 \sin \gamma_{61} = (1 + e_2) \sin \gamma_6 \cos \gamma_{61}. \quad (3.89d)$$

Now, dividing by $\cos \gamma_{61}$ and collecting terms yields

$$(1 + e_1) \tan \gamma_{61} + (1 + e_2) \cos \gamma_6 \tan \gamma_{61} = (1 + e_2) \sin \gamma_6 \quad (3.89e)$$

$$[(1 + e_1) + (1 + e_2) \cos \gamma_6] \tan \gamma_{61} = (1 + e_2) \sin \gamma_6 \quad (3.89f)$$

$$\tan \gamma_{61} = \frac{(1 + e_2) \sin \gamma_6}{(1 + e_1) + (1 + e_2) \cos \gamma_6} \quad (3.89g)$$

$$\gamma_{61} = \tan^{-1} \left[\frac{\sin \gamma_6}{\frac{(1+e_1)}{(1+e_2)} + \cos \gamma_6} \right]. \quad (3.89h)$$

¹²Atluri notes that the tensor $[\mathbf{r}]$ is sometimes referred to as the Jaumann stress tensor, citing Fraeijs de Veubeke (1972) and Atluri and Murakawa (1977). The tensor $[\mathbf{r}]$ thus described is, in fact, the Jaumann stress tensor $[\mathbf{J}]$ referred to herein (Pai and Palazotto 1995b).

The derivation for γ_{62} is analogous so, in summary:

$$\tan \gamma_{61} = \left[\frac{\sin \gamma_6}{\frac{(1+e_1)}{(1+e_2)} + \cos \gamma_6} \right], \quad \tan \gamma_{62} = \left[\frac{\sin \gamma_6}{\frac{(1+e_2)}{(1+e_1)} + \cos \gamma_6} \right]. \quad (3.90)$$

The unit vector normal to the deformed reference surface is found using Eqns (3.76):

$$\begin{aligned} \mathbf{i}_3 = \mathbf{j}_3 &= \frac{\mathbf{i}_1 \times \mathbf{i}_2}{\|\mathbf{i}_1 \times \mathbf{i}_2\|} = \frac{\hat{T}_{12}\hat{T}_{23} - \hat{T}_{13}\hat{T}_{22}}{R_0} \mathbf{j}_1 + \frac{\hat{T}_{13}\hat{T}_{21} - \hat{T}_{11}\hat{T}_{23}}{R_0} \mathbf{j}_2 + \frac{\hat{T}_{11}\hat{T}_{22} - \hat{T}_{12}\hat{T}_{21}}{R_0} \mathbf{j}_3, \quad \text{or} \\ \mathbf{i}_3 &= T_{31} \mathbf{j}_1 + T_{32} \mathbf{j}_2 + T_{33} \mathbf{j}_3 \end{aligned} \quad (3.91)$$

where the T_{3k} are found to be

$$T_{31} = (\hat{T}_{12}\hat{T}_{23} - \hat{T}_{13}\hat{T}_{22})/R_0 \quad (3.92a)$$

$$T_{32} = (\hat{T}_{13}\hat{T}_{21} - \hat{T}_{11}\hat{T}_{23})/R_0 \quad (3.92b)$$

$$T_{33} = (\hat{T}_{11}\hat{T}_{22} - \hat{T}_{12}\hat{T}_{21})/R_0 \quad (3.92c)$$

$$R_0 \equiv \sqrt{(\hat{T}_{12}\hat{T}_{23} - \hat{T}_{13}\hat{T}_{22})^2 + (\hat{T}_{13}\hat{T}_{21} - \hat{T}_{11}\hat{T}_{23})^2 + (\hat{T}_{11}\hat{T}_{22} - \hat{T}_{12}\hat{T}_{21})^2} = |\cos \gamma_6| \quad (3.92d)$$

The undeformed coordinate system xyz is related to the orthogonal coordinate system $\xi\eta\zeta$ at the deformed location (Figure 3.9) using Eqns (3.76) and (3.91). Given

$$\{\mathbf{i}_{123}\} = [\hat{\mathbf{T}}]\{\mathbf{j}_{123}\} \quad \text{and} \quad \{\mathbf{i}_{123}\} = [\mathbf{T}]\{\mathbf{i}_{123}\}, \quad (3.93a)$$

one obtains

$$\{\mathbf{i}_{123}\} = [\mathbf{T}][\hat{\mathbf{T}}]\{\mathbf{j}_{123}\} = [\mathbf{T}]\{\mathbf{j}_{123}\}, \quad (3.93b)$$

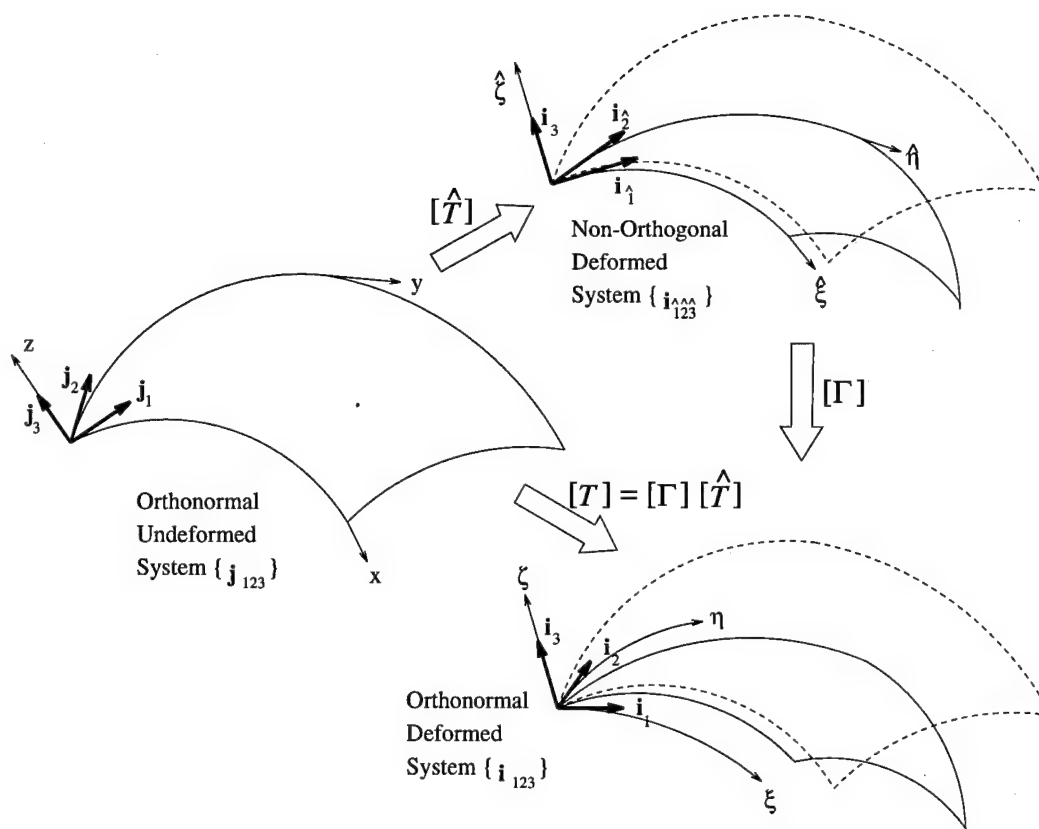


Figure 3.9 Transformation of infinitesimal shell element

where

$$[\mathbf{T}] = [\mathbf{R}][\hat{\mathbf{T}}] = \frac{1}{\cos \gamma_6} \begin{bmatrix} \cos \gamma_{62} & -\sin \gamma_{61} & 0 \\ -\sin \gamma_{62} & \cos \gamma_{61} & 0 \\ 0 & 0 & \cos \gamma_6 \end{bmatrix} \begin{bmatrix} \hat{T}_{11} & \hat{T}_{12} & \hat{T}_{13} \\ \hat{T}_{21} & \hat{T}_{22} & \hat{T}_{23} \\ T_{31} & T_{32} & T_{33} \end{bmatrix} \quad (3.93c)$$

and $\{\mathbf{i}_{123}\} \equiv \{\mathbf{i}_1, \mathbf{i}_2, \mathbf{i}_3\}^T$. Expanding the matrix equation of Eq (3.93c) yields

$$\begin{aligned} \mathbf{i}_1 = & \mathbf{j}_1 \left(\frac{\cos \gamma_{62} \hat{T}_{11}}{\cos \gamma_6} - \frac{\sin \gamma_{61} \hat{T}_{21}}{\cos \gamma_6} \right) + \mathbf{j}_2 \left(\frac{\cos \gamma_{62} \hat{T}_{12}}{\cos \gamma_6} - \frac{\sin \gamma_{61} \hat{T}_{22}}{\cos \gamma_6} \right) \\ & + \mathbf{j}_3 \left(\frac{\cos \gamma_{62} \hat{T}_{13}}{\cos \gamma_6} - \frac{\sin \gamma_{61} \hat{T}_{23}}{\cos \gamma_6} \right) \end{aligned} \quad (3.94a)$$

$$\begin{aligned} \mathbf{i}_2 = & \mathbf{j}_1 \left(-\frac{\sin \gamma_{62} \hat{T}_{11}}{\cos \gamma_6} + \frac{\cos \gamma_{61} \hat{T}_{21}}{\cos \gamma_6} \right) + \mathbf{j}_2 \left(-\frac{\sin \gamma_{62} \hat{T}_{12}}{\cos \gamma_6} + \frac{\cos \gamma_{61} \hat{T}_{22}}{\cos \gamma_6} \right) \\ & + \mathbf{j}_3 \left(-\frac{\sin \gamma_{62} \hat{T}_{13}}{\cos \gamma_6} + \frac{\cos \gamma_{61} \hat{T}_{23}}{\cos \gamma_6} \right) \end{aligned} \quad (3.94b)$$

$$\mathbf{i}_3 = \mathbf{j}_1 T_{31} + \mathbf{j}_2 T_{32} + \mathbf{j}_3 T_{33}. \quad (3.94c)$$

$$T_{11} = \frac{1}{\cos \gamma_6} (\hat{T}_{11} \cos \gamma_{62} - \hat{T}_{21} \sin \gamma_{61}) \quad (3.95a)$$

$$T_{12} = \frac{1}{\cos \gamma_6} (\hat{T}_{12} \cos \gamma_{62} - \hat{T}_{22} \sin \gamma_{61}) \quad (3.95b)$$

$$T_{13} = \frac{1}{\cos \gamma_6} (\hat{T}_{13} \cos \gamma_{62} - \hat{T}_{23} \sin \gamma_{61}) \quad (3.95c)$$

$$T_{21} = \frac{1}{\cos \gamma_6} (-\hat{T}_{11} \sin \gamma_{62} + \hat{T}_{21} \cos \gamma_{61}) \quad (3.95d)$$

$$T_{22} = \frac{1}{\cos \gamma_6} (-\hat{T}_{12} \sin \gamma_{62} + \hat{T}_{22} \cos \gamma_{61}) \quad (3.95e)$$

$$T_{23} = \frac{1}{\cos \gamma_6} (-\hat{T}_{13} \sin \gamma_{62} + \hat{T}_{23} \cos \gamma_{61}) \quad (3.95f)$$

(Recall that that T_{3k} are given by Eq 3.92.) Note that this approach could be called "corotational," in the sense that a reference frame is attached to a material point as it travels through

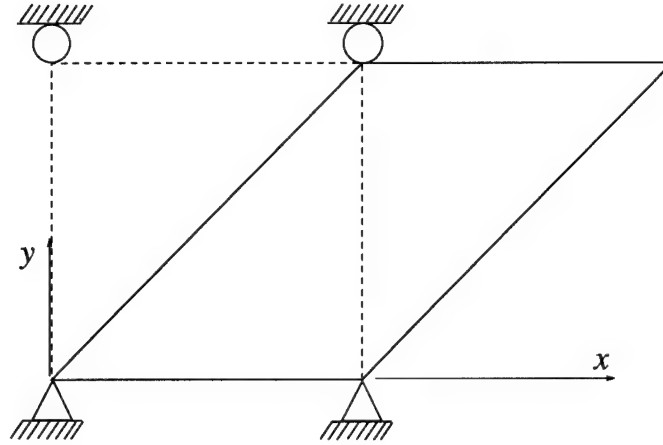


Figure 3.10 Deformation associated with displacement field of Eqns (3.96)

its deformation (according to Belytschko and Glaum 1979, corotational finite element formulations for straight beams were first presented by Argyris et al. 1964). But “corotational” often implies updating the reference configuration, which is not done—all deformation is referred back to the original undeformed configuration. So, in contrast to such updated-Lagrangian schemes in which the original configuration is discarded in favor of the most recent deformed configuration, in the present scheme the original configuration is not lost. Moreover, the transformation afforded by $[T]$ in the current theory is more exact than, say, the “ghost” reference (corotational) frame of Bergan (1981, 1984), since in the current formulation the unique angles γ_{61} and γ_{62} are found via polar (multiplicative) decomposition of the deformation gradient tensor. In the “ghost” reference frame, the corotated frame represents an “average” rotation of the initial (total-Lagrangian) or current (updated-Lagrangian) configuration (Nygård and Bergan 1989).

As a simple example illustrating the implementation of this transformation, consider the case of pure shear (Figure 3.10), where the displacement field is of the form

$$X(x, y, z) = x + k y, \quad Y(x, y, z) = y, \quad \text{and} \quad Z(x, y, z) = z, \quad (3.96)$$

where k is a constant. This leads to the following:

$$u = X - x = k y, \quad v = Y - y = 0, \quad z = Z - z = 0 \quad (3.97a)$$

$$u_{,y} = k, \quad u_{,x} = u_{,z} = 0, \quad v_{,i} = w_{,i} = 0 \text{ for all } i \quad (3.97b)$$

From Eqns (3.74) and Eqns (3.77) one obtains

$$e_1 = 0, \quad e_2 = \sqrt{k^2 + 1}, \quad \hat{T}_{11} = 1, \quad \hat{T}_{21} = k/\sqrt{k^2 + 1}, \quad (3.98a)$$

$$\hat{T}_{22} = 1/\sqrt{k^2 + 1}, \quad \hat{T}_{33} = 1, \quad \text{and all other } \hat{T}_{ij} = 0. \quad (3.98b)$$

From Eq (3.80) it is evident that $\sin \gamma_6 = k/\sqrt{k^2 + 1}$ and $\cos \gamma_6 = 1/\sqrt{k^2 + 1}$. Using Eq (3.90) and the identities

$$\sin \beta = \tan \beta / \sqrt{1 + \tan^2 \beta}, \quad \cos \beta = 1 / \sqrt{1 + \tan^2 \beta} \quad (3.99)$$

yields

$$\sin \gamma_{61} = k/\sqrt{k^2 + 4}, \quad \cos \gamma_{61} = 2/\sqrt{k^2 + 4} \quad (3.100a)$$

$$\sin \gamma_{62} = k/\sqrt{(k^2 + 1)(k^2 + 4)}, \quad \cos \gamma_{62} = (k^2 + 2)/\sqrt{(k^2 + 1)(k^2 + 4)}. \quad (3.100b)$$

Substituting these values into Eq (3.93c) yields

$$[\mathbf{T}] = [\mathbf{\Gamma}][\hat{\mathbf{T}}] = \frac{1}{\sqrt{k^2 + 4}} \begin{bmatrix} k^2 + 2 & -k\sqrt{k^2 + 1} & 0 \\ -k & 2\sqrt{k^2 + 1} & 0 \\ 0 & 0 & \sqrt{k^2 + 4} \end{bmatrix} \begin{bmatrix} 1 & 0 & 0 \\ k/\sqrt{k^2 + 1} & 1/\sqrt{k^2 + 1} & 0 \\ 0 & 0 & 1 \end{bmatrix} \quad (3.101a)$$

or

$$[\mathbf{T}] = \frac{1}{\sqrt{k^2 + 4}} \begin{bmatrix} 2 & -k & 0 \\ k & 2 & 0 \\ 0 & 0 & \sqrt{k^2 + 4} \end{bmatrix} \quad (3.101b)$$

It can be shown that this matrix, $[\mathbf{T}]$, is an orthogonal rotation matrix:

$$\begin{aligned} [\mathbf{T}]^T [\mathbf{T}] &= \frac{1}{\sqrt{k^2 + 4}} \begin{bmatrix} 2 & k & 0 \\ -k & 2 & 0 \\ 0 & 0 & \sqrt{k^2 + 4} \end{bmatrix} \frac{1}{\sqrt{k^2 + 4}} \begin{bmatrix} 2 & -k & 0 \\ k & 2 & 0 \\ 0 & 0 & \sqrt{k^2 + 4} \end{bmatrix} \\ &= \begin{bmatrix} 1 & 0 & 0 \\ 0 & 1 & 0 \\ 0 & 0 & 1 \end{bmatrix} \end{aligned} \quad (3.102)$$

As was done for taking derivatives of the unit vectors forming the basis for the coordinate system describing the undeformed configuration, the \mathbf{j} -frame, one may now set out to define curvature matrices for the unit vectors of the coordinate system associated with the deformed configuration, the \mathbf{i} -frame. Using Eqns (3.93b) and (3.66) and the identities

$$\frac{\partial \mathbf{i}_{(j)}}{\partial x} \cdot \mathbf{i}_{(j)} = \frac{\partial \mathbf{i}_{(j)}}{\partial y} \cdot \mathbf{i}_{(j)} = 0, \quad \frac{\partial \mathbf{i}_j}{\partial x} \cdot \mathbf{i}_k = -\frac{\partial \mathbf{i}_k}{\partial x} \cdot \mathbf{i}_j, \quad \frac{\partial \mathbf{i}_j}{\partial y} \cdot \mathbf{i}_k = -\frac{\partial \mathbf{i}_k}{\partial y} \cdot \mathbf{i}_j \quad \text{for } j, k = 1, 2, 3 \quad (3.103)$$

where parentheses suspend the summing convention, one may develop expressions for the derivatives of the \mathbf{i} -frame unit vectors just as was done for the \mathbf{j} -frame vectors. Beginning with

$$\{\mathbf{i}_{123}\} = [\mathbf{T}]\{\mathbf{j}_{123}\}, \quad (3.104)$$

where $\mathbf{i}_{123} = \{\mathbf{i}_1, \mathbf{i}_2, \mathbf{i}_3\}^T$ and $\mathbf{j}_{123} = \{\mathbf{j}_1, \mathbf{j}_2, \mathbf{j}_3\}^T$, the derivative (for the x -coordinate direction) may be expressed as

$$\begin{aligned}\frac{\partial}{\partial x}\{\mathbf{i}_{123}\} &= \frac{\partial}{\partial x}([\mathbf{T}]\{\mathbf{j}_{123}\}) \\ &= \frac{\partial[\mathbf{T}]}{\partial x}\{\mathbf{j}_{123}\} + [\mathbf{T}]\frac{\partial\{\mathbf{j}_{123}\}}{\partial x}\end{aligned}\quad (3.105)$$

Substituting Eq (3.64) for $\partial\{\mathbf{j}_{123}\}/\partial x$ yields

$$\frac{\partial}{\partial x}\{\mathbf{i}_{123}\} = \frac{\partial[\mathbf{T}]}{\partial x}\{\mathbf{j}_{123}\} + [\mathbf{T}][\mathbf{K}_1^0]\{\mathbf{j}_{123}\}. \quad (3.106)$$

Noting from Eq (3.93b) that

$$\{\mathbf{j}_{123}\} = [\mathbf{T}]^{-1}\{\mathbf{i}_{123}\}, \quad (3.107)$$

it is evident that

$$\frac{\partial}{\partial x}\{\mathbf{i}_{123}\} = \frac{\partial[\mathbf{T}]}{\partial x}[\mathbf{T}]^{-1}\{\mathbf{i}_{123}\} + [\mathbf{T}][\mathbf{K}_1^0][\mathbf{T}]^{-1}\{\mathbf{i}_{123}\}. \quad (3.108)$$

The matrix $[\mathbf{T}]$ is orthonormal (Pai and Palazotto 1995b), that is, $[\mathbf{T}]^T = [\mathbf{T}]^{-1}$, leading to

$$\frac{\partial}{\partial x}\{\mathbf{i}_{123}\} = \left(\frac{\partial[\mathbf{T}]}{\partial x}[\mathbf{T}]^T + [\mathbf{T}][\mathbf{K}_1^0][\mathbf{T}]^T \right) \{\mathbf{i}_{123}\}. \quad (3.109)$$

This expression leads to a new curvature matrix, $[\mathbf{K}]$, describing the curvatures associated with the *deformed* body:

$$\frac{\partial}{\partial x}\{\mathbf{i}_{123}\} = [\mathbf{K}_1]\{\mathbf{i}_{123}\}, \quad \text{where} \quad [\mathbf{K}_1] = \frac{\partial[\mathbf{T}]}{\partial x}[\mathbf{T}]^T + [\mathbf{T}][\mathbf{K}_1^0][\mathbf{T}]^T. \quad (3.110)$$

Likewise, for derivatives in the other in-plane coordinate,

$$\frac{\partial}{\partial y}\{\mathbf{i}_{123}\} = [\mathbf{K}_2]\{\mathbf{i}_{123}\}, \quad \text{where} \quad [\mathbf{K}_2] = \frac{\partial[\mathbf{T}]}{\partial y}[\mathbf{T}]^T + [\mathbf{T}][\mathbf{K}_2^0][\mathbf{T}]^T. \quad (3.111)$$

The deformed curvature matrices $[\mathbf{K}_1]$ and $[\mathbf{K}_2]$ may be written in the same manner as was Eq (3.66):

$$[\mathbf{K}_1] \equiv \begin{bmatrix} 0 & k_5 & -k_1 \\ -k_5 & 0 & -k_{61} \\ k_1 & k_{61} & 0 \end{bmatrix}, \quad [\mathbf{K}_2] \equiv \begin{bmatrix} 0 & k_4 & -k_{62} \\ -k_4 & 0 & -k_2 \\ k_{62} & k_2 & 0 \end{bmatrix}, \quad (3.112)$$

where the elements of these matrices are

$$k_1 \equiv -\frac{\partial \mathbf{i}_1}{\partial x} \cdot \mathbf{i}_3 = -T_{1m,x} T_{3m} - T_{21} k_{61}^0 + T_{22} k_1^0 + T_{23} k_5^0 \quad (3.113a)$$

$$k_2 \equiv -\frac{\partial \mathbf{i}_2}{\partial y} \cdot \mathbf{i}_3 = -T_{2m,y} T_{3m} + T_{11} k_2^0 - T_{12} k_{62}^0 - T_{13} k_4^0 \quad (3.113b)$$

$$k_{61} \equiv -\frac{\partial \mathbf{i}_2}{\partial x} \cdot \mathbf{i}_3 = -T_{2m,x} T_{3m} + T_{11} k_{61}^0 - T_{12} k_1^0 - T_{13} k_5^0 \quad (3.113c)$$

$$k_{62} \equiv -\frac{\partial \mathbf{i}_1}{\partial y} \cdot \mathbf{i}_3 = -T_{1m,y} T_{3m} - T_{21} k_2^0 + T_{22} k_{62}^0 + T_{23} k_4^0 \quad (3.113d)$$

$$k_5 \equiv \frac{\partial \mathbf{i}_1}{\partial x} \cdot \mathbf{i}_2 = T_{1m,x} T_{2m} - T_{31} k_{61}^0 + T_{32} k_1^0 + T_{33} k_5^0 \quad (3.113e)$$

$$k_4 \equiv -\frac{\partial \mathbf{i}_2}{\partial y} \cdot \mathbf{i}_1 = -T_{2m,y} T_{1m} - T_{31} k_2^0 + T_{32} k_{62}^0 + T_{33} k_4^0, \quad (3.113f)$$

where the repeated subscripts employ the well known tensor summation convention such that, for example

$$T_{1m,x} T_{3m} = T_{11,x} T_{31} + T_{12,x} T_{32} + T_{13,x} T_{33}. \quad (3.114)$$

It is noted that these curvatures are not, in general, the "real" deformed curvatures for two reasons (Pai and Palazotto 1995a): (1) the deformed dx (dy) is along the \mathbf{i}_1 (\mathbf{i}_2) direction, not along the \mathbf{i}_1 (\mathbf{i}_2) direction (since the in-plane shear is nonzero), and (2) differentiation of the local unit vectors has been taken with respect to the undeformed lengths dx and dy rather than the deformed lengths $(1 + e_1)dx$ and $(1 + e_2)dy$.

3.4 Strain-Displacement Relations

Having characterized the behavior of the reference surface, attention may now be turned toward generalizing the displacements to three-dimensions. This is necessary to describe the behavior of material points not located on the reference surface.

In this development, the concept of a "local displacement field" is used (Pai and Nayfeh 1991). Consider a displacement vector, \mathbf{u} , associated with a particular material point A located by a position vector, $\mathbf{P}(\mathbf{A})$ (Figure 3.11). In the infinitesimal region surrounding point A , consider the vector displacement field, $\mathbf{u}(\mathbf{P})$. The derivatives of this displacement field will yield the strain field, *as will the derivative of any displacement field that differs from $\mathbf{u}(\mathbf{P})$ by a constant*. If this constant is chosen to be $-\mathbf{u}(\mathbf{P}(\mathbf{A}))$, a new displacement field is generated:

$$\hat{\mathbf{u}}(\mathbf{P}) = \mathbf{u} - \mathbf{u}(\mathbf{P}(\mathbf{A})) \quad (3.115)$$

such that the *displacement* at point A , in this new displacement field, is now zero. In doing this, the *derivatives* of the displacements, which give rise to the strains, are unchanged (since this new displacement field differs from the previous one by only a constant). In a layered composite consisting of N layers (Figure 3.12), the local displacement vector (with respect to the local $\xi\eta\zeta$ coordinate system of Figure 3.7) as presented by Pai and Palazotto (1995a) and based upon the work of Bhimaraddi (1984), Reddy and Liu (1985), and (Kovářík 1980) is defined as (see Figure 3.13)

$$\mathbf{u} = u_1^{(i)} \mathbf{i}_1 + u_2^{(i)} \mathbf{i}_2 + u_3^{(i)} \mathbf{i}_3 \quad (3.116)$$

where

$$u_1^{(i)} = u_1^0(x, y) + z[\theta_2(x, y) - \theta_2^0(x, y)] + \gamma_5 z + \alpha_1^{(i)}(x, y)z^2 + \beta_1^{(i)}(x, y)z^3$$

$$u_2^{(i)} = u_2^0(x, y) - z[\theta_1(x, y) - \theta_1^0(x, y)] + \gamma_4 z + \alpha_2^{(i)}(x, y)z^2 + \beta_2^{(i)}(x, y)z^3$$

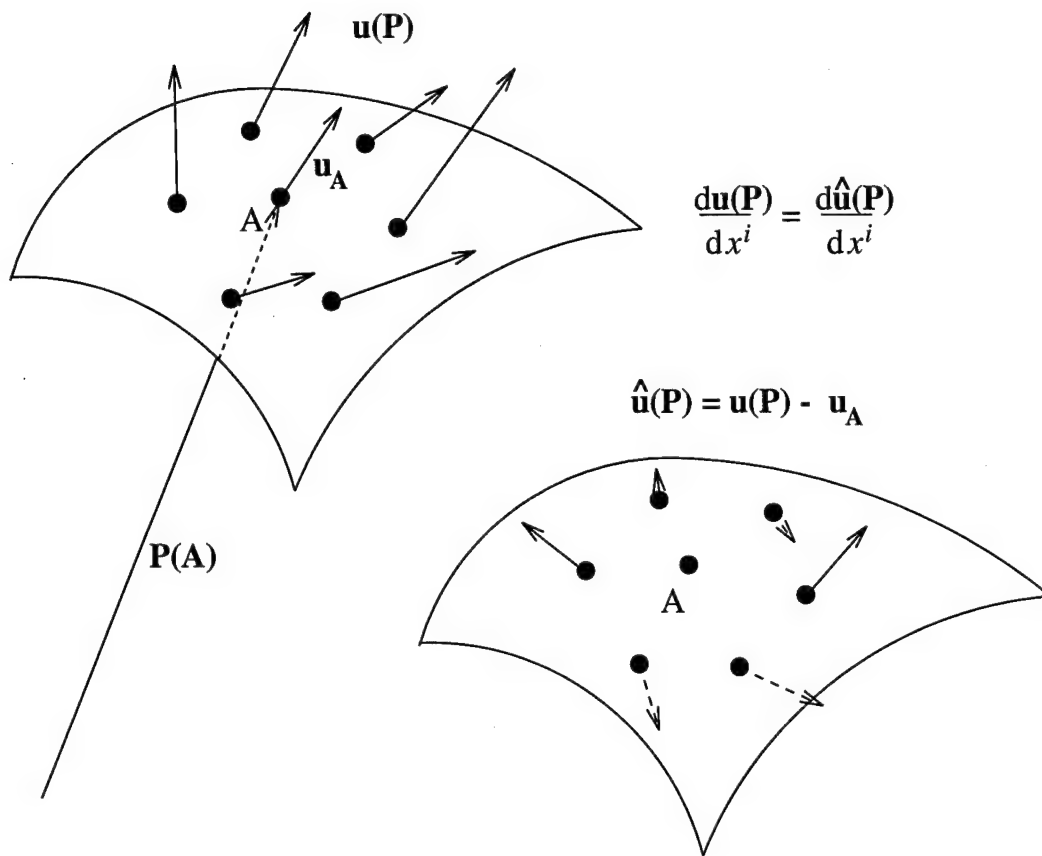


Figure 3.11 Displacement field in the vicinity of point A

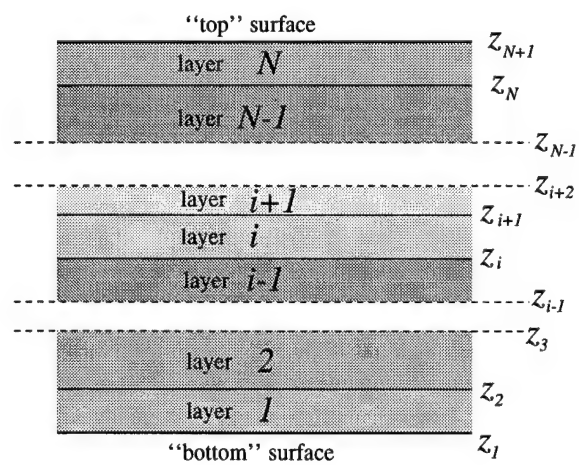


Figure 3.12 A layered composite of N layers indicating ply numbering scheme and interface coordinates, z_i

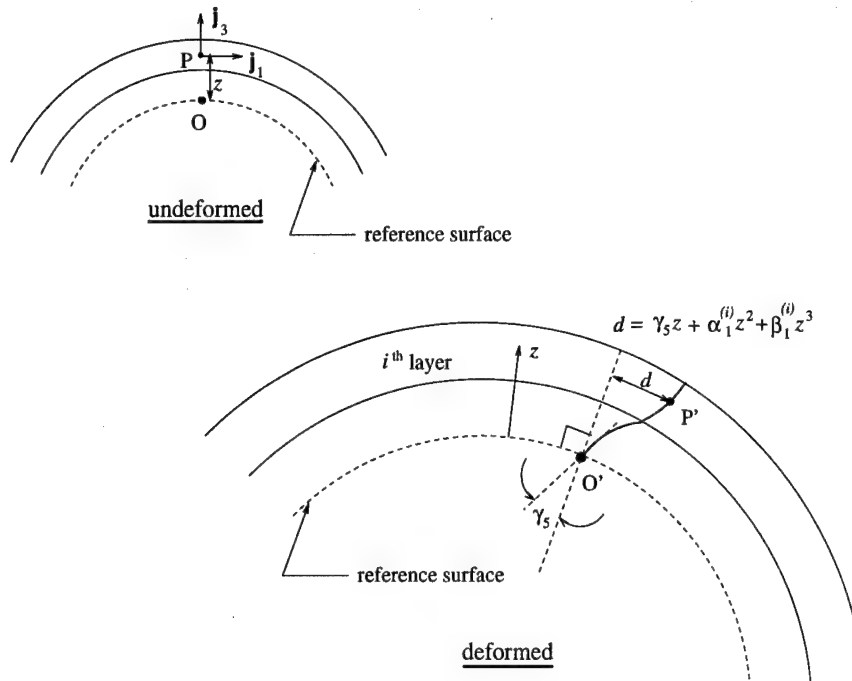


Figure 3.13 Shear warping in a layered composite

$$u_3^{(i)} = u_3^0(x, y) + \alpha_3^{(i)}(x, y)z + \beta_3^{(i)}(x, y)z^2 \quad (3.117)$$

Here, u_j^0 ($j = 1, 2, 3$) are the components of displacement (with respect to the local coordinate system $\xi\eta\zeta$) of a point which is located on the reference surface at (x, y) before deformation. The rigid body rotations and shear rotations are given by θ and γ respectively. In Figure 3.14, these angles are graphically depicted in the xz plane. Referring to Figure 3.14(a), the angle between the transverse coordinate (z) and the normal to the reference surface *in the undeformed configuration* as measured in the xz plane is given by θ_1^0 . The corresponding angle in the yz plane (not shown) is given by $-\theta_2^0$ (the minus sign arises in employing the right-hand rule for rotation about the x -axis). The shear rotation angle in the xz plane at the reference surface is denoted γ_5 , and represents the rotation of the normal to the reference surface due to transverse shear deformation. The corresponding angle in the yz plane is γ_4 (the rotation direction for γ_4 is chosen such that a positive value of γ_4 gives positive displacement for points above the reference surface hence,

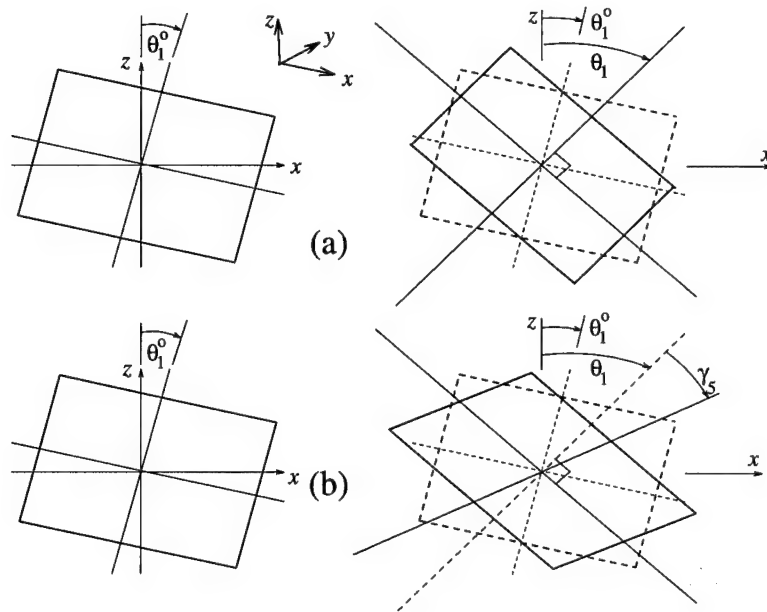


Figure 3.14 Rigid rotations and shear rotations in an originally undeformed parallelogram; (a) rigid rotation without shear rotation; (b) rigid rotation with shear rotation

unlike θ_2 , its sign remains positive). At this point, having described the displacements u_j^0 and the rotations θ_j^0 , θ_j , and γ_j , the ingredients are present for the so-called Reissner-Mindlin kinematic (see Reissner 1945, 1947, Mindlin 1951): normals to the reference surface may rotate due to shear, but must remain straight and of unchanged length. As mentioned in Chapter II, this assumption is inappropriate when dealing with laminated composites. A means is needed of including warping and stretching of the normal. For this the remaining terms of Eq (3.117) are used.

These terms, the $\alpha_k^{(i)}$ and $\beta_k^{(i)}$, are referred to as shear warping and thickness stretch functions. These functions are used to describe the kinematic behavior, *beyond simple rotation of the rigid normal*, of the material away from the reference surface, and allow coupling of the displacements $u_1^{(i)}$ and $u_2^{(i)}$ via the shear angles at the reference surface. That is, γ_4 can affect displacement $u_1^{(i)}$ through the warping functions and, likewise, γ_5 can affect $u_2^{(i)}$. The functions are developed in Section 3.6. By defining the shear warping functions, G_1 and G_2 , and the thickness stretch

function, G_3 as

$$G_1 \equiv \gamma_5 z + \alpha_1^{(i)} z^2 + \beta_1^{(i)} z^3, \quad G_2 \equiv \gamma_4 z + \alpha_2^{(i)} z^2 + \beta_2^{(i)} z^3, \quad \text{and} \quad G_3 \equiv \alpha_3^{(i)} z + \beta_3^{(i)} z^2, \quad (3.118)$$

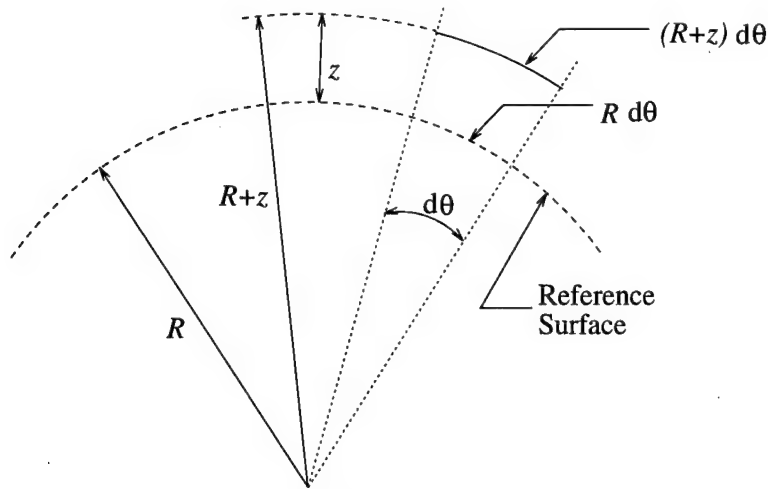
the kinematics of Eq (3.117) may be written as

$$\begin{aligned} u_1^{(i)} &= u_1^0(x, y) + z[\theta_2(x, y) - \theta_2^0(x, y)] + G_1 \\ u_2^{(i)} &= u_2^0(x, y) - z[\theta_1(x, y) - \theta_1^0(x, y)] + G_2 \\ u_3^{(i)} &= u_3^0(x, y) + G_3 \end{aligned} \quad (3.119)$$

Conspicuous by their absence in Eqns (3.117) are the $(1 \pm z/R)$ terms associated with shell kinematics. These are the terms that account for the fact that, along a coordinate curve, normals separated by a finite distance are, in general, not parallel. The kinematics of Eq (3.117) neglect the "trapezoidal cross-section" effect, and hence are not "true" shell kinematics (see Figure 3.15). The differential length subtended by a differential angle $d\theta$ changes with the thickness coordinate. This change in length is neglected in the analysis. While greatly simplifying the formulation, this does introduce an error. The error can be calculated as

$$\epsilon = \frac{(R + \delta) d\theta - R d\theta}{R d\theta} = \delta/R, \quad (3.120)$$

Where $\delta = \max \{|z_{N+1}|, |z_1|\}$ is the maximum distance of a fiber from the reference surface and R is the radius to the reference surface. Clearly, thick, deep shells will suffer the most error. Also note that while the kinematics for u_1 and u_2 are cubic in the thickness coordinate, they are quadratic for u_3 .



Assumption: $(R+z) d\theta \approx R d\theta$

Figure 3.15 Trapezoidal cross-section effect

Note that by choosing a local displacement field (as shown in Figure 3.11) one always has

$$u_1^0 = u_2^0 = u_3^0 = 0. \quad (3.121a)$$

Furthermore, by choosing the in-plane coordinates to lie in the undeformed reference surface, one finds

$$\theta_1^0 = \theta_2^0 = 0, \quad (3.121b)$$

that is, the normal to the undeformed reference surface corresponds to the z -axis. Likewise, note that the curvilinear coordinate system associated with the deformed reference surface (Figure 3.7), denoted by the \mathbf{i} -basis, has a similar characteristic: the normal to the deformed reference surface, by definition, corresponds to the ζ axis, hence

$$\theta_1 = \theta_2 = 0. \quad (3.121c)$$

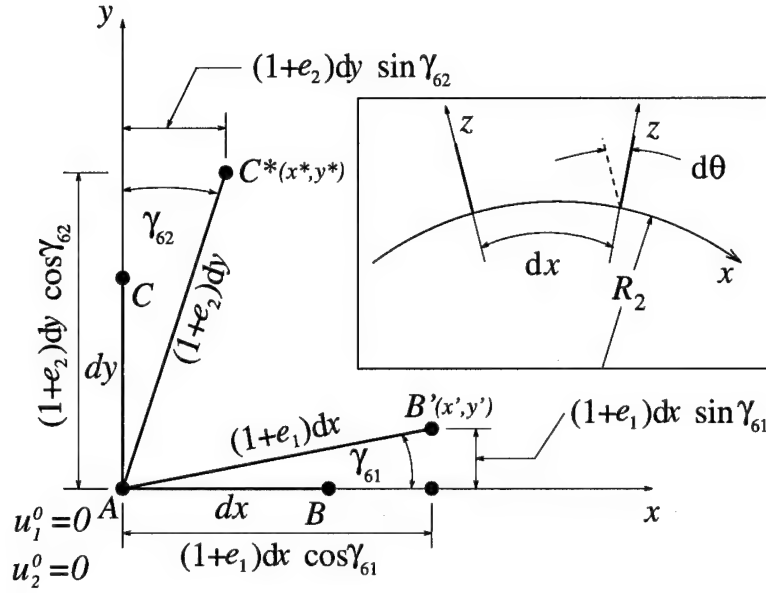


Figure 3.16 In-plane deformations relating to derivatives of displacement components

Finally, since the new \mathbf{i} -basis is tangent to the deformed reference surface, it is evident that

$$\partial u_3^0 / \partial x = \partial u_3^0 / \partial y = 0. \quad (3.121d)$$

Differentiation of the kinematics of Eq (3.119) with respect to the global coordinates gives rise to the Jaumann strains for the i th layer. First consider the in-plane deformations. In Figure 3.16 two originally mutually perpendicular infinitesimal lengths joined at point A , located at (x_0, y_0) are again considered. Now observe the displacements associated with point B , located at (dx, y_0) . The final x location of this point, denoted as x' , may be expressed analytically as

$$x' = x_0 + dx + \frac{\partial u_1^0}{\partial x} dx, \quad (3.122)$$

or geometrically, from the figure, as

$$x' = x_0 + (1 + e_1) dx \cos \gamma_{61}. \quad (3.123)$$

Equating the two expressions leads to

$$\frac{\partial u_1^0}{\partial x} = (1 + e_1) \cos \gamma_{61} - 1. \quad (3.124)$$

Similarly, the final y location of the point, denoted y' , is seen to be

$$y' = y_0 + \frac{\partial u_2^0}{\partial x} dx = y_0 + (1 + e_1) dx \sin \gamma_{61}, \quad (3.125)$$

which leads to

$$\frac{\partial u_2^0}{(1 + e_1) \partial x} = \sin \gamma_{61}. \quad (3.126)$$

Similar expressions are easily developed for point C , which moves during deformation to point C^* .

The derivatives of the rotations of the normals, θ_i^0 and θ_i , are seen to be identical to the curvatures as follows. In the inset of Figure 3.16, the infinitesimal rotation of the normal in moving from point A to point A' on the x axis in the xz plane is observed. The rate of change of this normal, $\partial \theta_1^0 / \partial x$ (or $\partial \theta_1 / \partial x$ in the deformed configuration) is simply the reciprocal of the radius of curvature for the x (ξ) axis:

$$\frac{\partial \theta_2^0}{\partial x} = k_1^0, \text{ and } \frac{\partial \theta_2}{\partial x} = k_1. \quad (3.127)$$

The other derivatives have similar definitions. To summarize, the derivatives associated with the components of the displacement vector $\{\mathbf{u}\}$ are given by

$$\frac{\partial u_2^0}{(1 + e_1) \partial x} = \sin \gamma_{61}, \quad \frac{\partial u_1^0}{(1 + e_2) \partial y} = \sin \gamma_{62} \quad (3.128a)$$

$$\frac{\partial u_1^0}{\partial x} = (1 + e_1) \cos \gamma_{61} - 1, \quad \frac{\partial u_2^0}{\partial y} = (1 + e_2) \cos \gamma_{62} - 1 \quad (3.128b)$$

$$\frac{\partial \theta_2^0}{\partial x} = -\frac{\partial \mathbf{j}_1}{\partial x} \cdot \mathbf{j}_3 = k_1^0, \quad \frac{\partial \theta_1^0}{\partial y} = -k_2^0, \quad \frac{\partial \theta_1^0}{\partial x} = -k_{61}^0, \quad \frac{\partial \theta_2^0}{\partial y} = k_{62}^0 \quad (3.128c)$$

$$\frac{\partial \theta_2}{\partial x} = -\frac{\partial \mathbf{i}_1}{\partial x} \cdot \mathbf{i}_3 = k_1, \quad \frac{\partial \theta_1}{\partial y} = -k_2, \quad \frac{\partial \theta_1}{\partial x} = -k_{61}, \quad \frac{\partial \theta_2}{\partial y} = k_{62} \quad (3.128d)$$

Like their undeformed counterparts, the curvatures k_{61} and k_{62} are the curvatures describing the "twisting" of the normal about the x and y axes respectively with respect to the deformed geometry. For example, k_{61} describes the rotation of the normal about the x axis as one moves along that (x) axis.

Substituting the expressions of Eqns (3.128) into Eq (3.119) yields the derivatives of the displacement vector \mathbf{u} with respect to x , y , and z :

$$\begin{aligned} \frac{\partial \mathbf{u}}{\partial x} &= \frac{\partial u_1}{\partial x} \mathbf{i}_1 + \frac{\partial u_2}{\partial x} \mathbf{i}_2 + \frac{\partial u_3}{\partial x} \mathbf{i}_3 + u_1 \frac{\partial \mathbf{i}_1}{\partial x} + u_2 \frac{\partial \mathbf{i}_2}{\partial x} + u_3 \frac{\partial \mathbf{i}_3}{\partial x} \\ &= [(1 + e_1) \cos \gamma_{61} - 1 + z(k_1 - k_1^0) + G_{1,x} - k_5 G_2 + k_1 G_3] \mathbf{i}_1 \\ &\quad + [(1 + e_1) \sin \gamma_{61} + z(k_{61} - k_{61}^0) + G_{2,x} + k_5 G_1 + k_{61} G_3] \mathbf{i}_2 \\ &\quad + [G_{3,x} - k_1 G_1 - k_{61} G_2] \mathbf{i}_3, \end{aligned} \quad (3.129a)$$

$$\begin{aligned} \frac{\partial \mathbf{u}}{\partial y} &= \frac{\partial u_1}{\partial y} \mathbf{i}_1 + \frac{\partial u_2}{\partial y} \mathbf{i}_2 + \frac{\partial u_3}{\partial y} \mathbf{i}_3 + u_1 \frac{\partial \mathbf{i}_1}{\partial y} + u_2 \frac{\partial \mathbf{i}_2}{\partial y} + u_3 \frac{\partial \mathbf{i}_3}{\partial y} \\ &= [(1 + e_2) \sin \gamma_{62} + z(k_{62} - k_{62}^0) + G_{1,y} - k_4 G_2 + k_{62} G_3] \mathbf{i}_1 \\ &\quad + [(1 + e_2) \cos \gamma_{62} - 1 + z(k_2 - k_2^0) + G_{2,y} + k_4 G_1 + k_2 G_3] \mathbf{i}_2 \\ &\quad + [G_{3,y} - k_{62} G_1 - k_2 G_2] \mathbf{i}_3, \end{aligned} \quad (3.129b)$$

$$\frac{\partial \mathbf{u}}{\partial z} = \frac{\partial u_1}{\partial z} \mathbf{i}_1 + \frac{\partial u_2}{\partial z} \mathbf{i}_2 + \frac{\partial u_3}{\partial z} \mathbf{i}_3 = G_{1,z} \mathbf{i}_1 + G_{2,z} \mathbf{i}_2 + G_{3,z} \mathbf{i}_3. \quad (3.129c)$$

So from Eq (3.128)–(3.129c), the Jaumann strains B_{mn} are

$$B_{mn} = \frac{1}{2} \left(\frac{\partial \mathbf{u}}{\partial x^m} \cdot \mathbf{i}_n + \frac{\partial \mathbf{u}}{\partial x^n} \cdot \mathbf{i}_m \right) \quad (3.130a)$$

$$B_{11}^{(i)} = \frac{\partial \mathbf{u}}{\partial x} \cdot \mathbf{i}_1 = (1 + e_1) \cos \gamma_{61} - 1 + z(k_1 - k_1^0) + G_{1,x} - k_5 G_2 + \underbrace{k_1 G_3} \quad (3.130b)$$

$$B_{22}^{(i)} = \frac{\partial \mathbf{u}}{\partial y} \cdot \mathbf{i}_2 = (1 + e_2) \cos \gamma_{62} - 1 + z(k_2 - k_2^0) + G_{2,y} + k_4 G_1 + \underbrace{k_2 G_3}_{(3.130c)}$$

$$B_{33}^{(i)} = \frac{\partial \mathbf{u}}{\partial z} \cdot \mathbf{i}_3 = G_{3,z} \quad (3.130d)$$

$$2B_{23}^{(i)} = \frac{\partial \mathbf{u}}{\partial y} \cdot \mathbf{i}_3 + \frac{\partial \mathbf{u}}{\partial z} \cdot \mathbf{i}_2 = G_{2,z} - k_{62} G_1 - k_2 G_2 + \underbrace{G_{3,y}}_{(3.130e)}$$

$$2B_{13}^{(i)} = \frac{\partial \mathbf{u}}{\partial x} \cdot \mathbf{i}_3 + \frac{\partial \mathbf{u}}{\partial z} \cdot \mathbf{i}_1 = G_{1,z} - k_1 G_1 - k_{61} G_2 + \underbrace{G_{3,x}}_{(3.130f)}$$

$$\begin{aligned} 2B_{12}^{(i)} &= \frac{\partial \mathbf{u}}{\partial x} \cdot \mathbf{i}_2 + \frac{\partial \mathbf{u}}{\partial y} \cdot \mathbf{i}_1 \\ &= (1 + e_1) \sin \gamma_{61} + (1 + e_2) \sin \gamma_{62} + z(k_6 - k_6^0) \\ &\quad + G_{1,y} + G_{2,x} + k_5 G_1 - k_4 G_2 + \underbrace{k_6 G_3}_{(3.130g)} \end{aligned}$$

where $k_6 \equiv k_{61} + k_{62}$ and $k_6^0 \equiv k_{61}^0 + k_{62}^0$.

At this point, a simplification suggested by Pai and Palazotto (1995a) is performed: because G_3 , the stretch in the thickness direction, is usually small, especially for thin shells¹³, one may neglect G_3 and its derivatives in all strain-displacement expressions *except* in that of the direct normal strain, $B_{33}^{(i)}$. This is based upon the claim that the effect of transverse normal strain on the in-plane strains is negligible. So the strain-displacement relations of Eq (3.130) are re-written, eliminating the terms marked with an underbrace.

$$B_{11}^{(i)} = \frac{\partial \mathbf{u}}{\partial x} \cdot \mathbf{i}_1 = (1 + e_1) \cos \gamma_{61} - 1 + z(k_1 - k_1^0) + G_{1,x} - k_5 G_2 \quad (3.131a)$$

$$B_{22}^{(i)} = \frac{\partial \mathbf{u}}{\partial y} \cdot \mathbf{i}_2 = (1 + e_2) \cos \gamma_{62} - 1 + z(k_2 - k_2^0) + G_{2,y} + k_4 G_1 \quad (3.131b)$$

$$B_{33}^{(i)} = \frac{\partial \mathbf{u}}{\partial z} \cdot \mathbf{i}_3 = G_{3,z} \quad (3.131c)$$

$$2B_{23}^{(i)} = \frac{\partial \mathbf{u}}{\partial y} \cdot \mathbf{i}_3 + \frac{\partial \mathbf{u}}{\partial z} \cdot \mathbf{i}_2 = G_{2,z} - k_{62} G_1 - k_2 G_2 \quad (3.131d)$$

$$2B_{13}^{(i)} = \frac{\partial \mathbf{u}}{\partial x} \cdot \mathbf{i}_3 + \frac{\partial \mathbf{u}}{\partial z} \cdot \mathbf{i}_1 = G_{1,z} - k_1 G_1 - k_{61} G_2 \quad (3.131e)$$

$$\begin{aligned} 2B_{12}^{(i)} &= \frac{\partial \mathbf{u}}{\partial x} \cdot \mathbf{i}_2 + \frac{\partial \mathbf{u}}{\partial y} \cdot \mathbf{i}_1 \\ &= (1 + e_1) \sin \gamma_{61} + (1 + e_2) \sin \gamma_{62} + z(k_6 - k_6^0) \end{aligned}$$

¹³The impact of not simplifying the equations is discussed further in Chapter VII where thick shells (tires) are considered.

$$+ G_{1,y} + G_{2,x} + k_5 G_1 - k_4 G_2 \quad (3.131f)$$

where, again, $k_6 \equiv k_{61} + k_{62}$ and $k_6^0 \equiv k_{61}^0 + k_{62}^0$.

Though trapezoidal cross-section effect has been neglected in these kinematics, the z/R -like terms of shell kinematics are present in these equations, arising from taking derivatives of the rotation angles θ_i^0 (recall the inset of Figure 3.16). For example, the B_{22} strain contains the term $-z k_2^0$, which is, for the cylindrical shell, just $-z/R_2$, where R_2 is a shell radius. The appearance of these terms is another by-product of referring displacement derivatives to the global coordinate system, i.e., the total Lagrangian approach.

Before moving on to the development of the constitutive relations, the earlier numerical example is now used to compare the results of the current description of mid-surface behavior to that using the theory of Pai and Palazotto. Using the equations for e_1 and e_2 from the theory (Eq 3.74) with all initial curvatures $k_i^0 = 0$, it is seen that

$$\begin{aligned} e_1 &= \frac{\|\mathbf{A}'\mathbf{B}'\| - dx}{dx} \\ &= \sqrt{(1 + u_{,x})^2 + v_{,x}^2 + w_{,x}^2} - 1 \end{aligned} \quad (3.132a)$$

$$\begin{aligned} e_2 &= \frac{\|\mathbf{A}'\mathbf{C}'\| - dy}{dy} \\ &= \sqrt{u_{,y}^2 + (1 + v_{,y})^2 + w_{,y}^2} - 1, \end{aligned} \quad (3.132b)$$

and $e_1 = 1.0$ and $e_2 = \sqrt{5}$. The expressions for the Jaumann strains at the reference surface ($z = 0$) are given by

$$B_{11}^{(i)} = \frac{\partial \mathbf{u}}{\partial x_1} \cdot \mathbf{i}_1 = (1 + e_1) \cos \gamma_{61} - 1 \quad (3.133a)$$

$$B_{22}^{(i)} = \frac{\partial \mathbf{u}}{\partial x_2} \cdot \mathbf{i}_2 = (1 + e_2) \cos \gamma_{62} - 1$$

(3.133b)

$$\begin{aligned}
2B_{12}^{(i)} &= \frac{\partial \mathbf{u}}{\partial x_1} \cdot \mathbf{i}_2 + \frac{\partial \mathbf{u}}{\partial x_2} \cdot \mathbf{i}_1 \\
&= (1 + e_1) \sin \gamma_{61} + (1 + e_2) \sin \gamma_{62}
\end{aligned}
\tag{3.133c}$$

Substituting the values of e_1 , e_2 , γ_{61} , and γ_{62} into the above leads to

$$[\mathbf{B}] = \begin{bmatrix} 0.94029 & 0.485071 \\ 0.485071 & 1.18282 \end{bmatrix}
\tag{3.134}$$

where the γ_{61} and γ_{62} were found through the relationships

$$\gamma_{61} + \gamma_{62} = \sin^{-1}(\mathbf{i}_1 \cdot \mathbf{i}_2)
\tag{3.135}$$

$$(1 + e_1) \sin \gamma_{61} = (1 + e_2) \sin \gamma_{62}
\tag{3.136}$$

which is exactly the result of the polar decomposition formulation.

3.5 Constitutive Relations

Having developed the relationships between the local displacements and the strains, the constitutive relations are now developed. These are the relationships between the strains and the stresses produced by them. As mentioned in Chapter II, the current analysis treats all materials as perfectly elastic over their entire range of deformation. That is, there is a *linear* relationship between strains and stresses regardless of the magnitudes of either. The kinematics developed in the last section do not explicitly limit the current theory to small strains, but prudence dictates that results are always interpreted in the light of what is known about the behavior of the material under study. In assessing the finite element results based on this theory, questions to consider would include: (1) Over what range of strains/stresses is the material elastic? (2) When the ma-

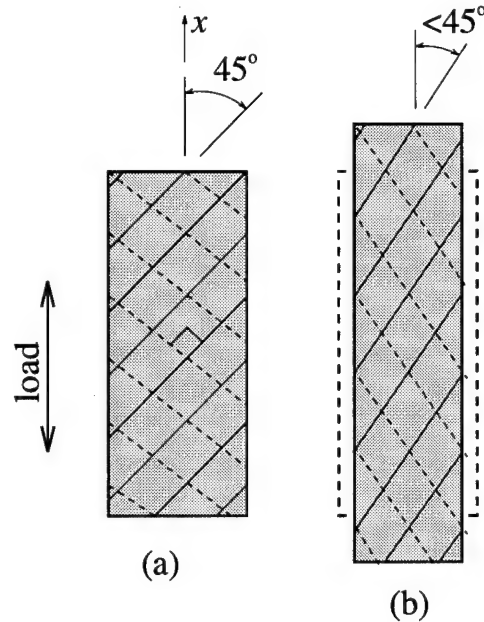


Figure 3.17 Change in orientation of fibers during deformation; (a) angle-ply laminate before deformation, (b) after deformation

terial becomes inelastic, are the changes in properties slight or dramatic? (3) When and how does the material fail?

To characterize a laminated composite made of transversely isotropic (sometimes called specially orthotropic or cross anisotropic) plies, well known tensor transformations are used (Whitney 1987) to obtain the transformed stiffness matrix $[\bar{Q}^{(i)}]$ for the i^{th} lamina (see Figure 3.12) from its principal stiffness matrix $[Q^{(i)}]$ and its ply angle, which is measured with respect to the x axis. Note that in this theoretical development, changes in the relative fiber orientations from ply-to-ply due to deformation are neglected. That is, under the assumption of a perfect interply bond, the deformation cannot cause the relative angle between fibers in, for example, the i^{th} ply, to *change* their orientation relative to the fibers of the $i - 1^{\text{st}}$ or $i + 1^{\text{st}}$ plies. In actuality, such orientation changes do take place, as illustrated in Figure 3.17. In the figure, a two-ply laminated composite is depicted. The “top” ply has fibers originally oriented 45° to the x -axis, while the “bottom” ply has fibers oriented at -45° (the fibers of this ply are depicted as dashed lines). During deformation,

a “scissoring” of the fibers takes place due to the stretching of the material in the x -direction. In the current formulation, such changes in orientation are not accounted for. To account for such deformation would require tracing the in-plane deformation at each location (in x , y , and z), and recalculating the constitutive relations based on any changes in the orientations. In large strain analyses using a Green’s strain total-Lagrangian approach, such as that of Schimmels and Palazotto (1994), expensive transformations of material and constitutive frames-of-reference are used to follow global changes of fiber orientations.

A transversely isotropic material can be described in terms of five independent elastic constants:

$$E_{11}, \quad E_{22} = E_{33}, \quad G_{23} \text{ or } \nu_{23}, \quad G_{12} = G_{13}, \quad \nu_{12} = \nu_{13}. \quad (3.137)$$

The quantities G_{23} and ν_{23} are related by (Whitney 1987, p. 11):

$$G_{23} = \frac{E_{23}}{2(1 + \nu_{23})}, \quad (3.138)$$

so either, but not both, may be specified.

The relationship between the Jaumann stresses, J_{mn} , and the Jaumann (or Biot-Cauchy) strains, B_{mn} , for the i^{th} lamina of a transversely isotropic material may then be written as (for the transformed relationships)

$$\begin{Bmatrix} J_{11}^{(i)} \\ J_{22}^{(i)} \\ J_{33}^{(i)} \\ J_{12}^{(i)} \\ J_{23}^{(i)} \\ J_{13}^{(i)} \end{Bmatrix} = \begin{bmatrix} \bar{Q}_{11}^{(i)} & \bar{Q}_{12}^{(i)} & \bar{Q}_{13}^{(i)} & \bar{Q}_{16}^{(i)} & 0 & 0 \\ \bar{Q}_{12}^{(i)} & \bar{Q}_{22}^{(i)} & \bar{Q}_{23}^{(i)} & \bar{Q}_{26}^{(i)} & 0 & 0 \\ \bar{Q}_{13}^{(i)} & \bar{Q}_{23}^{(i)} & \bar{Q}_{33}^{(i)} & \bar{Q}_{36}^{(i)} & 0 & 0 \\ \bar{Q}_{16}^{(i)} & \bar{Q}_{26}^{(i)} & \bar{Q}_{36}^{(i)} & \bar{Q}_{66}^{(i)} & 0 & 0 \\ 0 & 0 & 0 & 0 & \bar{Q}_{44}^{(i)} & \bar{Q}_{45}^{(i)} \\ 0 & 0 & 0 & 0 & \bar{Q}_{45}^{(i)} & \bar{Q}_{55}^{(i)} \end{bmatrix} \begin{Bmatrix} B_{11}^{(i)} \\ B_{22}^{(i)} \\ B_{33}^{(i)} \\ 2 B_{12}^{(i)} \\ 2 B_{23}^{(i)} \\ 2 B_{13}^{(i)} \end{Bmatrix} \quad (3.139)$$

3.6 Shear Warping Functions

In developing the transverse shear warping functions it is assumed that there is no delamination in the N -ply laminate, and that the in-plane displacements u_1 and u_2 and interlaminar shear stresses J_{13} and J_{23} are continuous across the interface of two adjacent layers. If there are no applied shear loads on the bounding surfaces, then $J_{13} = J_{23} = B_{13} = B_{23} = 0$ on the $z = z_1$ and $z = z_{N+1}$ surfaces, where N is the total number of layers (see Figure 3.12). If the above requirements are enforced, the result is $4N$ algebraic equations that can be stated as:

$$B_{23}^{(1)}(x, y, z_1, t) = 0 \quad (3.140a)$$

$$B_{13}^{(1)}(x, y, z_1, t) = 0 \quad (3.140b)$$

$$u_1^{(i)}(x, y, z_{i+1}, t) - u_1^{(i+1)}(x, y, z_{i+1}, t) = 0 \quad \text{for } i = 1, \dots, N-1 \quad (3.140c)$$

$$u_2^{(i)}(x, y, z_{i+1}, t) - u_2^{(i+1)}(x, y, z_{i+1}, t) = 0 \quad \text{for } i = 1, \dots, N-1 \quad (3.140d)$$

$$J_{23}^{(i)}(x, y, z_{i+1}, t) - J_{23}^{(i+1)}(x, y, z_{i+1}, t) = 0 \quad \text{for } i = 1, \dots, N-1 \quad (3.140e)$$

$$J_{13}^{(i)}(x, y, z_{i+1}, t) - J_{13}^{(i+1)}(x, y, z_{i+1}, t) = 0 \quad \text{for } i = 1, \dots, N-1 \quad (3.140f)$$

$$B_{23}^{(N)}(x, y, z_{N+1}, t) = 0 \quad (3.140g)$$

$$B_{13}^{(N)}(x, y, z_{N+1}, t) = 0 \quad (3.140h)$$

where the u_i are in the local orthogonal frame and from which the $4N$ unknown shear warping function coefficients $\alpha_1^{(i)}$, $\alpha_2^{(i)}$, $\beta_1^{(i)}$, $\beta_2^{(i)}$ for $i = 1, \dots, N$ may be determined in terms of γ_4 and γ_5 as follows.

Given that

$$\begin{aligned} \alpha_1^{(i)} &= a_{14}^{(i)}\gamma_4 + a_{15}^{(i)}\gamma_5, \quad \alpha_2^{(i)} = a_{24}^{(i)}\gamma_4 + a_{25}^{(i)}\gamma_5 \\ \beta_1^{(i)} &= b_{14}^{(i)}\gamma_4 + b_{15}^{(i)}\gamma_5, \quad \beta_2^{(i)} = b_{24}^{(i)}\gamma_4 + b_{25}^{(i)}\gamma_5 \end{aligned} \quad (3.141)$$

where $a_{kl}^{(i)}$ and $b_{kl}^{(i)}$ are functions of z_j , $\overline{Q}_{44}^{(j)}$, $\overline{Q}_{45}^{(j)}$, and $\overline{Q}_{55}^{(j)}$, one may write

$$G_1 = \gamma_5 g_{15}^{(i)} + \gamma_4 g_{14}^{(i)}, \quad G_2 = \gamma_4 g_{24}^{(i)} + \gamma_5 g_{25}^{(i)} \quad (3.142)$$

where $g_{14}^{(i)}$, $g_{15}^{(i)}$, $g_{24}^{(i)}$, and $g_{25}^{(i)}$ are polynomial functions of z , defined as

$$g_{14}^{(i)} \equiv a_{14}^{(i)} z^2 + b_{14}^{(i)} z^3, \quad g_{15}^{(i)} \equiv z + a_{15}^{(i)} z^2 + b_{15}^{(i)} z^3 \quad (3.143a)$$

$$g_{24}^{(i)} \equiv z + a_{24}^{(i)} z^2 + b_{24}^{(i)} z^3, \quad g_{25}^{(i)} \equiv a_{25}^{(i)} z^2 + b_{25}^{(i)} z^3 \quad (3.143b)$$

These are the functions suggested by Pai and Palazotto (1995a). The $4N$ equations of (3.140), upon separation of γ_4 and γ_5 , produce the $8N$ equations needed to solve for the coefficients of Eqns (3.143). However, note that the functions of Eqns (3.143) are constrained to pass through the origin *regardless of the ply to which they belong*. While this is required for the ply containing the reference surface, it is not required (or even desirable) for plies away from the reference surface.

While studying the work of Pagano (1969) (see Chapter V) under the current research, it was found that certain choices of shear moduli and ply thicknesses of a $[0/90/0]$ laminated plate strip could induce artificially high shear stiffness. In a phenomenon just the opposite of shear-locking, these conditions cause the coefficients of Eqns (3.143) to become unbounded, leading to a laminate infinitely stiff in shear. This phenomenon could be generated regardless of the gross thickness of the laminate. Thus, even for a very thick plate, the Kirchhoff kinematic could be artificially (and potentially unknowingly) applied to the analysis.

To further explore the weakness in this choice of functions, consider the three-ply laminate of Figure 3.18. The outer plies are of identical thickness, and the reference surface is at the center of the middle ply, the thickness of which may vary. If the plate is considered to be infinitely long in the y direction, one may consider only the transverse shear deformation in the x - z plane. For the warping functions of Eqns (3.143), this generates a 6×6 coefficient matrix to solve for the six

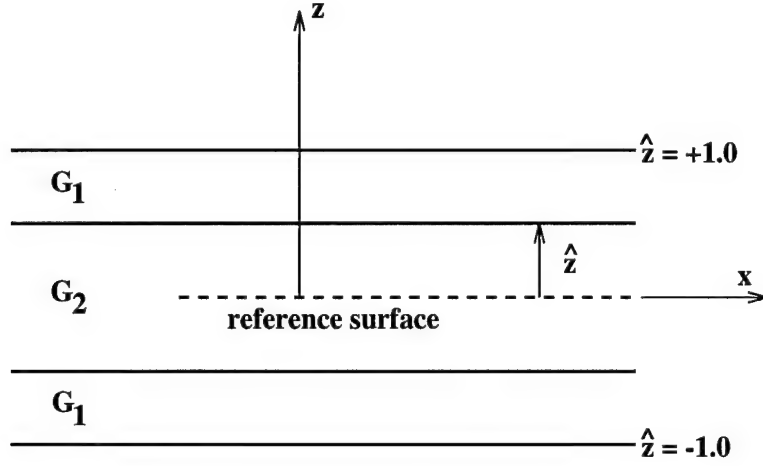


Figure 3.18 The three-ply laminate

unknowns, $a_{15}^{(i)}, b_{15}^{(i)}, i = 1, 2, 3$. The determinant of this coefficient matrix, calling it $[A]$, is

$$\det[A] = 12 (9 \hat{z}^7 - 15 g \hat{z}^7 + 6 g^2 \hat{z}^7 - 12 \hat{z}^8 + 25 g \hat{z}^8 - 12 g^2 \hat{z}^8 + 4 \hat{z}^9 - 10 g \hat{z}^9 + 6 g^2 \hat{z}^9), \quad (3.144)$$

where $g = G_1/G_2$. Thus, for unfortunate choices of \hat{z} and g , $\det[A]$ can be made to be zero. These conditions are:

$$\hat{z} = \frac{3(-1+g)}{-2+3g}, \quad \hat{z} = \frac{-3+2g}{2(-1+g)}, \quad g = \frac{-3+2\hat{z}}{2(-1+\hat{z})}, \quad g = \frac{-3+2\hat{z}}{3(-1+\hat{z})} \quad (3.145)$$

A more recent work of Pai (1995), while not mentioning the singularity problem mentioned above, suggests an alternate choice of warping functions: one set of functions, of the form of Eqns (3.143), to be used for the ply containing the reference surface, and another set of functions to be used for all other plies. Note that the cubic warping function has the general form

$$g_{mn}^{(i)} = c_{mn}^{(i)} + d_{mn}^{(i)} z + a_{mn}^{(i)} z^2 + b_{mn}^{(i)} z^3. \quad (3.146)$$

There are four such functions for a given layer, hence $16N$ unknowns coefficients. With only $8N$ equations, one must specify (or omit) two of the coefficients. Pai proposes the following four functions:

$$g_{14}^{(i)} \equiv a_{14}^{(i)} z^2 + b_{14}^{(i)} z^3 \quad (3.147a)$$

$$g_{15}^{(i)} \equiv c_{15}^{(i)} + z + b_{15}^{(i)} z^3 \quad (3.147b)$$

$$g_{24}^{(i)} \equiv c_{24}^{(i)} + z + b_{24}^{(i)} z^3 \quad (3.147c)$$

$$g_{25}^{(i)} \equiv a_{25}^{(i)} z^2 + b_{25}^{(i)} z^3. \quad (3.147d)$$

Because they couple the shear in one plane to the displacement perpendicular to that plane, Pai refers to $g_{14}^{(i)}$ and $g_{25}^{(i)}$ as “shear-coupling functions.” The form of these functions coupling functions is unchanged from Eqns (3.143). However, the shear-warping functions $g_{15}^{(i)}$ and $g_{24}^{(i)}$ have changed—including a constant term and dropping the quadratic term. This allows for an offset from the origin at the reference surface. Pai’s rationale for eliminating the quadratic term in the shear-warping functions is that, for isotropic plates, elasticity solutions give rise to no linear terms in the shear strains (only quadratic ones). Hence differentiating, for example, $g_{15}^{(i)}$, yields a quadratic strain function.

Applying the functions of Eqns (3.147) to the problem of Figure 3.18 also yields a 6×6 system of equations. However, the determinant of the coefficient matrix, calling it $[\mathbf{B}]$, is

$$\det[\mathbf{B}] = -108\hat{z}^3. \quad (3.148)$$

This well-behaved determinant causes trouble only when \hat{z} approaches zero. Moreover, this determinant is independent of the material properties. Note, however, that the shear coupling functions are still constrained to pass through the origin. Analysis of the tire problem revealed that this restriction was corrupting the representation of shear. Hence, the equations were modified to their

present form of

$$g_{14}^{(i)} \equiv c_{14}^{(i)} + b_{14}^{(i)} z^3 \quad (3.149a)$$

$$g_{15}^{(i)} \equiv c_{15}^{(i)} + z + b_{15}^{(i)} z^3 \quad (3.149b)$$

$$g_{24}^{(i)} \equiv c_{24}^{(i)} + z + b_{24}^{(i)} z^3 \quad (3.149c)$$

$$g_{25}^{(i)} \equiv c_{25}^{(i)} + b_{25}^{(i)} z^3 \quad (3.149d)$$

for plies not containing the reference surface. This formulation leads to a more correct representation of the through-the-thickness warping.

Note, however, that in none of the aforementioned formulations of these warping functions may one use an *interlaminar boundary* as the shell reference surface. For example, were one to model a four-ply symmetric laminate, one could not use the shell middle surface as the reference surface. This is a consequence of the use of a piece-wise continuous polynomial field to represent displacements through the thickness. In order to solve the warping function equations (Eqns 3.140), the slopes of the warping functions ($g_{14,z}$, $g_{15,z}$, $g_{24,z}$, and $g_{25,z}$) must have continuity at the reference surface ($z = 0$). By definition, these functions are, in general, *discontinuous* at interlaminar boundaries. Furthermore, Pai recommends that an outer ply not be permitted to contain the reference surface. Where that is desired, he recommends splitting the outer ply into two plies and putting the reference surface in the inner one, thus freeing the warping function in the outer ply (Pai 1995, p. 2300).

3.7 Thickness Stretching Functions

To generate the quadratic polynomials describing the transverse normal displacement in the i th layer, one may use the following conditions: (1) normal displacement $u_3^{(i)}$ is continuous across each (perfectly bonded) bonding surface and (2) the normal direct stresses are fully described by

the appropriate transformed constitutive relationships at the bonding surfaces. From Eqns (3.139), (3.131), (3.117), and (3.121) the appropriate $2N$ equations are

$$\bar{Q}_{33}^{(1)}(\alpha_3^{(1)} + 2\beta_3^{(1)}z_1) = -\{\bar{Q}_{13}^{(1)}, \bar{Q}_{23}^{(1)}, \bar{Q}_{36}^{(1)}\}\{B_{11}^{(1)}, B_{22}^{(1)}, 2B_{12}^{(1)}\}_{z_1}^T \quad (3.150a)$$

$$\begin{aligned} & \bar{Q}_{33}^{(i)}(\alpha_3^{(i)} + 2\beta_3^{(i)}z_{i+1}) - \bar{Q}_{33}^{(i+1)}(\alpha_3^{(i+1)} + 2\beta_3^{(i+1)}z_{i+1}) \\ &= \{\bar{Q}_{13}^{(i+1)}, \bar{Q}_{23}^{(i+1)}, \bar{Q}_{36}^{(i+1)}\}\{B_{11}^{(i+1)}, B_{22}^{(i+1)}, 2B_{12}^{(i+1)}\}_{z_{i+1}}^T - \{\bar{Q}_{13}^{(i)}, \bar{Q}_{23}^{(i)}, \bar{Q}_{36}^{(i)}\}\{B_{11}^{(i)}, B_{22}^{(i)}, 2B_{12}^{(i)}\}_{z_{i+1}}^T, \\ & \quad \text{for } i = 1, \dots, N-1 \end{aligned} \quad (3.150b)$$

$$\alpha_3^{(i)}z_{i+1} + \beta_3^{(i)}z_{i+1}^2 - \alpha_3^{(i+1)}z_{i+1} - \beta_3^{(i+1)}z_{i+1}^2 = 0, \quad \text{for } i = 1, \dots, N-1 \quad (3.150c)$$

$$\bar{Q}_{33}^{(N)}(\alpha_3^{(N)} + 2\beta_3^{(N)}z_{N+1}) = -\{\bar{Q}_{13}^{(N)}, \bar{Q}_{23}^{(N)}, \bar{Q}_{36}^{(N)}\}\{B_{11}^{(N)}, B_{22}^{(N)}, 2B_{12}^{(N)}\}_{z_{N+1}}^T \quad (3.150d)$$

where it is assumed that there are no externally applied normal stresses on the deformed bonding surfaces. Eqns (3.150a) and (3.150d) describe the stress free condition at the bounding surfaces in terms of the transverse normal and in-plane strains via the constitutive relations of Eq (3.139). Eq (3.150b) describes the continuity of the transverse normal stress across the bonding (vs. bounding) surfaces. Eq (3.150c) describes the continuity of the displacement in the thickness direction at the bonding surface. Eq (3.150b) expresses the same balance in terms of the bonding (vs. bounding) surfaces. Eq (3.150c) describes the continuity of the displacement in the thickness direction at the bonding surface. The assumption of zero-stress conditions at the free surfaces is critical to the current formulation. This assumption allows the equations to be solved in terms of the reference-surface transverse shear angles, γ_4 and γ_5 , since the equations are of the general form

$$f\left(a_{ij}^{(i)}, b_{ij}^{(i)}, x, y, z_i, z_{i+1}, [\bar{Q}^{(i)}]\right)\gamma_4 + g\left(a_{ij}^{(i)}, b_{ij}^{(i)}, x, y, z_i, z_{i+1}, [\bar{Q}^{(i)}]\right)\gamma_5 = J^{(i)} = 0 \quad (3.151)$$

where the $a_{ij}^{(i)}$ and $b_{ij}^{(i)}$ represent the unknown coefficients of the shear warping and thickness stretch functions for which one is solving. Notice that by insisting that the functions f and g *independently* go to zero, one gets *two* equations:

$$f(a_{ij}^{(i)}, b_{ij}^{(i)}, x, y, z_i, z_{i+1}, [\bar{Q}^{(i)}]) = 0 \quad (3.152a)$$

$$g(a_{ij}^{(i)}, b_{ij}^{(i)}, x, y, z_i, z_{i+1}, [\bar{Q}^{(i)}]) = 0. \quad (3.152b)$$

A non-zero stress at the boundary halves the available number of equations, and the warping/stretch function coefficients cannot be solved for in the present fashion.

Equations (3.150) can be used to solve for the $2N$ unknowns $\alpha_3^{(i)}$ and $\beta_3^{(i)}$, $i = 1, \dots, N$, in terms of the elements of the strain components (Eq 3.131) as

$$\begin{aligned} \begin{Bmatrix} \alpha_3^{(i)} \\ \beta_3^{(i)} \end{Bmatrix} &= \begin{bmatrix} a_{30}^{(i)} & a_{31}^{(i)} & a_{32}^{(i)} \\ b_{30}^{(i)} & b_{31}^{(i)} & b_{32}^{(i)} \end{bmatrix} \begin{Bmatrix} (1 + e_1) \cos \gamma_{61} - 1 \\ (1 + e_2) \cos \gamma_{62} - 1 \\ (1 + e_1) \sin \gamma_{61} + (1 + e_2) \sin \gamma_{62} \end{Bmatrix} \\ &+ \begin{bmatrix} a_{33}^{(i)} & a_{34}^{(i)} & a_{35}^{(i)} \\ b_{33}^{(i)} & b_{34}^{(i)} & b_{35}^{(i)} \end{bmatrix} \begin{Bmatrix} k_1 - k_1^0 \\ k_2 - k_2^0 \\ k_6 - k_6^0 \end{Bmatrix} \\ &+ \begin{bmatrix} a_{36}^{(i)} & a_{37}^{(i)} & a_{38}^{(i)} & a_{39}^{(i)} \\ b_{36}^{(i)} & b_{37}^{(i)} & b_{38}^{(i)} & b_{39}^{(i)} \end{bmatrix} \begin{Bmatrix} \gamma_{4,x} \\ \gamma_{4,y} \\ \gamma_{5,x} \\ \gamma_{5,y} \end{Bmatrix} + \begin{bmatrix} k_4 a_{41}^{(i)} + k_5 a_{42}^{(i)} & k_4 a_{43}^{(i)} + k_5 a_{44}^{(i)} \\ k_4 b_{41}^{(i)} + k_5 b_{42}^{(i)} & k_4 b_{43}^{(i)} + k_5 b_{44}^{(i)} \end{bmatrix} \begin{Bmatrix} \gamma_4 \\ \gamma_5 \end{Bmatrix} \end{aligned} \quad (3.153)$$

In enforcing the continuity of displacements and shear stresses at interlaminar boundaries, the transverse strains across these boundaries are not, in general, continuous. That is

$$B_{k3}^{(i)}(z_j) \neq B_{k3}^{(i+1)}(z_j), \quad i = 1, \dots, N-1; \quad j = 1, \dots, N+1; \quad k = 1, 2, 3. \quad (3.154)$$

Recall that earlier in this chapter, the strain-displacement expressions (Eqns 3.131) were simplified by eliminating the effect of $G_3^{(i)}$ on all other strains. One effect of this simplification is the violation of strain compatibility. These relationships, given by (Saada 1989, p. 90)

$$\frac{\partial^2 e_{jk}}{\partial x_i \partial x_l} + \frac{\partial^2 e_{il}}{\partial x_j \partial x_k} - \frac{\partial^2 e_{ik}}{\partial x_j \partial x_l} - \frac{\partial^2 e_{jl}}{\partial x_i \partial x_k} = 0, \quad (3.155)$$

lead to six non-trivial equations which are the necessary and sufficient conditions for the strain components, e_{ij} , to yield unique displacements for a simply connected region. For example, consider one of the compatibility equations in terms of the Jaumann strains:

$$\frac{1}{2} \frac{\partial^2 B_{33}}{\partial x \partial y} = \frac{\partial}{\partial z} \left(-\frac{\partial B_{12}}{\partial z} + \frac{\partial B_{23}}{\partial x} + \frac{\partial B_{13}}{\partial y} \right). \quad (3.156)$$

To indicate how the simplification of Eq (3.130) affects this equation, consider the transverse shear strain, B_{13} . In Eq (3.156), the term involving B_{13} is

$$\frac{\partial}{\partial z} \left(\frac{\partial B_{13}}{\partial y} \right). \quad (3.157)$$

In the unsimplified strain-displacement relations of Eq (3.130), this term is

$$\frac{\partial}{\partial z} \left(\frac{\partial B_{13}}{\partial y} \right) = \frac{1}{2} [G_{1,yzz} - k_1 G_{1,yz} - k_{61} G_{2,yz} + G_{3,xyz}]. \quad (3.158)$$

But using the simplified kinematics of Eq (3.131), the last term is omitted. The practical impact of this simplification will be addressed in Chapter VII, where the current theory is applied to the finite element analysis of the aircraft tire.

Casting the current theory into finite element form is the topic of the next chapter.

3.8 Summary

The shell theory developed in this chapter attaches a rigidly translated and rotated orthogonal coordinate system to a deformed infinitesimal volume element. The Jaumann stresses and strains, whose components are resolved along the axes of this new orthogonal system, are derived. These stress and strain measures differ from the second-Piola/Green and Cauchy measures, and the differences are described. Particle displacements due to through-the-thickness shear are described in terms of warping functions. The warping functions are cubic (for relating the transverse shear deformation to activity on the reference surface), and the thickness stretch functions are quadratic (for thickness direction displacements) polynomials. The coefficients of these polynomials are found by enforcing certain conditions at the laminar interfaces and the shell bounding surfaces, and the quantities describing these conditions are always related to the behavior at the two-dimensional reference surface. These warping functions preserve the continuity of displacements and through-the-thickness shear stresses across the bonding surfaces. They are also able to represent the direct normal (thickness) strain and hence interlaminar peeling stresses. This is accomplished through enforcing continuity of the direct normal stress at the bonding surfaces and the normal stress-free boundary condition on the shell exterior. Note that the transverse shear stresses are independent of the in-plane strains, while the transverse normal stresses are coupled with them via the constitutive equations (3.139). However, *all* of the strains are coupled through the warping/stretch functions since all of the strains contain these functions, and the coefficients of these functions are themselves functions of the various terms of the strain-displacement relations of Eq (3.131).

Two important simplifications in the theory incorporated by Pai and Palazotto 1995a are worth reiterating: (1) the trapezoidal cross section effect has been ignored, such that the kinematics of Eq (3.117) are not "true" shell kinematics, and (2) the transverse normal stretch function, G_3 of Eqns (3.118), is not coupled to the in-plane strains via the strain displacement relations. The first assumption is a "shallow shell" assumption, while the second is a "thin shell" assumption. Moreover, the current method of finding thickness stretch and shear warping functions does not permit inclusion of either non-zero normal or shear stresses on the bounding surfaces of the shell.

IV. Finite Element Formulation

In this chapter, the theoretical formulation of Chapter III is cast in terms suitable for numerical solution. In fact, the solution to the partial differential equations of the previous chapter are not tractable by classical analytical means, so the *only* recourse is to employ a numerical means of solution. The use of a numerical method of solution, which will involve some sort of “discretization” process, brings with it the consequence that the solution will usually not be exact (though for some special simple cases it may be), but it will, by processing a sufficient number of equations, usually be accurate enough for engineering purposes (Cook et al. 1989, p. 1).

There are a number of possible means, under the wide umbrella of “numerical solution techniques,” that could be employed, but finite element methods lend themselves well to problems that can be expressed in terms of potential energy. Such methods typically involve minimizing a *functional*, which is an integral expression describing the potential energy of a system in a given configuration. The mathematical expressions of Chapter III may be used to develop this potential energy functional, which will then be used to develop the finite element equations.

The finite element formulation presented here is that of Pai and Palazotto (1995a) where, as in the previous chapter, the development is expanded where warranted for the sake of clarity and completeness. The formulation of the two specific finite elements (the 36 DOF and 44 DOF elements) is newly developed here.

The principle of virtual work, which will be used in the finite element development, states (Washizu 1982)

$$\int_0^T (-\delta\Pi + \delta W_{nc})dt = 0 \quad (4.1)$$

where Π and W_{nc} denote the elastic energy and the non-conservative energy due to applied loads¹. The non-conservative energy includes the energy due to surface loads (distributed or concentrated).

The principle of minimum potential energy states that a displacement field satisfying Eq (4.1) does not merely make the total potential energy stationary, but is an *absolute minimum*. This is due to the fact that, for problems involving elastic deformation (i.e., a strain energy density function exists), the strain energy function is a positive definite function of the strain components. (Zienkiewicz 1977, Washizu 1982)

Note that the principle of minimum potential energy is applicable whether or not the load versus deformation relation is linear (Cook et al. 1989, p. 71). Nor must the stress-strain relations be linear (Saada 1989, p. 452). Nevertheless, a caveat is in order. In *unstable* regions of the solution space where snapping or bifurcation of the solution may occur, the claim of positive-definiteness may not be made. For example, during the snapping phenomenon, an increase in displacement is accompanied by a decrease in load. In such regions, the solution found from $\delta\Pi = 0$ cannot be guaranteed to be a global minimum potential energy solution. So, while the theory of Chapter III permits very general descriptions of the initial geometry (configuration) of structures to be analyzed, the analyst must exercise caution in assessing the validity of a finite element result. In particular, if a structure is loaded in such a fashion that snapping or buckling is possible, results in such regions of the solution should be viewed with healthy skepticism. (Note that in some cases, behavior of a single nodal degree of freedom may be used to determine the unstable regions of the solution space (Palazotto et al. 1992).) While recognizing that the potential for such regions exist in the current work, exploring these regions of instability is not a goal of this research.

The development of the elastic energy functional and its first variation is now performed.

¹By letting W consist of both conservative and non-conservative forces, Eq (4.1) is sometimes referred to as the *extended Hamilton principle* (Meirovitch 1967, p. 45)

4.1 Element Independent Formulation

In Chapter III it was stated that the Jaumann stresses and strains are *work conjugate*, that is, the elastic energy, Π , of the structure may be entirely accounted for by integrating the product of the stresses and strains over the entire volume of the structure:

$$\Pi = \frac{1}{2} \sum_{i=1}^N \iiint_V [\mathbf{J}^{(i)}]^T [\mathbf{B}^{(i)}] dV. \quad (4.2)$$

Or, since $[\mathbf{J}^{(i)}] = [\bar{\mathbf{Q}}^{(i)}][\mathbf{B}^{(i)}]$ and $[\bar{\mathbf{Q}}^{(i)}]$ is symmetric,

$$\Pi = \frac{1}{2} \sum_{i=1}^N \iiint_V [\mathbf{B}^{(i)}]^T [\bar{\mathbf{Q}}^{(i)}] [\mathbf{B}^{(i)}] dV. \quad (4.3)$$

The first variation of the potential energy is then found through

$$\begin{aligned} \delta \Pi &= \frac{1}{2} \sum_{i=1}^N \iiint_V \delta [\mathbf{B}^{(i)}]^T [\bar{\mathbf{Q}}^{(i)}] [\mathbf{B}^{(i)}] + [\mathbf{B}^{(i)}]^T [\bar{\mathbf{Q}}^{(i)}] \delta [\mathbf{B}^{(i)}] dV \\ &= \sum_{i=1}^N \iiint_V \delta [\mathbf{B}^{(i)}]^T [\bar{\mathbf{Q}}^{(i)}] [\mathbf{B}^{(i)}] dV, \end{aligned} \quad (4.4)$$

where V is the undeformed volume of the shell structure and (i) refers to the value of the function in the i^{th} layer of the laminate. From the strain-displacement relations of Eq (3.131) and the definitions of the shear warping and thickness stretch functions given in Eqns (3.142), (3.118), and (3.153), the terms in the Jaumann strains may be separated into those that depend only on the thickness coordinate, z , and those that do not. For example, consider the direct in-plane strain $B_{11}^{(i)}$. From Eq (3.131), it is seen that

$$B_{11}^{(i)} = (1 + e_1) \cos \gamma_{61} - 1 + z(k_1 - k_1^0) + G_{1,x} - k_5 G_2.$$

But since (Eq 3.142)

$$G_1 = \gamma_5 g_{15}^{(i)} + \gamma_4 g_{14}^{(i)}, \quad \text{and} \quad G_2 = \gamma_4 g_{24}^{(i)} + \gamma_5 g_{25}^{(i)},$$

it is evident that

$$B_{11}^{(i)} = (1 + e_1) \cos \gamma_{61} - 1 + z(k_1 - k_1^0) + \gamma_{5,x} g_{15}^{(i)} + \gamma_{4,x} g_{14}^{(i)} - k_5 (\gamma_4 g_{24}^{(i)} + \gamma_5 g_{25}^{(i)}). \quad (4.5)$$

Note that the terms $(1 + e_1) \cos \gamma_{61}$, $k_1 - k_1^0$, γ_4 , $\gamma_{4,x}$, γ_5 , and $\gamma_{5,x}$ are *reference surface* quantities, while $g_{15}^{(i)}$, $g_{14}^{(i)}$, $g_{24}^{(i)}$, and $g_{25}^{(i)}$, are dependent only upon the thickness coordinate z . In this manner, one may write all of the strains as the product of a matrix, $[\mathbf{S}^{(i)}]$, whose values depend solely on the thickness coordinate, z , and a vector, $\{\psi\}$, of displacement quantities at the reference surface, and are hence functions of only x and y :

$$\begin{Bmatrix} B_{11}^{(i)} \\ B_{22}^{(i)} \\ B_{33}^{(i)} \\ 2B_{12}^{(i)} \\ 2B_{23}^{(i)} \\ 2B_{13}^{(i)} \end{Bmatrix} = \begin{bmatrix} 1 & 0 & 0 & z & 0 & 0 & g_{14}^{(i)} & 0 & g_{15}^{(i)} & 0 & -k_5 g_{24}^{(i)} & -k_5 g_{25}^{(i)} \\ 0 & 1 & 0 & 0 & z & 0 & 0 & g_{24}^{(i)} & 0 & g_{25}^{(i)} & k_4 g_{14}^{(i)} & k_4 g_{15}^{(i)} \\ g_{30}^{(i)} & g_{31}^{(i)} & g_{32}^{(i)} & g_{33}^{(i)} & g_{34}^{(i)} & g_{35}^{(i)} & g_{36}^{(i)} & g_{37}^{(i)} & g_{38}^{(i)} & g_{39}^{(i)} & g_{51}^{(i)} & g_{61}^{(i)} \\ 0 & 0 & 1 & 0 & 0 & z & g_{24}^{(i)} & g_{14}^{(i)} & g_{25}^{(i)} & g_{15}^{(i)} & g_{52}^{(i)} & g_{62}^{(i)} \\ 0 & 0 & 0 & 0 & 0 & 0 & 0 & 0 & 0 & 0 & g_{53}^{(i)} & g_{63}^{(i)} \\ 0 & 0 & 0 & 0 & 0 & 0 & 0 & 0 & 0 & 0 & g_{54}^{(i)} & g_{64}^{(i)} \end{bmatrix} \begin{Bmatrix} \psi_1 \\ \psi_2 \\ \psi_3 \\ \psi_4 \\ \psi_5 \\ \psi_6 \\ \psi_7 \\ \psi_8 \\ \psi_9 \\ \psi_{10} \\ \psi_{11} \\ \psi_{12} \end{Bmatrix}, \quad (4.6a)$$

or

$$\{\mathbf{B}^{(i)}\} = [\mathbf{S}^{(i)}] \{\psi\}, \quad (4.6b)$$

$\begin{matrix} 6 \times 1 & 6 \times 12 & 12 \times 1 \end{matrix}$

where the elements of $\{\psi\}$ are given by

$$\begin{aligned}
\psi_1 &= (1 + e_1) \cos \gamma_{61} - 1, & \psi_5 &= k_2 - k_2^0, & \psi_9 &= \gamma_{5,x}, \\
\psi_2 &= (1 + e_2) \cos \gamma_{62} - 1, & \psi_6 &= k_6 - k_6^0, & \psi_{10} &= \gamma_{5,y}, \\
\psi_3 &= (1 + e_1) \sin \gamma_{61} + (1 + e_2) \sin \gamma_{62}, & \psi_7 &= \gamma_{4,x}, & \psi_{11} &= \gamma_4, \\
\psi_4 &= k_1 - k_1^0, & \psi_8 &= \gamma_{4,y}, & \psi_{12} &= \gamma_5.
\end{aligned} \tag{4.7}$$

The values of the shear warping and thickness stretch functions, $g_{kl}^{(i)}$, are

$$g_{51}^{(i)} = k_4 g_{41}^{(i)} + k_5 g_{42}^{(i)}, \quad g_{52}^{(i)} = k_5 g_{14}^{(i)} - k_4 g_{24}^{(i)} \tag{4.8a}$$

$$g_{61}^{(i)} = k_4 g_{43}^{(i)} + k_5 g_{44}^{(i)}, \quad g_{62}^{(i)} = k_5 g_{15}^{(i)} - k_4 g_{25}^{(i)}, \tag{4.8b}$$

$$g_{3j}^{(i)} \equiv a_{3j}^{(i)} + 2b_{3j}^{(i)}z, \quad j = 0, 1, \dots, 9; \quad g_{4j}^{(i)} \equiv a_{4j}^{(i)} + 2b_{4j}^{(i)}z, \quad j = 1, \dots, 4 \tag{4.9}$$

and

$$g_{53}^{(i)} = g_{24,z}^{(i)} - (k_2 g_{24} + k_{62} g_{14}), \quad g_{63}^{(i)} = g_{25,z}^{(i)} - (k_2 g_{25} + k_{62} g_{15}) \tag{4.10a}$$

$$g_{54}^{(i)} = g_{14,z}^{(i)} - (k_{61} g_{24} + k_1 g_{14}), \quad g_{64}^{(i)} = g_{15,z}^{(i)} - (k_{61} g_{25} + k_1 g_{15}) \tag{4.10b}$$

Hence one may write Eq (4.4) as

$$\delta \Pi = \sum_{i=1}^N \iiint_V \delta \{\psi\}^T [\mathbf{S}^{(i)}]^T [\bar{\mathbf{Q}}^{(i)}] [\mathbf{S}^{(i)}] \{\psi\} dV. \tag{4.11}$$

Now, by noticing that the quantity $[\mathbf{S}^{(i)}]^T [\bar{\mathbf{Q}}^{(i)}] [\mathbf{S}^{(i)}]$ is dependent only upon the thickness coordinate, z , one may formulate a new matrix $[\Phi]$, such that

$$[\Phi]_{12 \times 12} = \sum_{i=1}^N \int_{z_i}^{z_{i+1}} [\mathbf{S}^{(i)}]_{12 \times 6}^T [\bar{\mathbf{Q}}^{(i)}]_{6 \times 6} [\mathbf{S}^{(i)}]_{6 \times 12} dz. \tag{4.12}$$

Here, $[\Phi]$ is a 12×12 symmetric matrix. In this manner one may “integrate out” all of the quantities that are thickness dependent, and one may write a new expression representing the first variation of the potential energy as

$$\delta\Pi = \iint \delta\{\psi\}^T [\Phi] \{\psi\} dx dy, \quad (4.13)$$

which is an integral over the *surface* described by coordinates x and y . Note that the integration through the thickness is exact, since the integrand is a polynomial in z of known order, $\mathcal{O}(z^6)$, the use of fourth order Gauss quadrature yields an exact solution (Cook et al. 1989, p. 172).

In finding an expression for $\delta\{\psi\}$ of Eq (4.13), one needs to find expressions for each of the quantities used in expressing the vector $\{\psi\}$ of Eq (4.7). Beginning with the stretches, e_1 and e_2 of Eqns (3.74), it is seen that

$$(1 + e_1)^2 = (1 + u_{,x} - v k_5^0 + w k_1^0)^2 + (v_{,x} + u k_5^0 + w k_{61}^0)^2 + (w_{,x} - u k_1^0 - v k_{61}^0)^2 \quad (4.14a)$$

$$(1 + e_2)^2 = (u_{,y} - v k_4^0 + w k_{62}^0)^2 + (1 + v_{,y} + u k_4^0 + w k_2^0)^2 + (w_{,y} - u k_{62}^0 - v k_2^0)^2. \quad (4.14b)$$

Now define t_{ij} such that

$$t_{11} = 1 + u_{,x} - v k_5^0 + w k_1^0, \quad t_{12} = v_{,x} + u k_5^0 + w k_{61}^0, \quad t_{13} = w_{,x} - u k_1^0 - v k_{61}^0 \quad (4.15a)$$

$$t_{21} = u_{,y} - v k_4^0 + w k_{62}^0, \quad t_{22} = 1 + v_{,y} + u k_4^0 + w k_2^0, \quad t_{23} = w_{,y} - u k_{62}^0 - v k_2^0, \quad (4.15b)$$

such that Eqns (4.14) become

$$(1 + e_1)^2 = t_{11}^2 + t_{12}^2 + t_{13}^2 \quad (4.16a)$$

$$(1 + e_2)^2 = t_{21}^2 + t_{22}^2 + t_{23}^2. \quad (4.16b)$$

Taking the variation of Eqns (4.16) results in

$$2(1 + e_1) \delta e_1 = 2t_{11} \delta t_{11} + 2t_{12} \delta t_{12} + 2t_{13} \delta t_{13} \quad (4.17a)$$

$$2(1 + e_2) \delta e_2 = 2t_{21} \delta t_{21} + 2t_{22} \delta t_{22} + 2t_{23} \delta t_{23}. \quad (4.17b)$$

From Eqns (4.15) and Eqns (3.77) one may write the relationship

$$\frac{t_{(k)l}}{(1 + e_{(k)})} = \hat{T}_{kl} \quad (\text{no sum on } k), \quad (4.18)$$

where, for example,

$$\hat{T}_{11} = \frac{t_{11}}{1 + e_1} = \frac{1 + u_{,x} - vk_5^0 + wk_1^0}{1 + e_1}. \quad (4.19)$$

Dividing Eqns (4.17) through by $2(1 + e_k)$ and using Eq (4.18) yields the expressions for the variation of the stretches, e_1 and e_2 :

$$\delta e_1 = \hat{T}_{11} \delta t_{11} + \hat{T}_{12} \delta t_{12} + \hat{T}_{13} \delta t_{13} \quad (4.20a)$$

$$\delta e_2 = \hat{T}_{21} \delta t_{21} + \hat{T}_{22} \delta t_{22} + \hat{T}_{23} \delta t_{23}. \quad (4.20b)$$

The variations of the t_{ij} , are (from Eqs 4.15, with k_1^0 , k_2^0 , k_4^0 , k_5^0 , k_{61}^0 , and k_{62}^0 constant)

$$\delta t_{11} = \delta(1 + u_{,x} - vk_5^0 + wk_1^0) = \delta u_{,x} - k_5^0 \delta v + k_1^0 \delta w \quad (4.21a)$$

$$\delta t_{12} = \delta(v_{,x} + uk_5^0 + wk_{61}^0) = \delta v_{,x} + k_5^0 \delta u + k_{61}^0 \delta w \quad (4.21b)$$

$$\delta t_{13} = \delta(w_{,x} - uk_1^0 - vk_{61}^0) = \delta w_{,x} - k_1^0 \delta u - k_{61}^0 \delta v \quad (4.21c)$$

$$\delta t_{21} = \delta(u_{,y} - vk_4^0 + wk_{62}^0) = \delta u_{,y} - k_4^0 \delta v + k_{62}^0 \delta w \quad (4.21d)$$

$$\delta t_{22} = \delta(1 + v_{,y} + uk_4^0 + wk_2^0) = \delta v_{,y} + k_4^0 \delta u + k_2^0 \delta w \quad (4.21e)$$

$$\delta t_{23} = \delta(w_{,y} - uk_{62}^0 - vk_2^0) = \delta w_{,y} - k_{62}^0 \delta u - k_2^0 \delta v \quad (4.21f)$$

The variation of the in-plane shear rotation angle γ_6 is found by taking the variation of Eq (3.80), repeated here in the form of

$$\sin \gamma_6 = \hat{\mathbf{i}}_1 \cdot \hat{\mathbf{i}}_2 \quad (4.22a)$$

$$= \hat{T}_{11}\hat{T}_{21} + \hat{T}_{12}\hat{T}_{22} + \hat{T}_{13}\hat{T}_{23} \quad (4.22b)$$

$$\delta(\sin \gamma_6) = \delta \left(\hat{T}_{11}\hat{T}_{21} + \hat{T}_{12}\hat{T}_{22} + \hat{T}_{13}\hat{T}_{23} \right) \quad (4.22c)$$

$$\delta \gamma_6 \cos \gamma_6 = \hat{T}_{11} \delta \hat{T}_{21} + \hat{T}_{12} \delta \hat{T}_{22} + \hat{T}_{13} \delta \hat{T}_{23} + \delta \hat{T}_{11} \hat{T}_{21} + \delta \hat{T}_{12} \hat{T}_{22} + \delta \hat{T}_{13} \hat{T}_{23} \quad (4.22d)$$

$$= \hat{T}_{11} \delta \left(\frac{t_{21}}{1+e_2} \right) + \hat{T}_{12} \delta \left(\frac{t_{22}}{1+e_2} \right) + \hat{T}_{13} \delta \left(\frac{t_{23}}{1+e_2} \right) + \delta \left(\frac{t_{11}}{1+e_1} \right) \hat{T}_{21} + \delta \left(\frac{t_{12}}{1+e_1} \right) \hat{T}_{22} + \delta \left(\frac{t_{13}}{1+e_1} \right) \hat{T}_{23} \quad (4.22e)$$

Taking the variation of the parenthetical quantities yields

$$\begin{aligned} \delta \gamma_6 \cos \gamma_6 = & \hat{T}_{11} \left(\frac{(1+e_2) \delta t_{21} - t_{21} \delta e_2}{(1+e_2)^2} \right) + \hat{T}_{12} \left(\frac{(1+e_2) \delta t_{22} - t_{22} \delta e_2}{(1+e_2)^2} \right) + \\ & \hat{T}_{13} \left(\frac{(1+e_2) \delta t_{23} - t_{23} \delta e_2}{(1+e_2)^2} \right) + \left(\frac{(1+e_1) \delta t_{11} - t_{11} \delta e_1}{(1+e_1)^2} \right) \hat{T}_{21} + \\ & \left(\frac{(1+e_1) \delta t_{12} - t_{12} \delta e_1}{(1+e_1)^2} \right) \hat{T}_{22} + \left(\frac{(1+e_1) \delta t_{13} - t_{13} \delta e_1}{(1+e_1)^2} \right) \hat{T}_{23}, \end{aligned} \quad (4.23)$$

or

$$\begin{aligned} \delta \gamma_6 = & \frac{1}{\cos \gamma_6 (1+e_2)} \left[\hat{T}_{11} \left(\frac{(1+e_2) \delta t_{21} - t_{21} \delta e_2}{(1+e_2)} \right) + \right. \\ & \left. \hat{T}_{12} \left(\frac{(1+e_2) \delta t_{22} - t_{22} \delta e_2}{(1+e_2)} \right) + \hat{T}_{13} \left(\frac{(1+e_2) \delta t_{23} - t_{23} \delta e_2}{(1+e_2)} \right) \right] + \\ & \frac{1}{\cos \gamma_6 (1+e_1)} \left[\left(\frac{(1+e_1) \delta t_{11} - t_{11} \delta e_1}{(1+e_1)} \right) \hat{T}_{21} + \right. \\ & \left. \left(\frac{(1+e_1) \delta t_{12} - t_{12} \delta e_1}{(1+e_1)} \right) \hat{T}_{22} + \left(\frac{(1+e_1) \delta t_{13} - t_{13} \delta e_1}{(1+e_1)} \right) \hat{T}_{23} \right]. \end{aligned} \quad (4.24)$$

Now use Eq (4.18) to get

$$\begin{aligned}\delta\gamma_6 = & \frac{1}{\cos \gamma_6 (1 + e_2)} \left[\hat{T}_{11} (\delta t_{21} - \hat{T}_{21} \delta e_2) + \right. \\ & \left. \hat{T}_{12} (\delta t_{22} - \hat{T}_{22} \delta e_2) + \hat{T}_{13} (\delta t_{23} - \hat{T}_{23} \delta e_2) \right] + \\ & \frac{1}{\cos \gamma_6 (1 + e_1)} \left[(\delta t_{11} - \hat{T}_{11} \delta e_1) \hat{T}_{21} + \right. \\ & \left. (\delta t_{12} - \hat{T}_{12} \delta e_1) \hat{T}_{22} + (\delta t_{13} - \hat{T}_{13} \delta e_1) \hat{T}_{23} \right] \quad (4.25a)\end{aligned}$$

$$\begin{aligned}= & \frac{1}{\cos \gamma_6 (1 + e_2)} \left[(\hat{T}_{11} \delta t_{21} - \hat{T}_{11} \hat{T}_{21} \delta e_2) + \right. \\ & \left. (\hat{T}_{12} \delta t_{22} - \hat{T}_{12} \hat{T}_{22} \delta e_2) + (\hat{T}_{13} \delta t_{23} - \hat{T}_{13} \hat{T}_{23} \delta e_2) \right] + \\ & \frac{1}{\cos \gamma_6 (1 + e_1)} \left[(\hat{T}_{21} \delta t_{11} - \hat{T}_{21} \hat{T}_{11} \delta e_1) + \right. \\ & \left. (\hat{T}_{22} \delta t_{12} - \hat{T}_{22} \hat{T}_{12} \delta e_1) + (\hat{T}_{23} \delta t_{13} - \hat{T}_{23} \hat{T}_{13} \delta e_1) \right]. \quad (4.25b)\end{aligned}$$

Recalling from Eq (3.80) that $\sin \gamma_6 = \hat{T}_{11} \hat{T}_{21} + \hat{T}_{12} \hat{T}_{22} + \hat{T}_{13} \hat{T}_{23}$, terms are grouped as follows:

$$\begin{aligned}\delta\gamma_6 = & \frac{1}{\cos \gamma_6 (1 + e_2)} \left[\hat{T}_{11} \delta t_{21} + \right. \\ & \left. \hat{T}_{12} \delta t_{22} + \hat{T}_{13} \delta t_{23} - (\hat{T}_{11} \hat{T}_{21} + \hat{T}_{12} \hat{T}_{22} + \hat{T}_{13} \hat{T}_{23}) \delta e_2 \right] + \\ & \frac{1}{\cos \gamma_6 (1 + e_1)} \left[\hat{T}_{21} \delta t_{11} + \right. \\ & \left. \hat{T}_{22} \delta t_{12} + \hat{T}_{23} \delta t_{13} - (\hat{T}_{21} \hat{T}_{11} + \hat{T}_{22} \hat{T}_{12} + \hat{T}_{23} \hat{T}_{13}) \delta e_1 \right] \quad (4.26a)\end{aligned}$$

$$\begin{aligned}= & \frac{1}{\cos \gamma_6 (1 + e_2)} \left[\hat{T}_{11} \delta t_{21} + \hat{T}_{12} \delta t_{22} + \hat{T}_{13} \delta t_{23} - \sin \gamma_6 \delta e_2 \right] + \\ & \frac{1}{\cos \gamma_6 (1 + e_1)} \left[\hat{T}_{21} \delta t_{11} + \hat{T}_{22} \delta t_{12} + \hat{T}_{23} \delta t_{13} - \sin \gamma_6 \delta e_1 \right] \quad (4.26b)\end{aligned}$$

Now recall that

$$\delta e_1 = \hat{T}_{11} \delta t_{11} + \hat{T}_{12} \delta t_{12} + \hat{T}_{13} \delta t_{13} \quad (4.20a)$$

$$\delta e_2 = \hat{T}_{21} \delta t_{21} + \hat{T}_{22} \delta t_{22} + \hat{T}_{23} \delta t_{23}. \quad (4.20b)$$

Substituting Eqns (4.20a) and (4.20b) into Eq (4.26b) one obtains

$$\begin{aligned} \delta\gamma_6 = & \frac{(\hat{T}_{21} - \sin \gamma_6 \hat{T}_{11})\delta t_{11} + (\hat{T}_{22} - \sin \gamma_6 \hat{T}_{12})\delta t_{12} + (\hat{T}_{23} - \sin \gamma_6 \hat{T}_{13})\delta t_{13}}{\cos \gamma_6(1 + e_1)} \\ & + \frac{(\hat{T}_{11} - \sin \gamma_6 \hat{T}_{21})\delta t_{21} + (\hat{T}_{12} - \sin \gamma_6 \hat{T}_{22})\delta t_{22} + (\hat{T}_{13} - \sin \gamma_6 \hat{T}_{23})\delta t_{23}}{\cos \gamma_6(1 + e_2)} \end{aligned} \quad (4.27)$$

Now having the variation of γ_6 , one is able to calculate the variations of its two components, γ_{61} and γ_{62} as follows. Taking the variation of Eq (3.86) and using the fact that $\delta\gamma_6 = \delta\gamma_{61} + \delta\gamma_{62}$, one obtains

$$(1 + e_1) \sin \gamma_{61} = (1 + e_2) \sin \gamma_{62} \quad (3.86)$$

$$(1 + e_1) \delta(\sin \gamma_{61}) + \delta(1 + e_1) \sin \gamma_{61} = (1 + e_2) \delta(\sin \gamma_{62}) + \delta(1 + e_2) \sin \gamma_{62} \quad (4.28a)$$

$$(1 + e_1) \delta\gamma_{61}(\cos \gamma_{61}) + \delta e_1 \sin \gamma_{61} = (1 + e_2) \delta\gamma_{62}(\cos \gamma_{62}) + \delta e_2 \sin \gamma_{62} \quad (4.28b)$$

Now recall

$$\delta\gamma_6 = \delta\gamma_{61} + \delta\gamma_{62}$$

or

$$\delta\gamma_{62} = \delta\gamma_6 - \delta\gamma_{61}$$

resulting in

$$(1 + e_1) \delta\gamma_{61}(\cos \gamma_{61}) + \delta e_1 \sin \gamma_{61} = (1 + e_2) (\delta\gamma_6 - \delta\gamma_{61}) (\cos \gamma_{62}) + \delta e_2 \sin \gamma_{62}. \quad (4.29)$$

Solving for γ_{61} results in

$$\delta\gamma_{61} = \frac{(1 + e_2) \cos \gamma_{62} \delta\gamma_6 - \sin \gamma_{61} \delta e_1 + \sin \gamma_{62} \delta e_2}{(1 + e_1) \cos \gamma_{61} + (1 + e_2) \cos \gamma_{62}}. \quad (4.30a)$$

In an analogous manner, $\delta\gamma_{62}$ is found to be

$$\delta\gamma_{62} = \frac{(1 + e_1) \cos \gamma_{61} \delta\gamma_6 + \sin \gamma_{61} \delta e_1 - \sin \gamma_{62} \delta e_2}{(1 + e_1) \cos \gamma_{61} + (1 + e_2) \cos \gamma_{62}}. \quad (4.30b)$$

Expressions for the variations of the in-plane stretches, e_1 and e_2 , and for the in-plane shear rotation angles, γ_6 , γ_{61} , and γ_{62} have now been formed. One may now formulate the variation of the *deformed* curvatures (again, the *undeformed* curvatures are constant, based on the undeformed geometry, and so have no variation). Since finite rotations in space are not true vectorial quantities (Nygård and Bergan 1989, p. 313), the concept of orthogonal virtual rotations (Pai and Nayfeh 1991) is used. First, one notes that the variations of the unit vectors \mathbf{i}_k are caused by the virtual (and infinitesimal) rotations, $\delta\theta_i$, of the shell element about three orthogonal axes. This may be expressed as

$$\delta \{\mathbf{i}_{123}\} = [\delta\theta] \{\mathbf{i}_{123}\}, \quad [\delta\theta] \equiv \begin{bmatrix} 0 & \delta\theta_3 & -\delta\theta_2 \\ -\delta\theta_3 & 0 & \delta\theta_1 \\ \delta\theta_2 & -\delta\theta_1 & 0 \end{bmatrix} \quad (4.31)$$

where $\delta\theta_1$, $\delta\theta_2$, and $\delta\theta_3$ are the virtual rigid-body rotations of the shell element with respect to the axes ξ , η , and ζ , respectively. As an example, consider the variation of \mathbf{i}_3 , depicted in Figure 4.1. In the figure, the variation $\delta\mathbf{i}_3$ is shown to be a vector; the components of which are generated by two infinitesimal rotations about the ξ and η axes.

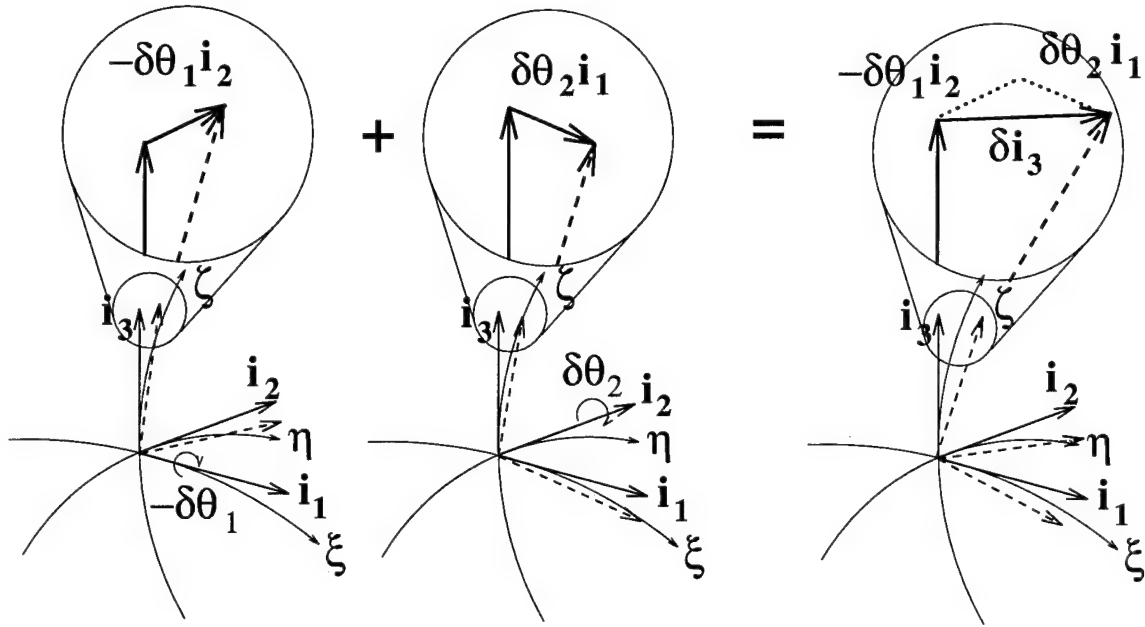


Figure 4.1 The variation of unit vector \mathbf{i}_3 , shown as the sum of two infinitesimal rotations

Note that Eq (4.31) is the matrix representation of the cross product

$$\delta \mathbf{i}_{123} = \mathbf{i}_{123} \times \delta \theta \quad (4.32)$$

where $\delta \theta = \{\delta \theta_1, \delta \theta_2, \delta \theta_3\}^T$. This cross product reflects the fact that an infinitesimal change in direction of a unit vector, say \mathbf{i}_1 , can be expressed as the sum of two virtual rotations, $\delta \theta_2$ and $\delta \theta_3$, about the two other unit vectors. This dovetails with the argument used in defining the curvatures of Eq (3.66). Recall from Figure 3.6 that the derivative, or change in direction of, a unit vector may be described in terms of infinitesimal rotations about the other two unit vectors mutually perpendicular to it. In the same way, one may note that the $\delta \theta_i$ are infinitesimal and mutually perpendicular rotations and hence they are vector quantities. Now these principles are used to find the variations of the deformed curvatures of Eqns (3.113). The variation δk_1 is used as an example, as all of the other variations of curvature are found similarly.

Recall (Eq 3.113a)

$$k_1 \equiv -\frac{\partial \mathbf{i}_1}{\partial x} \cdot \mathbf{i}_3.$$

Hence its variation is given by

$$\delta k_1 = -\frac{\partial \delta \mathbf{i}_1}{\partial x} \cdot \mathbf{i}_3 - \frac{\partial \mathbf{i}_1}{\partial x} \cdot \delta \mathbf{i}_3. \quad (4.33a)$$

Substituting Eqns (4.31) into the above yields

$$\delta k_1 = -\frac{\partial}{\partial x} (\delta \theta_3 \mathbf{i}_2 - \delta \theta_2 \mathbf{i}_3) \cdot \mathbf{i}_3 - \frac{\partial \mathbf{i}_1}{\partial x} \cdot \delta \mathbf{i}_3. \quad (4.33b)$$

Using the deformed curvature matrices of Eqns (3.111), and (3.112), one may write

$$\begin{aligned} \delta k_1 = & \left(-\frac{\partial \delta \theta_3}{\partial x} \mathbf{i}_2 - \delta \theta_3 (-k_5 \mathbf{i}_1 - k_{61} \mathbf{i}_3) + \frac{\partial \delta \theta_2}{\partial x} \mathbf{i}_3 + \delta \theta_2 (k_1 \mathbf{i}_1 + k_{61} \mathbf{i}_2) \right) \cdot \mathbf{i}_3 \\ & - (k_5 \mathbf{i}_2 - k_1 \mathbf{i}_3) \cdot (\delta \theta_2 \mathbf{i}_1 - \delta \theta_1 \mathbf{i}_2) \end{aligned} \quad (4.33c)$$

$$= \left(-\delta \theta_3 (-k_{61}) + \frac{\partial \delta \theta_2}{\partial x} \right) + (k_5)(\delta \theta_1), \quad (4.33d)$$

or

$$\delta k_1 = \frac{\partial}{\partial x} \delta \theta_2 - (-k_5 \delta \theta_1 - k_{61} \delta \theta_3). \quad (4.33e)$$

Pai and Nayfeh (1991,1994b) used this approach for the remaining undeformed curvatures to show that

$$\begin{Bmatrix} -\delta k_{61} \\ \delta k_1 \\ \delta k_5 \end{Bmatrix} = \frac{\partial}{\partial x} \begin{Bmatrix} \delta \theta_1 \\ \delta \theta_2 \\ \delta \theta_3 \end{Bmatrix} - [K_1] \begin{Bmatrix} \delta \theta_1 \\ \delta \theta_2 \\ \delta \theta_3 \end{Bmatrix} \quad (4.34a)$$

$$\begin{Bmatrix} -\delta k_2 \\ \delta k_{62} \\ \delta k_4 \end{Bmatrix} = \frac{\partial}{\partial y} \begin{Bmatrix} \delta \theta_1 \\ \delta \theta_2 \\ \delta \theta_3 \end{Bmatrix} - [K_2] \begin{Bmatrix} \delta \theta_1 \\ \delta \theta_2 \\ \delta \theta_3 \end{Bmatrix} \quad (4.34b)$$

At present, the unknowns in this equation are the variations of the rotation angles, $\delta\theta_k$. Defining these variations requires the variations of the unit vectors \mathbf{i}_1 and \mathbf{i}_2 . These are found as follows. Using Eqns (3.76) and the relationship of Eq (4.18), one has

$$\mathbf{i}_1 = \hat{T}_{11}\mathbf{j}_1 + \hat{T}_{12}\mathbf{j}_2 + \hat{T}_{13}\mathbf{j}_3 \quad (3.76)$$

$$= \frac{1}{(1+e_1)} (t_{11}\mathbf{j}_1 + t_{12}\mathbf{j}_2 + t_{13}\mathbf{j}_3). \quad (4.35)$$

So the variation is

$$\delta\mathbf{i}_1 = \delta \left[\frac{1}{(1+e_1)} (t_{11}\mathbf{j}_1 + t_{12}\mathbf{j}_2 + t_{13}\mathbf{j}_3) \right] \quad (4.36a)$$

$$= \frac{1}{(1+e_1)} \delta (t_{11}\mathbf{j}_1 + t_{12}\mathbf{j}_2 + t_{13}\mathbf{j}_3) + \delta \left[\frac{1}{(1+e_1)} \right] (t_{11}\mathbf{j}_1 + t_{12}\mathbf{j}_2 + t_{13}\mathbf{j}_3) \quad (4.36b)$$

$$= \frac{1}{(1+e_1)} (\delta t_{11}\mathbf{j}_1 + \delta t_{12}\mathbf{j}_2 + \delta t_{13}\mathbf{j}_3) - \frac{\delta e_1}{(1+e_1)^2} (t_{11}\mathbf{j}_1 + t_{12}\mathbf{j}_2 + t_{13}\mathbf{j}_3) \quad (4.36c)$$

$$= \frac{1}{(1+e_1)} (\delta t_{11}\mathbf{j}_1 + \delta t_{12}\mathbf{j}_2 + \delta t_{13}\mathbf{j}_3) - \frac{\delta e_1}{(1+e_1)} \mathbf{i}_1 \quad (4.36d)$$

$$= \frac{1}{(1+e_1)} (\delta t_{11}\mathbf{j}_1 + \delta t_{12}\mathbf{j}_2 + \delta t_{13}\mathbf{j}_3 - \delta e_1 \mathbf{i}_1). \quad (4.36e)$$

The derivation of $\delta\mathbf{i}_2$ is virtually identical, so in summary,

$$\delta\mathbf{i}_1 = \frac{1}{1+e_1} (\mathbf{j}_1\delta t_{11} + \mathbf{j}_2\delta t_{12} + \mathbf{j}_3\delta t_{13} - \mathbf{i}_1\delta e_1) \quad (4.37a)$$

$$\delta\mathbf{i}_2 = \frac{1}{1+e_2} (\mathbf{j}_1\delta t_{21} + \mathbf{j}_2\delta t_{22} + \mathbf{j}_3\delta t_{23} - \mathbf{i}_2\delta e_2). \quad (4.37b)$$

Now one may find the variations of the θ_i . From Eq (4.31) it is evident that

$$\delta\mathbf{i}_2 = -\delta\theta_3\mathbf{i}_1 + \delta\theta_1\mathbf{i}_3, \quad (4.38)$$

so one may write

$$\delta\mathbf{i}_2 \cdot \mathbf{i}_3 = \delta\theta_1. \quad (4.39)$$

But Eqns (3.93a) and (3.93c) describe the relationship between $\{\mathbf{i}_{123}\}$ and $\{\mathbf{i}_{123}\}$ such that

$$\mathbf{i}_2 = -\frac{\sin \gamma_{62}}{\cos \gamma_6} \mathbf{i}_1 + \frac{\cos \gamma_{61}}{\cos \gamma_6} \mathbf{i}_2. \quad (4.40)$$

So

$$\delta \mathbf{i}_2 = -\delta \left(\frac{\sin \gamma_{62}}{\cos \gamma_6} \right) \mathbf{i}_1 - \frac{\sin \gamma_{62}}{\cos \gamma_6} \delta \mathbf{i}_1 + \delta \left(\frac{\cos \gamma_{61}}{\cos \gamma_6} \right) \mathbf{i}_2 + \frac{\cos \gamma_{61}}{\cos \gamma_6} \delta \mathbf{i}_2. \quad (4.41)$$

Substituting the above into Eq (4.39) yields

$$\delta \theta_1 = \left[-\delta \left(\frac{\sin \gamma_{62}}{\cos \gamma_6} \right) \mathbf{i}_1 - \frac{\sin \gamma_{62}}{\cos \gamma_6} \delta \mathbf{i}_1 + \delta \left(\frac{\cos \gamma_{61}}{\cos \gamma_6} \right) \mathbf{i}_2 + \frac{\cos \gamma_{61}}{\cos \gamma_6} \delta \mathbf{i}_2 \right] \cdot \mathbf{i}_3. \quad (4.42)$$

But since $\mathbf{i}_3 \cdot \mathbf{i}_1 = \mathbf{i}_3 \cdot \mathbf{i}_2 = 0$, it is clear that

$$\delta \theta_1 = \delta \mathbf{i}_2 \cdot \mathbf{i}_3 = \frac{\cos \gamma_{61}}{\cos \gamma_6} \delta \mathbf{i}_2 \cdot \mathbf{i}_3 - \frac{\sin \gamma_{62}}{\cos \gamma_6} \delta \mathbf{i}_1 \cdot \mathbf{i}_3. \quad (4.43)$$

Now, from Eqns (4.37), one obtains

$$\delta \mathbf{i}_1 \cdot \mathbf{i}_3 = \frac{1}{1 + e_1} (\mathbf{j}_1 \delta t_{11} + \mathbf{j}_2 \delta t_{12} + \mathbf{j}_3 \delta t_{13} - \mathbf{i}_1 \delta e_1) \cdot \mathbf{i}_3, \quad (4.44)$$

where, again, $\mathbf{i}_3 \cdot \mathbf{i}_1 = 0$ leads to

$$\delta \mathbf{i}_1 \cdot \mathbf{i}_3 = \frac{1}{1 + e_1} (\mathbf{j}_1 \delta t_{11} + \mathbf{j}_2 \delta t_{12} + \mathbf{j}_3 \delta t_{13}) \cdot \mathbf{i}_3. \quad (4.45)$$

From Eq (3.93b), it is seen that

$$\mathbf{i}_3 = T_{31} \mathbf{j}_1 + T_{32} \mathbf{j}_2 + T_{33} \mathbf{j}_3. \quad (4.46)$$

Substituting this into Eq (4.45) gives

$$\begin{aligned}\delta \mathbf{i}_1 \cdot \mathbf{i}_3 &= \frac{1}{1+e_1} (\mathbf{j}_1 \delta t_{11} + \mathbf{j}_2 \delta t_{12} + \mathbf{j}_3 \delta t_{13}) \cdot (T_{31} \mathbf{j}_1 + T_{32} \mathbf{j}_2 + T_{33} \mathbf{j}_3) \\ &= \frac{1}{1+e_1} (T_{31} \delta t_{11} + T_{32} \delta t_{12} + T_{33} \delta t_{13}).\end{aligned}\quad (4.47a)$$

Similar reasoning is used to find

$$\delta \mathbf{i}_2 \cdot \mathbf{i}_3 = \frac{1}{1+e_2} (T_{31} \delta t_{21} + T_{32} \delta t_{22} + T_{33} \delta t_{23}). \quad (4.47b)$$

Substituting Eqns (4.47) into Eq (4.43) yields

$$\begin{aligned}\delta \theta_1 &= \frac{\cos \gamma_{61}}{\cos \gamma_6 (1+e_2)} (T_{31} \delta t_{21} + T_{32} \delta t_{22} + T_{33} \delta t_{23}) \\ &\quad - \frac{\sin \gamma_{62}}{\cos \gamma_6 (1+e_1)} (T_{31} \delta t_{11} + T_{32} \delta t_{12} + T_{33} \delta t_{13}).\end{aligned}\quad (4.48a)$$

In the same way, the variation (virtual rotation) of θ_2 is found to be

$$\begin{aligned}\delta \theta_2 &= -\delta \mathbf{i}_1 \cdot \mathbf{i}_3 = \frac{\sin \gamma_{61}}{\cos \gamma_6} \delta \mathbf{i}_2 \cdot \mathbf{i}_3 - \frac{\cos \gamma_{62}}{\cos \gamma_6} \delta \mathbf{i}_1 \cdot \mathbf{i}_3 \\ &= \frac{\sin \gamma_{61}}{\cos \gamma_6 (1+e_2)} (T_{31} \delta t_{21} + T_{32} \delta t_{22} + T_{33} \delta t_{23}) \\ &\quad - \frac{\cos \gamma_{62}}{\cos \gamma_6 (1+e_1)} (T_{31} \delta t_{11} + T_{32} \delta t_{12} + T_{33} \delta t_{13}).\end{aligned}\quad (4.48b)$$

One finds the variation of θ_3 as follows. From Eq (4.31),

$$\delta \mathbf{i}_1 = \delta \theta_3 \mathbf{i}_2 - \delta \theta_2 \mathbf{i}_3 \quad (4.49a)$$

$$\delta \mathbf{i}_2 = -\delta \theta_3 \mathbf{i}_1 + \delta \theta_1 \mathbf{i}_3. \quad (4.49b)$$

Forming the inner product of the above equations with \mathbf{i}_2 and \mathbf{i}_1 respectively leads to

$$\delta \mathbf{i}_1 \cdot \mathbf{i}_2 = \delta \theta_3 \quad (4.50a)$$

$$\delta \mathbf{i}_2 \cdot \mathbf{i}_1 = -\delta \theta_3. \quad (4.50b)$$

Subtracting Eq (4.50b) from Eq (4.50a) leads to

$$\delta \theta_3 = \frac{1}{2} (\delta \mathbf{i}_1 \cdot \mathbf{i}_2 - \delta \mathbf{i}_2 \cdot \mathbf{i}_1). \quad (4.51)$$

Consider the first term in the parenthesis of Eq (4.51). From Eq (3.93c),

$$\begin{aligned} \delta \mathbf{i}_1 \cdot \mathbf{i}_2 &= \delta \left(\frac{\cos \gamma_{62}}{\cos \gamma_6} \mathbf{i}_1 - \frac{\sin \gamma_{61}}{\cos \gamma_6} \mathbf{i}_2 \right) \cdot \left(-\frac{\sin \gamma_{62}}{\cos \gamma_6} \mathbf{i}_1 + \frac{\cos \gamma_{61}}{\cos \gamma_6} \mathbf{i}_2 \right) \\ &= \left(\delta \frac{\cos \gamma_{62}}{\cos \gamma_6} \mathbf{i}_1 + \frac{\cos \gamma_{62}}{\cos \gamma_6} \delta \mathbf{i}_1 - \delta \frac{\sin \gamma_{61}}{\cos \gamma_6} \mathbf{i}_2 - \frac{\sin \gamma_{61}}{\cos \gamma_6} \delta \mathbf{i}_2 \right) \cdot \left(-\frac{\sin \gamma_{62}}{\cos \gamma_6} \mathbf{i}_1 + \frac{\cos \gamma_{61}}{\cos \gamma_6} \mathbf{i}_2 \right) \\ &= \left(-\frac{\sin \gamma_{62}}{\cos \gamma_6} \delta \frac{\cos \gamma_{62}}{\cos \gamma_6} - \frac{\cos \gamma_{61}}{\cos \gamma_6} \delta \frac{\sin \gamma_{61}}{\cos \gamma_6} \right) + \left(\frac{\sin \gamma_{61} \sin \gamma_{62}}{\cos^2 \gamma_6} \right) (\mathbf{i}_1 \cdot \delta \mathbf{i}_2) \\ &\quad + \left(\frac{\cos \gamma_{61} \cos \gamma_{62}}{\cos^2 \gamma_6} \right) (\mathbf{i}_2 \cdot \delta \mathbf{i}_1). \end{aligned} \quad (4.52a)$$

Likewise, the second term of Eq (4.51) is

$$\begin{aligned} \delta \mathbf{i}_2 \cdot \mathbf{i}_1 &= \left(-\frac{\cos \gamma_{62}}{\cos \gamma_6} \delta \frac{\sin \gamma_{62}}{\cos \gamma_6} - \frac{\sin \gamma_{61}}{\cos \gamma_6} \delta \frac{\cos \gamma_{61}}{\cos \gamma_6} \right) + \left(\frac{\cos \gamma_{61} \cos \gamma_{62}}{\cos^2 \gamma_6} \right) (\mathbf{i}_1 \cdot \delta \mathbf{i}_2) \\ &\quad + \left(\frac{\sin \gamma_{61} \sin \gamma_{62}}{\cos^2 \gamma_6} \right) (\mathbf{i}_2 \cdot \delta \mathbf{i}_1). \end{aligned} \quad (4.52b)$$

Substituting Eqns (4.52) into Eq (4.51) yields

$$\begin{aligned} \delta \theta_3 &= \frac{1}{2} \left\{ \left[-\frac{\sin \gamma_{62}}{\cos \gamma_6} \delta \frac{\cos \gamma_{62}}{\cos \gamma_6} - \frac{\cos \gamma_{61}}{\cos \gamma_6} \delta \frac{\sin \gamma_{61}}{\cos \gamma_6} + \frac{\cos \gamma_{62}}{\cos \gamma_6} \delta \frac{\sin \gamma_{62}}{\cos \gamma_6} + \frac{\sin \gamma_{61}}{\cos \gamma_6} \delta \frac{\cos \gamma_{61}}{\cos \gamma_6} \right] \right. \\ &\quad \left. + \left(\frac{\sin \gamma_{61} \sin \gamma_{62} - \cos \gamma_{61} \cos \gamma_{62}}{\cos^2 \gamma_6} \right) (\mathbf{i}_1 \cdot \delta \mathbf{i}_2) + \left(\frac{\cos \gamma_{61} \cos \gamma_{62} - \sin \gamma_{61} \sin \gamma_{62}}{\cos^2 \gamma_6} \right) (\mathbf{i}_2 \cdot \delta \mathbf{i}_1) \right\}. \end{aligned}$$

(4.53)

Collecting the last two terms of the above leaves

$$\delta \theta_3 = \frac{1}{2} \left\{ \left[-\frac{\sin \gamma_{62}}{\cos \gamma_6} \delta \frac{\cos \gamma_{62}}{\cos \gamma_6} - \frac{\cos \gamma_{61}}{\cos \gamma_6} \delta \frac{\sin \gamma_{61}}{\cos \gamma_6} + \frac{\cos \gamma_{62}}{\cos \gamma_6} \delta \frac{\sin \gamma_{62}}{\cos \gamma_6} + \frac{\sin \gamma_{61}}{\cos \gamma_6} \delta \frac{\cos \gamma_{61}}{\cos \gamma_6} \right] + \frac{1}{\cos^2 \gamma_6} (\sin \gamma_{61} \sin \gamma_{62} - \cos \gamma_{61} \cos \gamma_{62}) (\mathbf{i}_1 \cdot \delta \mathbf{i}_2 - \mathbf{i}_2 \cdot \delta \mathbf{i}_1) \right\}. \quad (4.54)$$

Noting that

$$\sin \gamma_{61} \sin \gamma_{62} - \cos \gamma_{61} \cos \gamma_{62} = -\cos(\gamma_{61} + \gamma_{62}) = -\cos \gamma_6, \quad (4.55)$$

further simplification leads to:

$$\delta \theta_3 = \frac{1}{2} \left\{ \left[-\frac{\sin \gamma_{62}}{\cos \gamma_6} \delta \frac{\cos \gamma_{62}}{\cos \gamma_6} - \frac{\cos \gamma_{61}}{\cos \gamma_6} \delta \frac{\sin \gamma_{61}}{\cos \gamma_6} + \frac{\cos \gamma_{62}}{\cos \gamma_6} \delta \frac{\sin \gamma_{62}}{\cos \gamma_6} + \frac{\sin \gamma_{61}}{\cos \gamma_6} \delta \frac{\cos \gamma_{61}}{\cos \gamma_6} \right] - \frac{1}{\cos \gamma_6} (\mathbf{i}_1 \cdot \delta \mathbf{i}_2 - \mathbf{i}_2 \cdot \delta \mathbf{i}_1) \right\}. \quad (4.56)$$

Expanding each of the four terms in the brackets [] above leads to

$$-\frac{\sin \gamma_{62}}{\cos \gamma_6} \delta \frac{\cos \gamma_{62}}{\cos \gamma_6} = -\frac{\sin \gamma_{62}}{\cos \gamma_6} \left(\frac{-\cos \gamma_6 \delta \gamma_{62} \sin \gamma_{62} + \cos \gamma_{62} \delta \gamma_6 \sin \gamma_6}{\cos^2 \gamma_6} \right) \quad (4.57a)$$

$$-\frac{\cos \gamma_{61}}{\cos \gamma_6} \delta \frac{\sin \gamma_{61}}{\cos \gamma_6} = -\frac{\cos \gamma_{61}}{\cos \gamma_6} \left(\frac{\cos \gamma_6 \delta \gamma_{61} \cos \gamma_{61} + \sin \gamma_{61} \delta \gamma_6 \sin \gamma_6}{\cos^2 \gamma_6} \right) \quad (4.57b)$$

$$\frac{\cos \gamma_{62}}{\cos \gamma_6} \delta \frac{\sin \gamma_{62}}{\cos \gamma_6} = \frac{\cos \gamma_{62}}{\cos \gamma_6} \left(\frac{\cos \gamma_6 \delta \gamma_{62} \cos \gamma_{62} + \sin \gamma_{62} \delta \gamma_6 \sin \gamma_6}{\cos^2 \gamma_6} \right) \quad (4.57c)$$

$$\frac{\sin \gamma_{61}}{\cos \gamma_6} \delta \frac{\cos \gamma_{61}}{\cos \gamma_6} = \frac{\sin \gamma_{61}}{\cos \gamma_6} \left(\frac{-\cos \gamma_6 \delta \gamma_{61} \sin \gamma_{61} + \cos \gamma_{61} \delta \gamma_6 \sin \gamma_6}{\cos^2 \gamma_6} \right) \quad (4.57d)$$

Eqns (4.57a) and (4.57c) sum to

$$-\frac{\sin \gamma_{62}}{\cos \gamma_6} \delta \frac{\cos \gamma_{62}}{\cos \gamma_6} + \frac{\cos \gamma_{62}}{\cos \gamma_6} \delta \frac{\sin \gamma_{62}}{\cos \gamma_6} = \frac{1}{\cos^2 \gamma_6} \delta \gamma_{62}, \quad (4.58a)$$

while Eqns (4.57b) and (4.57d) sum to

$$-\frac{\cos \gamma_{61}}{\cos \gamma_6} \delta \frac{\sin \gamma_{61}}{\cos \gamma_6} + \frac{\sin \gamma_{61}}{\cos \gamma_6} \delta \frac{\cos \gamma_{61}}{\cos \gamma_6} = -\frac{1}{\cos^2 \gamma_6} \delta \gamma_{61}. \quad (4.58b)$$

Substituting Eqns (4.58) into Eq (4.56) yields

$$\delta \theta_3 = \frac{1}{2 \cos^2 \gamma_6} (\delta \gamma_{62} - \delta \gamma_{61}) + \frac{1}{2 \cos \gamma_6} (\delta \mathbf{i}_1 \cdot \mathbf{i}_2 - \delta \mathbf{i}_2 \cdot \mathbf{i}_1). \quad (4.59)$$

The inner product term $(\delta \mathbf{i}_1 \cdot \mathbf{i}_2 - \delta \mathbf{i}_2 \cdot \mathbf{i}_1)$ is now examined. Consider the first half of the term. From Eq (4.37a), it is evident that

$$\delta \mathbf{i}_1 \cdot \mathbf{i}_2 = \frac{1}{1 + e_1} (\mathbf{j}_1 \delta t_{11} + \mathbf{j}_2 \delta t_{12} + \mathbf{j}_3 \delta t_{13} - \mathbf{i}_1 \delta e_1) \cdot \mathbf{i}_2. \quad (4.60)$$

Noting from Eqns (3.76) and (4.22a) that

$$\mathbf{i}_1 = \hat{T}_{11} \mathbf{j}_1 + \hat{T}_{12} \mathbf{j}_2 + \hat{T}_{13} \mathbf{j}_3, \quad \text{and} \quad \sin \gamma_6 = \mathbf{i}_1 \cdot \mathbf{i}_2, \quad (4.61)$$

Eq (4.60) becomes

$$\delta \mathbf{i}_1 \cdot \mathbf{i}_2 = \frac{1}{1 + e_1} (\hat{T}_{21} \delta t_{11} + \hat{T}_{22} \delta t_{12} + \hat{T}_{23} \delta t_{13} - \sin \gamma_6 \delta e_1). \quad (4.62)$$

Substituting Eq (4.20a) for δe_1 into the above and simplifying yields

$$\delta \mathbf{i}_1 \cdot \mathbf{i}_2 = \frac{1}{(1 + e_1)} (\hat{T}_{21} - \sin \gamma_6 \hat{T}_{11}) \delta t_{11} + (\hat{T}_{22} - \sin \gamma_6 \hat{T}_{12}) \delta t_{12} + (\hat{T}_{23} - \sin \gamma_6 \hat{T}_{13}) \delta t_{13} \quad (4.63a)$$

Similarly,

$$\delta \mathbf{i}_2 \cdot \mathbf{i}_1 = \frac{1}{(1 + e_2)} (\hat{T}_{11} - \sin \gamma_6 \hat{T}_{21}) \delta t_{21} + (\hat{T}_{12} - \sin \gamma_6 \hat{T}_{22}) \delta t_{22} + (\hat{T}_{13} - \sin \gamma_6 \hat{T}_{23}) \delta t_{23} \quad (4.63b)$$

Substituting Eqns (4.63) into Eq (4.59) produces

$$\begin{aligned} \delta \theta_3 = & \frac{1}{2 \cos^2 \gamma_6} (\delta \gamma_{62} - \delta \gamma_{61}) \\ & + \frac{1}{2 \cos \gamma_6} \left\{ \left(\frac{1}{(1 + e_1)} (\hat{T}_{21} - \sin \gamma_6 \hat{T}_{11}) \delta t_{11} + (\hat{T}_{22} - \sin \gamma_6 \hat{T}_{12}) \delta t_{12} + (\hat{T}_{23} - \sin \gamma_6 \hat{T}_{13}) \delta t_{13} \right) \right. \\ & \left. - \left(\frac{1}{(1 + e_2)} (\hat{T}_{11} - \sin \gamma_6 \hat{T}_{21}) \delta t_{21} + (\hat{T}_{12} - \sin \gamma_6 \hat{T}_{22}) \delta t_{22} + (\hat{T}_{13} - \sin \gamma_6 \hat{T}_{23}) \delta t_{23} \right) \right\} \quad (4.64) \end{aligned}$$

Note that this result differs from that of Eq (30) of Pai and Palazotto (1995a, p. 3057), in which the coefficient of the $(\delta \gamma_{62} - \delta \gamma_{61})$ term is $\frac{1}{2}$, rather than $\frac{1}{2 \cos^2 \gamma_6}$. This is of no consequence to the finite element formulation given the method of describing $\delta\{\psi\}$ in Eq (4.69). That is, in the process of describing the variation of $\{\psi\}$ for the finite element method, one need never explicitly form the variation of θ_3 via Eq (4.64).

Having now succeeded in formulating the variations of each of the kinematic quantities comprising the vector $\{\psi\}$ of Eq (4.7), and hence the derivatives of these variations as well, they may now be represented in terms of the variations of the *global* displacement variables and their derivatives: δu , δv , δw , $\delta u_{,x}$, $\delta v_{,x}$, $\delta w_{,x}$, $\delta u_{,y}$, $\delta v_{,y}$, $\delta w_{,y}$, $\delta u_{,xx}$, $\delta v_{,xx}$, $\delta w_{,xx}$, $\delta u_{,yy}$, $\delta v_{,yy}$, $\delta w_{,yy}$, $\delta u_{,xy}$, $\delta v_{,xy}$, and $\delta w_{,xy}$.

Development of the finite element formulation is now resumed from Eq (4.13), restated here:

$$\delta \Pi = \iint \delta\{\psi\}^T [\Phi] \{\psi\} dx dy, \quad (4.13)$$

where

$$[\Phi] = \sum_{i=1}^N \int_{z_i}^{z_{i+1}} [\mathbf{S}^{(i)}]^T [\bar{\mathbf{Q}}^{(i)}] [\mathbf{S}^{(i)}] dz. \quad (4.12)$$

At this point in the work of Pai and Palazotto (1995a), a simplification is made: the deformed curvatures, k_i , in $[\mathbf{S}^{(i)}]$ are replaced by their undeformed counterparts, k_i^0 . The validity of this assumption was examined using the problem of Section 6.3, a composite cylindrical shell subjected to a transverse load. Using this simplification resulted in a slightly more flexible structure. The displacement increased a maximum of 0.2% (usually far less) and the stresses and strains increased a maximum of 0.5% (only the transverse shear values were affected to any degree). These results support the use of the simplification for this geometry. It will be examined again in the context of tire inflation in Chapter VII.

A slight detour in formulating the equations is now taken in order to highlight an important difference between the Jaumann and Green/Lagrange formulations. As will be shown, the difference in the two approaches is fundamental and has a major impact on the linearization of the equations and therefore on the finite element formulation as a whole. In particular, it will be shown that because the vector $\{\psi\}$ cannot be separated neatly into linear and nonlinear parts, one must modify the Newton-Raphson linearization scheme to represent the elements of $\{\psi\}$ in the formulation.

First, because the Jaumann strains are defined geometrically, square root terms appear in their terms (see Eq 3.74). This is avoided in the Green/Lagrange formulation, which is derived from the change in *squared* length of an infinitesimal element. The Green's strain formulation allows a simpler form for the variation of the strains. As an example, consider a component of the Green's strain at the reference surface, denoted E_{11}^{ref} (see Palazotto and Dennis 1992, p. 71 for details):

$$E_{11}^{\text{ref}} = u_{,x} + \frac{1}{2} (u_{,x}^2 + v_{,x}^2 + w_{,x}^2) \quad (4.65a)$$

$$= \{\mathbf{L}\}^T \{\mathbf{U}\} + \frac{1}{2} \{\mathbf{U}\}^T [\mathbf{H}] \{\mathbf{U}\}, \quad (4.65b)$$

Where $\{\mathbf{U}\}$ is the displacement gradient vector, $\{\mathbf{L}\}$ is a vector of constants, and $[\mathbf{H}]$ is a symmetric matrix of constants. Note that the strain is neatly separated into a linear and nonlinear part. In addition, the variation of the strain may be written as

$$\delta E_{11}^{\text{ref}} = (\{\mathbf{L}\}^T + \{\mathbf{U}\}^T[\mathbf{H}]) \delta\{\mathbf{U}\} \quad (4.66)$$

In contrast, the corresponding Jaumann strain at the reference surface is

$$B_{11}^{\text{ref}} = (1 + e_1) \cos \gamma_{61} - 1, \quad (4.67)$$

where the expressions for e_1 and γ_{61} are given by Eqns (3.74) and (3.90) respectively. These equations cannot be easily separated into linear and nonlinear parts, as can Eqns (4.65). Nonetheless, as shown in Eq (4.6a), one may write a vector of "strain-like" quantities at the reference surface to define the strains, a vector referred to as $\{\psi\}$. Still, though, this does not facilitate writing the strains as a simple product of matrices and the displacement gradient vector. So in order to take the variation of the strains, one resorts to the following method.

Recall that $\{\psi\}$ is a function of the global displacement quantities and their derivatives. There are 24 such quantities, and they may be arranged in a vector, $\{\mathbf{U}\}$, the *displacement gradient vector*. The variation of the vector $\{\psi\}$, in terms of the elements of the displacement gradient vector, may be written as (see, e.g.², Apostol 1974, p. 353)

$$\begin{aligned} \delta\{\psi\} = & \frac{\partial\psi_1}{\partial U_1}\delta U_1 + \frac{\partial\psi_1}{\partial U_2}\delta U_2 + \frac{\partial\psi_1}{\partial U_3}\delta U_3 + \cdots + \frac{\partial\psi_1}{\partial U_{24}}\delta U_{24} + \\ & \frac{\partial\psi_2}{\partial U_1}\delta U_1 + \frac{\partial\psi_2}{\partial U_2}\delta U_2 + \frac{\partial\psi_2}{\partial U_3}\delta U_3 + \cdots + \frac{\partial\psi_2}{\partial U_{24}}\delta U_{24} + \\ & \vdots \end{aligned}$$

²The reference deals with differentiation and is here extended to the variation, as the rules for both operations are similar. (Differentiation deals with the effect of infinitesimal changes in an independent variable on the dependent variable. The variation deals with the effect of a small variation of a dependent variable upon a function.) See, e.g., Weinstock (1974), Meirovitch (1967).

$$\frac{\partial \psi_{12}}{\partial U_1} \delta U_1 + \frac{\partial \psi_{12}}{\partial U_2} \delta U_2 + \frac{\partial \psi_{12}}{\partial U_3} \delta U_3 + \dots \frac{\partial \psi_{12}}{\partial U_{24}} \delta U_{24} \quad (4.68)$$

or, more compactly,

$$\delta\{\psi\} = [\Psi] \delta\{\mathbf{U}\} \quad (4.69)$$

where the displacement gradient vector, $\{\mathbf{U}\}$, is given by

$$\begin{aligned} \{\mathbf{U}\} = & \{u, u_x, u_y, u_{xx}, u_{xy}, u_{yy}, v, v_x, v_y, v_{xx}, v_{xy}, v_{yy}, \\ & w, w_x, w_y, w_{xx}, w_{xy}, w_{yy}, \gamma_4, \gamma_{4,x}, \gamma_{4,y}, \gamma_5, \gamma_{5,x}, \gamma_{5,y}\}^T, \end{aligned} \quad (4.70)$$

and

$$\Psi_{ij} = \frac{\partial \psi_i}{\partial U_j}. \quad (4.71)$$

The expressions in $[\Psi]$ are complicated and were developed using *Mathematica* for the current work (see Appendix A). Consider the term $\Psi(6, 4)$ as an example of the complexity:

$$\begin{aligned} \Psi(6, 4) &= \partial \psi_6 / \partial U_4 \\ &= \partial (k_6 - k_6^0) / \partial u_{xx} \\ &= \partial (k_{61} + k_{62} - k_{61}^0 - k_{62}^0) / \partial u_{xx} \end{aligned} \quad (4.72)$$

Substituting Eqns (3.113) into the above yields

$$\begin{aligned} \Psi(6, 4) &= \partial (-T_{21,x} T_{31} - T_{22,x} T_{32} - T_{23,x} T_{33} + T_{11} k_{61}^0 - T_{12} k_{61}^0 - T_{13} k_{61}^0 - T_{11,y} T_{31} \\ &\quad - T_{12,y} T_{32} - T_{13,y} T_{33} - T_{21} k_{62}^0 + T_{22} k_{62}^0 + T_{23} k_{62}^0) / \partial u_{xx} \end{aligned} \quad (4.73)$$

The only terms of the above equation that have can be functions of $u_{,xx}$ are those having terms of the form $u_{,x}$, so the above equation is simplified by eliminating all other terms to yield

$$\Psi (6,4) = \partial (-T_{21,x}T_{31} - T_{22,x}T_{32} - T_{23,x}T_{33}) / \partial u_{,xx} \quad (4.74)$$

Using Eqns (3.72), (3.77), (3.80), (3.90)³, and the identities

$$\sin (\tan^{-1} x) = \frac{x}{\sqrt{1+x^2}}, \quad \cos (\sin^{-1} x) = \sqrt{1-x^2}, \quad (4.75)$$

the numerator, $\Psi (6,4)_N$, and denominator, $\Psi (6,4)_D$, of $\Psi (6,4)$ are seen to be

$$\begin{aligned} \Psi (6,4)_N = & c \left(-(ab) + b^2 + d^2 \right) \sqrt{a \left(a^5 - 2a^3b + ab^2 + 3a^2d^2 - bd^2 - 2\sqrt{a}d^2\sqrt{ab-d^2} \right)} \\ & (- (c_3c_5) + c_2c_6) \end{aligned} \quad (4.76a)$$

$$\begin{aligned} \Psi (6,4)_D = & \sqrt{a} \sqrt{(a^3 - ab + d^2)^2} \left(b + \sqrt{ab - d^2} \right) \\ & \sqrt{b \left(a^2b - 2ab^2 + b^3 - ad^2 + 3bd^2 - 2d^2\sqrt{ab - d^2} \right)} \\ & \sqrt{c_2^2c_4^2 + c_3^2c_4^2 - 2c_1c_2c_4c_5 + c_1^2c_5^2 + c_3^2c_5^2 - 2c_1c_3c_4c_6 - 2c_2c_3c_5c_6 + c_1^2c_6^2 + c_2^2c_6^2} \end{aligned} \quad (4.76b)$$

where

$$c_1 = 1 + u_{,x} - vk_5^0 + wk_1^0 \quad (4.77a)$$

$$c_2 = v_{,x} + uk_5^0 + wk_{61}^0 \quad (4.77b)$$

$$c_3 = w_{,x} - uk_1^0 - vk_{61}^0 \quad (4.77c)$$

$$c_4 = u_{,y} - vk_4^0 + wk_{62}^0 \quad (4.77d)$$

$$c_5 = 1 + v_{,y} + uk_4^0 + wk_2^0 \quad (4.77e)$$

³These calculations were carried out using *Mathematica*.

$$c_6 = w_{,y} - u k_{\delta 2}^0 - v k_2^0 \quad (4.77f)$$

$$a = \sqrt{c_1^2 + c_2^2 + c_3^2} \quad (4.77g)$$

$$b = \sqrt{c_4^2 + c_5^2 + c_6^2} \quad (4.77h)$$

$$c = c_1 c_4 + c_2 c_5 + c_3 c_6 \quad (4.77i)$$

$$d = 1/\sqrt{ab} \quad (4.77j)$$

The calculations of the elements of $[\Psi]$ and the elements of $[\Upsilon]$, a second-derivative matrix (developed later as a result of the modified linearization scheme), make up the bulk of the computer code. Note that the displacements u , v , and w and their derivatives are written in terms of the local, undeformed, curvilinear axis system, xyz . The local, orthogonal, deformed axis system is brought into play via the T_{ij} and \hat{T}_{ij} in the elements of the matrix $[\Psi]$.

In Eq (4.69), $\delta\{\psi\}$ was written as $[\Psi]\delta\{U\}$. In a similar fashion, one can write $\{\psi\}$ in terms of the displacement gradient vector, $\{U\}$ as

$$\{\psi\} = [\hat{\Psi}]\{U\}, \quad \text{where} \quad \hat{\Psi}_{ij} = \frac{\psi_i}{24 U_j}. \quad (4.78a)$$

This comes about from the fact that the i^{th} element of $\{\psi\}$ may be written as⁴

$$\psi_i = \frac{1}{24} \frac{\psi_i}{U_j} U_j, \quad j = 1, 2, \dots, 24. \quad (4.78b)$$

Unfortunately, Eq (4.78a) becomes problematic when generating the initial stiffness matrix, where usually both $\{\psi\}$ and $\{U\}$ are the vectors consisting of all zeroes. Also, note that in general $[\hat{\Psi}]$ is not equal to $[\Psi]$. For example, consider $\Psi(6, 4) = \partial\psi_6/\partial U_4$ and $\hat{\Psi}(6, 4) = \psi_6/(24 U_4)$. The terms in $\Psi(6, 4)$ were derived earlier and can easily be seen to be quite different from $\hat{\Psi}(6, 4) =$

⁴For example, $\psi_1 = \frac{1}{24} \left(\frac{\psi_1}{U_1} U_1 + \frac{\psi_1}{U_2} U_2 + \dots + \frac{\psi_1}{U_{24}} U_{24} \right) = \frac{1}{24} (24 \psi_1) = \psi_1$. Note that the factor of 24 is missing from Eq (63) in the work by Pai and Palazotto (1995a, p. 3064).

$(k_{62} - k_{62}^0)/(24 u_{,xx})$. This will lead to an asymmetric stiffness matrix as implied by Eq (4.79), and this undesirable characteristic will be addressed later in this section.

Substituting Eqns (4.69) and (4.78a) into Eq (4.13) yields

$$\delta\Pi = \iint \{\delta\mathbf{U}\}^T [\Psi]^T [\Phi] [\dot{\Psi}] \{\mathbf{U}\} dx dy. \quad (4.79)$$

Before moving on to a specific choice of a finite element, note that the middle three terms of Eq (4.79) represent the 24×24 element-independent stiffness matrix. Its characteristics are described in the next section.

4.2 Element-Independent Stiffnesses and Coupling

The element-independent stiffness matrix (EISM) may be used to represent the strain energy of an element in the vicinity of its current state of deformation in terms of the elements of the displacement gradient vector of Eq (4.70) repeated here:

$$\begin{aligned} \{\mathbf{U}\}_{24 \times 1} = \{ & u, u_{,x}, u_{,y}, u_{,xx}, u_{,xy}, u_{,yy}, v, v_{,x}, v_{,y}, v_{,xx}, v_{,xy}, v_{,yy}, \\ & w, w_{,x}, w_{,y}, w_{,xx}, w_{,xy}, w_{,yy}, \gamma_4, \gamma_{4,x}, \gamma_{4,y}, \gamma_5, \gamma_{5,x}, \gamma_{5,y} \}^T. \end{aligned} \quad (4.70)$$

The strain-energy density is of the form

$$\{\mathbf{U}\}^T [EISM] \{\mathbf{U}\}, \quad (4.80)$$

where the $[EISM]$ is of the form $[\Psi]^T [\Phi] [\Psi]$ (see Eq 4.79), such that non-zero terms in the EISM indicate the strain-energy-producing members of $\{\mathbf{U}\}$. In this section, the "state of deformation" is the initial, undeformed state. The EISM gives some insight into how the deformations of various shell geometries are coupled to each other, with these various geometries having different initial

curvatures. From Eq (4.79), it is seen that the EISM depends on the constitutive make-up of the shell as well, via the $[\Phi]$ matrix. However, in this section, the examination is restricted to coupling due to curvature by examining only isotropic shells.

In the following figures describing the EISMs for several initial configurations, a “.” symbol represents a zero entry in the EISM, a “•” symbol represents a zero element on the diagonal of the matrix, and a “□” represents a non-zero element of the matrix. The numbers 1–24 represent the respective elements of the displacement gradient vector, $\{U\}$ (Eq 4.70).

The entries of the EISM represent something quite different from the entries in the element-dependent stiffness matrix (EDSM). This is most easily seen in the diagonal entries. Note that for geometries with no curvature in the x -direction (the plate and the cylindrical shell of Figures 4.3 and 4.4) there is no stiffness associated with u (entry (1,1)). This is because rigid body displacement in the u -direction is a permissible mode for these geometries. In contrast, this entry for an EDSM is *not* zero, as the diagonal entry represents the force generated in the x direction at the node in question *with all other DOF fixed*.

As curvatures are added, the element-independent matrix becomes more populated as more rigid-body displacements are ruled out. It is also worth noting that the entries of the EISM represent forces associated with infinitesimal movement, which is why a v -displacement rigid-body movement is permissible for the cylindrical shell (a *finite* displacement in the v direction would not be, since deformation would be generated). This is illustrated in Figure 4.2. Figure 4.2(a) attempts to illustrate the movement associated with an infinitesimal displacement of each material point along an arc in its v (tangential) direction. Note that for a sufficiently small (i.e., infinitesimal) displacement, the motion causes no deformation, only a rigid-body movement. In Figure 4.2(b), the effect of finite movement in the v direction of points along the arc is shown. Note that deformation occurs.

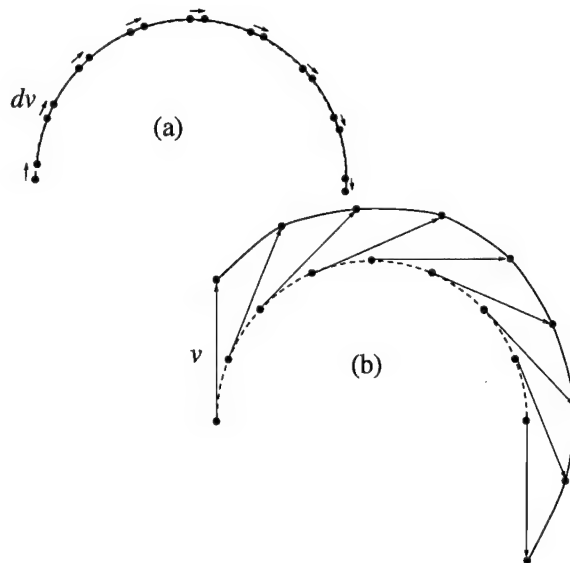


Figure 4.2 (a) Rigid-body movement associated with small v displacements, (b) Deformation associated with finite v displacements

4.2.1 Flat Plate. In this configuration, all initial curvatures are zero, and so the EISM is quite sparse due to the lack of coupling between deformations (Figure 4.3).

4.2.2 Cylindrical Shell. The cylindrical shell element has non-zero curvature k_2^0 , with all other curvatures zero. This curvature corresponds to $1/R_2$, where R_2 is the radius of an $x = \text{constant}$ coordinate curve. In going from the plate to the shell, coupling between extension and bending due to an initial curvature has been introduced, hence this matrix (Figure 4.4) has more non-zero elements than that of the flat plate. Most notably, entry (13,13), which correlates to energy associated with the displacement w , is now populated. This is because the initial curvature has eliminated the rigid body motion in the w direction. This effect is illustrated in Figure 4.5. In Figure 4.5(a) and (b), both displacements are meant to illustrate small (infinitesimal) movement. Note that for the line (plate), w movement causes no deformation. However, for the arc (shell) depicted in (b), simultaneous movement of all points along the arc in the w (in this case $-w$) direction causes deformation. *This is true even for infinitesimal displacement.* Hence, the element in the EISM corresponding to this movement is populated.

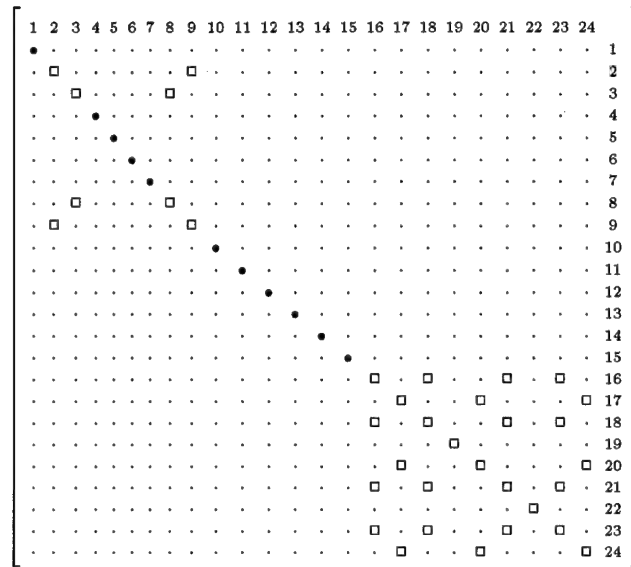


Figure 4.3 Element independent stiffness matrix for flat plate, undeformed configuration

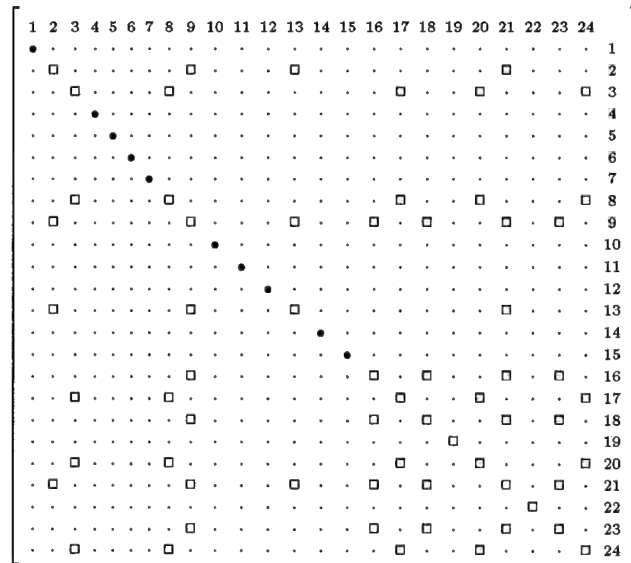


Figure 4.4 Element independent stiffness matrix for cylindrical shell, undeformed configuration

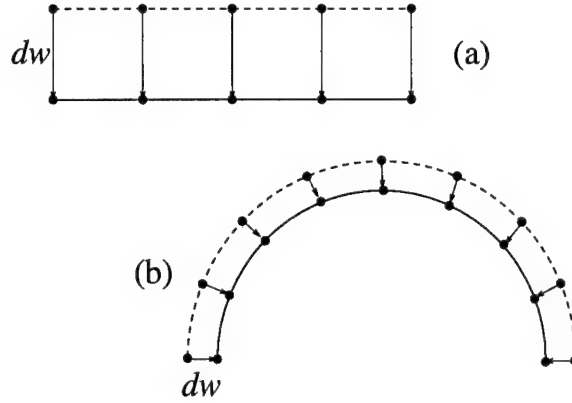
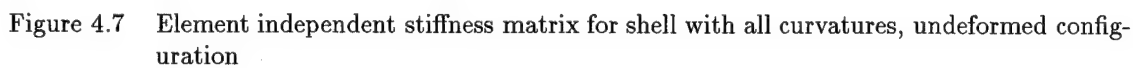
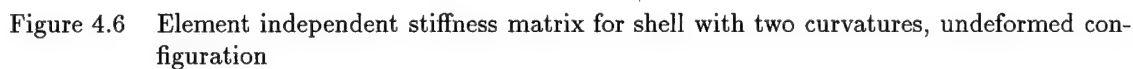


Figure 4.5 (a) Rigid body motion associated with small w displacement; (b) deformation caused by small w displacement when initial curvature is present

4.2.3 Bi-Curved Shell (Spherical/Toroidal). This configuration has non-zero curvatures k_1^0 , k_2^0 , and k_3^0 . For the circular torus, the value of k_2^0 is constant at $1/R_2$. Even though in this case the major radius R_1 is constant, curvatures k_1^0 and k_3^0 vary with location on the reference surface. The EISM for this configuration is depicted in Figure 4.6. More coupling terms have appeared. The population of elements (1,1) and (7,7) correspond to the deformations resulting from u and v movement respectively.

4.2.4 Shell with All Curvatures Present. This is an unlikely shell having all curvatures non-zero. In addition to bi-directional curvature, such a shell would have twisting curvatures about the x and y axes. And, for all curvatures to be non-zero, it would have to be represented using a non-orthogonal coordinate system. Nevertheless, the EISM for this configuration (Figure 4.7) illustrates how the current formulation has permissible displacement gradients with no associated *linear* stiffness (in the initial, undeformed state), namely, second derivatives of the in-plane displacements.



4.3 Element-Dependent Formulation

To this point, the displacement field has not been approximated, so the expressions for the elastic energy and its variation could be considered "exact." But in order to numerically solve the equations, the displacements must be approximated. This is done by assuming that the displacement field may be represented by polynomial functions (shape functions) over some finite region (the finite element). Moreover, it is assumed that if the domain is made up of a sufficient number of such elements, the solution will provide acceptable results.

Toward this end, the components of $\{\mathbf{U}\}$ are approximated through the choice of a specific finite element. Using shape functions to discretize the displacements, one obtains

$$\{u, v, w, \gamma_4, \gamma_5\}^T = [\mathbf{N}(r, s)]\{\mathbf{q}^{[j]}\}, \quad (4.81)$$

where $\{\mathbf{q}^{[j]}\}$ is the vector whose members are the nodal displacements of element j , and $[\mathbf{N}(r, s)]$ is a matrix of two-dimensional finite element shape functions written in terms of natural coordinates

r and s , and given by

$$[N] \equiv \begin{bmatrix} \mathcal{H}_1^1 & 0 & 0 & 0 & 0 \\ \mathcal{H}_2^1 & 0 & 0 & 0 & 0 \\ \mathcal{H}_3^1 & 0 & 0 & 0 & 0 \\ 0 & \mathcal{H}_1^1 & 0 & 0 & 0 \\ 0 & \mathcal{H}_2^1 & 0 & 0 & 0 \\ 0 & \mathcal{H}_3^1 & 0 & 0 & 0 \\ 0 & 0 & \mathcal{H}_1^1 & 0 & 0 \\ 0 & 0 & \mathcal{H}_2^1 & 0 & 0 \\ 0 & 0 & \mathcal{H}_3^1 & 0 & 0 \\ 0 & 0 & 0 & \mathcal{L}_1 & 0 \\ 0 & 0 & 0 & 0 & \mathcal{L}_1 \\ \mathcal{H}_1^2 & 0 & 0 & 0 & 0 \\ \mathcal{H}_2^2 & 0 & 0 & 0 & 0 \\ \mathcal{H}_3^2 & 0 & 0 & 0 & 0 \\ 0 & \mathcal{H}_1^2 & 0 & 0 & 0 \\ 0 & \mathcal{H}_2^2 & 0 & 0 & 0 \\ 0 & \mathcal{H}_3^2 & 0 & 0 & 0 \\ 0 & 0 & \mathcal{H}_1^2 & 0 & 0 \\ 0 & 0 & \mathcal{H}_2^2 & 0 & 0 \\ 0 & 0 & \mathcal{H}_3^2 & 0 & 0 \\ 0 & 0 & 0 & \mathcal{L}_2 & 0 \\ 0 & 0 & 0 & 0 & \mathcal{L}_2 \\ \mathcal{H}_1^3 & 0 & 0 & 0 & 0 \\ \mathcal{H}_2^3 & 0 & 0 & 0 & 0 \\ \mathcal{H}_3^3 & 0 & 0 & 0 & 0 \\ 0 & \mathcal{H}_1^3 & 0 & 0 & 0 \\ 0 & \mathcal{H}_2^3 & 0 & 0 & 0 \\ 0 & \mathcal{H}_3^3 & 0 & 0 & 0 \\ 0 & 0 & \mathcal{H}_1^3 & 0 & 0 \\ 0 & 0 & \mathcal{H}_2^3 & 0 & 0 \\ 0 & 0 & \mathcal{H}_3^3 & 0 & 0 \\ 0 & 0 & 0 & \mathcal{L}_3 & 0 \\ 0 & 0 & 0 & 0 & \mathcal{L}_3 \\ \mathcal{H}_1^4 & 0 & 0 & 0 & 0 \\ \mathcal{H}_2^4 & 0 & 0 & 0 & 0 \\ \mathcal{H}_3^4 & 0 & 0 & 0 & 0 \\ 0 & \mathcal{H}_1^4 & 0 & 0 & 0 \\ 0 & \mathcal{H}_2^4 & 0 & 0 & 0 \\ 0 & \mathcal{H}_3^4 & 0 & 0 & 0 \\ 0 & 0 & \mathcal{H}_1^4 & 0 & 0 \\ 0 & 0 & \mathcal{H}_2^4 & 0 & 0 \\ 0 & 0 & \mathcal{H}_3^4 & 0 & 0 \\ 0 & 0 & 0 & \mathcal{L}_4 & 0 \\ 0 & 0 & 0 & 0 & \mathcal{L}_4 \end{bmatrix}^T \quad (4.82)$$

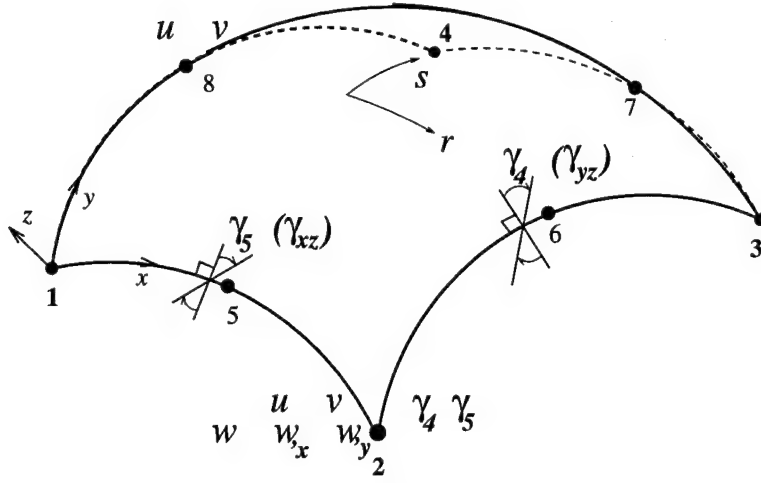


Figure 4.8 The 36-DOF shell element

The shape functions are given by

$$\mathcal{H}_1^k = 1/8(1 + r_k r)(1 + s_k s)(2 + r_k r + s_k s - r^2 - s^2) \quad (4.83a)$$

$$\mathcal{H}_2^k = (a/8)r_k(1 + r_k r)^2(r_k r - 1)(1 + s_k s) \quad (4.83b)$$

$$\mathcal{H}_3^k = (b/8)s_k(1 + r_k r)(s_k s - 1)(1 + s_k s)^2 \quad (4.83c)$$

$$\mathcal{L}^k = (1/4)(1 + r_k r)(1 + s_k s) \quad (4.83d)$$

where $2a$ and $2b$ are dimensions along x and y of the rectangular (in curvilinear coordinates) element, and the values of r_k and s_k are determined by the local coordinates (r, s) of the k^{th} node.

Again, u , v , and w are displacements relative to the undeformed local curvilinear system, and γ_4 and γ_5 represent reference surface shear rotation angles in the η - ζ and ξ - η planes respectively, expressed in terms of the global coordinates.

For the present research, two finite elements are used: an eight-noded isoparametric shell element having 36 degrees-of-freedom and a four-noded, 44 DOF element.

The eight-noded 36 DOF element (Figure 4.8) has seven DOF at each corner node: u , v , w , $w_{,x}$, $w_{,y}$, γ_4 , and γ_5 . At each mid-side node are two DOF: u and v . Hermitian shape functions are

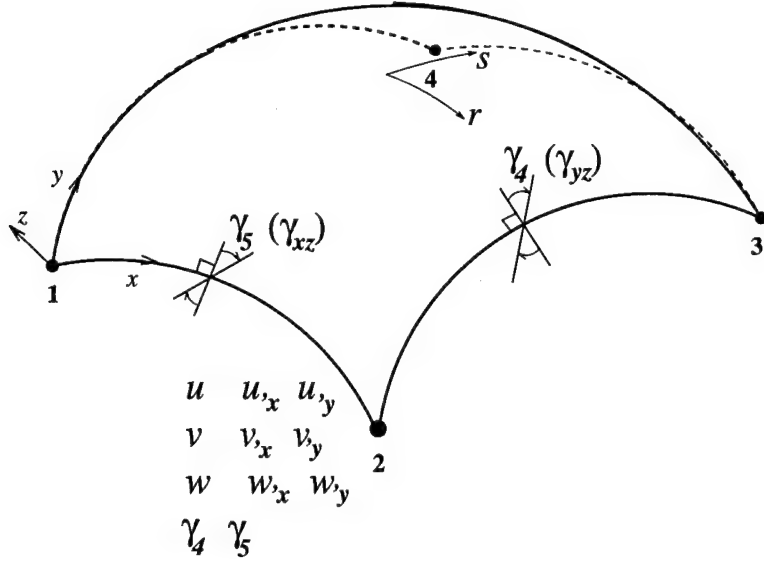


Figure 4.9 The 44-DOF shell element

used for the w DOF, bi-quadratic Lagrangian shape functions are used for the in-plane displacements u and v , and bi-linear shape functions are used for the transverse shear quantities γ_4 and γ_5 . This is a non-conforming element and, as will be shown later, the discontinuity of derivatives of u and v at inter-element boundaries causes problems in analyses involving very large rotations.

Figure 4.9 shows the four-noded 44 DOF element. The degrees of freedom at each corner are $u, u_x, u_y, v, v_x, v_y, w, w_x, w_y, \gamma_4$, and γ_5 . Hermitian shape functions are used for all DOF except the transverse shear DOF, γ_4 and γ_5 , which use bi-linear shape functions.

The element-dependent formulation is now continued with matrix dimensions as shown reflecting the use of the 44 DOF element. Substituting Eq (4.81) into Eq (4.70) yields

$$\{\mathbf{U}(x, y)\}_{24 \times 1} = [\mathbf{D}(x, y)]_{24 \times 44} \{\mathbf{q}(x, y)^{[j]}\}_{44 \times 1} = [\mathbf{\Lambda}]_{24 \times 24} [\mathcal{D}(r, s)]_{24 \times 44} \{\mathbf{q}(x, y)^{[j]}\}_{44 \times 1} \quad (4.84)$$

$$[\mathbf{D}(x, y)]_{24 \times 44} \equiv [\mathbf{\Lambda}]_{24 \times 24} [\partial(r, s)]_{24 \times 5} [\mathbf{N}(r, s)]_{5 \times 44} \quad (4.85)$$

where $[\partial]$ is a 24×5 differential operator matrix given by

$$[\partial] \equiv \begin{bmatrix} 1 & \frac{\partial}{\partial r} & \frac{\partial}{\partial s} & \frac{\partial^2}{\partial r^2} & \frac{\partial^2}{\partial r \partial s} & \frac{\partial^2}{\partial s^2} & 0 & 0 & 0 & 0 & 0 & 0 & 0 & 0 & 0 & 0 & 0 & 0 & 0 & 0 & 0 & 0 & 0 \\ 0 & 0 & 0 & 0 & 0 & 0 & 1 & \frac{\partial}{\partial r} & \frac{\partial}{\partial s} & \frac{\partial^2}{\partial r^2} & \frac{\partial^2}{\partial r \partial s} & \frac{\partial^2}{\partial s^2} & 0 & 0 & 0 & 0 & 0 & 0 & 0 & 0 & 0 & 0 & 0 \\ 0 & 0 & 0 & 0 & 0 & 0 & 0 & 0 & 0 & 0 & 0 & 0 & 1 & \frac{\partial}{\partial r} & \frac{\partial}{\partial s} & \frac{\partial^2}{\partial r^2} & \frac{\partial^2}{\partial r \partial s} & \frac{\partial^2}{\partial s^2} & 0 & 0 & 0 & 0 & 0 \\ 0 & 0 & 0 & 0 & 0 & 0 & 0 & 0 & 0 & 0 & 0 & 0 & 0 & 0 & 0 & 0 & 0 & 1 & \frac{\partial}{\partial r} & \frac{\partial}{\partial s} & 0 & 0 & 0 \\ 0 & 1 & \frac{\partial}{\partial r} & \frac{\partial}{\partial s} \end{bmatrix}^T \quad (4.86)$$

The matrix $[\mathcal{D}]$ is in terms of the natural coordinates r and s of the isoparametric formulation and must be expressed in terms of the global coordinates x and y for Eq (4.84) to hold true. The matrix $[\Lambda]$ is used to perform the necessary conversion. Because only rectangular elements whose axes x and y are aligned with the natural axes r and s are used in the current formulation, the matrix $[\Lambda]$ is diagonal, with elements:

$$\Lambda_{1,1} = \Lambda_{7,7} = \Lambda_{13,13} = \Lambda_{19,19} = \Lambda_{22,22} = 1 \quad (4.87a)$$

$$\Lambda_{2,2} = \Lambda_{8,8} = \Lambda_{14,14} = \Lambda_{20,20} = \Lambda_{23,23} = 1/a \quad (4.87b)$$

$$\Lambda_{3,3} = \Lambda_{9,9} = \Lambda_{15,15} = \Lambda_{21,21} = \Lambda_{24,24} = 1/b \quad (4.87c)$$

$$\Lambda_{4,4} = \Lambda_{10,10} = \Lambda_{16,16} = 1/a^2 \quad (4.87d)$$

$$\Lambda_{5,5} = \Lambda_{11,11} = \Lambda_{17,17} = 1/ab \quad (4.87e)$$

$$\Lambda_{6,6} = \Lambda_{12,12} = \Lambda_{18,18} = 1/b^2. \quad (4.87f)$$

The differentiated shape function matrix in natural coordinates is given by

$$[\mathcal{D}(r, s)]_{24 \times 44} = \begin{bmatrix} \mathbf{H}_1 & \mathbf{0} & \mathbf{H}_2 & \mathbf{0} & \mathbf{H}_3 & \mathbf{0} & \mathbf{H}_4 & \mathbf{0} \\ 6 \times 3 & 6 \times 8 & 6 \times 3 & 6 \times 8 & 6 \times 3 & 6 \times 8 & 6 \times 3 & 6 \times 8 \\ \mathbf{0} & \mathbf{H}_1 & \mathbf{0} & \mathbf{H}_2 & \mathbf{0} & \mathbf{H}_3 & \mathbf{0} & \mathbf{H}_4 & \mathbf{0} \\ 6 \times 3 & 6 \times 3 & 6 \times 8 & 6 \times 3 & 6 \times 8 & 6 \times 3 & 6 \times 8 & 6 \times 3 & 6 \times 5 \\ \mathbf{0} & \mathbf{H}_1 & \mathbf{0} & \mathbf{H}_2 & \mathbf{0} & \mathbf{H}_3 & \mathbf{0} & \mathbf{H}_4 & \mathbf{0} \\ 6 \times 6 & 6 \times 3 & 6 \times 8 & 6 \times 3 & 6 \times 8 & 6 \times 3 & 6 \times 8 & 6 \times 3 & 6 \times 2 \\ \mathbf{0} & \mathbf{L}_1 & \mathbf{0} & \mathbf{L}_2 & \mathbf{0} & \mathbf{L}_3 & \mathbf{0} & \mathbf{L}_4 & \mathbf{0} \\ 3 \times 9 & 3 \times 1 & 3 \times 10 & 3 \times 1 & 3 \times 10 & 3 \times 1 & 3 \times 10 & 3 \times 1 & 3 \times 1 \\ \mathbf{0} & \mathbf{L}_1 & \mathbf{0} & \mathbf{L}_2 & \mathbf{0} & \mathbf{L}_3 & \mathbf{0} & \mathbf{L}_4 & \\ 3 \times 10 & 3 \times 1 & 3 \times 10 & 3 \times 1 & 3 \times 10 & 3 \times 1 & 3 \times 10 & 3 \times 1 & \end{bmatrix}, \quad (4.88)$$

where

$$\mathbf{H}_k = \begin{bmatrix} \mathcal{H}_1^k & \mathcal{H}_2^k & \mathcal{H}_3^k \\ \mathcal{H}_{1,r}^k & \mathcal{H}_{2,r}^k & \mathcal{H}_{3,r}^k \\ \mathcal{H}_{1,s}^k & \mathcal{H}_{2,s}^k & \mathcal{H}_{3,s}^k \\ \mathcal{H}_{1,rr}^k & \mathcal{H}_{2,rr}^k & 0 \\ \mathcal{H}_{1,rs}^k & \mathcal{H}_{2,rs}^k & \mathcal{H}_{3,rs}^k \\ \mathcal{H}_{1,ss}^k & 0 & \mathcal{H}_{3,ss}^k \end{bmatrix}, \quad \text{and} \quad \mathbf{L}_k = \begin{bmatrix} \mathcal{L}^k \\ \mathcal{L}_{,r}^k \\ \mathcal{L}_{,s}^k \end{bmatrix}, \quad (4.89)$$

and the shape functions are given in Eqns (4.83).

Substituting Eq (4.84) into Eq (4.79) yields

$$\begin{aligned} \delta \Pi &= \sum_{j=1}^{N_e} \int \int_{A^{[j]}} \{\delta \mathbf{q}^{[j]}\}^T [\mathbf{D}]^T [\Psi]^T [\Phi] [\dot{\Psi}] [\mathbf{D}] \{\mathbf{q}^{[j]}\} dx dy \\ &= \sum_{j=1}^{N_e} \{\delta \mathbf{q}^{[j]}\}^T [\mathbf{K}^{[j]}] \{\mathbf{q}^{[j]}\} \\ &= \{\delta \mathbf{q}\}^T [\mathbf{K}] \{\mathbf{q}\}, \end{aligned} \quad (4.90)$$

where

$$[\mathbf{K}^{[j]}] \equiv \int \int_{A^{[j]}} [\mathbf{D}]^T [\Psi]^T [\Phi] [\dot{\Psi}] [\mathbf{D}] dx dy. \quad (4.91)$$

Or, in terms of the isoparametric formulation,

$$[\mathbf{K}^{[j]}]_{44 \times 44} \equiv \int_{-1}^1 \int_{-1}^1 [\mathbf{D}]^T [\Psi]^T [\Phi] [\dot{\Psi}] [\mathbf{D}] \det([\mathbf{J}]) \, dr \, ds. \quad (4.92)$$

N_e is the total number of elements in the mesh, $A^{[j]}$ is the area of the j th element, $[\mathbf{K}^{[j]}]$ is the stiffness matrix of the j^{th} element, $[\mathbf{K}]$ is the assembled global structural stiffness matrix, and $\{\mathbf{q}\}$ is the global structural displacement vector referenced to the coordinate system associated with the undeformed structure (Lagrangian).

In a typical Green's strain formulation, determining the order of the integrand of Eq (4.92) is a straight-forward task, as the elements of the integrand are polynomials of known order. Not so in the current formulation. The integrand contains the square root expressions generated by Eqns (3.74) and (3.90) and is not a polynomial. For the current analyses, no significant improvement in the result occurred beyond a four-by-four Gauss quadrature scheme.

Since, in general, $[\Psi] \neq [\dot{\Psi}]$, $[\mathbf{K}^{[j]}]$ and hence $[\mathbf{K}]$ may be asymmetric. This is not a consequence of some physical feature of the formulation, such as nonconservative loading; the asymmetry is due to the scheme used in formulating the variational expressions. In a finite element description of a conservative system having a potential, the stiffness matrix will be symmetric (Schweizerhof and Ramm 1984). The asymmetry of the the stiffness matrix of Eq (4.92) arises from using an inconsistent approach in formulating the integrand of Eq (4.13). The expression for $\delta\{\psi\}$ is only exact for infinitesimal increments of $\{\mathbf{U}\}$, just as the differential of a dependent variable is only exact for infinitesimal increments of the independent variable (Ayres and Mendelson 1990, p. 196). On the other hand, the expression $\{\psi\} = [\dot{\Psi}]\{\mathbf{U}\}$ of Eq (4.78a) is exact for *any* size of increment in $\{\mathbf{U}\}$. Obviously, in the numerical implementation of the theory, one cannot apply infinitesimal increments of displacement. So, in practice, this asymmetric stiffness is not calculated from Eq (4.92), but from the equation for the tangent stiffness, formulated later (Eq 4.106). This expression for the tangent stiffness yields a symmetric matrix, hence the initial stiffness is found by evaluating

the tangent stiffness in the undeformed configuration, $\{\mathbf{q}\} = \{\mathbf{0}\}$. This circumvents having to store or manipulate asymmetric matrices. Another severe drawback in attempting to use Eq (4.78a) for the stiffness matrix is the singularity (division by zero) that would occur in attempting to generate the $[\dot{\Psi}]$ matrix at $\{\mathbf{U}\} = \{\mathbf{0}\}$, the undeformed state.

Note also that the matrix $[\mathbf{K}]$ is dependent upon the displacements (and their derivatives) present in the displacement gradient vector, $\{\mathbf{U}\}$. As in the development of $\delta\{\psi\}$, this precludes direct application of the Newton-Raphson scheme to $[\mathbf{K}]$, since $[\mathbf{K}]$ is a function of $\{\mathbf{U}\}$, not $\{\mathbf{q}\}$. The square-root terms present in Eq (3.74) and (3.90) again cause the problem.

Thus to implement the Newton-Raphson scheme, one first must derive the incremental forms of $\{\mathbf{q}^{[j]}\}$, $\{\mathbf{U}\}$, $\{\psi\}$, and $[\Psi]$:

$$\{\mathbf{q}^{[j]}\} = \{\mathbf{q}^0\} + \{\Delta\mathbf{q}^{[j]}\}, \quad \{\mathbf{U}\} = \{\mathbf{U}^0\} + \{\Delta\mathbf{U}\}, \quad (4.93)$$

where $\{\mathbf{q}^0\}$ is the equilibrium solution (at the last converged increment) and $\{\Delta\mathbf{q}^{[j]}\}$ is the incremental displacement vector. One may generate the first-order Taylor series expansions of $\{\psi\}$ and $[\Psi]$ as follows. Starting with the vector $\{\psi\}$, assume the value of this vector is known at some known value of the displacement gradient vector, $\{\mathbf{U}\} = \{\mathbf{U}^0\}$. The quantity $\{\mathbf{U}^0\}$ could represent an initial condition or the condition satisfying the convergence criteria at some increment. This known vector value is defined as

$$\{\psi^0\} = \{\psi\}|_{\{\mathbf{U}\}=\{\mathbf{U}^0\}}. \quad (4.94)$$

A new value of $\{\mathbf{U}\}$ is now specified based upon an incremental change, as $\{\mathbf{U}\} = \{\mathbf{U}^0\} + \{\Delta\mathbf{U}\}$.

One may find the new value of $\{\psi\}$ via a Taylor series expansion:

$$\{\psi\}|_{\{\mathbf{U}\}+\{\Delta\mathbf{U}\}} = \{\psi\}|_{\{\mathbf{U}\}=\{\mathbf{U}^0\}} + \Delta U_j \left. \frac{\partial \psi_i}{\partial U_j} \right|_{\{\mathbf{U}\}=\{\mathbf{U}^0\}} + \frac{\Delta U_j \Delta U_k}{2} \left. \frac{\partial^2 \psi_i}{\partial U_j \partial U_k} \right|_{\{\mathbf{U}\}=\{\mathbf{U}^0\}} + \dots \quad (4.95)$$

Ignoring higher order terms, one may write

$$\{\psi\} = \{\psi^0\} + [\Psi^0]\{\Delta U\}, \quad (4.96)$$

where $\{\psi^0\} = \{\psi\}|_{\{U\}=\{U^0\}}$ and $[\Psi^0] = \frac{\partial \psi_i}{\partial U_j} \Big|_{\{U\}=\{U^0\}}$. But the matrix $[\Psi]$ appears in Eq (4.92) and must also be written in incremental form. Just as was done with $\{\psi\}$, one may write

$$[\Psi] = [\Psi^0] + [\Xi]. \quad (4.97)$$

The entry Ξ_{ij} of $[\Xi]$ is given by

$$\Xi_{ij} = \frac{\partial^2 \psi_i}{\partial U_j \partial U_k} \Delta U_k. \quad (4.98)$$

Notice that having to represent $\delta\{\psi\}$ as in Eq (4.69) has led to a second derivative matrix *though, strictly speaking, this is only a "first-order" expansion* of $[\Psi]$. Once again, this is due to the use of the Jaumann strain measure, which is based upon an engineering-strain-type of definition and leads to the square-root terms of Eqns (3.74). Eqns (4.96) and (4.97) are then used to expand $[\mathbf{K}^{[j]}]\{\mathbf{q}^{[j]}\}$ into a Taylor series as follows. Recall from Eqns (4.78a) and (4.84) that

$$\{\psi\} = [\dot{\Psi}]\{U\} = [\dot{\Psi}][D]\{q\}, \quad (4.99)$$

so that Eq (4.92) may be used to write

$$[\mathbf{K}^{[j]}]\{\mathbf{q}^{[j]}\} = \int \int_{A^{[j]}} [D]^T [\Psi]^T [\Phi] \{\psi\} \, dx \, dy. \quad (4.100)$$

Now substituting Eqns (4.96) and (4.97) into the above yields

$$[\mathbf{K}^{[j]}]\{\mathbf{q}^{[j]}\} = \int \int_{A^{[j]}} \{ [D]^T [\Psi^0]^T [\Phi] \{\psi^0\} + [D]^T [\Psi^0]^T [\Phi] [\Psi^0] \{\Delta U\} + [D]^T [\Xi]^T [\Phi] \{\psi^0\} \} \, dx \, dy \quad (4.101)$$

In substituting Eqns (4.96) and (4.97) into Eq (4.100), a higher-order term that produces $\{\Delta \mathbf{U}\}^T \{\Delta \mathbf{U}\}$ has been discarded.

Using Eq (4.98) one may define a new symmetric matrix, $[\Upsilon]$, from (Pai 1994):

$$\text{Given } \Xi_{ij} = \frac{\partial^2 \psi_i}{\partial U_j \partial U_k} \Delta U_k, \quad (4.102a)$$

$$\begin{aligned} [\Xi]^T [\Phi] \{\psi^0\} &= \Xi_{ji} \Phi_{jk} \psi_k^0 \\ &= \frac{\partial^2 \psi_j}{\partial U_i \partial U_m} \Delta U_m \Phi_{jk} \psi_k^0 \\ &= \frac{\partial^2 \psi_j}{\partial U_i \partial U_m} \Phi_{jk} \psi_k^0 \Delta U_m \\ &= \psi_k^0 \Phi_{jk} \frac{\partial^2 \psi_j}{\partial U_i \partial U_m} \Delta U_m \\ &= \Upsilon_{im} \Delta U_m \end{aligned} \quad (4.102b)$$

Symmetry of Υ_{im} is shown as follows:

$$\begin{aligned} \Upsilon_{im} &= \psi_k^0 \Phi_{jk} \frac{\partial^2 \psi_j}{\partial U_i \partial U_m} \\ &= \psi_k^0 \Phi_{kj} \frac{\partial^2 \psi_j}{\partial U_i \partial U_m}, \text{ since } [\Phi] \text{ is symmetric} \\ &= \psi_k^0 \Phi_{kj} \frac{\partial^2 \psi_j}{\partial U_m \partial U_i}, \text{ since the order of partial differentiation is interchangeable} \\ &= \Upsilon_{mi} \end{aligned} \quad (4.102c)$$

$$[\Xi]^T [\Phi] \{\psi^0\} = [\Upsilon] \{\Delta \mathbf{U}\}, \quad (4.103)$$

and the entries of Υ_{ij} are

$$\Upsilon_{ij} = \Upsilon_{ji} = \psi_m^0 \Phi_{mn} \frac{\partial^2 \psi_n}{\partial U_i \partial U_j} = \psi_m^0 \Phi_{mn} \frac{\partial \Psi_{ni}^0}{\partial U_j}. \quad (4.104)$$

Substituting Eqns (4.103) and (4.84) into Eq (4.101) yields

$$\underbrace{[\mathbf{K}^{[j]}]\{\mathbf{q}^{[j]}\}}_{44 \times 1} = [\check{\mathbf{K}}^{[j]}\{\Delta \mathbf{q}^{[j]}\} + [\mathbf{K}^{[j]}\{\mathbf{q}^{[j]}\}]_{\{\mathbf{q}^{[j]}\}=\{\mathbf{q}^0\}} \cdot \quad (4.105)$$

Eq (4.105) corresponds to a modified Newton iteration method (Bathe 1982), where $[\check{\mathbf{K}}^{[j]}]$ is the element tangent stiffness matrix given by

$$\underbrace{[\check{\mathbf{K}}^{[j]}]}_{44 \times 44} = \int \int_{A^{[j]}} [\mathbf{D}]^T ([\Psi^0]^T [\Phi] [\Psi^0] + [\Upsilon]) [\mathbf{D}] dx dy \quad (4.106)$$

and

$$[\mathbf{K}^{[j]}\{\mathbf{q}^{[j]}\}]_{\{\mathbf{q}^{[j]}\}=\{\mathbf{q}^0\}} = \int \int_{A^{[j]}} [\mathbf{D}]^T [\Psi^0]^T [\Phi] \{\psi^0\} dx dy. \quad (4.107)$$

Note that the $[\check{\mathbf{K}}^{[j]}]$ of Eq (4.106) is a symmetric matrix. Furthermore, note that Eq (4.107) describes the resultant force vector

$$\{\mathbf{R}^{[j]}\} = [\mathbf{K}^{[j]}\{\mathbf{q}^{[j]}\}]_{\{\mathbf{q}^{[j]}\}=\{\mathbf{q}^0\}} \cdot \quad (4.108)$$

This will be useful for calculation of nodal loads in subsequent sections.

4.4 External Loads

Using Eq (4.81) the variation of non-conservative energy due to external loads is

$$\begin{aligned} \delta W_{nc} &= \int \int \{\delta u, \delta v, \delta w, \delta \gamma_4, \delta \gamma_5\} \{R_1, R_2, R_3, 0, 0\}^T dx dy \\ &= \sum_{j=1}^{N_e} \int \int_{A^{[j]}} \{\delta \mathbf{q}^{[j]}\}^T [\mathbf{N}]^T \{R_1, R_2, R_3, 0, 0\}^T dx dy \\ &= \sum_{j=1}^{N_e} \{\delta \mathbf{q}^{[j]}\}^T \{\mathbf{R}^{[j]}\} \\ &= \{\delta \mathbf{q}\}^T \{\mathbf{R}\} \end{aligned} \quad (4.109)$$

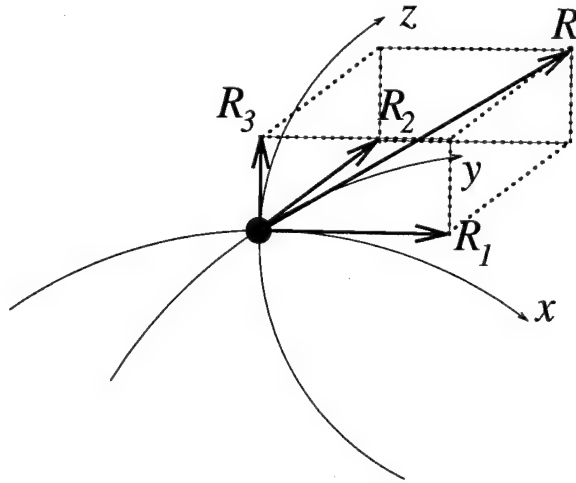


Figure 4.10 Load \mathbf{R} acting at a node and its components along the Lagrangian coordinate axes

where R_1 , R_2 , and R_3 are distributed external loads along the directions of the axes x , y , and z , respectively (see Figure 4.10. Normal and

tangential loads on the shell are most easily described in terms of these shell curvilinear coordinates. The global structural loading vector is $\{\mathbf{R}\}$, and $\{\mathbf{R}^{[j]}\}$ is the elemental nodal loading vector, which is given by

$$\{\mathbf{R}^{[j]}\}_{44 \times 1} \equiv \iint_{A^{[j]}} [\mathbf{N}]^T \{R_1, R_2, R_3, 0, 0\}^T dx dy \quad (4.110)$$

Here, it is assumed that R_1 , R_2 , and R_3 are functions of x and y only and not functions of displacements u , v , and w . Some loading scenarios, such as tire pressurization, may need to be described in terms of the deformed surface. This is easily handled by applying the load incrementally. This point is discussed further in Chapter VII.

4.5 Solution to Incremental Equations

An incremental/iterative Newton-Raphson method is used to solve the nonlinear finite element equations. Substituting Eqns (4.90), (4.105), and (4.109) into Eq (4.1) yields the incremental

equations of motion:

$$\sum_{j=1}^{N_e} [\check{\mathbf{K}}^{[j]}] \{\Delta \mathbf{q}^{[j]}\} = \sum_{j=1}^{N_e} (\{\mathbf{R}^{[j]}\} - [\mathbf{K}^{[j]}] \{\mathbf{q}^{[j]}\})_{\{\mathbf{q}^{[j]}\} = \{\mathbf{q}^0\}}. \quad (4.111)$$

Again, the asymmetric stiffness matrix $[\mathbf{K}^{[j]}]$ need never be formulated, since the product $[\mathbf{K}^{[j]}] \{\mathbf{q}^{[j]}\}$ is a vector described by Eq (4.107). Hence, in the implementation of the algorithm, routines for manipulating and storing real symmetric matrices may be employed.

In nonlinear analyses, the solution to Eq (4.111) is found through an iterative process. In this iterative process, some sort of criterion must be used to determine when the “correct” solution to the finite element equations has been found. In the finite element literature, such criteria are referred as *convergence* (Owen and Hinton 1980, p. 65) or, more correctly *termination* criteria⁵ (Cook et al. 1989, p. 508–509).

The criterion used in the current work (Owen and Hinton 1980, p. 65, Palazotto and Dennis 1992, p. 134) compares successive displacement solution vectors to quantitatively assess the “correctness” of the solution. The global displacement solution vector $\{\mathbf{q}\}$ for the $i + 1^{\text{st}}$ iteration is compared to that of the i^{th} iteration in the current displacement increment as follows:

$$\left| \frac{\|\{\mathbf{q}\}\|_{i+1} - \|\{\mathbf{q}\}\|_i}{\|\{\mathbf{q}\}\|_1} \right| \times 100 \leq \epsilon, \quad (4.112)$$

where $\|\{\mathbf{q}\}\|$ is the Euclidean norm of the displacement vector $\{\mathbf{q}\}$ having n elements such that

$$\|\{\mathbf{q}\}\| = \sqrt{\sum_{i=1}^n (q_i)^2}. \quad (4.113)$$

⁵The word *convergence* implies certain strict mathematical properties (see, e.g., Apostol 1974, p. 189) not satisfied by termination criteria. Furthermore, *convergence* in the finite element sense is more properly applied to characteristics of particular finite elements to provide convergent solutions—a topic of an enormous body of literature that *does* involve convergence in the mathematically rigorous sense.

Note that Eq (4.112) could be (wrongly) satisfied by two vectors, $\{\mathbf{q}\}_{i+1}$ and $\{\mathbf{q}\}_i$ having the same Euclidean norm, but different "directions" (in n -dimensional space, where n is the number of degrees of freedom in the model). That is, two very different solution vectors could, coincidentally, have norms close enough to each other to satisfy the convergence criterion. But the incremental algorithm, applied with good judgment, can mitigate the possibility of such a coincidence. First, the state vector $\{\mathbf{q}\}$ represents the physical deformed configuration of the structure, so state vectors having "very different" directions correspond to states of deformed geometry that are very different. In our incremental approach, we are searching for a "nearby" equilibrium state. If we are searching in a *stable portion of the load-deflection solution space*, a nearby solution will not be very different from the current one. However, when in the neighborhood of a critical (snapping) or bifurcation (multiple solutions) point, a "nearby" equilibrium state may be found having a very different geometry. But the likelihood of this new state vector having the same norm as its predecessor, while extant, is arguably remote for the following reasons: (1) snapping is a jump discontinuity, and the new deformed configuration (state or "direction") is usually, in the author's experience, very different from the state just prior to snapping and, (2) in an incremental approach, the bifurcated state found will be close to the previous one though, by definition, will not be unique.

Clearly, some foreknowledge of the behavior of the structure (vis-à-vis possible snapping, bifurcation buckling, etc.) as well as good engineering judgment and caution must be applied in the context of each problem to be solved.

4.6 Summary

In this chapter, the equations of the theory of Chapter III have been written in a form suitable for numerical solution. In the following chapters, this formulation will be applied to various shell structures having progressively increasing levels of complexity in both initial configuration (geometrically and materially) and in degree of deformation (progressing to geometric nonlinearity).

V. Linear Results

In this chapter, the finite element formulation is evaluated in the context of geometrically linear (small displacement) analyses. (Recall that in all of the analyses presented under the current research, material linearity is assumed, regardless of the magnitude of displacements.) Here the interest is in taking the first steps in demonstrating that the finite element formulation of Chapter IV has been properly implemented (coded). First, the patch test is applied to a plane-stress problem of in-plane loading of a flat plate, then a plate loaded by a transverse pressure is analyzed, followed by a pinched cylindrical shell and, to further assess the stress formulation, the stress results of the current finite element solution are compared to some known elasticity solutions using the infinite plate strip of Pagano (1969). Finally, the formulation is applied to a shell having two (different) radii of curvature: the circular torus. This problem anticipates the subject of Chapter VII, where the formulation is applied to another shell of revolution, namely the aircraft tire.

For the finite element models presented in this chapter (and the next two), solution convergence for a particular model were assessed through modeling each problem with progressively finer meshes until, in the author's judgment, further mesh refinement would not produce an appreciably better solution. To assess the quality of the solution, comparisons with previously published experimental and analytical data are made.

The code developed under the present research is referred to as *JAGS*, for "Jaumann Analysis of General Shells." The text and table headings will use this acronym for the sake of brevity. Also note that for all isotropic problems, the reference surface is chosen to be the middle-surface.

5.1 Patch Test for 44-DOF Element

The patch test, originated by Irons (Bazeley et al. 1965, Taylor et al. 1986), was used to assess the quality of the 44-DOF element. The goal of the patch test is to ensure that, for the element in question, refinement of a mesh modeling a structure results in a sequence of approximate

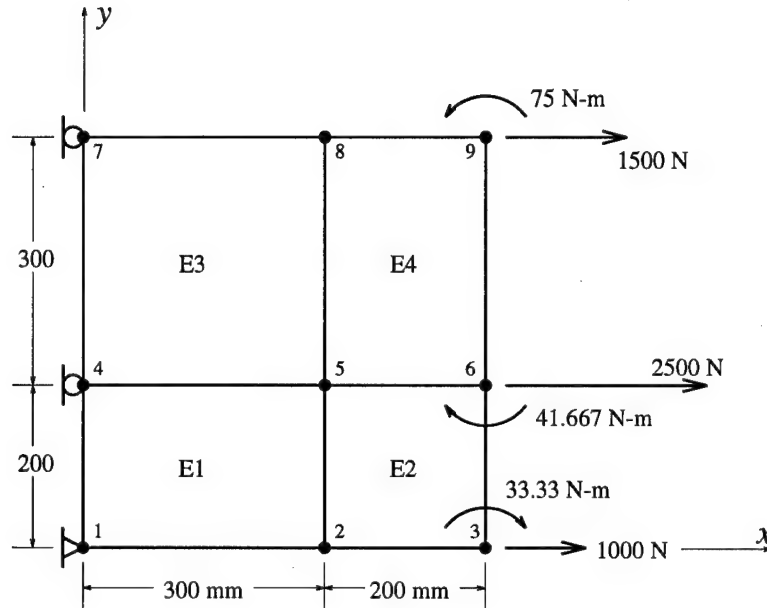


Figure 5.1 In-plane patch test of the 44-DOF shell element

solutions that converge (in the theoretical limit) to the exact solution of the problem. The patch test is passed if, throughout each element, the computed stresses agree exactly (within the limits of machine precision) with the stresses for the physical problem modeled (Cook et al. 1989, p. 129).

Note that certain restrictions on the program limit the scope of the test, and so limit the generality of the conclusions drawn from it. Normally, the patch test serves as a necessary and sufficient condition to declare an element valid (for *linear* problems), in the sense of convergence. For the current program, which only allows quadrilateral elements and has no DOF corresponding directly to bending modes, the patch test serves as a falsifying tool. That is, while failure of the test sufficiently proves a “bad” element, passing the test does not guarantee a “good” one. Or, to put it another way, for the current approach, passing the patch test is a necessary, but not sufficient, condition for the element.

With these limitations in mind, an in-plane patch test was conducted as shown in Figure 5.1. The “moments” appearing in the figure are applied to the in-plane degrees of freedom u_y , which correspond to in-plane rotation. They arise from applying equivalent nodal loads along the edge

$x = 500$ mm to represent a uniform load of 1 MPa along that edge¹, given a plate thickness of 10 mm. The material properties of plate are $E = 200$ GPa, $\nu = 0.3$, and $G = 76.923$ GPa. The boundary conditions applied at nodes 1, 4, and 7 are $u = u_{,y} = v = w = w_{,x} = w_{,y} = 0$; $u = u_{,y} = 0$; and $u = u_{,y} = 0$, respectively. These conditions lead to the correct calculated stresses of $J_{11} = 1$ MPa, all other $J_{mn} = 0$, and strains of $B_{11} = 5$ μ strain, $B_{22} = B_{33} = -1.5$ μ strain, all other $B_{mn} = 0$.

Since there are no DOF corresponding directly to shell bending, linear or otherwise, the patch test cannot be used directly for such deformation. However, simple problems having a known solution may be performed to assess the quality of the element in bending, and such problems are the subject of Section 5.4.

5.2 The Square Isotropic Plate Subjected to Uniform Transverse Pressure

A simply supported square isotropic plate is subjected to a uniform transverse pressure. The nondimensionalized transverse displacement of the plate at its center is given by

$$\bar{w} = \frac{w_c h^3 E}{q_0 a^4}, \quad (5.1)$$

where w_c is the displacement at the center, $E = 1$ GPa is the Young's modulus of the material, $h = 100$ mm is the plate thickness, $q_0 = 1$ MPa is the magnitude of the transverse pressure, and $a = 1$ meter is the length of one side of the square plate. The plate is simply supported along its edges, and the boundary conditions are given by

$$\begin{aligned} \text{at } x = 0, \text{ (} yz\text{-symmetric)} : u = u_{,y} = v_{,x} = w_{,x} = \gamma_5 = 0 \\ \text{at } x = a/2, \text{ (simple)} : u_{,y} = v_{,x} = w = w_{,y} = \gamma_4 = 0 \\ \text{at } y = 0, \text{ (} xz\text{-symmetric)} : u_{,y} = v = v_{,x} = w_{,y} = \gamma_4 = 0 \\ \text{at } y = a/2, \text{ (simple)} : u_{,y} = v_{,x} = w = w_{,x} = \gamma_5 = 0 \end{aligned} \quad (5.2)$$

¹See Section 7.3.1 for a discussion of equivalent nodal loads.

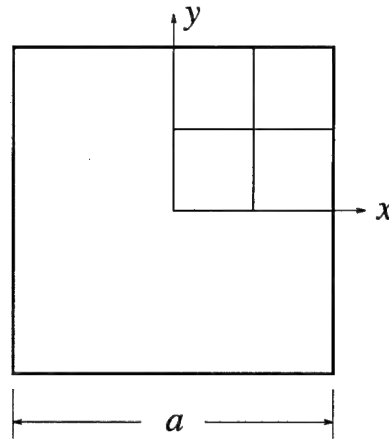


Figure 5.2 Isotropic square flat plate problem indicating 2×2 mesh of square elements modeling one fourth of plate

Because of symmetric loading and boundary conditions, one fourth of the plate is modeled (see Figure 5.2). The results are compared to the closed-form Navier series solutions of Reddy (1984a), as well as to those of Palazotto and Dennis (1992). Uniform meshes of various size were used to assess the convergence characteristics of the 44-DOF element, and the results for three thickness ratios, $S = a/h$, are presented in Table 5.1. Reddy's result for this problem was found by assuming a displacement field of the form

$$w(x, y) = \sum_{n=1}^N \sum_{m=1}^M W_{mn} \sin \frac{m\pi}{a} \sin \frac{n\pi}{b}, \quad (5.3)$$

where M and N were chosen to be 19. A higher order shear deformation theory was used but, as with the work of Palazotto and Dennis (1992), no thickness stretching was included. Note that for the very thin plate, $S = 100$, the present method has a slightly more flexible response for a given mesh size than that of Palazotto and Dennis (+0.11% for the 8×8 mesh), while for the thicker plates, $S = 10$ and $S = 5$, the present code yields what appears to be a slightly stiffer (−0.17% and −0.22%, respectively) response. The more flexible response for the thin plate may be attributed to the use of a higher order element in the *JAGS* code. The apparently stiffer response for the thicker plates, however, is due to strain energy going into thickness stretching, making less available

$S = a/h$	Mesh	Palazotto and Dennis 1992	JAGS	Reddy 1984a
100	1 × 1		0.01616	
	2 × 2	0.02397	0.04304	
	3 × 3		0.04381	
	4 × 4	0.04253	0.04406	
	5 × 5		0.04418	
	6 × 6		0.04424	
	8 × 8	0.04425	0.04430	
				0.0444
10	1 × 1		0.01623	
	2 × 2	0.04613	0.04536	
	3 × 3		0.04607	
	4 × 4	0.04662	0.04634	
	5 × 5		0.04645	
	6 × 6		0.04651	
	8 × 8	0.04666	0.04658	
				0.0467
5	1 × 1		0.02012	
	2 × 2	0.05378	0.05238	
	3 × 3		0.05291	
	4 × 4	0.05360	0.05319	
	5 × 5		0.05331	
	6 × 6		0.05338	
	8 × 8	0.05356	0.05344	
				0.0535

Table 5.1 Nondimensionalized displacement, \bar{w} , at center of simply supported plate transversely loaded with uniform pressure

Integration Order	\bar{w} (<i>JAGS</i>)
1	0.3796701121549270
2	0.04657749159481588
3	0.04657744309154569
4	0.04657744309154816

Table 5.2 Comparison of Gauss integration order to nondimensionalized displacement at center of simply supported plate transversely loaded with uniform pressure (8×8 mesh, $S = 10$)

for transverse displacement. So the response, while appearing to be less flexible, is actually just trading a small amount of transverse displacement for thickness stretching. Also note that, for all three thicknesses, the *JAGS* code exhibits monotonic convergence. That is, as the number of elements is increased, the response becomes monotonically more flexible. This is not the case for the thickest plate, $S = 5$, of Palazotto and Dennis, where the solution appears to become stiffer (though convergent) as more elements are employed.

As mentioned in the previous chapter, the integral equation that yields the stiffness matrix (Eq 4.92) is not a polynomial expression, and hence is not amenable to exact integration via Gauss quadrature. Table 5.2 indicates the effect of varying the order of integration for the current problem. In all of the analyses in the current research, a fourth order Gauss quadrature scheme was used for integrating the stiffness equations. Further increases in integration order changed the result only near the order of machine precision which, for these analyses, was 16-digits.

5.3 The Isotropic Pinched Cylinder

In this problem, an isotropic cylinder of length $L = 262.9$ mm, radius $R = 125.8026$ mm, and thickness $h = 2.3876$ mm is pinched at opposite points along its length by transverse point loads (see Figure 5.3). The cylinder is modeled with the 44-DOF element and with four elements in the x direction and 15 elements in the y directions, with all elements of equal size. The material properties are given by $E = 72.395$ GPa and $\nu = 0.3125$. The boundary conditions used for the

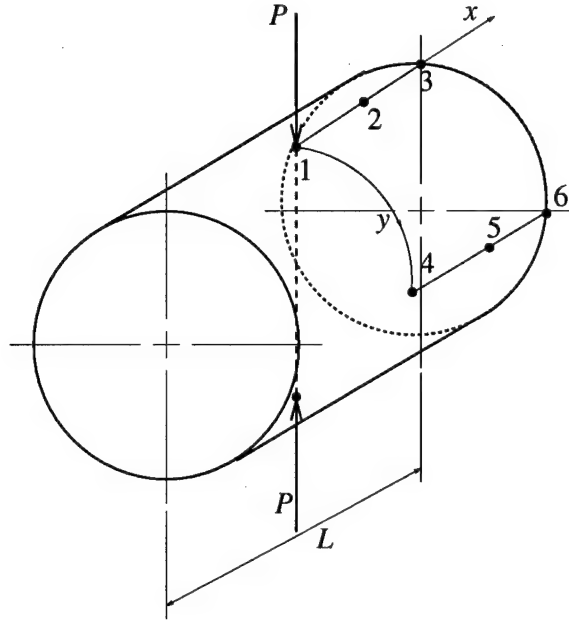


Figure 5.3 Isotropic cylinder pinched by transverse point loads at mid-length indicating region used in modeling one eighth of cylinder

problem are

$$\begin{aligned}
 &\text{at } x = 0, \text{ (} yz\text{-symmetric) : } u = u_{,y} = v_{,x} = w_{,x} = \gamma_5 = 0 \\
 &\text{at } x = L/2, \text{ free} \\
 &\text{at } y = 0, \text{ (} xz\text{-symmetric) : } u_{,y} = v = v_{,x} = w_{,y} = \gamma_4 = 0 \\
 &\text{at } y = R\frac{\pi}{2}, \text{ (} xz\text{-symmetric) : } u_{,y} = v = v_{,x} = w_{,y} = \gamma_4 = 0.
 \end{aligned} \tag{5.4}$$

The deflections at each of the six points shown in Figure 5.3 (point 2 lies midway between points 1 and 3, likewise point 5 between 4 and 6) are listed in Table 5.3. Timoshenko's result is based upon the theory of inextensional deformations of shells. In this approach, the straining at the mid-surface of the (thin) shell is entirely neglected, and only bending is considered. A by-product of this approach is that bending along the x -axis is neglected, hence identical values of deflection are indicated along an x coordinate (see Table 5.3). The present (*JAGS*) approach, which includes

Source	1	2	3	4	5	6
Timoshenko and Woinowski-Krieger 1959	-2.753	-2.753	-2.753	2.540	2.540	2.540
Palazotto and Dennis 1992	-2.791	-2.756	-2.687	2.503	2.504	2.516
JAGS	-2.884	-2.765	-2.741	2.551	2.552	2.565

Table 5.3 Comparison of displacements at six points on the pinched isotropic cylinder; displacements in millimeters

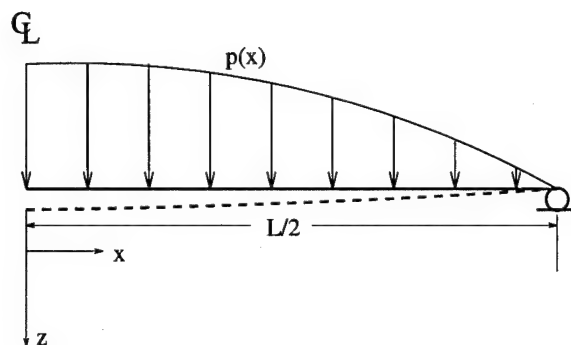


Figure 5.4 Half plate strip in circular bending

not only transverse shear deformation but thickness stretching, yields a result only slightly more flexible than that of Palazotto and Dennis. This is a “thin shell” problem, as the ratio of the shell’s radius to its thickness, $S = R/h \approx 53$, is large enough to neglect both transverse shear and thickness stretch effects. As was seen with the thin flat plate, for a given mesh the *JAGS* model yields a slightly more flexible response when thickness stretching is negligible, due to the use of a higher order element.

5.4 Elasticity Solutions of Pagano and the Flat Plate Strip

To evaluate the element in bending, the finite element scheme is assessed against the work of Pagano (1969), in which elasticity solutions are presented for the infinitely wide plate strip loaded with a transverse sinusoidal pressure load as in Figure 5.4. The load is defined as

$$p(x) = p_0 \sin \left[\pi \frac{(x + L/2)}{L} \right], \quad (5.5)$$

$S = L/h$	\bar{w} (JAGS)	\bar{w} (Pagano)
50	0.5256	0.5270
20	0.6092	0.6173
10	0.9033	0.9316
5	2.0164	2.0908

Table 5.4 Finite element results as compared to Pagano (1969) for the [0/90/0] laminated plate strip of various thickness ratios S

and the normalized center displacement, \bar{w} , is given by

$$\bar{w} = \frac{100 E_{22} h^3 w_c}{p_0 L^4}, \quad (5.6)$$

where w_c is the displacement at the center of the strip, and L is the strip length. A comparison of the \bar{w} values generated by the current finite element program to those of Pagano for a [0/90/0] laminated composite are presented in Table 5.4. The material properties used in the analysis are

$$E_{11} = 172.37 \text{ GPa} \quad (5.7a)$$

$$E_{22} = E_{33} = 6.8948 \text{ GPa} \quad (5.7b)$$

$$\nu_{12} = \nu_{13} = \nu_{23} = 0.25 \quad (5.7c)$$

$$G_{12} = G_{13} = 3.4474 \text{ GPa} \quad (5.7d)$$

$$G_{23} = 1.37896 \text{ GPa} \quad (5.7e)$$

$$(5.7f)$$

A length dimensions of $L = 400\text{mm}$ was held constant, while the thickness, h , was varied to generate different values of $S = L/h$. Twenty elements were used to model half the strip, so the element width was 10mm. The boundary conditions used were:

$$\text{at } x = 0, \text{ (} yz\text{-symmetric) : } u = u_{,y} = v = v_{,x} = v_{,y} = w_{,x} = w_{,y} = \gamma_4 = \gamma_5 = 0$$

$$\text{at } x = L/2, \text{ (simple) : } u_{,y} = v = v_{,x} = v_{,y} = w = w_{,y} = \gamma_4 = 0$$

along $y = 0$ and $y = 2b$ (plane strain and symmetry) : $u_{,y} = v = v_{,x} = v_{,y} = w_{,y} = \gamma_4 = 0$.

(5.8)

The middle of the middle ply is used as the reference surface. Note that all degrees of freedom in the width direction are zeroed, as infinite width is being modeled in that direction (a condition of plane strain in the x - z plane).

The displacements and stresses generated by the finite element program approximate the elasticity solution with varying success. The displacement $\bar{u}_1 = (E_{22}u_1)/(p_0h)$ is matched very well except in the middle (90°) ply (Figure 5.5). The reason for this difference between the \bar{u}_1 displacement function of the current work and that of Pagano's elasticity solution lies in how the warping function is defined. Recall from the definitions of Eqns (3.118) the displacement due to warping in the xz -plane:

$$G_1 \equiv \gamma_5 z + \alpha_1^{(i)} z^2 + \beta_1^{(i)} z^3.$$

Now consider the slope of this function as reference surface is approached:

$$\lim_{z \rightarrow 0} G_{1,z} = \lim_{z \rightarrow 0} \gamma_5 + 2\alpha_1^{(i)} z + 3\beta_1^{(i)} z^2 = \gamma_5. \quad (5.9)$$

Unlike the solution from the equations of elasticity, the slope of the displacement \bar{u}_1 is constrained to take on the value of the shear at the reference surface. The "wiggle" in the middle ply reflects this constraint on the displacement function, which is still required to yield a match between displacements and (transverse shear and normal) stresses at the interface. Despite the "wiggle", though, note how the use of a layer-wise displacement field has allowed the displacement to "zig-zag" at the ply interface. This allows for a very good approximation of the displacement. The results based upon classical laminated plate theory (CLPT) are also shown.

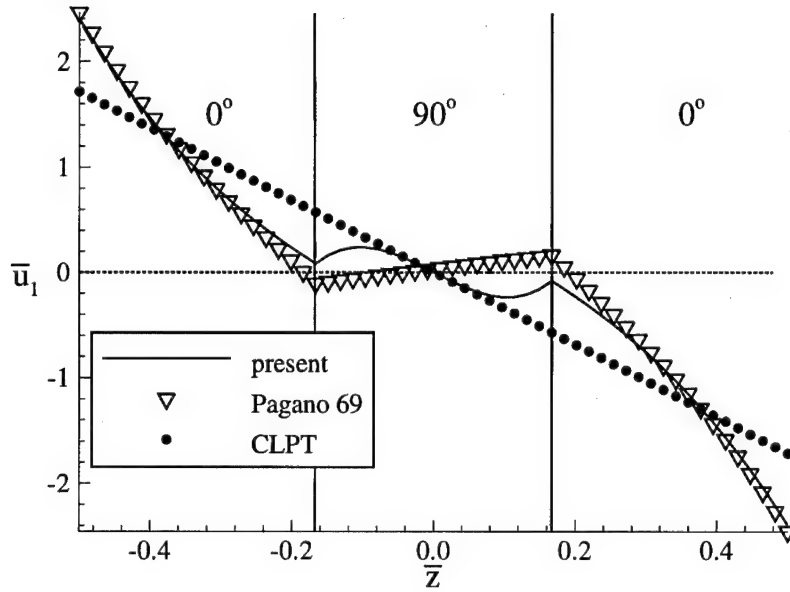


Figure 5.5 Displacement u_1 at plate strip end, $S = 6$

The in-plane stress $\bar{J}_{11} = J_{11}/p_0$ at the plate strip center is plotted in Figure 5.6. The finite element stresses are nearly identical to the elasticity solution. (The effect of the “wiggle” in the displacement \bar{u}_1 will be seen in the transverse shear stress, J_{13} .)

Transverse shear stresses $\bar{J}_{13} = J_{13}/p_0$ are shown in Figure 5.7. The current results model the stresses fairly well, albeit only in the average sense over the center ply. Note how the “zig-zag” displacement function facilitates continuous stresses across the ply boundary. The CLPT solution which, as a matter of course, neglects transverse shear effects, is derived from the equilibrium equations,

$$\tau_{xz,x} = -\sigma_{x,x} \quad (5.10a)$$

$$\sigma_{z,z} = -\tau_{xz,x}. \quad (5.10b)$$

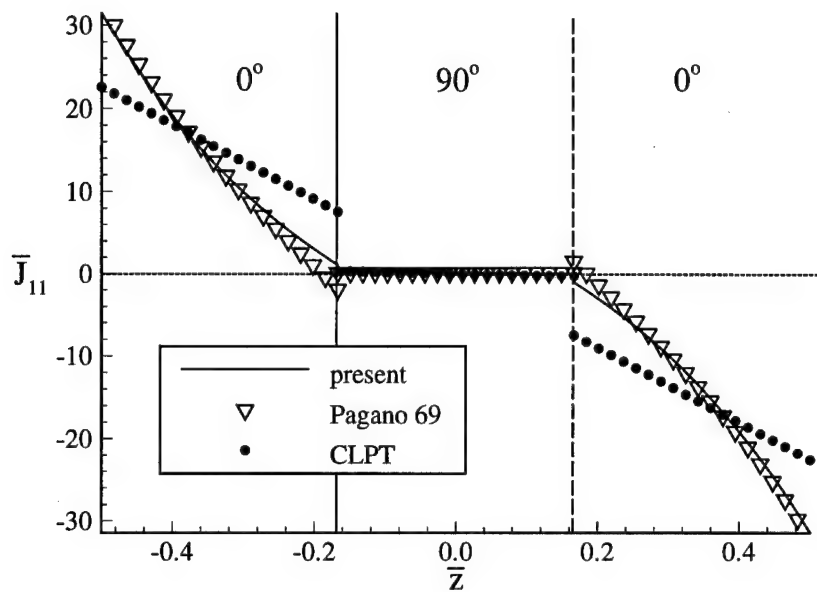


Figure 5.6 Membrane stress J_{11} at plate strip center, $S = 6$

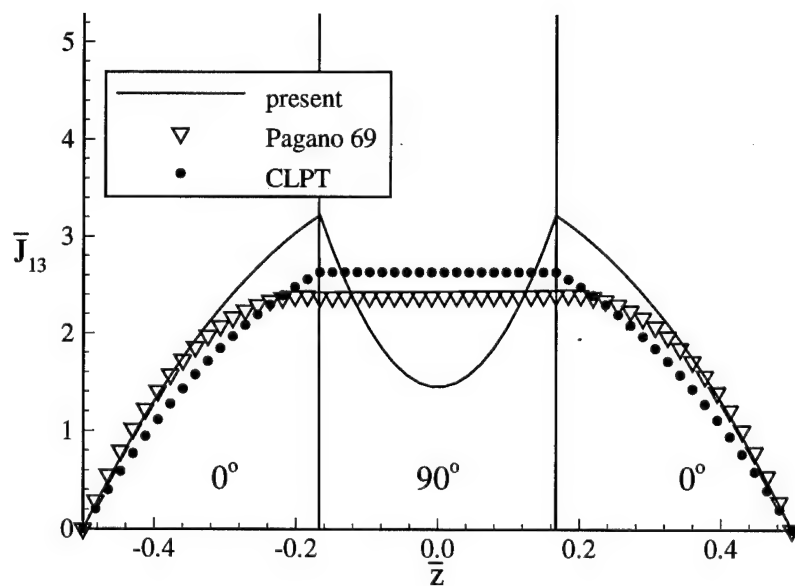


Figure 5.7 Transverse shear stress J_{13} at plate strip end, $S = 6$

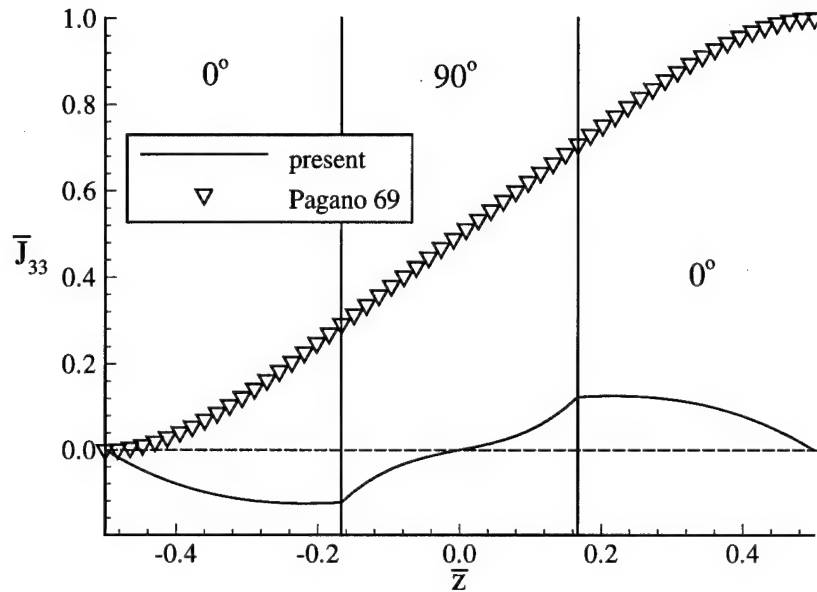


Figure 5.8 Transverse normal stress J_{33} at plate strip center, $S = 6$

The normal stress J_{33} , shown in Figure 5.8, is poorly modeled, as the finite element plate strip is loaded by equivalent nodal loads, not a transverse pressure. The scheme for determining the transverse stretching (see Section 3.7) assumes stress free boundary conditions, which are incorrect for this problem. Using the current formulation, matching non-zero stresses at the boundaries would require incorporation of an iterative scheme that would vary the stretch functions such that the additional constraint(s) would be matched.

5.5 The Toroidal Shell

A linear analysis of a toroidal shell section was undertaken to verify model validity with more than one curvature. The analysis was chosen to be linear for comparison purposes with work done by Zhang and Redekop (1992), not because of any limitations to the algorithm in the current research.

The 90-degree section of circular toroidal pipe is loaded over a small portion of its surface by a prescribed pressure load (Figure 5.9). This loading condition simulates the trunnion pipe configuration of Lewis and Chao (1990). The toroidal section is simply supported at both ends in a fashion that allows movement of the end in the circumferential direction, but not in the meridional direction. Hence the boundary conditions for the 36 DOF element model are:

$$\begin{aligned}
 &\text{at } x = 0, \text{ simple : } v = w = \gamma_5 = 0 \\
 &\text{at } x = 264.37\text{mm, simple : } v = w = \gamma_5 = 0 \\
 &\text{at } y = 0, \text{ } xz\text{-symmetric : } v = w_{,y} = \gamma_4 = 0 \\
 &\text{at } y = 264.37\text{mm, } xz\text{-symmetric : } v = w_{,y} = \gamma_4 = 0.
 \end{aligned} \tag{5.11}$$

These conditions constrain the ends to remain circular and of constant radii.

The results using an 80 element model are depicted in Figure 5.10 and Figure 5.11, indicating good agreement with the finite element work of Zhang and Redekop (1992), who used an 80 element model 16-noded, two-dimensional thin shell elements. Their model contained 775 nodes and 3873 DOF, compared to 277 nodes and 1049 DOF in the *JAGS* model. In this analysis, only displacements have been compared. Stress analysis of bi-curved shells will be included in the tire analysis of Chapter VII.

5.6 Summary

In the next chapter, the analyses will no longer be limited to geometric linearity (small displacements) and will examine the finite element formulation in the context of large displacements and rotations for both isotropic and composite structures.

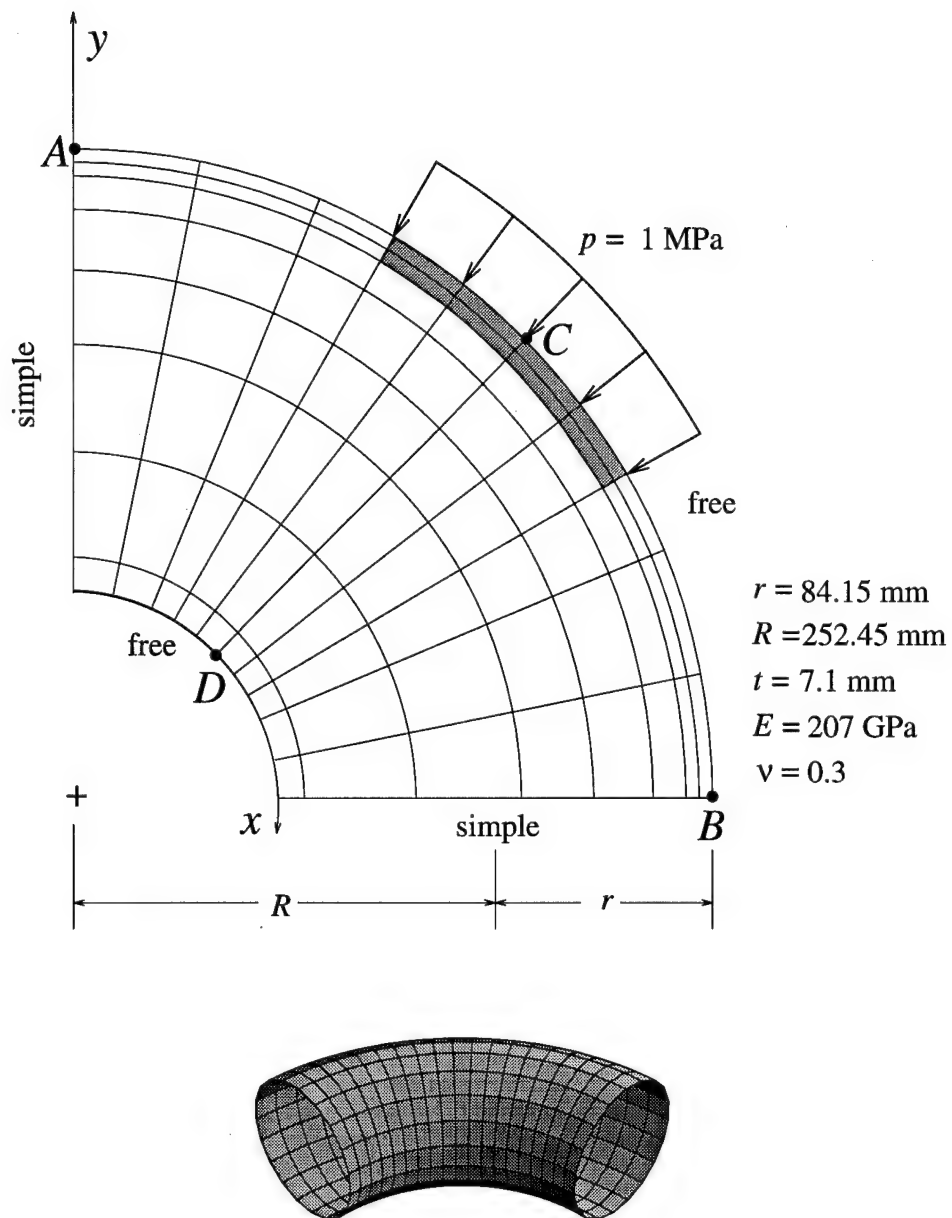


Figure 5.9 Isotropic toroidal shell segment subjected to a pressure load over a portion of its surface

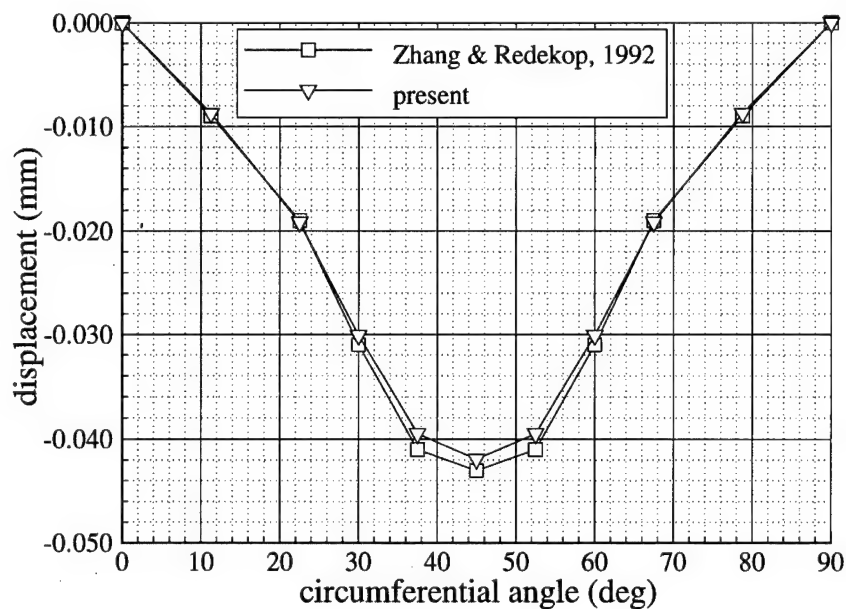


Figure 5.10 Displacement along outer circumference of toroidal shell section between simply supported ends (curve *AB* in Figure 5.9)

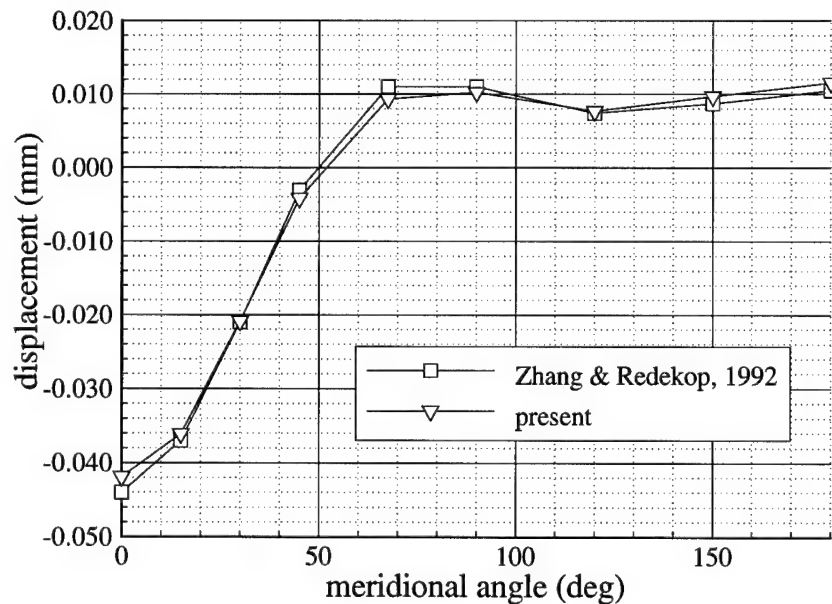


Figure 5.11 Displacement along meridional line 45 degrees to shell free ends, with zero degrees corresponding to the outer circumference of the torus (curve *CD* of Figure 5.9)

VI. Nonlinear Results

To assess the validity of the finite element formulation, it is applied to a composite beam, three isotropic shallow cylindrical panels of varying thicknesses, a composite circular cylindrical arch, and a deep isotropic arch displaying large rotations. As the finite element code is displacement-based, the results in this section primarily compare displacement, rather than stress results.

Prescribed displacement steps (rather than load steps) are used in these analyses. This is done to facilitate capturing the unstable portions of the load-displacement response curves that arise in snap-buckling problems.

A convergence tolerance of $\epsilon = 0.0001\%$ is used in all of the analyses presented herein in accordance with Eq (4.112).

6.1 The Composite Beam

A cantilevered composite beam¹ is subjected to a concentrated end load. The layup of the 12-ply beam is $[0/90]_{3S}$, and the properties of the AS4/3501-6 specially orthotropic laminae are: $E_{11} = 142$ GPa, $E_{22} = E_{33} = 9.8$ GPa, $G_{12} = G_{13} = 6$ GPa, $G_{23} = 3.63$ GPa, $\nu_{12} = \nu_{13} = 0.3$, $\nu_{23} = 0.35$, $t = 0.124$ mm. The beam is modeled with the 36 DOF element and 1×22 mesh, exploiting the symmetry of the beam with respect to the x - z plane (Figure 6.1). The beam is cantilevered at one end and free at the end subjected to the transverse point-load. The following boundary conditions were applied:

$$\begin{aligned} \text{at } x = 0, \text{ (clamped)} : u = v = w = w_{,x} = w_{,y} = \gamma_4 = \gamma_5 = 0 \\ \text{at } y = 0, \text{ (} xz\text{-symmetric)} : v = w_{,y} = \gamma_5 = 0. \end{aligned} \quad (6.1)$$

¹The finite element is a shell element, so the term "beam" is used loosely here. In fact, a very narrow shell is being considered.

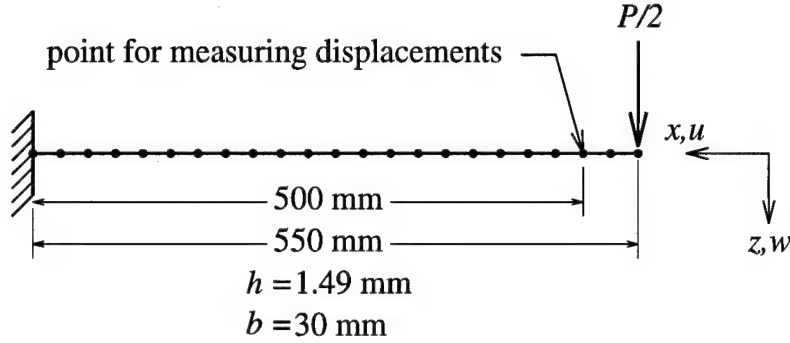


Figure 6.1 Composite cantilever beam subjected to an end-load

The reference surface was chosen to be the middle of the seventh ply, numbering from the bottom². Sixteen uniform ($w=25\text{mm}$) displacement steps are applied to the beam tip, while the displacements are measured 50mm from the tip. The results are compared (Figure 6.2) to the experiments of Minguet and Dugundji (1990) on high aspect ratio, thin laminated beams. The finite element results in the current research indicate a slightly stiffer response than that of the experiments, as expected, but the agreement with the experimental data is quite good. The resultant load, R_i , at the node of interest (node i) is found through the use of Eq (4.108), restated here:

$$\{\mathbf{R}\} = [\mathbf{K}]\{\mathbf{q}\} \mid_{\{\mathbf{q}\}=\{\mathbf{q}^0\}},$$

where the global stiffness matrix, $[\mathbf{K}]$, is calculated based upon the converged value of the displacement vector $\{\mathbf{q}\} \mid_{\{\mathbf{q}\}=\{\mathbf{q}^0\}}$. It is noted that the laminate thicknesses used for the analysis are values corrected for loss of material due to sanding of the laminate given by Minguet and Dugundji.

6.2 The Shallow Cylindrical Panel

The shallow isotropic cylindrical panel of Figure 6.3 is subjected to a transverse point load. The response of the panel varies significantly as the shell thickness is changed, making this a popular

²Recall from Section 3.6 that an interlaminar boundary may not be used as the reference surface due to the definitions of the warping functions.

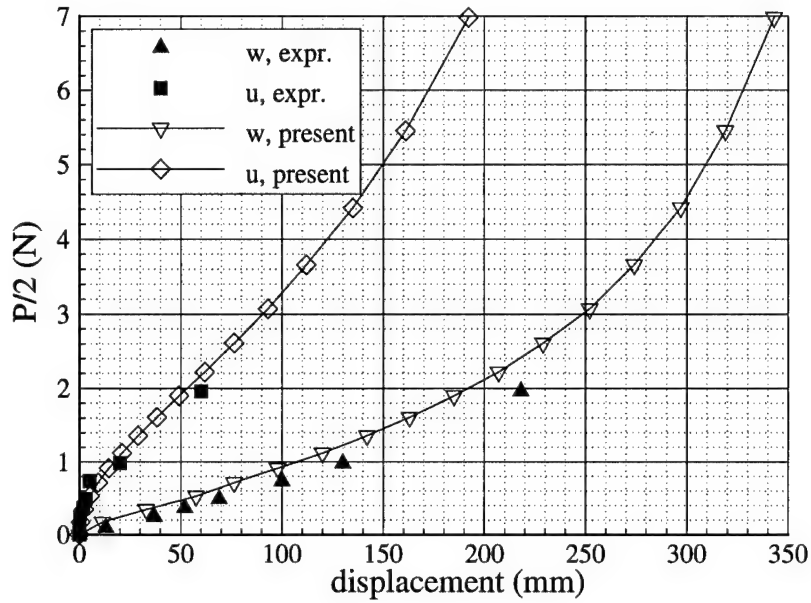


Figure 6.2 Load versus displacement for composite cantilever beam; experimental results are from (Minguet and Dugundji 1990)

validation problem (Palazotto and Dennis 1992). A uniform 24-element mesh having 4 elements in the x direction and 6 elements in the y direction is used to model one quarter of the panel. The panel is hinged along both straight edges and free on both curved ends, so the boundary conditions for the 36 DOF element are given by:

$$\begin{aligned}
 &\text{at } x = 0, (yz\text{-symmetric}) : u = w_{,x} = \gamma_4 = 0 \\
 &\text{at } y = 0, (xz\text{-symmetric}) : v = w_{,y} = \gamma_5 = 0 \\
 &\text{at } y = 254\text{mm, (hinged)} : u = v = w = \gamma_5 = 0.
 \end{aligned} \tag{6.2}$$

The reference surface is the middle surface. The results are compared with the work of other researchers (Sabir and Lock 1972, Palazotto and Dennis 1992, Crisfield 1981, Sabir and Djoudi 1995) in Figure 6.4, Figure 6.5, and Figure 6.6 for thicknesses of 25.4 mm, 12.7 mm, and 6.35 mm respectively. There is excellent agreement in all cases. Note that while the use of an in-

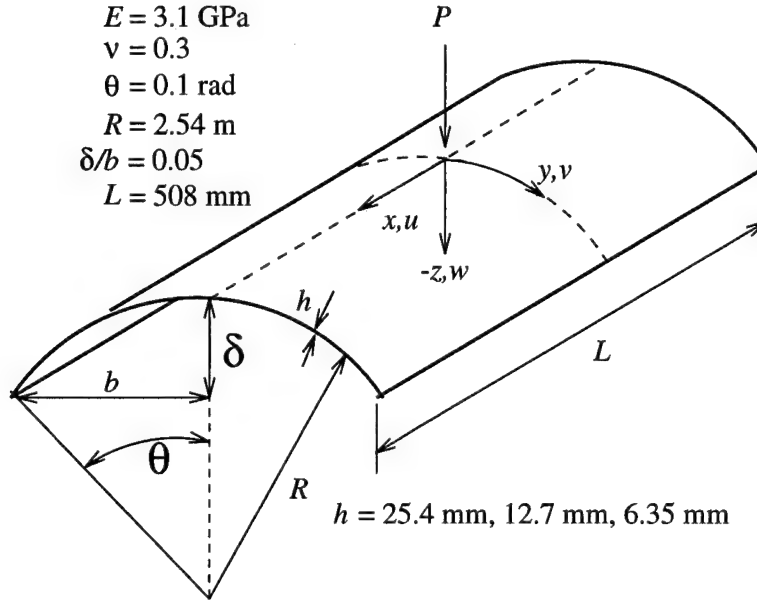


Figure 6.3 Shallow circular cylindrical panel subjected to a transverse point load

cremental displacement scheme allows the snap-through phenomenon to be captured, it precludes depicting the snap-back phenomenon that occurs in the thinnest panel (Figure 6.6). A combination load/displacement scheme, or one of the constrained search path algorithms, such as that of Riks (1979), can capture equilibrium states along very complex and convoluted equilibrium paths, including the snap-back (see, e.g. Miller and Palazotto 1995).

6.3 The Composite Cylindrical Shell

One quarter of a composite cylindrical shell is modeled exploiting the symmetric loading and boundary conditions, and the fact that the laminate is of cross-ply construction. A mesh of 96 uniform elements, eight in the x -direction and twelve in the y -direction, was found to be convergent for the 36-DOF element. The geometry and material properties are depicted in Figure 6.7. The shell thickness is $h = 1.016 \text{ mm}$ (0.04 in). The shell is fully-clamped along its straight edges and

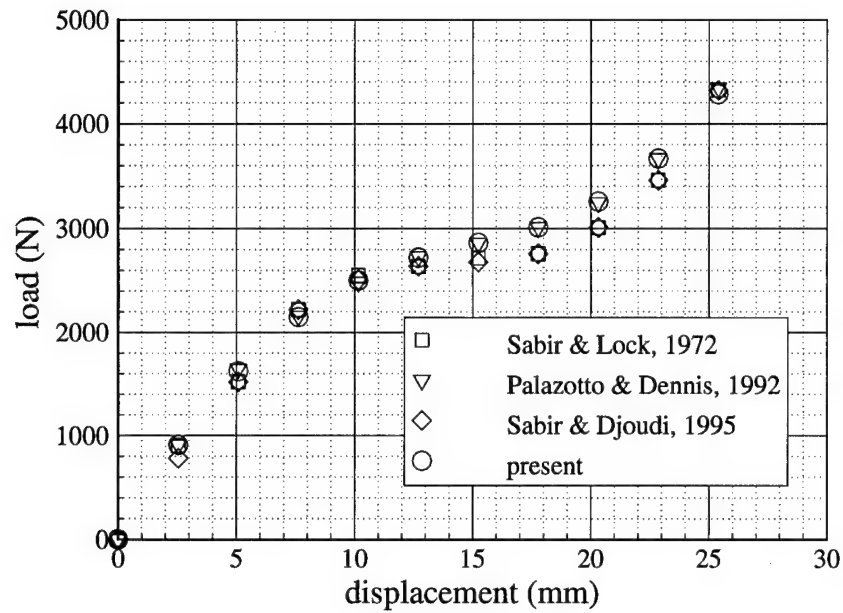


Figure 6.4 Shallow circular cylindrical panel subjected to a transverse point load, $h = 25.4$ mm

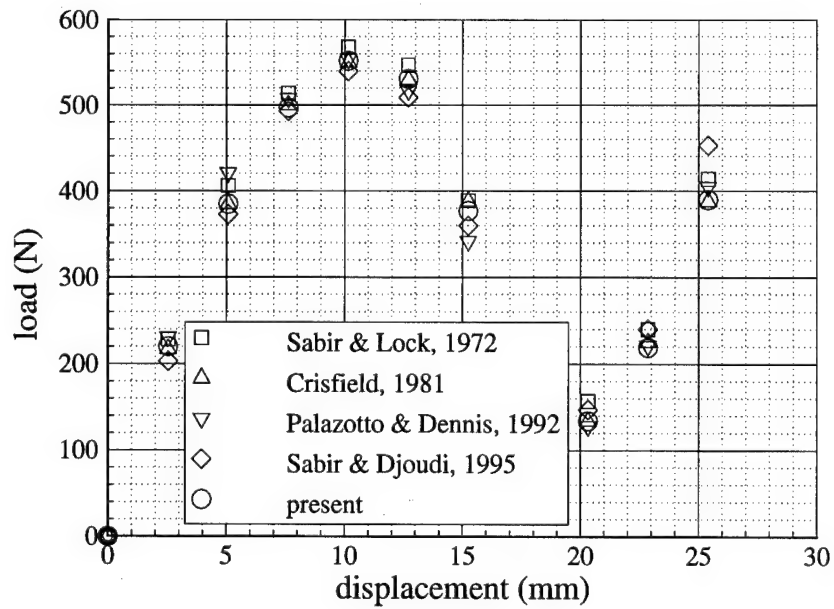


Figure 6.5 Shallow circular cylindrical panel subjected to a transverse point load, $h = 12.7$ mm

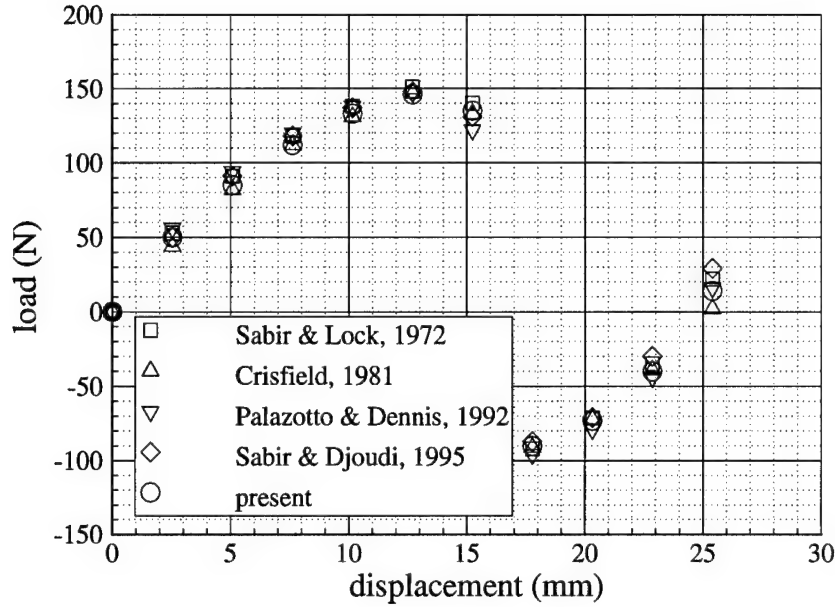


Figure 6.6 Shallow circular cylindrical panel subjected to a transverse point load, $h = 6.35$ mm

free on both curved ends, i.e.,

$$\text{at } x = 0, (yz\text{-symmetric}) : u = w_{,x} = \gamma_4 = 0$$

$$\text{at } y = 0, (xz\text{-symmetric}) : v = w_{,y} = \gamma_5 = 0$$

$$\text{at } y = 152.4\text{mm, (clamped)} : u = v = w = w_{,x} = w_{,y} = \gamma_4 = \gamma_5 = 0. \quad (6.3)$$

The reference surface is chosen to be middle of the second ply, numbering from the bottom. Thirty-two displacement steps of various sizes ranging from 5mm to 25mm were used, and the load-displacement curve for the point-loaded structure is shown in Figure 6.8. Agreement with the work of Palazotto and Dennis (1992) is good, though the the current work indicates a stiffer response in the unstable (snapping) region of the curve. In this region the transverse normal stresses approach $J_{33} = -16$ MPa, and it is possible that the inclusion of these stresses leads to the difference. (For comparison purposes, the membrane stresses J_{11} and J_{22} are on the order of 500 MPa.) Were this

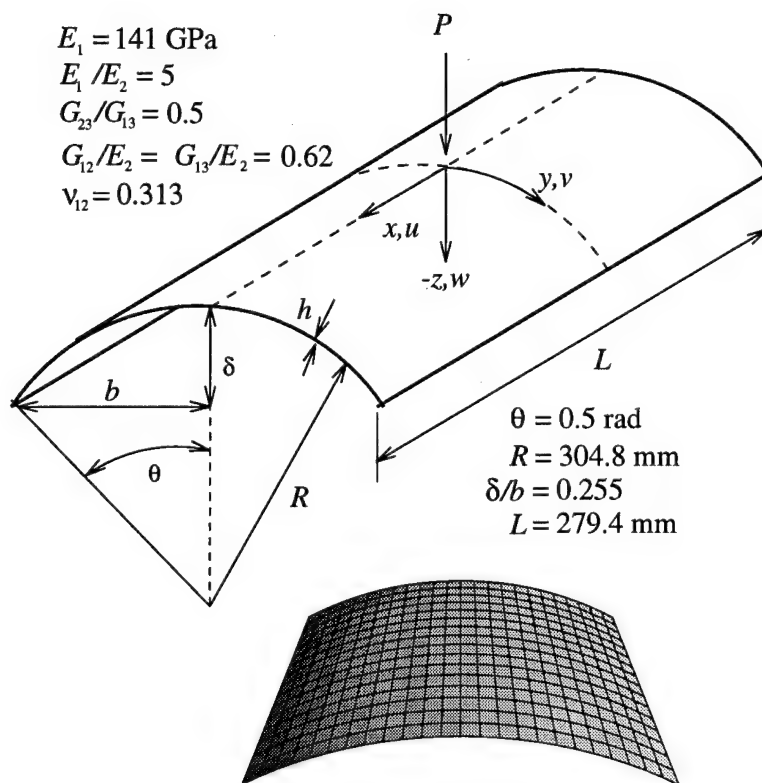


Figure 6.7 Composite circular cylindrical shell subjected to a transverse point load

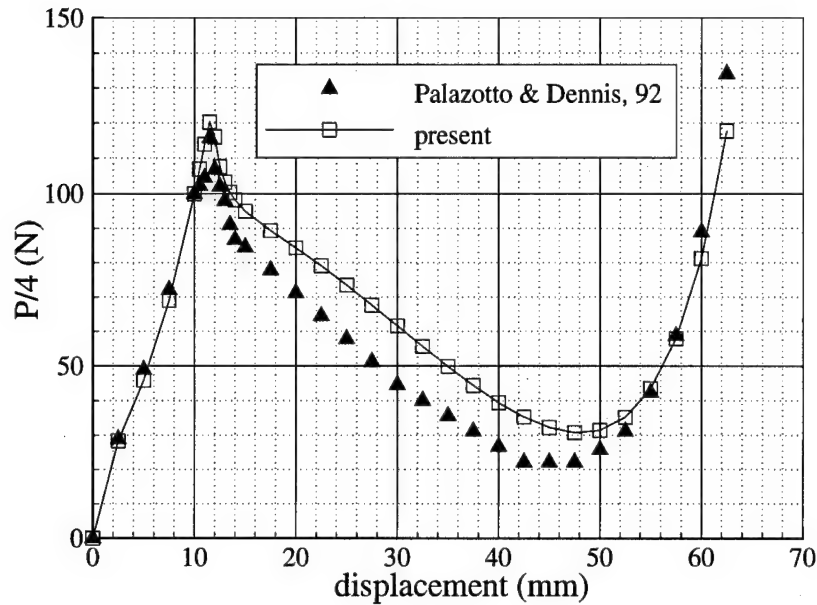


Figure 6.8 Load versus displacement for composite cylindrical shell at point of load application

an isotropic shell, the transverse normal stress would be an unlikely contributor, as this is a “thin” shell ($R/h = 300$). But in a composite shell, rules-of-thumb are difficult to apply (Reissner 1950). Another possible, though less likely, source of disparity is the use of an entirely different solution algorithm by Palazotto and Dennis. They apply a constrained search path solution algorithm (see, e.g., Tsai and Palazotto 1990) to the problem, versus the displacement control method used in the present research.

6.4 The Isotropic Deep Arch

A deep isotropic arch is modeled with a 1×32 mesh (Figure 6.9). Again, symmetry in the x - z plane is assumed, allowing the finite element mesh to model only one-half (in the width direction) of the arch. The boundary conditions of the arch are asymmetric: the left end is clamped and the

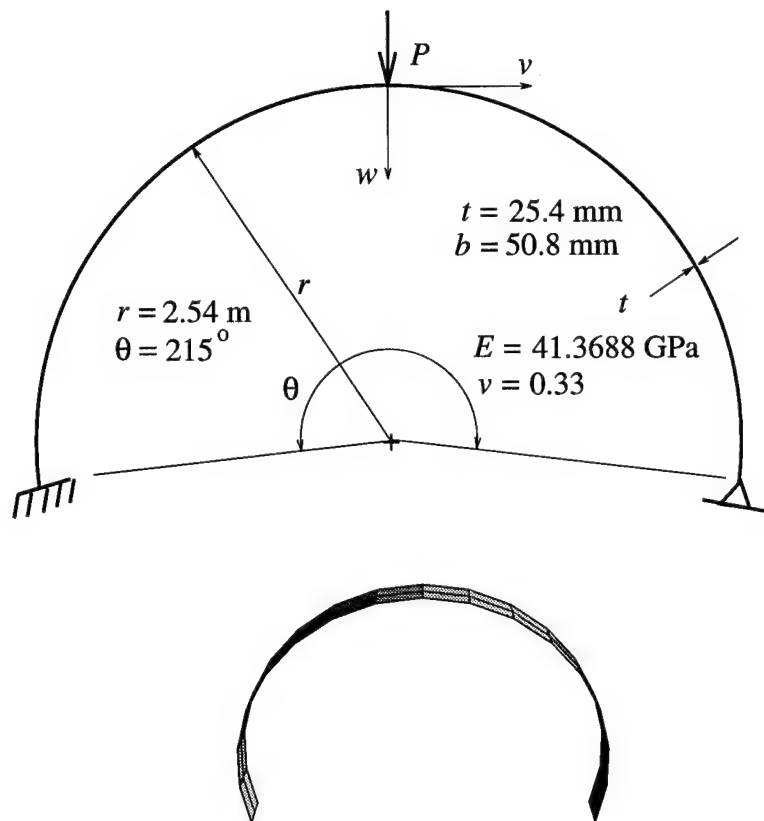


Figure 6.9 Isotropic deep circular arch with asymmetric boundary conditions subjected to transverse point load

right end is hinged. In terms of the nodal degrees of freedom, the boundary conditions are:

$$\begin{aligned}
 &\text{at } x = 25.4\text{mm, } yz\text{-symmetric : } u = w_{,x} = \gamma_5 = 0 \\
 &\text{at } y = 0, \text{ clamped : } u = v = w = w_{,x} = w_{,y} = \gamma_4 = \gamma_5 = 0 \\
 &\text{at } y = 9531\text{mm, hinged : } u = v = w = w_{,x} = \gamma_5 = 0,
 \end{aligned} \tag{6.4}$$

and the reference surface is the middle surface. This asymmetry, coupled with the large opening angle of the arch, presents a challenging geometrically nonlinear problem. A variety of displacement increment sizes were used in an attempt to solve this problem.

Comparing the results with those of Surana (1983), who used a total Lagrangian scheme based on the degenerated shell element of Ahmad et al. (1970). Hence normals to the reference surface may neither stretch nor warp. In the present analysis, the arch is modeled with the 36 DOF element (656 DOF total) and fails to capture the deformation beyond $w/R \doteq 0.7$ (Figure 6.10). This is the case despite using twice the number of elements as Surana, who used 16 eight-noded elements having five DOF at each node (415 DOF in the assembled configuration). Note that the largest rotation in this unsatisfactory simulation is about 90 degrees and takes place at the hinge side of the arch at the maximum deflection attained (Figure 6.11). As mentioned earlier, the 36 DOF element is not C^1 continuous in the in-plane displacements u and v . That is, the values of $u_{,x}$, $u_{,y}$, $v_{,x}$, and $v_{,y}$ are not continuous across inter-element boundaries. Consider the impact of this discontinuity. At any point on the (deforming) reference surface, the rigidly translated and rotated reference frame, $\{\mathbf{i}_{123}\}$ is given by Eq (3.104) to be

$$\{\mathbf{i}_{123}\} = [\mathbf{T}]\{\mathbf{j}_{123}\}. \tag{3.104}$$

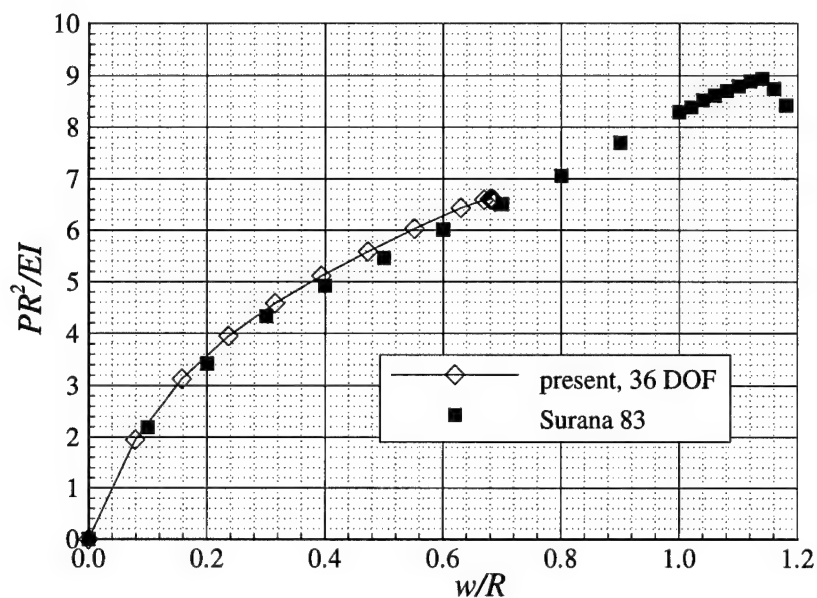


Figure 6.10 Load versus displacement for crown of deep arch, 36 degree-of-freedom element; failure to converge occurs near $w/R = 0.7$ (see text)

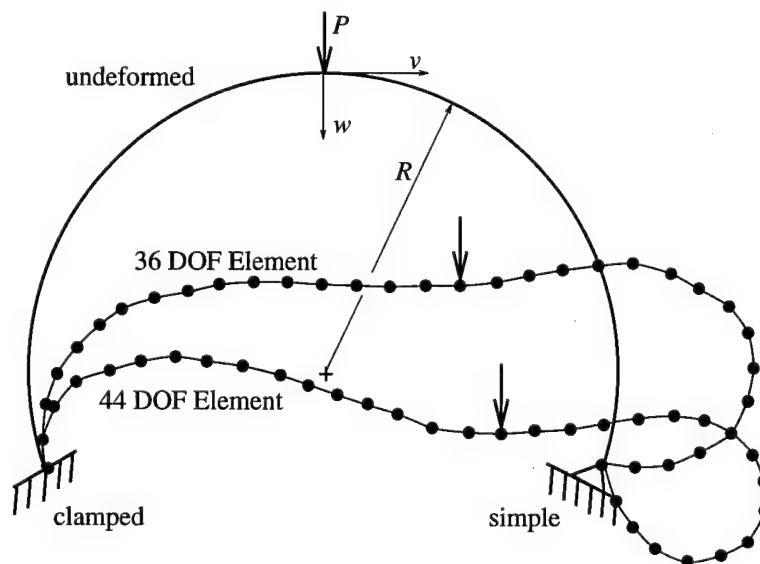


Figure 6.11 Deformed geometry of deep arch indicating maximum deflection achieved for 36 and 44 degree-of-freedom elements

Now recall from Eqns (3.92), and (3.95) that

$$T_{11} = \frac{1}{\cos \gamma_6} (\hat{T}_{11} \cos \gamma_{62} - \hat{T}_{21} \sin \gamma_{61}) \quad (3.95a)$$

$$T_{12} = \frac{1}{\cos \gamma_6} (\hat{T}_{12} \cos \gamma_{62} - \hat{T}_{22} \sin \gamma_{61}) \quad (3.95b)$$

$$T_{13} = \frac{1}{\cos \gamma_6} (\hat{T}_{13} \cos \gamma_{62} - \hat{T}_{23} \sin \gamma_{61}) \quad (3.95c)$$

$$T_{21} = \frac{1}{\cos \gamma_6} (-\hat{T}_{11} \sin \gamma_{62} + \hat{T}_{21} \cos \gamma_{61}) \quad (3.95d)$$

$$T_{22} = \frac{1}{\cos \gamma_6} (-\hat{T}_{12} \sin \gamma_{62} + \hat{T}_{22} \cos \gamma_{61}) \quad (3.95e)$$

$$T_{23} = \frac{1}{\cos \gamma_6} (-\hat{T}_{13} \sin \gamma_{62} + \hat{T}_{23} \cos \gamma_{61}) \quad (3.95f)$$

$$T_{31} = (\hat{T}_{12}\hat{T}_{23} - \hat{T}_{13}\hat{T}_{22})/R_0 \quad (3.92a)$$

$$T_{32} = (\hat{T}_{13}\hat{T}_{21} - \hat{T}_{11}\hat{T}_{23})/R_0 \quad (3.92b)$$

$$T_{33} = (\hat{T}_{11}\hat{T}_{22} - \hat{T}_{12}\hat{T}_{21})/R_0 \quad (3.92c)$$

$$R_0 \equiv \sqrt{(\hat{T}_{12}\hat{T}_{23} - \hat{T}_{13}\hat{T}_{22})^2 + (\hat{T}_{13}\hat{T}_{21} - \hat{T}_{11}\hat{T}_{23})^2 + (\hat{T}_{11}\hat{T}_{22} - \hat{T}_{12}\hat{T}_{21})^2} = |\cos \gamma_6| \quad (3.92d)$$

where, from Eqns (3.77)

$$\hat{T}_{11} = \frac{1 + u_{,x} - vk_5^0 + wk_1^0}{1 + e_1}, \quad \hat{T}_{12} = \frac{v_{,x} + uk_5^0 + wk_{61}^0}{1 + e_1}, \quad \hat{T}_{13} = \frac{w_{,x} - uk_1^0 - vk_{61}^0}{1 + e_1},$$

$$\hat{T}_{21} = \frac{u_{,y} - vk_4^0 + wk_{62}^0}{1 + e_2}, \quad \hat{T}_{22} = \frac{1 + v_{,y} + uk_4^0 + wk_2^0}{1 + e_2}, \quad \hat{T}_{23} = \frac{w_{,y} - uk_{62}^0 - vk_2^0}{1 + e_2}.$$

From these equations, it can be seen that if the DOF in question are not continuous at a point, then there can be multiple values of the $\{\mathbf{i}_{123}\}$ triad at that point. This is a serious defect, since the change in the orientation of this triad as one moves along the reference surface yields the deformed curvatures through Eqns (3.113), repeated here:

$$k_1 \equiv -\frac{\partial \mathbf{i}_1}{\partial x} \cdot \mathbf{i}_3 = -T_{1m,x} T_{3m} - T_{21} k_{61}^0 + T_{22} k_1^0 + T_{23} k_5^0$$

$$k_2 \equiv -\frac{\partial \mathbf{i}_2}{\partial y} \cdot \mathbf{i}_3 = -T_{2m,y} T_{3m} + T_{11} k_2^0 - T_{12} k_{62}^0 - T_{13} k_4^0$$

$$\begin{aligned}
k_{61} &\equiv -\frac{\partial \mathbf{i}_2}{\partial x} \cdot \mathbf{i}_3 = -T_{2m,x}T_{3m} + T_{11}k_{61}^0 - T_{12}k_1^0 - T_{13}k_5^0 \\
k_{62} &\equiv -\frac{\partial \mathbf{i}_1}{\partial y} \cdot \mathbf{i}_3 = -T_{1m,y}T_{3m} - T_{21}k_2^0 + T_{22}k_{62}^0 + T_{23}k_4^0 \\
k_5 &\equiv \frac{\partial \mathbf{i}_1}{\partial x} \cdot \mathbf{i}_2 = T_{1m,x}T_{2m} - T_{31}k_{61}^0 + T_{32}k_1^0 + T_{33}k_5^0 \\
k_4 &\equiv -\frac{\partial \mathbf{i}_2}{\partial y} \cdot \mathbf{i}_1 = -T_{2m,y}T_{1m} - T_{31}k_2^0 + T_{32}k_{62}^0 + T_{33}k_4^0.
\end{aligned}$$

The difference between the deformed and undeformed curvatures are directly responsible for strain energy due to bending. For example, in the current problem ($k_2 - k_2^0$), where $k_2^0 = 1/R$ (the arch radius) gives rise to the largest contributor to strain energy: that due to bending of the arch. The discontinuity of this strain at the inter-element boundaries causes the program to fail to converge when the discrepancy gets large enough to induce a numerical instability.

So the problem is run again with the 44 DOF element and the following boundary conditions:

$$\text{at } x = 25.4\text{mm, (yz-symmetric): } u = u_{,y} = v_{,x} = w_{,x} = \gamma_5 = 0$$

$$\text{at } y = 0, \text{ (clamped): } u = u_{,x} = u_{,y} = v = v_{,x} = w = w_{,x} = w_{,y} = \gamma_4 = \gamma_5 = 0$$

$$\text{at } y = 9531\text{mm, (hinged): } u = u_{,y} = v = v_{,x} = w = w_{,x} = \gamma_5 = 0$$

(6.5)

As mentioned before, this element is C^1 continuous in all displacement variables (though not in the transverse shear variables). The result, generated with a 1×16 mesh (374 DOF), is shown in Figure 6.12. These displacement results are in good agreement with Surana. For comparison purposes, the maximum rotation for this problem is about 150 degrees, again at the hinged end of the arch (Figure 6.11). To examine the convergence properties of the element, the number of elements used in the model was successively reduced (Figure 6.13). As can be seen, 12 elements (286 DOF total) are adequate to model the arch. Furthermore, 8 elements (198 DOF) appear satisfactory for displacements up to $w/R \doteq 0.8$. An additional analysis was made to determine

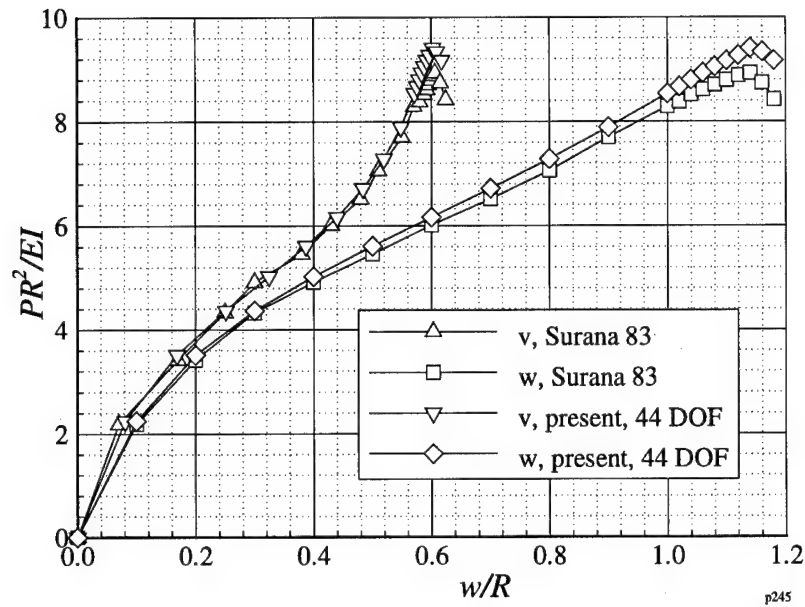


Figure 6.12 Load versus displacement for crown of deep arch, 44 degree-of-freedom element

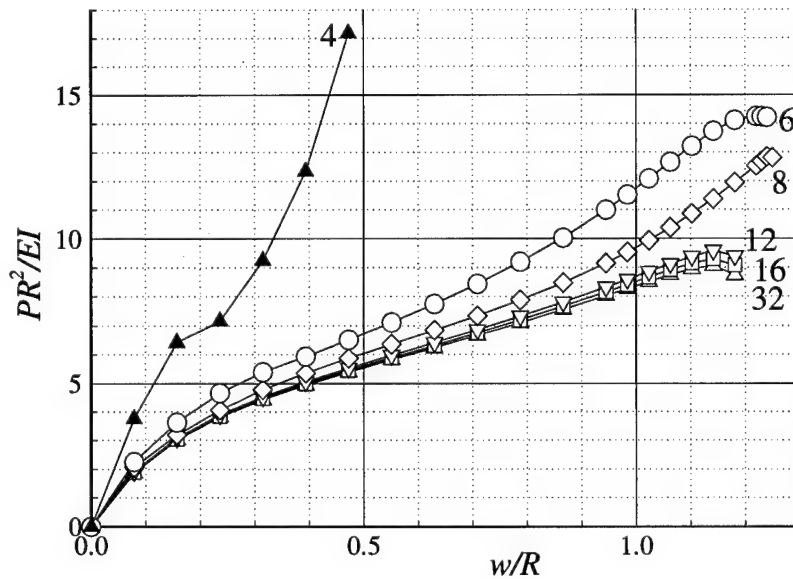


Figure 6.13 Load versus displacement for crown of deep arch indicating response with different numbers of equal size elements

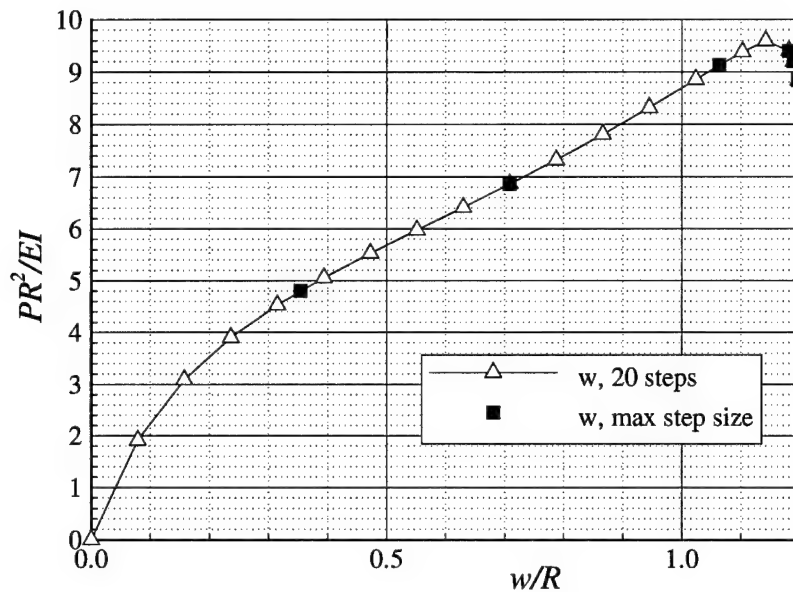


Figure 6.14 Load versus displacement for crown of deep arch indicating maximum displacement step size

the maximum displacement increment that could be used with the model (see Figure 6.14). It was found that the maximum load condition could be reached in slightly more than three displacement steps; Surana used 17 displacement steps, though the authors do not claim that any effort was made by Surana to optimize in this regard.

6.5 Summary

Now having exercised the finite element program in some nonlinear applications, the next step will be to attempt to model a more complex structure. One having properties which vary along the reference surface as well as through the thickness, and having a very general shape: the aircraft tire.

VII. Application to the Aircraft Tire

As presented in Chapter II, there is a large body of excellent work in the analysis of tires through the use of the finite element method. Nonetheless, the present research is novel in its combining of a number of heretofore disparate features: (1) A high-fidelity geometric model of the anisotropic tire is developed entirely with two-dimensional finite elements. (2) This model incorporates a higher order and layer-wise shear deformation shell theory and includes thickness stretching. (3) The model includes the effects of large displacements and rotations (i.e., geometric nonlinearity). (4) Surface contact of the tire is modeled using a boundary condition modification scheme and two-dimensional finite elements.

By way of comparison, the work of Kim and Noor (1990) incorporated a geometrically high-fidelity tire model, but not higher order shear nor thickness stretching, and the contact problem was handled via linear solution of application of a distributed load. Many simplified models, such as the ring on an elastic foundation or simple shells of revolution (see the works of Padovan 1975, Padovan 1976, Padovan 1977, Kennedy and Padovan 1987, and Brockman et al. 1992) have been used for analytical and finite element dynamic analyses, usually employing the Galilean transform (Sve and Herrmann 1974) in concert with traveling load methods. Others have used three-dimensional finite elements (Kennedy and Padovan 1987, Brockman et al. 1992, Wu and Du 1995) having, to varying degrees, simplified material models. Such simplifications often take the form of generating single-ply models having "equivalent orthotropic" properties or just including fewer plies in the model than exist in the actual tire. Others simplify the finite element itself, as did DeEskinazi et al. (1978), who used flat triangular plate elements to model the radial tire in contact with a flat surface. Tire contact has been handled in a number of ways, including gap elements in concert with three-dimensional finite element models (Kennedy and Padovan 1987), traveling loads (as mentioned above) and boundary condition modification schemes (Wu and Du 1995). Incorporation of the viscoelastic properties of rubber, not included herein, has also been done using the finite

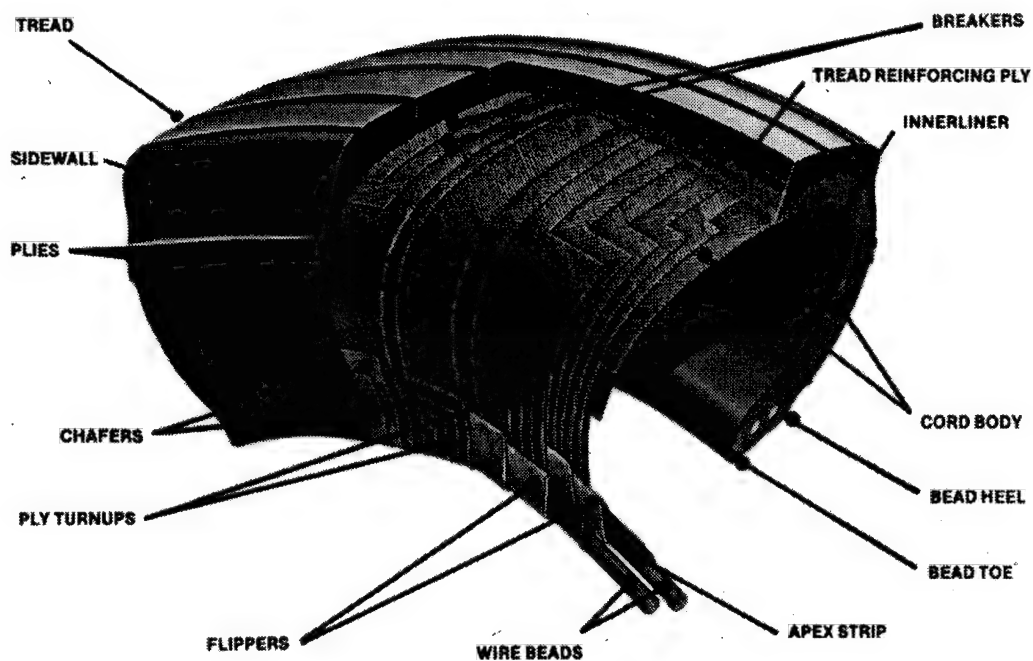


Figure 7.1 Typical bias-ply aircraft tire indicating complexity of construction

element method (see, e.g., Padovan 1976 and Kennedy and Padovan 1987). It is clear that the complex three-dimensional structure of the tire presents a formidable challenge to two-dimensional finite element analysis. The finite element model developed in Chapter IV is now applied to the modeling of the aircraft tire.

The aircraft tire (Figure 7.1) is a toroidal shell of non-circular cross-section. Furthermore, it may be described as a laminated shell, owing to its corded-rubber ply construction. The structure is complicated by the presence of bead rings and tread grooves, as well as by the varying thickness of the cross-section in the meridional direction¹. The thickness, number of plies, ply orientation, and constitutive properties all change in the meridional direction.

¹Throughout this chapter, "circumferential" refers to the x , or "rolling" direction, while "meridional" refers to the y , or "minor radius" direction.

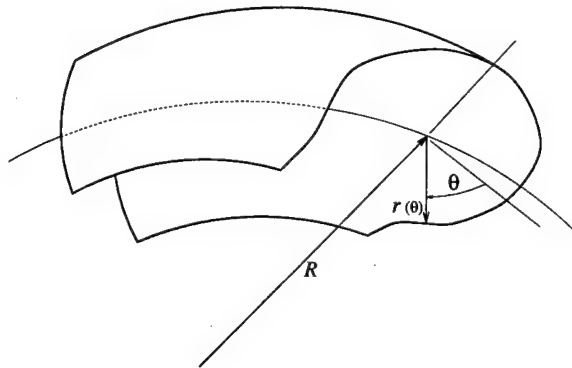


Figure 7.2 Shell of revolution with irregular cross section

The two types of mechanical loads on the tire are inflation loads and loads caused by contact with a surface. Inflation forces are easily described by the "tire pressure", while the loads due to contact depend on many factors, including aircraft weight, braking, pavement roughness and flexibility, tire camber, turning loads, etc. One objective of the current research is to demonstrate an initial capability in analyzing the tire with respect to these loads.

7.1 Tire Geometry

The tire geometry is toroidal, but of non-circular cross section. For this reason, the curvature terms of the circular torus given by Eqns (3.66), below (with θ replacing y^2), are not valid:

$$k_1^0 = \frac{-\sin \theta}{(R - y^3 \sin \theta)} \quad (7.1a)$$

$$k_2^0 = \frac{1}{y^3} \quad (7.1b)$$

$$k_5^0 = \frac{\cos \theta}{(R - y^3 \sin \theta)} \quad (7.1c)$$

In the tire cross section, the minor radius of the torus ($y^3 = r$) is now a function of the meridional angle ($y^2 = \theta$), as shown in Figure 7.2. This leads to very different curvature terms. Consider the

coordinate transformations of the circular torus from Chapter III:

$$\begin{aligned} X^1 &= (R - y^3 \sin y^2) \sin y^1 \\ X^2 &= (R - y^3 \sin y^2) \cos y^1 \\ X^3 &= -y^3 \cos y^2. \end{aligned} \quad (3.38)$$

Now substitute θ for y^2 and $r(\theta)$ for y^3 :

$$\begin{aligned} X^1 &= (R - r \sin \theta) \sin y^1 \\ X^2 &= (R - r \sin \theta) \cos y^1 \\ X^3 &= -r \cos \theta. \end{aligned} \quad (7.2)$$

There are now only two independent variables in y -space, since r is now dependent upon θ . This leads to a 3×2 Jacobian matrix of (cf. Eq 3.46)

$$[\mathbf{J}] = \begin{bmatrix} (R - r \sin \theta) \cos y^1 & -(r' \sin \theta + r \cos \theta) \sin y^1 \\ -(R - r \sin \theta) \sin y^1 & -(r' \sin \theta + r \cos \theta) \cos y^1 \\ 0 & -r' \cos \theta + r \sin \theta \end{bmatrix}, \quad (7.3)$$

where $r' = dr/d\theta$. From Eq (3.44) one obtains

$$\mathbf{a}_1 = (R - r \sin \theta) \cos y^1 \mathbf{e}_1 - (R - r \sin \theta) \sin y^1 \mathbf{e}_2 \quad (7.4a)$$

$$\begin{aligned} \mathbf{a}_2 &= -(r' \sin \theta + r \cos \theta) \sin y^1 \mathbf{e}_1 - (r' \sin \theta + r \cos \theta) \cos y^1 \mathbf{e}_2 \\ &\quad + (-r' \cos \theta + r \sin \theta) \mathbf{e}_3 \end{aligned} \quad (7.4b)$$

and, since

$$\|\mathbf{a}_1\| = \sqrt{\mathbf{a}_1 \cdot \mathbf{a}_1} = R - r \sin \theta \quad (7.5a)$$

$$\|\mathbf{a}_2\| = \sqrt{\mathbf{a}_2 \cdot \mathbf{a}_2} = \sqrt{r'^2 + r^2}, \quad (7.5b)$$

the unit vectors \mathbf{j}_1 and \mathbf{j}_2 are given by (cf. Eqns 3.41)

$$\mathbf{j}_1 = \mathbf{a}_1 / \|\mathbf{a}_1\| = \cos y^1 \mathbf{e}_1 - \sin y^1 \mathbf{e}_2 \quad (7.6a)$$

$$\begin{aligned} \mathbf{j}_2 = \mathbf{a}_2 / \|\mathbf{a}_2\| = & -\frac{(r' \sin \theta + r \cos \theta) \sin y^1}{\sqrt{r'^2 + r^2}} \mathbf{e}_1 - \frac{(r' \sin \theta + r \cos \theta) \cos y^1}{\sqrt{r'^2 + r^2}} \mathbf{e}_2 \\ & + \frac{(-r' \cos \theta + r \sin \theta)}{\sqrt{r'^2 + r^2}} \mathbf{e}_3 \end{aligned} \quad (7.6b)$$

The normal vector \mathbf{j}_3 is immediately available through

$$\begin{aligned} \mathbf{j}_3 = \mathbf{j}_1 \times \mathbf{j}_2 = & -\frac{\sin y^1 (-r' \cos \theta + r \sin \theta)}{\sqrt{r'^2 + r^2}} \mathbf{e}_1 - \frac{\cos y^1 (-r' \cos \theta + r \sin \theta)}{\sqrt{r'^2 + r^2}} \mathbf{e}_2 \\ & - \frac{r' \sin \theta + r \cos \theta}{\sqrt{r'^2 + r^2}} \mathbf{e}_3. \end{aligned} \quad (7.7)$$

From Eq (3.60) the following new curvature matrices are evident

$$[\mathbf{K}_1^0] = \begin{bmatrix} 0 & \frac{r \cos \theta + r' \sin \theta}{\sqrt{r'^2 + r^2}} & -\frac{-r \sin \theta + r' \cos \theta}{\sqrt{r'^2 + r^2}} \\ -\frac{(r \cos \theta + r' \sin \theta)}{\sqrt{r'^2 + r^2}} & 0 & 0 \\ -\frac{-r \sin \theta + r' \cos \theta}{\sqrt{r'^2 + r^2}} & 0 & 0 \end{bmatrix}, \quad (7.8a)$$

and

$$[\mathbf{K}_2^0] = \begin{bmatrix} 0 & 0 & 0 \\ 0 & 0 & -\frac{r^2 + 2r'^2 - rr''}{r^2 + r'^2} \\ 0 & \frac{r^2 + 2r'^2 - rr''}{r^2 + r'^2} & 0 \end{bmatrix}. \quad (7.8b)$$

Once again, these rates of change of unit vectors are mathematically correct, but not dimensionally consistent (i.e., they are not the physical curvatures). Again each matrix is multiplied by the reciprocal of its respective scale factor:

$$1/h_1 = 1/\sqrt{g_{11}} = 1/\|\mathbf{a}_1\| = 1/(R - r \sin \theta) \quad (7.9a)$$

$$1/h_2 = 1/\sqrt{g_{22}} = 1/\|\mathbf{a}_2\| = 1/\sqrt{r^2 + r'^2}, \quad (7.9b)$$

leading to the physical curvature matrices (cf. Eqns 3.66)

$$[\mathbf{K}_1^0]_{(P)} = \begin{bmatrix} 0 & \frac{r \cos \theta + r' \sin \theta}{(R - r \sin \theta)\sqrt{r^2 + r'^2}} & -\frac{-r \sin \theta + r' \cos \theta}{(R - r \sin \theta)\sqrt{r^2 + r'^2}} \\ -\frac{(r \cos \theta + r' \sin \theta)}{(R - r \sin \theta)\sqrt{r^2 + r'^2}} & 0 & 0 \\ \frac{-r \sin \theta + r' \cos \theta}{(R - r \sin \theta)\sqrt{r^2 + r'^2}} & 0 & 0 \end{bmatrix} \quad (7.10a)$$

and

$$[\mathbf{K}_2^0]_{(P)} = \begin{bmatrix} 0 & 0 & 0 \\ 0 & 0 & -\frac{r^2 + 2r'^2 - r r''}{(r^2 + r'^2)^{3/2}} \\ 0 & \frac{r^2 + 2r'^2 - r r''}{(r^2 + r'^2)^{3/2}} & 0 \end{bmatrix}. \quad (7.10b)$$

From Eq (3.65), it is evident that the physical curvatures for a shell of revolution having a smooth (but otherwise arbitrary) cross-section are

$$k_1^0 = \frac{-r \sin \theta + r' \cos \theta}{(R - r \sin \theta)\sqrt{r^2 + r'^2}} \quad (7.11a)$$

$$k_2^0 = \frac{r^2 + 2r'^2 - r r''}{(r^2 + r'^2)^{3/2}} \quad (7.11b)$$

$$k_3^0 = \frac{r \cos \theta + r' \sin \theta}{(R - r \sin \theta)\sqrt{r^2 + r'^2}}, \quad (7.11c)$$

where $r' = dr/d\theta$. Note that for $r = \text{constant}$, which corresponds to the circular torus, Eqns (7.11) degenerate to Eqns (7.1).

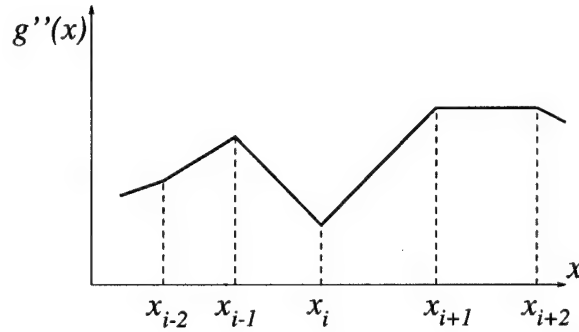


Figure 7.3 Piece-wise continuity of second derivative associated with classical cubic spline

For the finite element model, the generatrix (tire cross-section) for the shell of revolution is represented by a tension spline (Renka 1987) connecting user-defined nodes along the cross section. Rotating this generatrix about the origin of the major radius (axle) of the shell then generates the tire's reference surface. The tension spline is used because, in addition to having the continuous second derivative of the classical cubic spline (which results in continuous curvature), it may be formulated to preserve convexity of the curve over an interval. That is, the tension may be chosen such that the interpolant may not "wobble" (have an inflection point) between data points. This results in a smooth generatrix, making it suitable for modeling the tire cross section (Kim and Noor 1990). An overview of the tension spline technique follows.

In the classical implementation of the cubic spline (see, e.g., Hornbeck 1975, p. 47), the second derivative of the cubic interpolant, $g(x)$, is piecewise linear and continuous on the interval of interest, as shown in Figure 7.3, and the value of the second derivative at any point x , where $x_i \leq x \leq x_{i+1}$ is given by

$$g''(x) = g''(x_i) + \frac{x - x_i}{x_{i+1} - x_i} [g''(x_{i+1}) - g''(x_i)]. \quad (7.12)$$

Consider the interval $[x_1, x_2]$, where the associated data values and their derivatives are y_1, y_2, y'_1 , and y'_2 , respectively, and $y' = dy/dx$. Furthermore, define

$$h = x_2 - x_1, \quad b = (x_2 - x)/h, \quad s = (y_2 - y_1)/h, \quad d_1 = s - y'_1, \quad d_2 = y'_2 - s \quad (7.13)$$

By enforcing continuity of the first and second derivatives of the interpolant at the data points, the interpolating function on the interval $[x_1, x_2]$ is given by

$$g(x) = h_2 - h[y'_2 b + (d_1 - 2d_2)b^2 + (d_2 - d_1)b^2]. \quad (7.14)$$

Eq (7.14) represents the classical cubic spline.

In contrast, Renka's implementation of the tension spline applies a tension factor, σ_k , to each interval along the spline, such that

$$g \in C^1[x_1, x_n], \text{ and} \quad (7.15a)$$

$$g'''' - (\sigma_k/h_k)^2 g' = 0 \text{ in } [x_k, x_{k+1}], \quad (7.15b)$$

where $h_k = x_{k+1} - x_k$ is the length of the k^{th} interval. From Eq (7.15a), the interpolant is a function whose first derivative is continuous on the entire interval of interest. From Eq (7.15b), it is evident that as σ_k , the tension factor on the k^{th} interval, goes to zero, $g'''' = 0$, or g is a cubic function. That is, a tension of zero corresponds to the classical cubic spline of Eq (7.14). On the other hand, for $\sigma_k > 0$, one obtains (from multiplying Eq 7.15b by $(h_k/\sigma_k)^2$ and integrating twice)

$$(h_k/\sigma_k)^2 g'' - g = c_1 x + c_2, \quad (7.16)$$

where c_1 and c_2 are constants of integration. That is, as σ_k gets large, the first term of Eq (7.16) vanishes and the interpolating function, g , tends toward a linear function. In other words, for a sufficiently large value of σ_k (tension), the interpolant is simply a straight line connecting the two data points. Consider again the interval $[x_1, x_2]$, with associated data values and their derivatives are y_1, y_2, y'_1 , and y'_2 , respectively. Furthermore, define

$$\sinhm(z) = \sinh(z) - z, \quad \coshm(z) = \cosh(z) - 1 \quad (7.17a)$$

$$E = \coshm^2(\sigma) - \sinhm(\sigma) \sinh(\sigma) \quad (7.17b)$$

$$\alpha_1 = \sigma \coshm(\sigma) d_2 - \sinhm(\sigma) (d_1 + d_2) \quad (7.17c)$$

$$\alpha_2 = \sigma \sinh(\sigma) d_2 - \coshm(\sigma) (d_1 + d_2). \quad (7.17d)$$

Then the form of the interpolating function, based upon Eqns (7.15), is

$$g(x) = y_2 = y'_2 h b + h/(\sigma E) [\alpha_1 \coshm(\sigma b) - \alpha_2 \sinhm(\sigma b)]. \quad (7.18)$$

Renka's technique uses an iterative procedure to satisfy certain user-defined conditions on the interpolant with the minimum tension, σ , necessary. The interested reader is referred to the reference of Renka (1987) for the details of the algorithm.

The FORTRAN implementation of this technique downloaded from the world-wide-web site

$$\text{http} : // \text{netlib.att.com/netlib/master/readme.html} \quad (7.19)$$

provides for calculation of the derivatives of the fitted curve at any point along the curve, easing the formulation of Eqns (7.11).

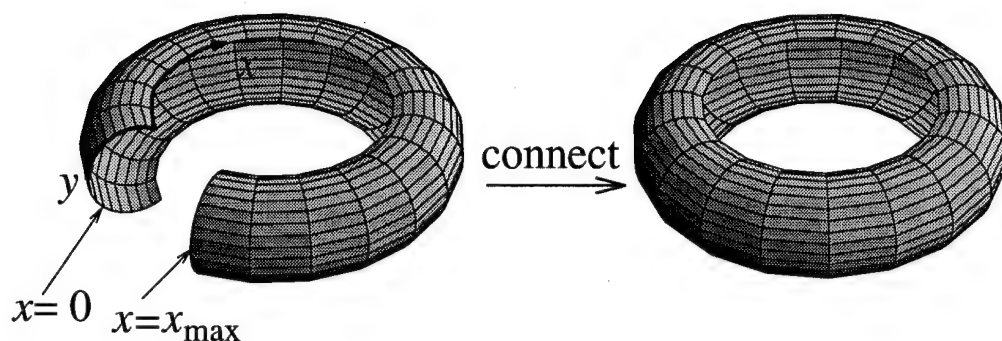


Figure 7.4 Connecting a mesh to itself to form a continuous shell

7.2 Connected Meshes

To adequately model the tire geometry, the computer program must have features allowing the mesh to be connected along the curves $x = 0$ and $x = x_{\max}$ as in Figure 7.4. That is, the mesh must be capable of being “closed” into a continuous shell. Though not required for the tire model, a more general modification was made to the program which includes the aforementioned feature along with the ability to connect the mesh along the curves $y = 0$ and $y = y_{\max}$, as well as simultaneously connecting the mesh along both sets of curves (as would be done to model an inner-tube, for example).

It is important to note that connecting the mesh affects the bandwidth of the symmetric-banded system of equations solved to find nodal displacements (Eq 4.111). The half bandwidth, hbw , of the system of equations is given by

$$hbw = \max_{i \in A} (\max(B) - \min(B))_i + 1, \quad (7.20)$$

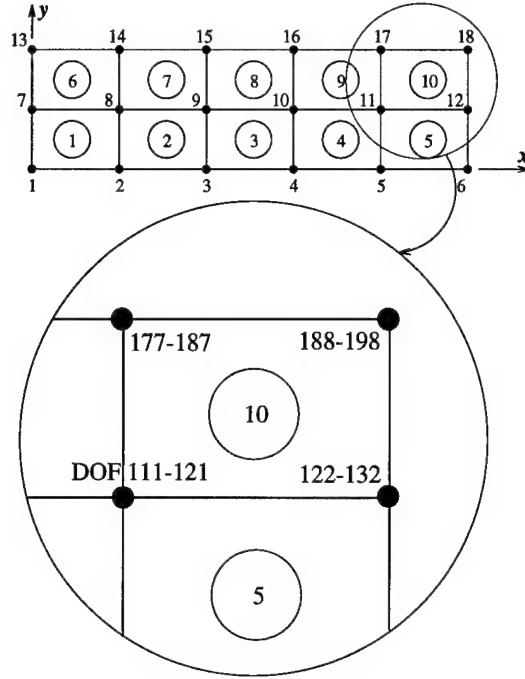


Figure 7.5 Unconnected 2×5 mesh indicating degrees-of-freedom associated with element 10

where $A = \{1, 2, 3, \dots, N_{\text{ele}}\}$, N_{ele} being the number of elements in the mesh, and B is the set containing all DOF numbers associated with the nodes of element i . For the four-noded, 44-DOF elements arranged in an ‘unconnected’ rectangular mesh (as would be used with a shell panel or flat plate) having M rows and N columns of elements, the half bandwidth of the equations will be $11(3 + N)$. (Note that the bandwidth depends only on the number of columns in the mesh. This is due to the convention of numbering nodes consecutively along the x -direction.) As an example, consider element number 10 of the unconnected mesh² of Figure 7.5. For this case $N_{\text{ele}} = 10$, $A = \{1, 2, 3, \dots, 10\}$, and $B = \{111, 112, 113, \dots, 132\} \cup \{177, 178, 179, \dots, 198\}$, yielding a half bandwidth of $hbw = (198 - 111) + 1 = 88$.

As will be shown, connecting the mesh has the following effects: (1) the number of nodes and degrees-of-freedom are always decreased while (2) the bandwidth of the equations almost always increases. This penalizes the solution algorithm, in that the expense of solution (in terms of number

²For this type of mesh, any element could be chosen to calculate the half bandwidth.

of calculations required to solve the system of equations) is strongly related to the half band-width of the equations. Letting \hat{e}_1 and \hat{e}_2 be the “expense” of solution for two systems of equations having half bandwidths b_1 and b_2 , respectively, leads to (Cook et al. 1989, p. 45)

$$\frac{\hat{e}_2}{\hat{e}_1} \approx \left(\frac{b_2}{b_1} \right)^2. \quad (7.21)$$

For example, doubling the half bandwidth of a system of equations results in a quadrupling of the number of calculations required to solve it.

Now consider the effect on the half bandwidth of joining the mesh in three different ways. The discussions here focus on the effect of the connections on the bandwidth of the system of equations that yield the solution to the finite element problem. Another consideration, while not discussed here in detail, is the effect on “book-keeping” tasks: when node numbers are reassigned, care must be taken so that the boundary conditions, loads, and degrees-of-freedom are applied correctly.

7.2.1 The x -connected mesh. Again, consider the mesh of Figure 7.5. If the ends of the mesh corresponding to $x = 0$ and $x = x_{\max}$ are connected, a strip is turned into a ring. This is depicted in Figure 7.6, which also shows the effect on the node numbering. It is this connection scheme that is used in modeling the tire in subsequent sections, where x is the circumferential direction and y is the meridional direction. In an $M \times N$ mesh of elements, the number of nodes is reduced by $M + 1$ and the number of DOF by $11(M + 1)$. The half bandwidth of the x -connected mesh is $22N$. It is a simple exercise to show that for $N > 3$, this mesh connection increases the bandwidth by a factor of $2N/(3 + N)$ and, in the limiting case of $N \rightarrow \infty$, doubles it.

7.2.2 The y -connected mesh. Again, this type of mesh connection is not required to form the tire model, but has application to other geometries, and so is included here for completeness. To see the impact of connecting the mesh along $y = 0$ and $y = y_{\max}$, again consider the flat mesh of Figure 7.5. If the mesh is “rolled up” in the y direction, a tube is formed, as shown in Figure 7.6.

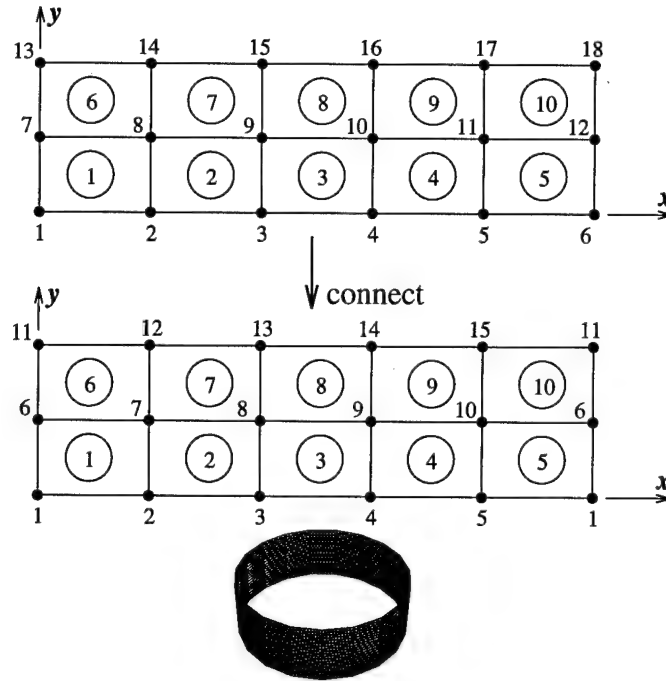


Figure 7.6 Mesh joined along constant x coordinate curves

The figure also indicates the node numbering changes that occur as a result. Again, connecting the mesh does not change the number of elements but, for an $M \times N$ mesh, reduces the number of nodes by $N + 1$, and the number of DOF by $11(N + 1)$. The half bandwidth for this arrangement is $11(1 + M - N + MN)$. For $M > 2$, the effect of the y -connection is to increase the half bandwidth by $(1 + M - N + MN)/(3 + N)$. This factor approaches $(M - 1)$ as $N \rightarrow \infty$. So whereas the growth in bandwidth is limited to a factor of 2 in the x -connection case, it is not so limited in this case.

7.2.3 Connecting in both directions. By taking the rolled up mesh of the previous section and joining the free ends, the mesh is closed in both directions forming a circular torus (Figure 7.8). In this case, the number of nodes in an $M \times N$ mesh is reduced by $M + N + 1$, the DOF by $11(M + N + 1)$, and the half bandwidth is simply $11MN$. Any practical mesh will have a larger bandwidth than its unconnected counterpart by a factor of $MN/(3 + N)$. Like the y -connected

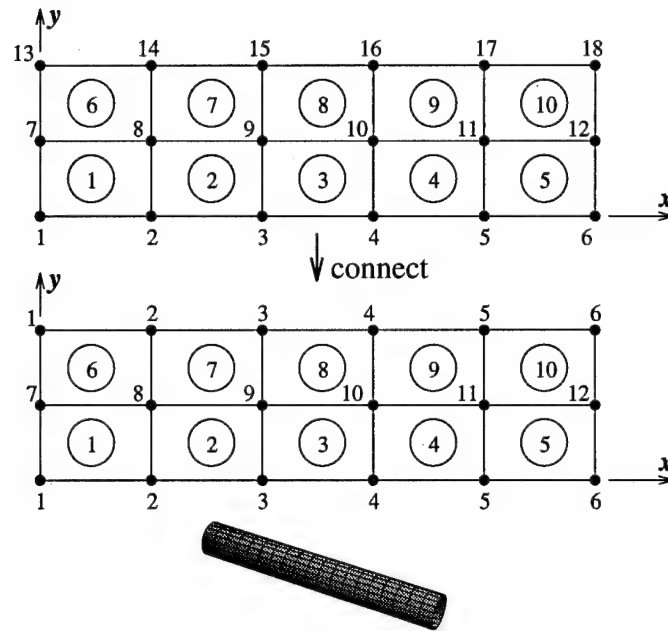


Figure 7.7 Mesh joined along constant y coordinate curves

Effect on $M \times N$ mesh	x -connected	y -connected	both x and y
Reduction in Nodes	$M + 1$	$N + 1$	$M + N + 1$
Reduction in DOF	$11(M + 1)$	$11(N + 1)$	$11(M + N + 1)$
Increase in hbw	$2N/(3 + N)^a$	$(1 + M - N + MN)/(3 + N)^b$	$MN/(3 + N)$

^aFor $N > 3$

^bFor $M > 2$

Table 7.1 Effect of different mesh connection schemes on number of nodes, number of DOF, and half bandwidth of system of equations for a mesh of M rows and N columns

mesh, the half bandwidth can grow quite large: it approaches M as $N \rightarrow \infty$, and becomes infinite as $M \rightarrow \infty$.

The results of connecting the finite element mesh to itself in these three ways are summarized in Table 7.1.

7.3 The Shuttle Tire

The nose wheel tire of the Space Transportation System or "Space Shuttle" is examined in the current research. The tire is modeled as a two-dimensional reference surface, and the ply thicknesses,

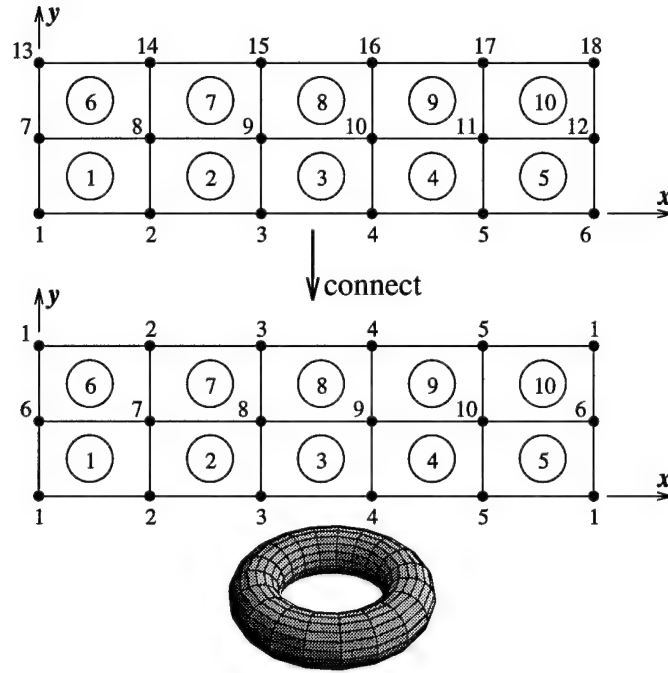


Figure 7.8 Mesh joined along both constant x and constant y coordinate curves

ply constitutive relations, and ply orientation angles are allowed to change from element to element in the meridional direction (elements in the circumferential direction have identical properties). The tire's construction details are described in the work of Kim and Noor (1990) whose results are used for comparison purposes in the current research.

7.3.1 Inflation. In the current work, a pressure loading is applied using equivalent nodal loads. The shape functions are used to calculate the applied nodal loads in an potential energy equivalent sense. That is,

$$\{\mathbf{r}_e\}_{44 \times 1} = \int_A [\mathbf{N}]^T_{44 \times 5} \{\mathbf{P}\}_{5 \times 1} dA \quad (7.22)$$

where $\{\mathbf{r}_e\}$ is the vector of equivalent nodal loads for the element, $[\mathbf{N}]$ is the matrix of shape functions (Eq 4.83), and

$$\{\mathbf{P}\} = \{p_u, p_v, p_w, 0, 0\} \quad (7.23)$$

is the pressure loading vector. The two zero entries in the pressure vector correspond to loads associated local rotations (moment-like quantities), which are not present in a pressure load. In keeping with the total Lagrangian formulation, the components of $\{\mathbf{P}\}$ must always be expressed in terms of coordinates associated with the initial (undeformed) configuration, represented by the $\{\mathbf{j}_{123}\}$ -basis (recall Figure 3.7). Since \mathbf{j}_3 is initially everywhere normal to the reference surface, as is the pressure load, the pressure vector originally has the form $\{\mathbf{P}\} = \{0, 0, p_w, 0, 0\} = P \mathbf{j}_3$, where P is the magnitude of the pressure. As the reference surface goes through its movement, the normal to the surface is represented by the basis vector \mathbf{i}_3 , and the pressure, which remains normal to the deforming surface, becomes $\{\mathbf{P}\} = P \mathbf{i}_3$. The basis vector \mathbf{i}_3 is related to \mathbf{j}_3 by (Eq 3.104)

$$\mathbf{i}_3 = T_{31}\mathbf{j}_1 + T_{32}\mathbf{j}_2 + T_{33}\mathbf{j}_3, \quad (7.24)$$

where the T_{3k} are available through the relationships of Eqns (3.92). Hence the direction of the normal pressure load can be "updated" at each increment by expressing it in terms of the *undeformed* reference surface through

$$\mathbf{P} = P \mathbf{i}_3 = P(T_{31}\mathbf{j}_1 + T_{32}\mathbf{j}_2 + T_{33}\mathbf{j}_3) = P_u \mathbf{j}_1 + P_v \mathbf{j}_2 + P_w \mathbf{j}_3, \quad (7.25)$$

where

$$P_u = P T_{31}, \quad P_v = P T_{32}, \quad P_w = P T_{33}. \quad (7.26)$$

For this formulation, the elements are always rectangular (in the curvilinear coordinate system) with dimensions $2a \times 2b$, and substituting Eqns (7.23) and (4.83) into Eq (7.22) leads to the following equivalent load vector:

$$\begin{aligned} \{\mathbf{r}_e\} = & \{abp_u, a^2bp_u/3, ab^2p_u/3, abp_v, a^2bp_v/3, ab^2p_v/3, abp_w, a^2bp_w/3, ab^2p_w/3, 0, 0, \\ & 44 \times 1 \\ & abp_u, -a^2bp_u/3, ab^2p_u/3, abp_v, -a^2bp_v/3, ab^2p_v/3, abp_w, -a^2bp_w/3, ab^2p_w/3, 0, 0, \end{aligned}$$

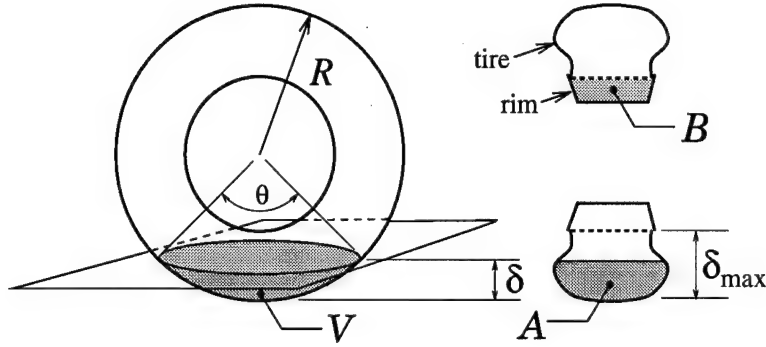


Figure 7.9 Estimating the effect of tire deflection on tire pressure

$$\begin{aligned}
 &abp_u, -a^2bp_u/3, -ab^2p_u/3, abp_v, -a^2bp_v/3, -ab^2p_v/3, abp_w, -a^2bp_w/3, -ab^2p_w/3, 0, 0, \\
 &abp_u, a^2bp_u/3, -ab^2p_u/3, abp_v, a^2bp_v/3, -ab^2p_v/3, abp_w, a^2bp_w/3, -ab^2p_w/3, 0, 0\}^T.
 \end{aligned}
 \tag{7.27}$$

Some scenarios benefit more from this updating scheme than others. In fact, one can easily visualize geometries for which such an updating scheme is superfluous (e.g., inflation of an isotropic sphere). In the following results, it will be noted for each case whether the updating scheme was used.

Of course the *magnitude* of the internal pressure changes with tire deflection as well, but this effect can be estimated using the method depicted in Figure 7.9. In this figure is a toroidal shell having the cross section of the shuttle nose wheel tire. The maximum deflection of the tire, δ_{\max} , is about 153 mm and, for most tires, deflections exceeding 40 % are rare. A 40 % deflection for this tire is $0.40 \times 153 \text{ mm} \approx 62 \text{ mm}$. Using a graphical plot of the shuttle tire cross section, the following relationship was developed to estimate the area of the region denoted A in the figure versus the deflection δ :

$$A(\delta) = \frac{170 \pi}{18} \int_0^\delta \sin\left(\frac{\pi}{18} \bar{\delta}\right) d\bar{\delta} \text{ cm}^2.
 \tag{7.28}$$

Using this relationship, the volume of region V may be estimated (via the geometric relationships of the figure) as

$$V(\delta) = \left[\left(R - \frac{\delta}{2} \right) A(\delta) \right] \int_0^{\theta(\delta)} \sin \left(\frac{\bar{\theta}}{\theta(\delta)} \right) d\bar{\theta}, \quad (7.29)$$

where the angle θ of Figure 7.9 is given by

$$\theta(\delta) = 2 \cos^{-1}(1 - \delta/R). \quad (7.30)$$

To calculate the change in tire pressure, the air in the volume V is placed in the truncated volume of the tire, \hat{V} , where

$$\hat{V}(\delta) = V_{\text{tot}} - V(\delta), \quad (7.31)$$

and V_{tot} is the initial volume of the undeflected tire. Using the equation of state for a perfect gas, a very conservative estimate of the pressure change ΔP can be made, given by

$$\Delta P(\delta) = \frac{\mathcal{R}T}{V_{\text{tot}}} - \frac{\mathcal{R}T}{V(\delta)}, \text{ or} \quad (7.32a)$$

$$\Delta P(\delta) = \mathcal{R}T \left(\frac{1}{V_{\text{tot}}} - \frac{1}{V(\delta)} \right), \quad (7.32b)$$

where \mathcal{R} is the gas constant for air and T is its absolute temperature. The result of this equation is plotted in Figure 7.10. Note that this estimate is *very* conservative for a number of reasons. First, it is assumed that the tire may not flex to accommodate the pressure increase. Second, it is assumed that the temperature of the air does not increase as the pressure increases. Finally, there is *additional initial volume* available that is being neglected: the volume shown in Figure 7.9 resulting from the area of region B . This volume is present due to the concave shape of the wheel at the wheel's outer radius. Because the exact shape is unknown, the attendant volume was not included. Had it been, the pressure change would have been smaller still. From Figure 7.10, the percentage change in pressure is of order $\Delta P_{\text{max}} \% \approx \mathcal{O}(\delta/10)$, where δ is the deflection in millimeters. In view

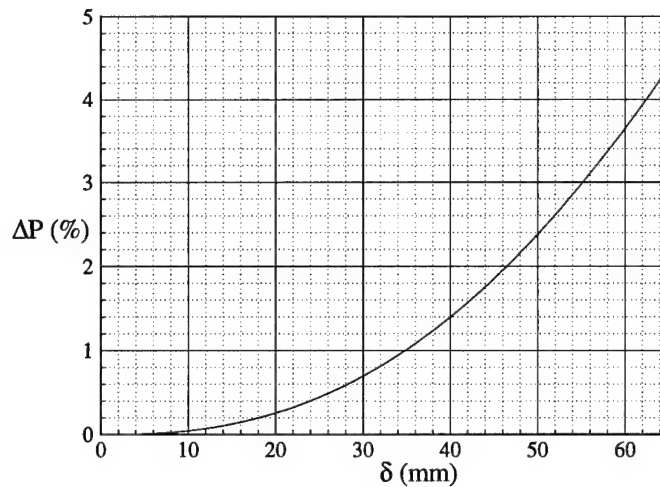


Figure 7.10 Conservative estimate of increase in shuttle nose wheel tire pressure due to inflation of the conservative assumptions, the actual change would be considerably less, hence no attempt is made to adjust the pressure *magnitude* during tire deflection.

The results of the finite element analysis for an inflation pressure of 2.206 MPa (320 psi) are compared to experimental results presented by Kim and Noor (1990) in Figure 7.11. The reference surface is chosen to satisfy three criteria: (1) along the meridian, the reference surface should be as near the middle of the laminate as possible, (2) the reference surface should be at the middle of the ply in which it resides, and (3) the outer surface of the elements should match that of the actual tire and be as smooth as possible. Criterion (1) arises from the desire to free the warping functions in the outer plies; The ply containing the reference surface must be constrained such that the warping functions are zero at the reference surface (see the discussion of Section 3.6). Criterion (2) reflects that fact that as the reference surface approaches a ply interface, the warping function equations (Eqns 3.140) have no unique solution, hence the middle of the ply is a desirable location (see Section 3.6). The third criterion is desirable from the standpoint of tire contact studies as, in reality, the outer surface is the contact surface. In the contact algorithm, the reference surface is used as the contact surface, then corrected for the thickness of the tire above the reference surface as

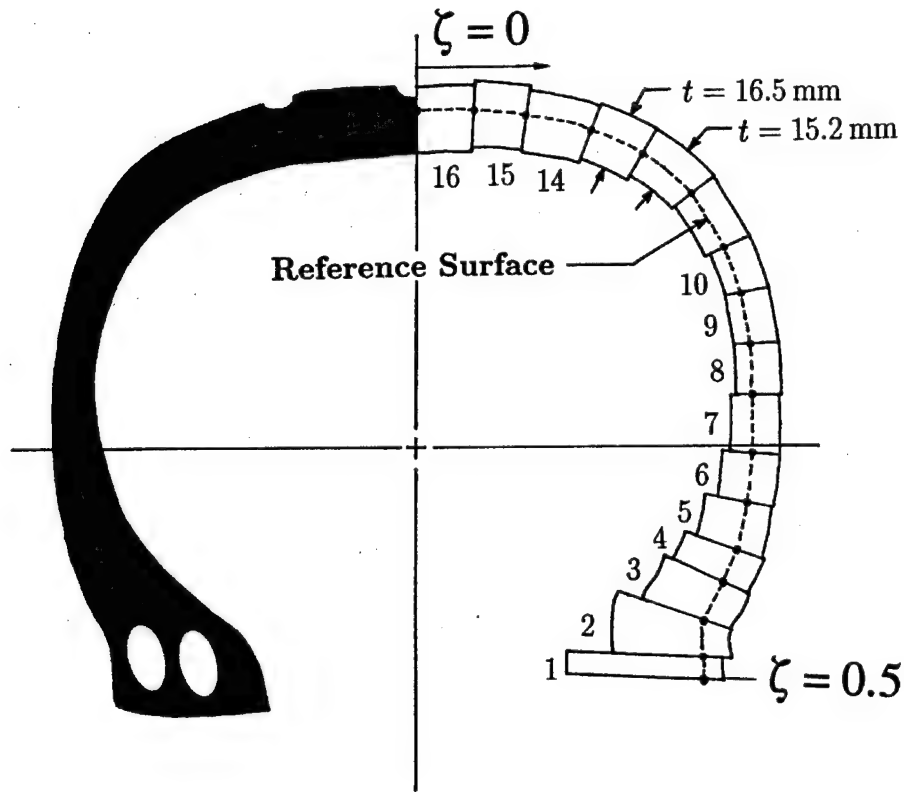


Figure 7.11 Finite element mesh vs. actual tire cross-section indicating element numbering and typical element thicknesses

well as the change in that thickness. Since the reference surface is continuous and smooth, criterion (3) ensures that the undeformed tire thickness above the reference surface is nearly uniform about the meridian.

Trying to satisfy these criteria leads to the element choices depicted in Figure 7.11, where ζ is the non-dimensionalized meridional coordinate, expressing the the fraction of the total curvilinear length along the meridian of the reference surface. The overall mesh employed in the inflation study is shown in Figure 7.12. The mesh employs 832 elements, 858 nodes, and has 9438 total DOF. The material properties used in the finite element model are presented in Appendix F. The boundary conditions for the analysis are given by

$$\text{at } y = 0, \text{ clamped: all DOF fixed} \quad (7.33)$$

$$\text{at } y = 9.13 \text{ mm, clamped: all DOF fixed}$$

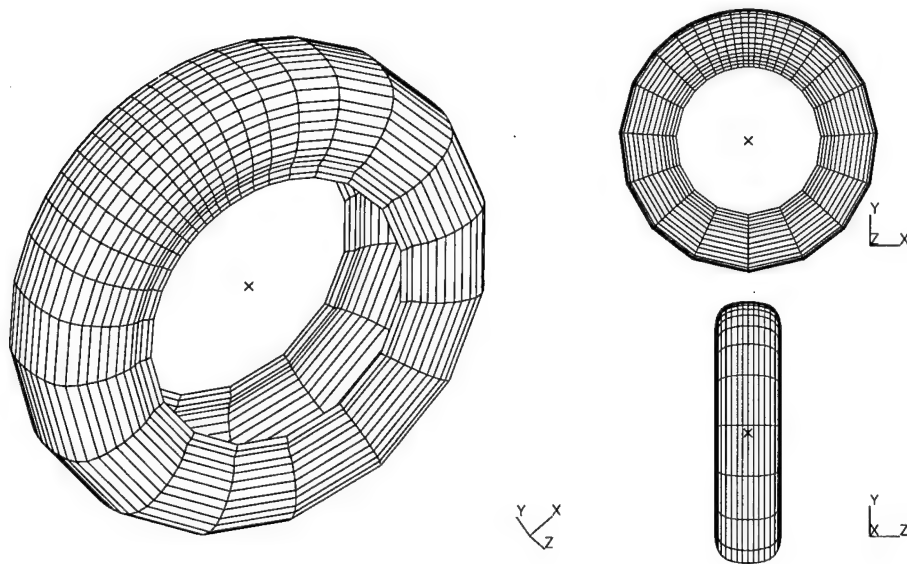


Figure 7.12 Three views of the shuttle nose wheel tire mesh; The figure does not reflect the fact that the finite element is actually bi-curved, not flat.

at $y = 16.60$ mm, clamped: all DOF fixed

at $y = 439.29$ mm, clamped: all DOF fixed

at $y = 446.75$ mm, clamped: all DOF fixed

at $y = 455.88$ mm, clamped: all DOF fixed.

These conditions reflect the fact that the first and last three (circumferential) rows of nodes are fixed at the tire/rim interfaces (see Figure 7.13). A convergence tolerance of $10^{-4}\%$ was used in the analysis, and the inflation loads were applied in six equal increments. The pressure vector directions were not updated in this portion of the study. The results of the inflation study are depicted in Figure 7.14. The “uncorrected” deflection represents the deflection of the reference surface, which, ignoring any thickness change, is also the displacement of the outer surface. The “corrected” data points adjust these displacements for thickness stretching, Δh , by numerically

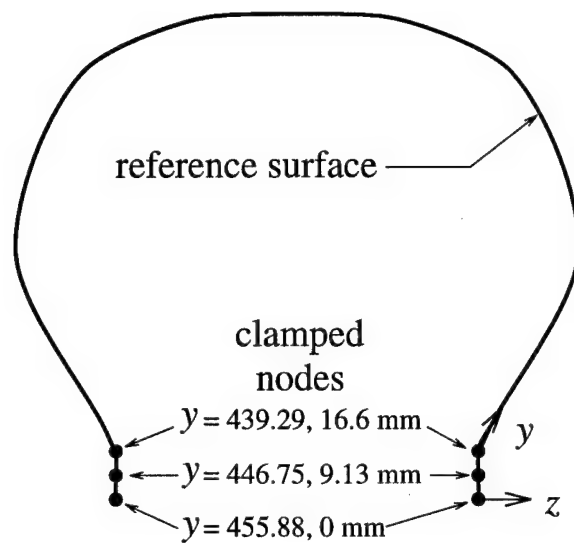


Figure 7.13 Tire cross section indicating coordinate system and boundary conditions

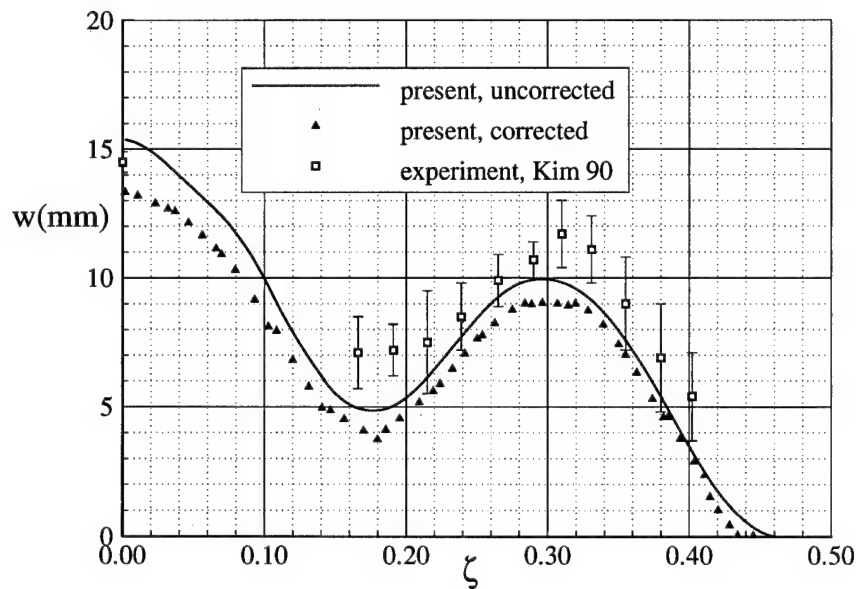


Figure 7.14 Finite element calculations compared to experimental (measured) values for space shuttle nose-wheel tire. See text for discussion of error bars.

integrating the strain, $B_{33}(z)$, from the reference surface to the outer surface at each Gauss point.

That is,

$$\Delta h = \int_0^{z_{N+1}} B_{33}(z) dz. \quad (7.34)$$

The error bars on the experimental data have two sources: (1) the measured radial displacement at a given meridional location may have slightly different values at different circumferential locations and the error bars encompass that variation, and (2) precision error is introduced in reading the graphical data from the plots of the work of Kim and Noor (1990). In any case, the calculated displacements are clearly less than the experimental ones. Two possible sources of this difference are (1) any finite element solution should be somewhat stiffer than its "real" counterpart, and (2) the present analysis models no viscoelastic properties. It is likely that the tire material exhibits some "creep" after inflation and, depending upon when the measurements were taken, these time-dependent properties may have influenced the result (according to DeEskinazi et al. 1978, the majority of this creep occurs shortly after inflation).

It is important to recall that the finite element formulation calculates the thickness stretching based upon the assumption of zero stress at the boundaries. For the tire inflation problem, this assumption is patently false. However, the thickness change calculated by the model, generated by the membrane stretching due to application of equivalent nodal loads, provides good results in predicting the displaced outer surface of the tire.

Stress resultants for the finite element results are calculated by integrating the stresses through the thickness:

$$N_x = \int_{z_1}^{z_{N+1}} J_{11}(z) dz, \quad N_y = \int_{z_1}^{z_{N+1}} J_{22}(z) dz, \quad N_z = \int_{z_1}^{z_{N+1}} J_{33}(z) dz, \quad (7.35a)$$

$$N_{xy} = \int_{z_1}^{z_{N+1}} J_{12}(z) dz, \quad N_{xz} = \int_{z_1}^{z_{N+1}} J_{13}(z) dz, \quad N_{yz} = \int_{z_1}^{z_{N+1}} J_{23}(z) dz. \quad (7.35b)$$

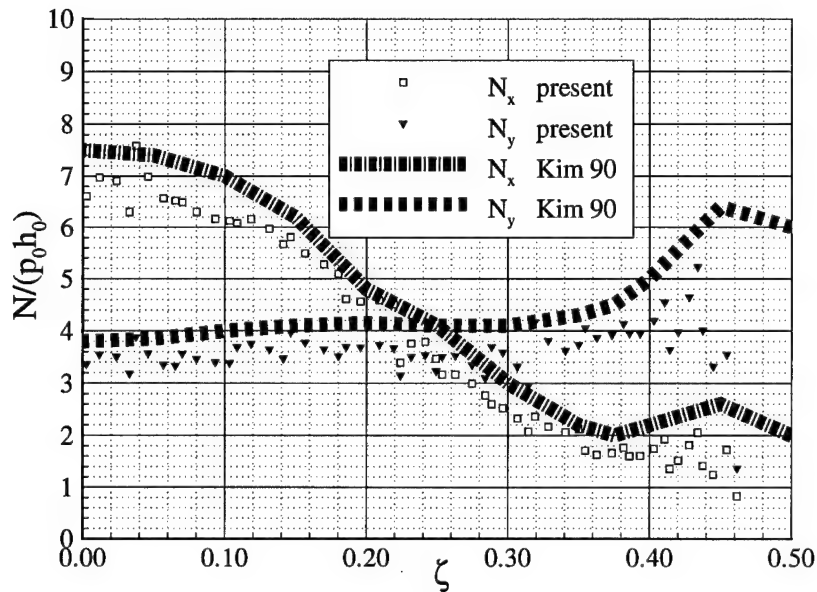


Figure 7.15 Finite element stress resultants compared to finite element calculations of Kim and Noor (1990)

They are then nondimensionalized by dividing by the inflation pressure, $p_0 = 2.206 \text{ MPa}$ (320 psi), and the tire thickness at the crown, $h_0 = 19.05 \text{ mm}$ (0.75 in). The resultants generated by the finite element model are shown in Figure 7.15. They are compared with the results of the finite element model of Kim and Noor (1990), who used a semi-analytic finite element model employing moderate-rotation Sanders-Budiansky shell theory and having the following properties: (1) the shell variables are represented by Fourier series in the circumferential direction and piecewise polynomials in the meridional direction, and (2) the fundamental unknowns in the model are strain-resultant parameters, stress-resultant parameters, and generalized displacements. The line thickness in the plot reflects the imprecision in reading the graphical data. As stress-resultants are a fundamental unknown in the model, it is likely that the values of Kim and Noor in Figure 7.15 are more reliable than those of the present research, in which the stresses are tertiary quantities calculated from strains generated by displacements. Still, the agreement between solutions is good, except near the tire/rim interface. In this region, the element thicknesses are changing rapidly, causing erratic

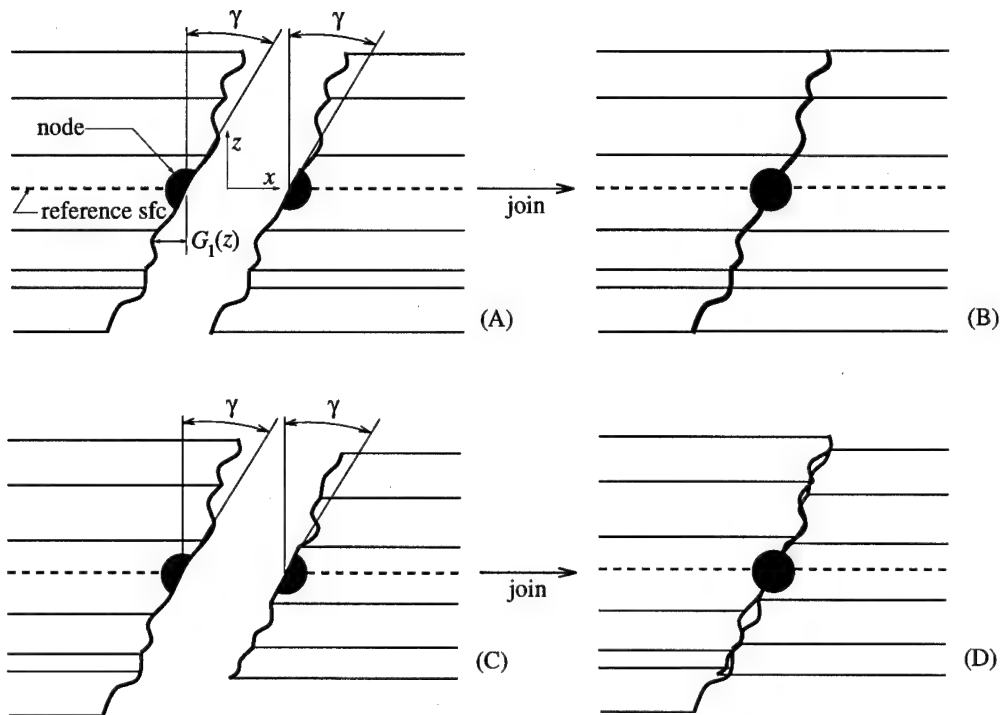


Figure 7.16 Discontinuity introduced by adjacent elements of different ply lay-up; Case (A) \rightarrow (B): adjacent elements of identical configuration; Case (C) \rightarrow (D): adjacent elements of different configuration

results. This is due to the discontinuity introduced by having different ply lay-ups adjacent to each other at nodes. Consider Figure 7.16, which depicts the effect of this difference. Recall that the displacements away from the shell reference surface are determined by enforcing stress and displacement continuity at interlaminar boundaries. Therefore, the element configuration (number, angles, thicknesses, and constitutive properties of the plies) and the displacements at the reference surface uniquely determine the values of these through-the-thickness displacements. If two adjacent elements have identical configurations (Case (A) \rightarrow (B) of Figure 7.16), then the displacement conditions at their common node(s) (on the reference surface) will determine the displacements away from the reference surface at the node. Furthermore, these displacements will be identical at the node whether it is approached from the element on the left or the right. On the contrary, if

Component (ij)	11	22	33	12	23	13
Stress J_{ij} (MPa)	36.91	27.76	4.022	27.428	-.5976	.2121
Occurs in element	16	10	3	10	10	11
Distance from ref sfc (z mm)	-0.8255	-0.5135	-15.93	-0.5135	0.5135	0.
Strain B_{ij} (%)	4.131	23.642	-55.25	-1.696	-25.01	13.212
Occurs in element	16	16	16	3	12	10
Distance from ref sfc (z mm)	+7.247	+7.247	+4.128	-18.41	-0.5745	-0.5135

Table 7.2 Maximum stresses and strains due to inflation of the shuttle tire model without pressure direction updates

the adjacent elements have different configurations (Case $(C) \rightarrow (D)$ of Figure 7.16) then, while the displacements at the common node(s) on the reference surface are unique, the difference in element configuration will cause a mis-match in the displacement functions through-the-thickness. Note that, unlike the problem generated by lack of element continuity seen in Section 6.4, *the element remains C^1 continuous at the reference surface*. The effect of the mis-match is to cause a discontinuity in the strain energy along interelement boundaries (since integration through the thickness is included in that calculation). In qualitative terms, it should be clear that very gradual changes in element properties are more desirable than sudden ones.

The peak stresses in the inflated tire are noted in Table 7.2. The element numbers in the table indicate numbering from the tire/rim interface to the crown, such that element 1 is at the tire/rim interface and elements 16 and 17 are astride the crown. The largest strains in Table 7.2 are located in the outer ply which is isotropic rubber. It has a modulus roughly two orders of magnitude less than that of the nylon-corded rubber of the other plies. The maximum transverse normal strain of $B_{33\max} = -55\%$ is large, but is on the order of that seen by Simo et al. (1990) in finite element modeling of a transversely loaded rubber sphere. In that instance, strains of 55% were seen.

Another source of the erratic results near the tire/wheel interface is that the current (displacement based) model imposes a fully-clamped boundary condition at the rim, while the stress-resultant parameters used by Kim and Noor (1990) permit non-zero stresses in the interface region. In this displacement-based scheme, the setting of the displacements in the clamped region to zero

Component (ij)	11	22	33	12	23	13
without updated warping functions:						
Stress J_{ij} (MPa)	36.91	27.76	4.022	27.428	-.5976	.2121
Occurs in element	16	10	3	10	10	11
Distance from ref sfc (z mm)	-0.8255	-0.5135	-15.93	-0.5135	0.5135	0.
Strain B_{ij} (%)	4.131	23.642	-55.25	-1.696	-25.01	13.212
Occurs in element	16	16	16	3	12	10
Distance from ref sfc (z mm)	+7.247	+7.247	+4.128	-18.41	-0.5745	-0.5135
with updated warping functions:						
Stress J_{ij} (MPa)	36.68	27.65	4.161	27.33	-.5982	.2123
Occurs in element	16	10	3	10	10	11
Distance from ref sfc (z mm)	-0.8255	-0.5135	-15.93	-0.5135	0.5135	0.
Strain B_{ij} (%)	4.275	23.42	-54.12	-1.774	-24.97	13.225
Occurs in element	16	16	16	3	12	10
Distance from ref sfc (z mm)	+7.247	+7.247	+4.128	-18.41	-0.5745	-0.5135

Table 7.3 Maximum stresses and strains due to inflation of the shuttle tire model without pressure direction updates indicating differences caused by updating warping functions in constitutive matrix

has the result of setting strains to zero and therefore stresses to zero. In contrast, when stress-resultant parameters are used as fundamental unknowns (as opposed to a derived quantity) they need not be *a priori* set to zero along a clamped boundary.

As mentioned in Chapter IV, the simplification incorporated by Pai and Palazotto (1995a) in which the deformed curvatures of the $[S]$ matrix of Eq (4.6a) are replaced by their undeformed counterparts will now be re-examined. Recall that the $[S]$ matrix specifies the constitutive matrix, $[\Phi]$. A comparison of the stresses and strains generated by the incorporating the simplification (the data of Table 7.2) to those generated without use of the simplification is shown in Table 7.3. As can be seen in the table, even with the thick shell of the tire, the effect of updating the warping functions in the constitutive matrix is not significant. Attention is now turned to the problem of static contact.

7.3.2 Static Contact. The static contact analyses are developed by bringing a flat surface (representing the pavement) into contact with the tire and moving it toward the axle incrementally as in Figure 7.17. The contact algorithm is similar to that of Wu and Du (1995) in that it is a

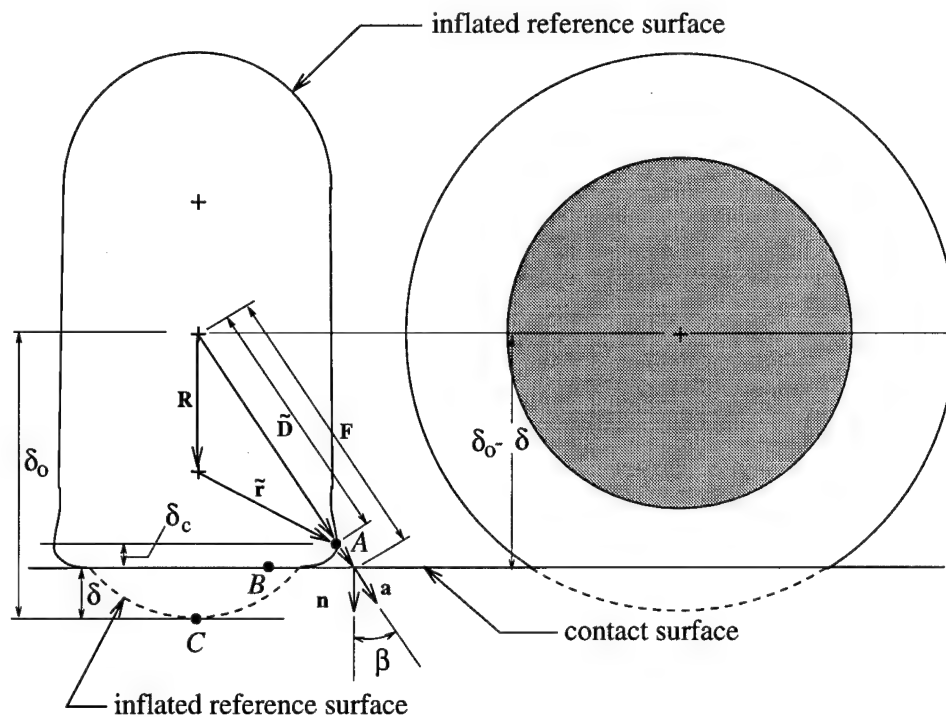


Figure 7.17 Geometry of deformed tire for contact algorithm

boundary condition modification scheme. In this first attempt at designing a contact algorithm for this finite element scheme, two simplifying assumptions are made: (1) once in contact with the surface, a node may not slide along the surface and (2) the contact surface is perfectly rigid. With these assumptions, the algorithm is implemented by checking the distance between each node³ and the contact surface and then, for nodes determined to be in contact, prescribing their displacements such that they move with the contact surface. The algorithm begins by locating the contact surface tangent to the tire crown at a specified node; in this case, node *C* of Figure 7.17. The distance from the axle of this tangent point is known, since it is merely the sum of the distance to this point in its undeformed location, d_0^c , and the displacement w that occurred as a result of inflation. That is

$$\delta_0 = d_0^c + w_c. \quad (7.36)$$

³In actuality, the *JAGS* user specifies a limited *group* of candidate nodes to check for contact.

The displacement of the reference surface is then incremented by an amount equal to the distance, δ^* , from the contact surface in the normal direction to the closest node not yet in contact. Note that this displacement increment is restricted by:

$$\delta_{\min} \leq \delta^* \leq \delta_{\max}, \quad (7.37)$$

where δ_{\min} and δ_{\max} are prescribed by the user. This normal distance is calculated as follows. Consider candidate node A of Figure 7.17. The vector to node A from the origin of the body-fixed coordinate system (the $\{\mathbf{e}_{123}\}$ -basis of Figure 3.5), is given by

$$\|\tilde{\mathbf{D}}\| = \|\mathbf{R}\| + \|\tilde{\mathbf{r}}\|, \quad (7.38)$$

where \mathbf{R} is the vector from this origin to the center of the tire cross-section, and $\tilde{\mathbf{r}}$ is the vector from that point to the *displaced* nodal location. (Both \mathbf{R} and $\tilde{\mathbf{r}}$ lie in the meridional plane of point A). The choice of \mathbf{R} is arbitrary (in terms of its length), but for this research \mathbf{R} was chosen such that $\|\mathbf{r}\|_{\theta=0} = \|\mathbf{r}\|_{\theta=\frac{\pi}{2}}$. The vector $\tilde{\mathbf{r}}$ is easily generated by knowing the original coordinates and the subsequent displacements u_A , v_A , and w_A of node A . Now note that the normal distance from point A to the contact surface, δ_c , is given by

$$\delta_c = \delta_0 - \delta - \|\tilde{\mathbf{D}}\|(\mathbf{n} \cdot \mathbf{a}), \quad (7.39)$$

where δ is the sum of all previous displacement increments, \mathbf{n} is the unit normal to the contact surface, and \mathbf{a} is a unit normal in the direction of $\tilde{\mathbf{D}}$. If this distance is zero (or less than zero) the node's translational degrees of freedom are fixed, and in subsequent displacement increments move with the contact surface. No attempt is made to modify the slopes $w_{,x}$ and $w_{,y}$ at the nodes in order to maintain an element shape congruent to the flat contact surface—only the node's displacements are considered. This implies that the shell surface between nodes could penetrate

the contact surface. However, if the mesh is fine enough in the contact region, such penetrations can be considered to be negligible.

The static contact algorithm was exercised on two tire models of the shuttle nose-wheel tire: an axisymmetric version of the tire model used in the inflation study, and materially simplified, but geometrically correct, whole-tire model.

The axisymmetric model of the shuttle nose-wheel tire consists of a 1×32 mesh modeling the entire tire meridian (Figure 7.11). The material properties are identical to those used in the inflation study (see Appendix F). The boundary conditions are set to represent axisymmetry: behavior of the structure may not vary in the circumferential (x) direction. For such a model, the boundary conditions are given by:

$$\text{at } y = 0, \text{ clamped: all DOF fixed} \quad (7.40)$$

$$\text{at } y = 9.13 \text{ mm, clamped: all DOF fixed}$$

$$\text{at } y = 16.60 \text{ mm, clamped: all DOF fixed except } v_y$$

$$\text{at } y = 439.29 \text{ mm, clamped: all DOF fixed except } v_y$$

$$\text{at } y = 446.75 \text{ mm, clamped: all DOF fixed}$$

$$\text{at } y = 455.88 \text{ mm, clamped: all DOF fixed}$$

$$\text{all other DOF axisymmetric: } u = u_x = u_y = v_x = w_x = \gamma_5 = 0$$

Since the loading is also axisymmetric, the "contact surface" for this case is best described as a flat hoop encircling the outer diameter of the tire, tangent at the crown, as shown in Figure 7.18. In the local sense, this approximates tire contact with a flat surface, though in the global sense, the load closely models the use of a device known as a "bead-popper." This device consists of an inflatable band which is placed around the circumference of an uninflated tire having a large gap between the tire bead and the rim. Such a gap prevents the tire from being inflated. By inflating

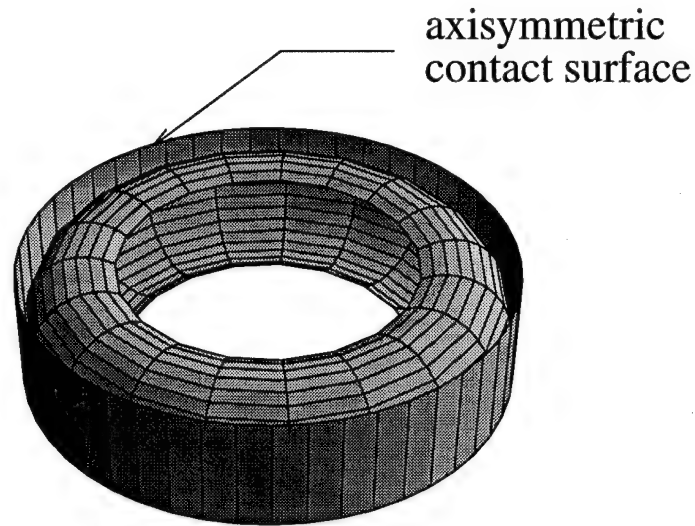


Figure 7.18 Configuration of axisymmetric loading case for contact study

Component (ij)	11	22	33	12	23	13
Stress J_{ij} (MPa)	46.17	32.54	4.157	32.06	-.6457	.1625
Occurs in element	16	8	3	16	10	11
Distance from ref sfc (z mm)	-0.8255	-0.4994	-15.93	-0.8255	0.	0.
Strain B_{ij} (%)	4.138	28.92	-68.15	-1.809	-27.13	-11.59
Occurs in element	16	16	16	13	11	11
Distance from ref sfc (z mm)	-11.75	+7.247	+4.128	+7.839	-0.5440	-0.5440

Table 7.4 Maximum stresses and strains due to inflation of the axisymmetric tire model without pressure direction updates

the bead-popper, the circumference of the tire is pinched, pushing the tire beads outward and into contact with the wheel rim. This allows the tire to then be inflated (Hensley 1995).

In the numerical study, the tire is first inflated to 2.206 MPa (320 psi) in four equal load increments without using the pressure vector updating scheme previously described. The convergence tolerance for inflation is $10^{-8}\%$. The peak deflection at the crown, not corrected for thickness stretch, is 15.56 mm. This gives a maximum permissible deflection of about 153 mm (deflection to the wheel rim). The percent-deflection values given herein refer to percent of that maximum deflection. The maximum calculated stresses and strains due to inflation are given in Table 7.4. Again,

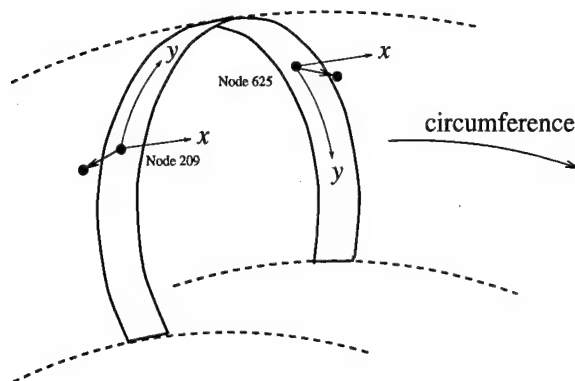


Figure 7.19 Displacements of opposing nodes on full tire model during inflation; displacements exaggerated—actual in-plane displacement is < 0.5 mm

the largest strains are in the isotropic rubber outer ply. Note that the values in Table 7.4 are larger than those of Table 7.2. This is due to constraining the tire from warping in the circumferential direction. Due to the highly anisotropic layup of the tire, it tries to warp. This is seen in the whole tire model. Nodes on opposite sides of the tire cross section move in opposite directions as shown in Figure 7.19. These nodes are not free to go through this movement in the axisymmetric model, hence higher stresses are generated.

Having inflated the tire, the axisymmetric displacement (load) is applied, and the boundary condition modification scheme previously described is implemented. In this portion of the analysis, the convergence tolerance is 10^{-5} %, and the prescribed minimum and maximum increment sizes for deflection are 1 mm and 3 mm respectively. The surface-normal (footprint) load is found by taking the component of the total load on a node (found from Eq (4.108)) that is normal to the surface, and subtracting from it the component of the internal pressure in that direction⁴. Recall that the *magnitude* of the pressure is assumed constant with deflection.). For example, consider the point on the tire crown tangent to the contact surface at the first instant of contact. At this first instant, the contact plane is merely “attached” to the tire—there is no deflection due to contact.

⁴Since no attempt is made to conform the deformed element to the contact surface (by, e.g., manipulating w_x and w_y), note that the pressure direction normal to the *element* (in the updated pressure scenario) may be in a slightly different direction than the normal to the contact surface.

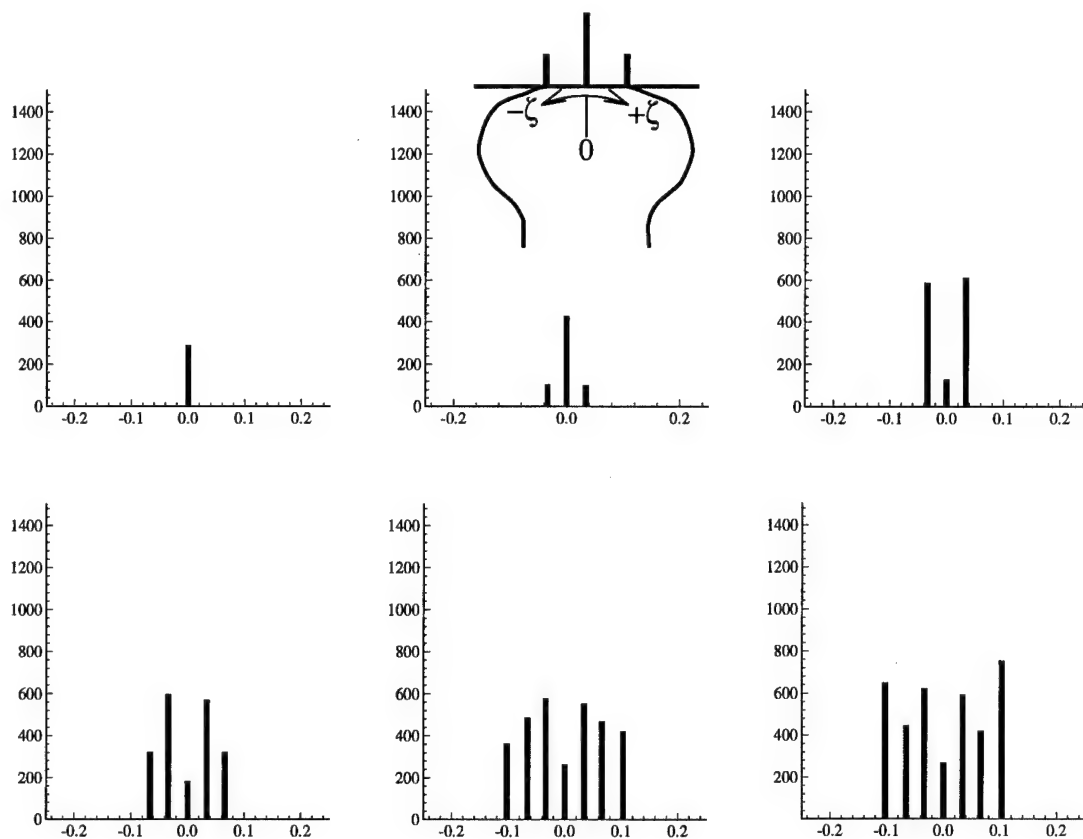


Figure 7.20 Surface-normal loads (Newtons) vs. nondimensionalized meridional coordinate (ζ) at nodes on axisymmetric tire slice without update of pressure direction; from left-to-right, top-to-bottom, deflections are: (1) 3.3 %, (2) 7.1 %, (3) 14 %, (4) 19 %, (5) 25 %, (6) 28 %

The normal component of the nodal load, L_N , is exactly equal to the normal component of the pressure load, P_N , hence the surface-normal (footprint) load, $F_N = P_N - L_N$ is zero. Now say the contact surface moves a small amount, δ , into the tire, but still with only one node in contact. The normal nodal load in the w direction is now calculated to be slightly less, say $L_N - \Delta L$. This yields a footprint load of $F_N = P_N - (L_N - \Delta L) = \Delta L$.

Refer now to Figure 7.20. It shows the surface-normal loads and the growth of the footprint region. The noticeable asymmetry in the magnitude of the loads is a by product of the cross-sectional anisotropy. The tire material warps slightly in the meridional direction within the constraints of

Component (ij)	11	22	33	12	23	13
Stress J_{ij} (MPa)	47.45	33.14	4.508	32.93	-.6536	.1648
Occurs in element	16	8	3	16	10	11
Distance from ref sfc (z mm)	-0.8255	-0.4994	-15.93	-0.8255	0.	0.
Strain B_{ij} (%)	3.680	30.57	-72.95	-1.783	-27.53	-11.75
Occurs in element	15	16	16	13	11	11
Distance from ref sfc (z mm)	-10.29	+7.247	+4.128	+7.839	-0.5440	-0.5440

Table 7.5 Maximum stresses and strains due to inflation of the axisymmetric tire model with pressure direction updates

the boundary conditions imposed. That is, while the tire may not deform asymmetrically in the circumferential direction, it is free to do so in the meridional one.

The same contact problem is run again, but this time the pressure vector direction-updating scheme described in Section 7.3.1 is used both in inflating the tire and during deflection due to contact. Again, four equal increments of pressure are applied, with the pressure vector directions updated at each iteration of each increment. Once again, a convergence tolerance of $10^{-8}\%$ is used for inflation. The peak deflection in this case (not corrected for thickness stretch), at 13.7 mm, is nearly two millimeters less than the previous case, though the average difference in inflation displacement around the meridian is only 2.9%. The updated-pressure model exhibits about 10% greater deflection in the sidewall area of the tire, and about 10% less deflection in the crown (tread) area of the tire. The maximum stresses and strains due to inflation are shown in Table 7.5. Note that the maximum stresses and strains observed in this case are slightly greater than the previous case, where the pressure loading vector direction was not updated. Once again, the largest strains are observed in the outer ply, which is isotropic rubber.

Applying the axisymmetric load to the inflated tire results in the surface-normal loads shown in Figure 7.21. The convergence tolerance, minimum displacement increment, and maximum displacement increment are $10^{-6}\%$, 1 mm, and 3 mm respectively. The maximum displacement for this analysis is about 151 mm, and the percent deflection figures refer to this amount. Again the growth of the footprint region can be seen, as can the marked increase in the loads near the footprint

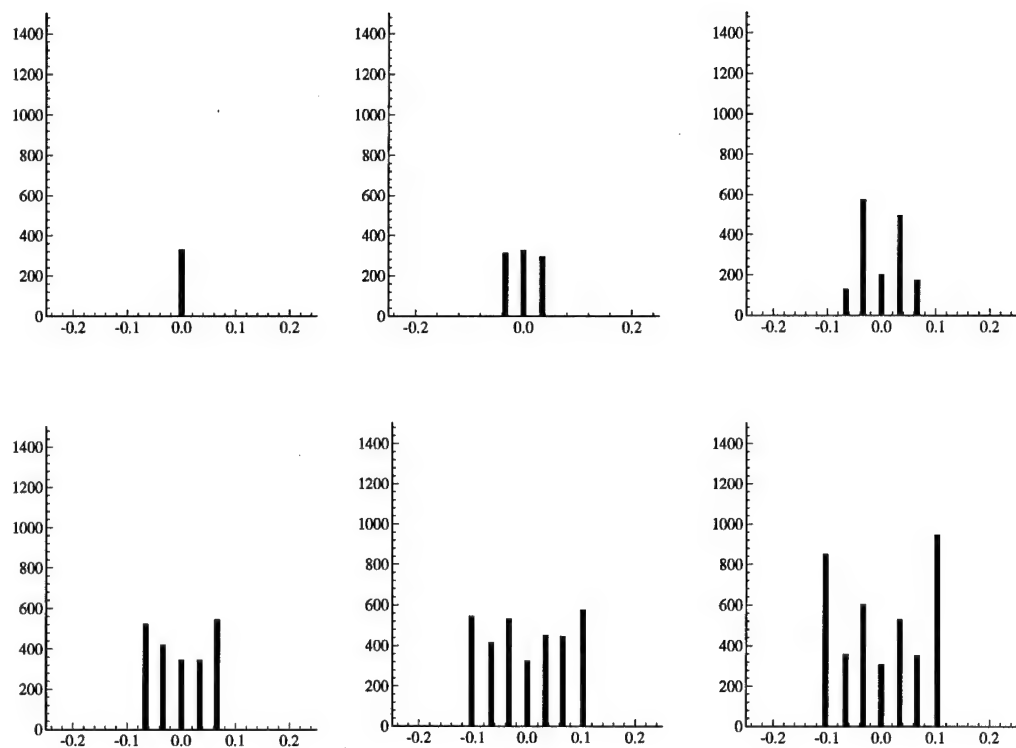


Figure 7.21 Surface-normal loads (Newtons) vs. nondimensionalized meridional coordinate (ζ) at nodes on axisymmetric tire slice with updated pressure vector directions; from left-to-right, top-to-bottom, deflections are: (1) 3.3 %, (2) 6.7 %, (3) 14 %, (4) 18 %, (5) 24 %, (6) 28 %

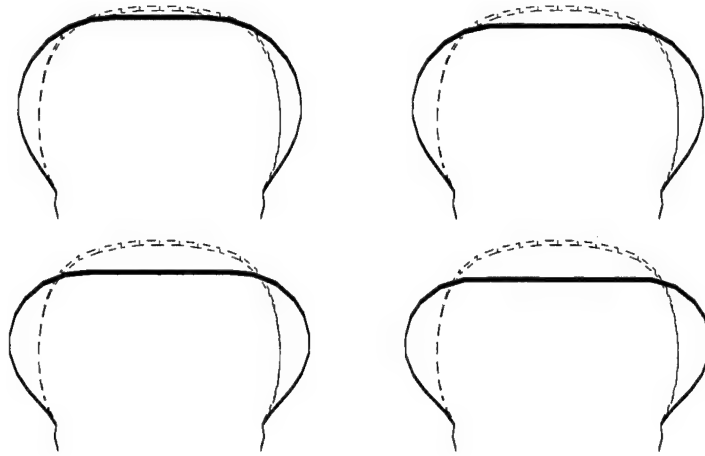


Figure 7.22 Four deformed geometries of axisymmetric tire model with updated pressure vectors; from left-to-right, top-to-bottom, deflections are: (1) 14 %, (2) 18 %, (3) 24 %, (4) 28 %; dotted outline indicates uninflated tire geometry

edge as 30 % deflection is approached. This is a phenomenon that has been observed experimentally (Mayer 1995). Some deformed tire geometries are shown in Figure 7.22, demonstrating the ability of the algorithm to maintain an approximately flat contact surface throughout the deformation.

Having considered the axisymmetric model, a model representing the whole tire is now considered. Recall that several assumptions in the theory of Pai and Palazotto (1995a) have been made which impact analysis of thick shells undergoing large deflections:

1. The trapezoidal cross-section effect has been neglected, hence the kinematics of Eqns (3.119) are not “true” shell kinematics.
2. Thickness stretching has been decoupled from in-plane strains in the strain displacement equations of Eqns (3.131).

The effect of the second assumption is known (see Eq 3.120), but the effect of the first assumption is more difficult to quantify. Recall that the thickness stretch function, $G_3^{(i)}$, is given by $G_3 \equiv$

$\alpha_3^{(i)} z + \beta_3^{(i)} z^2$, where

$$\begin{aligned}
 \begin{Bmatrix} \alpha_3^{(i)} \\ \beta_3^{(i)} \end{Bmatrix} &= \begin{bmatrix} a_{30}^{(i)} & a_{31}^{(i)} & a_{32}^{(i)} \\ b_{30}^{(i)} & b_{31}^{(i)} & b_{32}^{(i)} \end{bmatrix} \begin{Bmatrix} (1 + e_1) \cos \gamma_{61} - 1 \\ (1 + e_2) \cos \gamma_{62} - 1 \\ (1 + e_1) \sin \gamma_{61} + (1 + e_2) \sin \gamma_{62} \end{Bmatrix} \\
 &+ \begin{bmatrix} a_{33}^{(i)} & a_{34}^{(i)} & a_{35}^{(i)} \\ b_{33}^{(i)} & b_{34}^{(i)} & b_{35}^{(i)} \end{bmatrix} \begin{Bmatrix} k_1 - k_1^0 \\ k_2 - k_2^0 \\ k_6 - k_6^0 \end{Bmatrix} \\
 &+ \begin{bmatrix} a_{36}^{(i)} & a_{37}^{(i)} & a_{38}^{(i)} & a_{39}^{(i)} \\ b_{36}^{(i)} & b_{37}^{(i)} & b_{38}^{(i)} & b_{39}^{(i)} \end{bmatrix} \begin{Bmatrix} \gamma_{4,x} \\ \gamma_{4,y} \\ \gamma_{5,x} \\ \gamma_{5,y} \end{Bmatrix} + \begin{bmatrix} k_4 a_{41}^{(i)} + k_5 a_{42}^{(i)} & k_4 a_{43}^{(i)} + k_5 a_{44}^{(i)} \\ k_4 b_{41}^{(i)} + k_5 b_{42}^{(i)} & k_4 b_{43}^{(i)} + k_5 b_{44}^{(i)} \end{bmatrix} \begin{Bmatrix} \gamma_4 \\ \gamma_5 \end{Bmatrix}
 \end{aligned} \tag{3.153}$$

Including the effect of $G_3^{(i)}$ on the in-plane strains will require including terms like $G_{3,x}$ and $G_{3,y}$. From Eq (3.153), it is evident that this will result in a need for terms such as $\gamma_{4,xx}$, $\gamma_{4,xy}$, etc. The current formulation will not allow for such terms, as the shape functions are bilinear for the transverse shears and thus are not sufficiently differentiable to generate second derivative terms. Moreover, the solution to that problem is *not* to use hermitian shape functions (as are used for u , v , and w). This was attempted under the current research, but it was found that the stiffnesses associated with degrees of freedom like $\gamma_{4,x}$ are so small as to cause ill-conditioning of the stiffness array. From this it can be seen that one potential solution to the problem of including higher order derivatives could be the addition of mid-side nodes having degrees-of-freedom γ_4 and γ_5 . This would allow the use of a higher order shape function without including the low stiffnesses associated with the derivatives of the transverse shear. Introducing the coupling between thickness

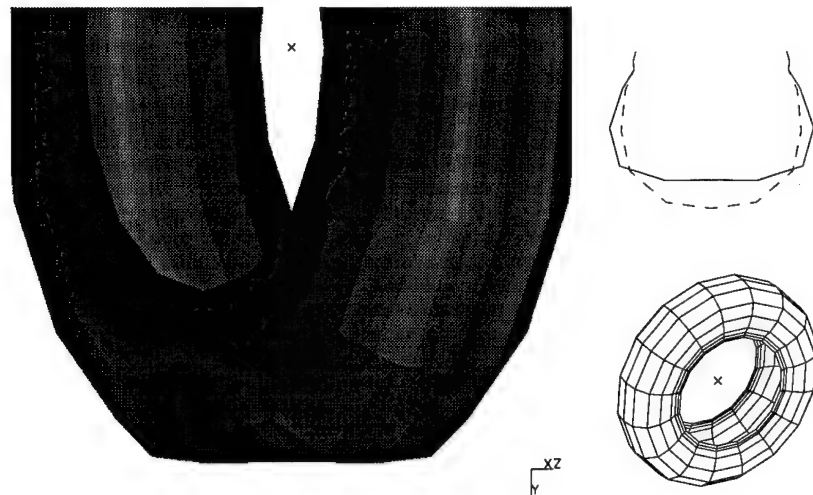


Figure 7.23 Full tire undergoing contact at 28.5% deflection; lower right is view of mesh; upper right is view of meridional section at maximum deformation; left is deformed tire, with contact surface at bottom of figure

stretching and in-plane strains, as well as inclusion of “true” shell kinematics are potential areas of future research.

Inclusion of these simplifying assumptions decreases the generality of the finite element model somewhat, requiring simplification of the whole-tire model for the contact study: a three ply lay-up (rather than the 13–16 ply lay-up used to this point) of orthotropic material having the properties of nylon-corded rubber will be used, as will a coarser mesh. These simplifications allow for successful demonstration of an initial capability of whole-tire contact with a flat surface. The full tire is modeled as a 16×14 mesh (16 elements in the x direction and 14 in the y , for a total of 224 elements). The mesh and deformed geometry of the tire is shown in Figure 7.23. As has been mentioned, the tire is materially simpler than the full tire model used for the inflation study. It is a three ply laminate of specially orthotropic plies having orientations $[29.8/90/-29.8]^5$. The material properties are given in Section F.2 of Appendix F. These properties are typical of nylon-corded

⁵The 29.8° plies are representative of typical ply orientations in the actual tire.

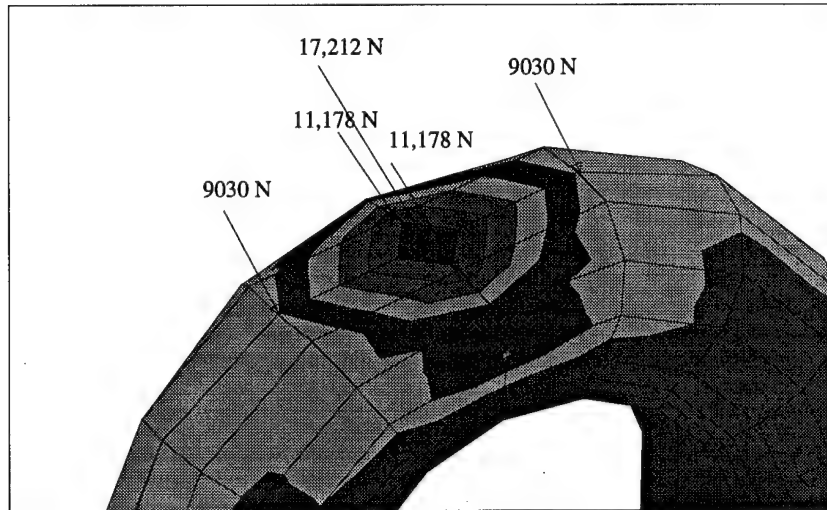


Figure 7.24 Surface-normal nodal loads and deformed geometry associated with the five nodes in contact; angle ply tire at 28.5% deflection

rubber. The tire is of uniform thickness of 25.4 mm (1 in), and the plies are of equal thickness. Reducing the number of plies was found to ameliorate the convergence problem.

The tire was inflated to 2.206 MPa (320 psi), and the crown deflection at this pressure (not corrected for thickness stretch) was 11.14 mm. This yields a maximum deflection (to the wheel rim) of about 148 mm. Percent deflection in the following refers to percentage of this maximum. The maximum deflection achieved was 33.7% (49.8 mm), at which point the program failed to converge.

As can be seen, the gross behavior of the tire is as expected, with the bulging of the side-wall in the region of contact. The surface-normal loads on the five nodes in contact nodes at 28.5% deflection (this deflection was chosen for the purpose of comparing results to the axisymmetric model) are shown in Figure 7.24. Given the coarseness of the mesh, these numbers should not be viewed as having great accuracy.

7.4 Summary

In this chapter the finite element model has been tailored for application to the aircraft tire: a highly complex structure presenting a serious challenge to two-dimensional finite element analysis. Inflation of the space shuttle nose wheel tire has been simulated and the results, corrected for thickness stretching, correlate well to experimental results. An initial capability of analyzing the tire with respect to static contact with a flat surface has been demonstrated using two models: (1) an axisymmetric tire model having the same material properties used in the inflation study and (2) a materially simplified angle-ply laminate modeling the whole tire. The simplification is the result of an attempt to circumvent convergence problems which arose in attempting to model the full tire in contact with a flat surface. These problems arise from simplifications made in the original theory, and future work could be directed toward removing these simplifications.

VIII. Summary and Conclusions

8.1 Summary

Chapter II introduced the baseline theory used in the current research, presenting it as a geometrically exact shell theory incorporating finite deformations, linear elastic constitutive laws, and geometric nonlinearity. Its relationship to the large body of literature on shell analysis was described as well.

In Chapter III, the theory of Pai and Palazotto (1995a) is thoroughly described pointing out two important shell assumptions incorporated therein: (1) the trapezoidal cross section effect has been ignored, such that the kinematics of Eq (3.117) are not "true" shell kinematics, and (2) the transverse normal stretch function, G_3 of Eqns (3.118), is not coupled to the in-plane strains via the strain displacement relations. The first assumption is a "shallow shell" assumption, while the second is a "thin shell" assumption. Moreover, the current method of finding thickness stretch and shear warping functions does not permit inclusion of either non-zero normal or shear stresses on the bounding surfaces of the shell. The shear warping functions are described in detail along with a needed modification. Likewise, the derivation of the thickness stretch function is presented.

Chapter IV casts the equations of the theory into finite element form, largely following the course laid out by Pai and Palazotto (1995a). The finite element code is first exercised on a series of linear problems in Chapter V, and geometric nonlinearity is the topic of the problems of Chapter VI. Finally, the finite element code is applied to the complex geometry of the tire in Chapter VII, demonstrating tire inflation and static contact of the Space Shuttle nose wheel tire.

8.2 Conclusions

The nonlinear shell theory of Pai and Palazotto (1995a) has been successfully implemented, with some modification, into a finite element model. The significant modifications to the theory were in the areas of the shear warping functions (Pai and Palazotto 1995a, Pai 1995), used to

describe displacements of material points away from the shell reference surface, and in extending the theory to the shell of revolution of arbitrary cross-section through a more general expression of the shell curvatures.

The total Lagrangian formulation described herein shows good displacement results when compared to experimental and other analytical work. In problems exhibiting truly large rotations, such as the arch problem, the non-conforming 36 DOF element is inadequate due to the discontinuity of the deformed curvatures at inter-element boundaries. The 44 DOF element models the large-rotation problem well, requiring much fewer elements and allowing a much larger displacement increment. When the shear warping functions were corrected, comparisons of the stress-state generated by the finite element model with the elasticity results of Pagano indicated good agreement, with the exception that the current formulation cannot match non-zero normal stresses at laminate boundaries. In such cases, transverse normal stress calculations are incorrect, but the global displacement field generated by the application of equivalent nodal loads can be remarkably good. The exceedingly complex structure of the aircraft tire is successfully modeled with the current theory. Tire inflation data agree very well with experimental data, and feasibility of the contact problem has been demonstrated with a materially, but not geometrically, simplified full tire and with an axisymmetric strip representing the tire cross-section. These simplifications could likely be removed if the theory were modified to eliminate these thin/shallow shell assumptions.

Future work in the tire area could be directed toward these assumptions, as well as more contact analyses including tire camber (leaning) and yaw (turning). And, of course, the model could be extended to dynamical analysis. Still, a caution is in order in that regard: the decomposition scheme is computationally intensive, and methods involving the removal of the time dependency, such as the Galilean transform, may be appropriate.

Bibliography

- Ahmad, S., B. M. Irons, and O. C. Zienkiewicz (1970). Analysis of thick and thin shell structures by curved finite elements. *International Journal for Numerical Methods in Engineering* 2, 419–451.
- Antman, S. S. (1989). Nonlinear problems of geometrically exact shell theories. In A. K. Noor, T. Belytschko, and J. C. Simo (Eds.), *Analytical and Computational Models of Shells*, pp. 109–131. New York: The American Society of Mechanical Engineers.
- Apostol, T. M. (1974). *Mathematical Analysis* (Second ed.). Reading, MA.: Addison-Wesley.
- Argyris, J., S. Kelsey, and H. Kamel (1964). Matrix methods of structural analysis: A précis of recent developments. In B. Fraeijs de Veubeke (Ed.), *Matrix Methods of Structural Analysis*, Number 72 in AGARDograph. Oxford: Published for and on behalf of Advisory Group for Aeronautical Research and Development, North Atlantic Treaty Organization, by Pergamon Press; distributed in the Western Hemisphere by Macmillan, New York. Papers submitted to the Structures and Materials Panel of AGARD.
- Atluri, S. N. (1984). Alternate stress and conjugate strain measures, and mixed variational formulations involving rigid rotations, for computational analyses of finitely deformed solids, with applications to plates and shells—I, theory. *Computers & Structures* 18(1), 93–116.
- Atluri, S. N. and H. Murakawa (1977, August). On hybrid finite element models in nonlinear mechanics. In P. G. B. et al. (Ed.), *Finite Elements in Nonlinear Mechanics: Papers Presented at the International Conference on Finite Elements in Nonlinear Solid and Structural Mechanics*, Trondheim, Norway, pp. 3–41. Tapir.
- Ayres, Jr., F. and E. Mendelson (1990). *Differential and Integral Calculus* (Third ed.). New York: McGraw-Hill.
- Babuška, I., H. C. Elman, and K. Markley (1992, November). Parallel implementation of the Hp-version of the finite element method on a shared-memory architecture. *SIAM Journal On Scientific and Statistical Computing* 13(6), 1433–1459.
- Başar, Y., Y. Ding, and R. Schultz (1993). Refined shear-deformation models for composite laminates with finite rotations. *International Journal of Solids and Structures* 30(19), 2611.
- Bagley, R. L. and P. J. Torvik (1983). Fractional calculus—a different approach to the analysis of viscoelastically damped structures. *AIAA J.* 21, 741.
- Bagley, R. L. and P. J. Torvik (1985). Fractional calculus in the transient analysis of viscoelastically damped structures. *AIAA J.* 23, 910.
- Barbero, E. J. and J. N. Reddy (1990). An accurate determination of stresses in thick laminates using a generalized plate theory. *International Journal for Numerical Methods in Engineering* 29, 1–14.
- Bathe, K.-J. (1982). *Finite Element Procedures in Engineering Analysis*. Englewood Cliffs, N.J.: Prentice-Hall, Inc.
- Bathe, K.-J., E. Ramm, and E. L. Wilson (1975). Finite element formulations for large deformation dynamic analysis. *International Journal for Numerical Methods in Engineering* 9, 353–386.
- Bazeley, G. P., Y. K. Cheung, B. M. Irons, and O. C. Zienkiewicz (1965). Triangular elements in plate bending—conforming and nonconforming solutions. In *Proc. First Conf. on Matrix Methods in Structural Mechanics*, Wright-Patterson Air Force Base, pp. 547–576. AFFDL-TR-66-80, Nov. 1966; AD-646-300, N.T.I.S.

- Belytschko, T. and L. W. Glaum (1979). Applications of higher order corotational stretch theories to nonlinear finite element analysis. *Computers & Structures* 10, 175-182.
- Belytschko, T. and M. O. Neal (1991). Contact-impact by the pinball algorithm with penalty and lagrangian methods. *International Journal for Numerical Methods in Engineering* 31, 547-572.
- Belytschko, T. and E. J. Plaskacz (1992, April). SIMD implementation of a non-linear transient shell program with partially structured meshes. *International Journal for Numerical Methods in Engineering* 33(5), 997-1026.
- Beran, P. S. (1994). The time-asymptotic behavior of vortex breakdown in tubes. *Computers & Fluids* 23(7), 913.
- Bergan, P. G. (1981). Lecture notes in nonlinear finite element analysis. Trondheim, Norway: Division of Structural Mechanics, The Norwegian Institute of Technology.
- Bergan, P. G. (1984). *FENRIS Manuals, Theory-Program Outline-Data Input*. Høvik, Norway: NTH, SINTEF, and A. S. Veritec.
- Bertrand, F. H. and P. A. Tanguy (1992, February). Parallel finite element computations on a network using ncs. *AIChE Journal* 38(2), 251-258.
- Bhimaraddi, A. (1984). A higher order theory for free vibration analysis of circular cylindrical shells. *International Journal of Solids and Structures* 20, 623-630.
- Brockman, R. A. and W. R. Braisted (1994, April-June). Critical speed estimation for aircraft tires. *Tire Science & Technology* 22(2), 121-144.
- Brockman, R. A., W. R. Braisted, J. Padovan, F. Tabaddor, and S. K. Clark (1992, February). Design and analysis of aircraft tires. Final Report WL-TR-91-3060, Flight Dynamics Directorate, Wright Laboratory, Air Force Systems Command, Wright-Patterson AFB, OH 45433-6553. University of Dayton Research Institute Report UDR-TR-91-41.
- Chandrashekhara, K. (1988). General nonlinear bending analysis of composite beams, plates, and shells. In *Proceedings of the International Conference on Composite Materials and Structures*, New Delhi, pp. 392-402. Indian Institute of Technology, Madus, India: McGraw-Hill.
- Cook, R. D., D. S. Malkus, and M. E. Plesha (1989). *Concepts and Applications of Finite Element Analysis*. New York: John Wiley & Sons.
- Crisfield, M. A. (1981). A fast incremental/iterative solution procedure that handles 'snap-through'. *Computers & Structures* 13, 55-62.
- Crisfield, M. A. (1991). *Non-linear Finite Element Analysis of Solids and Structures, Volume 1: Essentials*. New York: John Wiley & Sons.
- Danielson, D. A. and D. H. Hodges (1987, June). Nonlinear beam kinematics by decomposition of the rotation tensor. *Journal of Engineering Mechanics* 54(2), 258-262.
- DeEskinazi, J., T. Y. Yang, and W. Soedel (1978). Displacements and stresses resulting from contact of a steel belted radial tire with a flat surface. *Tire Science & Technology* 11(1), 48-70.
- Dennis, S. T. (1988). *Large Displacement and Rotational Formulation for Laminated, Cylindrical Shells Including Parabolic Transverse Shear*. Ph. D. dissertation, School of Engineering, Air Force Institute of Technology, Wright-Patterson Air Force Base, OH. Number AFIT/DS/AA/88-1.
- Dennis, S. T. and A. N. Palazotto (1989, October). Transverse shear deformation in orthotropic cylindrical pressure vessels using a higher-order shear theory. *AIAA J.* 27(10), 1441-1447.
- Di Sciuva, M. (1987, September). An improved shear-deformation theory for moderately thick multilayered anisotropic shells and plates. *Journal of Applied Mechanics* 54(3), 589-596.

- Dong, G. B. and F. K. W. Tso (1972). On a laminated orthotropic shell theory including transverse shear deformation. *Journal of Applied Mechanics* 39, 1091-1097.
- Doxsee, Jr., L. E. and G. S. Springer (1991, October). Measurements of temperature induced deformations in composite cylindrical shells. *Journal of Composite Materials* 25, 1340-1350.
- (ed.), S. K. C. (1981). *Mechanics of Pneumatic Tires*. Washington, D. C.: U. S. Department of Transportation. DOT HS 805 952.
- Eldred, L. B., W. P. Baker, and A. N. Palazotto (1995). Kelvin-voigt vs. fractional derivative model as constitutive relations for viscoelastic materials. *AIAA J.* 33(3), 547.
- Epstein, M. and P. G. Glockner (1977). Nonlinear analysis of multilayered shells. *International Journal of Solids and Structures* 13, 1081-1089.
- Epstein, M. and H.-P. Huttelmaier (1983). A finite element formulation for multilayered and thick plates. *Computers & Structures* 16(6), 645-650.
- Eringen, A. C. (1967). *Mechanics of Continua*. John Wiley & Sons, Inc.
- Farhat, C. and M. Geradin (1992, June). Using a reduced number of lagrange multipliers for assembling parallel incomplete field finite element approximations [CMA226]. *Computer Methods in Applied Mechanics and Engineering* 97(3), 333-354.
- Farhat, C. and F. X. Roux (1991). A method of finite element tearing and interconnecting and its parallel solution algorithm. *International Journal for Numerical Methods in Engineering* 32, 1205-1227.
- Faria, L. O., J. T. Oden, B. Yavari, W. W. Tworzydlo, J. M. Bass, and E. B. Becker (1992). Tire modeling by finite elements. *Tire Science & Technology* 20(1), 33-56.
- Forral, A. E. and A. N. Palazotto (1994). A finite element model considering nonlinear dynamically loaded composite plates and shells. *International Journal for Engineering Analysis and Design* 1, 379-393.
- Fraeijs de Veubeke, B. (1972). A new variational principle for finite elastic displacements. *International Journal of Engineering Science* 10(9), 745-763.
- Gander, W. (1990, November). Algorithms for the polar decomposition. *SIAM Journal On Scientific and Statistical Computing* 11(6), 1102.
- Gilbertsen, N. D. and T. Belytschko (1990, December). Explicit time integration of finite element models on a vectorized, concurrent computer with shared memory. *Finite Elements in Analysis and Design : the International Journal of Applied Finite Elements and Computer Aided Engineering* 7(3), 193-215.
- Greer, Jr., J. M. and A. N. Palazotto (1994, September). Some nonlinear response characteristics of collapsing composite shells (TN). *AIAA J.* 32(9), 1935-1938.
- Greer, Jr., J. M. and A. N. Palazotto (1995, June). Nonlinear dynamics of simple shell model with chaotic snapping behavior. *Journal of Engineering Mechanics* 121(6), 753-761.
- Griffin, Jr., O. H., E. R. Johnson, and M. D. Sensmeier (1993, March). Nonlinear response of graphite-epoxy wide columns subject to eccentric load. *Journal of Applied Mechanics* 60(1), 101-108.
- Grunwald, A. K. (1867). "veber begrentze", dervationen und deren anwendung. *Zeitschrift fur Mathematik und Physik* 12, 441.
- Gulati, S. T. and F. Essenburg (1967). Effects of anisotropy in axisymmetric cylindrical shells. *Journal of Applied Mechanics* 34(3), 659-666.

- Hensley, J. (1995, December). Personal Communication. Goodyear Tire & Rubber, Fairborn, OH.
- Higham, N. J. and R. S. Schreiber (1990, July). Fast polar decomposition of an arbitrary matrix. *SIAM Journal On Scientific and Statistical Computing* 11(4), 648.
- Hinrichsen, R. L. and A. N. Palazotto (1986, November). Nonlinear finite element analysis of thick composite plates using cubic spline functions. *AIAA J.* 24(11), 1836-1842.
- Hodges, D. H., A. R. Atigan, and D. A. Danielson (1993, March). A geometrically nonlinear theory of elastic plates. *Journal of Applied Mechanics* 60(1), 109-116.
- Hornbeck, R. W. (1975). *Numerical Methods*. New York: Quantum Publishers, Inc.
- Horrigmoer, G. and P. G. Bergan (1978). Instability analysis of free form shells by flat finite elements. *Computer Methods in Applied Mechanics and Engineering* 16, 11-35.
- Johan, Z., T. J. R. Hughes, K. K. Mathur, and S. L. Johnsson (1992). A data parallel finite element method for computational fluid dynamics on the connection machine system [CMA 248]. *Computer Methods in Applied Mechanics and Engineering* 99(1), 113-134.
- John, F. (1965). Estimates for the derivatives of the stresses in a thin shell and interior shell equations. *Communications on Pure and Applied Mathematics* 18, 235-267.
- Johnsson, S. L. and K. K. Mathur (1990, March). Data structures and algorithms for the finite element method on a data parallel supercomputer. *International Journal for Numerical Methods in Engineering* 29(4), 881.
- Katona, M. G. and O. C. Zienkiewicz (1985). A unified set of single step algorithms, part 3: The beta-*m* method, a generalization of the newmark scheme. *International Journal for Numerical Methods in Engineering* 21(7), 1345-1359.
- Kazempour, A. and J. Padovan (1989). Multibody instantly centered moving lagrangian observer schemes-part II. application to vehicular simulations. *Computers & Structures* 32(1), 101-111.
- Kennedy, R. and J. Padovan (1987). Finite element analysis of steady and transiently moving/rolling nonlinear viscoelastic structure-II. shell and three-dimensional simulations. *Computers & Structures* 27(2), 259-273.
- Kim, K. O. and A. K. Noor (1990). Modeling and analysis of the space shuttle nose-gear tire with semianalytic finite elements. NASA Technical Paper TP-2977, NASA.
- Kovařík, V. (1980). Cylindrical orthotropic sandwich-type shells under general loading. *Acta Technica ČSAV* 4, 499-518.
- Kulkarni, S. M., G. T. Hahn, C. A. Rubin, and V. Bhargava (1990, March). Elastoplastic finite element analysis of three-dimensional, pure rolling contact at the shakedown limit. *Journal of Applied Mechanics* 57(1), 57-65.
- Kulkarni, S. M., G. T. Hahn, C. A. Rubin, and V. Bhargava (1991, June). Elasto-plastic finite element analysis of three-dimensional pure rolling contact above the shakedown limit. *Journal of Applied Mechanics* 58(2), 347-353.
- Lamb, H. (1917). On waves in an elastic plate. *Proceedings of the Royal Society of London, England* 93, 114-128.
- Law, K. H. and D. R. Mackay (1993, September). A parallel row-oriented sparse solution method for finite element structural analysis. *International Journal for Numerical Methods in Engineering* 36(17), 2895.
- Lewis, G. D. and Y. J. Chao (1990, May). Flexibility of trunnion piping elbows. *Journal of Pressure Vessel Technology, ASME* 112(2), 184-187.

- Librescu, L. and R. Schmidt (1991). Substantiation of a shear-deformable theory of anisotropic composite laminated shells accounting for the interlaminae continuity conditions. *International Journal of Engineering Science* 29(6), 669-683.
- Likins, P. W. (1973). *Elements of Engineering Mechanics*. New York: McGraw-Hill.
- Lindsley, N. J. and J. P. Cusumano (1993). Critical speed analysis of a non-linear strain ring dynamical model for aircraft tires. *S.A.E. Transactions* 102(1), 1922-1932.
- Love, A. E. H. (1891). *Note on the Present State of the Theory of Thin Elastic Shells*. London: Harrison and Sons.
- Luo, J.-C. and M. B. Friedman (1990). A parallel computational model for the finite element method on a memory-sharing multiprocessor computer. *Computer Methods in Applied Mechanics and Engineering* 84(2), 193-210.
- Lutton, M. J. and P. S. Beran (1994). Hopf bifurcation in viscous, low-speed flows about an airfoil with structural coupling. *Computers & Fluids* 23(2), 323.
- Malvern, L. E. (1969). *Introduction to the Mechanics of a Continuous Medium*. Englewood Cliffs, New Jersey: Prentice-Hall, Inc.
- Malone, J. G. and N. L. Johnson (1994a, February). A parallel finite element contact/impact algorithm for non-linear explicit transient analysis: Part I-the search algorithm and contact mechanics. *International Journal for Numerical Methods in Engineering* 37(4), 559-590.
- Malone, J. G. and N. L. Johnson (1994b, February). A parallel finite element contact/impact algorithm for non-linear explicit transient analysis: Part II-parallel implementation. *International Journal for Numerical Methods in Engineering* 37(4), 591-603.
- Mayer, A. (1995, December). Personal Communication. Vehicle Subsystems Division, Flight Dynamics Directorate, Wright Laboratories, Wright-Patterson AFB, OH.
- Medzorian, J. (1992, August). Prediction of aircraft tire critical speed. Final Report WL-TR-92-3003, Flight Dynamics Directorate, Wright Laboratory, Air Force Materiel Command, Wright-Patterson AFB, OH 45433-6553.
- Meirovitch, L. (1967). *Analytical Methods in Vibrations*. New York: Macmillan.
- Miller, D. A. and A. N. Palazotto (1995). Nonlinear finite element analysis of composite beams and arches using a large rotation theory. *Finite Elements in Analysis and Design* 19(3), 131.
- Mindlin, R. D. (1951, March). Influence of rotatory inertia and shear on flexural motions of isotropic, elastic plates. *Journal of Applied Mechanics* 18(1), 31-38.
- Minguet, P. and J. Dugundji (1990, September). Experiments and analysis for composite blades under large deflections part I: Static behavior. *AIAA J.* 28(9), 1573-1579.
- Mirsky, I. and G. Herrmann (1957). Nonaxially symmetric motions of cylindrical shells. *The Journal of the Acoustic Society of America* 29, 1116-1124.
- Moran, K. J. and P. S. Beran (1994). Navier-stokes simulations of slender axisymmetric shapes in turbulent, supersonic flow. *AIAA J.* 32(7), 1446.
- Murakami, H. (1984). Laminated composite plate theories with improved inplane responses. In *ASME Pressure Vessels and Piping Conference*, pp. 257-263.
- Nakajima, Y. and J. Padovan (1987). Finite element analysis of steady and transiently moving/rolling nonlinear viscoelastic structure-III. impact/contact simulations. *Computers & Structures* 27(2), 275-286.

- Navon, I. M. and Y. Cai (1993, July). Domain decomposition and parallel processing of a finite element model of the shallow water equations. *Computer Methods in Applied Mechanics and Engineering* 106(1-2), 179-212.
- Noor, A. K., C. M. Andersen, and J. A. Tanner (1987). Exploiting symmetries in the modeling and analysis of tires. *Computer Methods in Applied Mechanics and Engineering* 63, 37-81.
- Noor, A. K. and W. S. Burton (1990, March). Three-dimensional solutions for antisymmetrically laminated anisotropic plates. *Journal of Applied Mechanics* 57(1), 182-188.
- Noor, A. K., K. O. Kim, and J. A. Tanner (1990, March). Analysis of aircraft tires via semi-analytic finite elements. *Finite Elements in Analysis and Design : the International Journal of Applied Finite Elements and Computer Aided Engineering* 6(3), 217-233.
- Noor, A. K. and J. A. Tanner (1985). Advances and trends in the development of computational models for tires. *Computers & Structures* 20(1-3), 517-533.
- Noor, A. K., J. A. Tanner, and J. M. Peters (1993). Reduced-basis technique for evaluating the sensitivity coefficients of the nonlinear tire response. *AIAA J.* 31(2), 370-376.
- Nygård, M. K. and P. G. Bergan (1989). Advances in treating large rotations for nonlinear problems. In A. K. Noor and J. T. Oden (Eds.), *State-of-the-Art Surveys on Computational Mechanics*, pp. 305-333. New York: The American Society of Mechanical Engineers.
- Oden, J. T. (1972). *Finite Elements of Nonlinear Continua*. New York: McGraw-Hill.
- Owen, D. R. J. and E. Hinton (1980). *Finite Elements in Plasticity: Theory and Practice*. Swansea, U. K.: Pineridge Press, Ltd.
- Padovan, J. (1975). Traveling waves vibrations and buckling of rotating anisotropic shells of revolution by finite elements. *International Journal of Solids and Structures* 11, 1367-1380.
- Padovan, J. (1976, November). On viscoelasticity and standing waves in tires. *Tire Science & Technology* 4(4), 233-246.
- Padovan, J. (1977). Circumferentially traveling radial loads on rings and cylinders. *International Journal of Non-Linear Mechanics* 12, 241-250.
- Padovan, J. (1982). Spectral/critical speed characteristics of structure subject to moving loads. *International Journal of Engineering Science* 20(1), 77-91.
- Padovan, J. (1987). Finite element analysis of steady and transiently moving/rolling nonlinear viscoelastic structure-I. theory. *Computers & Structures* 27(2), 249-257.
- Padovan, J. and A. Kazempour (1989). Multibody instantly centered moving lagrangian observer schemes-part I. formulation. *Computers & Structures* 32(1), 93-100.
- Padovan, J. and O. Paramadilok (1985). Transient and steady state viscoelastic rolling contact. *Computers & Structures* 20(1-3), 545-553.
- Padovan, J., S. Tovchakchaikul, and I. Zeid (1984). Finite element analysis of steadily moving contact fields. *Computers & Structures* 18(2), 191-200.
- Pagano, N. J. (1969, July). Exact solutions for composite laminates in cylindrical bending. *Journal of Composite Materials* 3, 398-411.
- Pai, P. F. (1994, September). Personal Communication.
- Pai, P. F. (1995). A new look at shear correction factors and warping functions of anisotropic laminates. *International Journal of Solids and Structures* 32(16), 2295-2313.
- Pai, P. F. and A. H. Nayfeh (1991). A nonlinear composite plate theory. *Nonlinear Dynamics* 2, 445-477.

- Pai, P. F. and A. H. Nayfeh (1992). A nonlinear composite beam theory. *Nonlinear Dynamics* 3, 273–303.
- Pai, P. F. and A. H. Nayfeh (1994a). A new method for the modeling of geometric nonlinearities in structures. *Computers & Structures* 53(4), 877–895.
- Pai, P. F. and A. H. Nayfeh (1994b). A unified nonlinear formulation for plate and shell theories. *Nonlinear Dynamics*, in press.
- Pai, P. F., A. H. Nayfeh, K. Oh, and D. T. Mook (1993). A refined nonlinear model of composite plates with integrated piezoelectric actuators and sensors. *International Journal of Solids and Structures* 30(12), 1603–1630.
- Pai, P. F. and A. N. Palazotto (1994, January). Correct stress and strain measures for nonlinear analyses of flexible composite structures. *International Journal of Solids and Structures*, accepted for publication.
- Pai, P. F. and A. N. Palazotto (1995a). Nonlinear displacement-based finite-element analyses of composite shells—a new total lagrangian formulation. *International Journal of Solids and Structures* 32(20), 3047–3073.
- Pai, P. F. and A. N. Palazotto (1995b). Polar decomposition theory in nonlinear analyses of solids and structures. *Journal of Engineering Mechanics* 121(4), 568.
- Palazotto, A. N., L. S. Chien, and W. W. Taylor (1992). Stability characteristics of laminated cylindrical panels under transverse loading. *AIAA J.* 30(6), 1649–1653.
- Palazotto, A. N. and S. T. Dennis (1992). *Nonlinear Analysis of Shell Structures*. AIAA Educational Series. Washington, D. C.: American Institute of Aeronautics and Astronautics, Inc.
- Palmerio, A. F., J. N. Reddy, and R. Schmidt (1990a). On a moderate rotation theory of laminated anisotropic shells— part 1. theory. *International Journal of Non-Linear Mechanics* 25(6), 687.
- Palmerio, A. F., J. N. Reddy, and R. Schmidt (1990b). On a moderate rotation theory of laminated anisotropic shells— part 2. finite-element analysis. *International Journal of Non-Linear Mechanics* 25(6), 701–714.
- Przemieniecki, J. S. (1963). Matrix structural analysis of substructures. *AIAA J.* 1, 138–147.
- Rayleigh (1889). On the free vibrations of an infinite plate of homogeneous isotropic elastic matter. *Proceedings of the London Mathematical Society* 20(357), 225–234.
- Reddy, J. N. (1984a). *Energy and Variational Methods in Applied Mechanics*. Wiley.
- Reddy, J. N. (1984b, December). A simple higher-order theory for laminated composite plates. *Journal of Applied Mechanics* 51, 745–752.
- Reddy, J. N. (1987). A generalization of two-dimensional theories of laminated composite plates. *Communications in Applied Numerical Methods* 3, 113–180.
- Reddy, J. N. (1989). On refined computational models of composite laminates. *International Journal for Numerical Methods in Engineering* 27, 361–382.
- Reddy, J. N. and C. F. Liu (1985). A higher order shear deformation theory of laminated composite shells. *International Journal of Engineering Science* 23(3), 319–330.
- Reissner, E. (1945). The effect of transverse shear deformation on the bending of elastic plates. *Journal of Applied Mechanics* 67, A–69.
- Reissner, E. (1947). On bending of elastic plates. *Quarterly of Applied Mathematics* 5, 55–68.

- Reissner, E. (1950). Small bending and stretching of sandwich-type shells. Technical Report NACA Report 975, NACA.
- Rembielinski, J. and W. Tybor (1992, November). Polar decomposition of the twisted derham complex for $C(\text{sub})q$. *Journal of Physics A: Mathematical and General* 25(21), L1209.
- Renka, R. J. (1987, May). Interpolatory tension splines with automatic selection of tension factors. *Siam Journal on Scientific and Statistical Computing* 8(3), 393–415.
- Rheinboldt, W. C. and E. Riks (1983). Solution techniques for nonlinear finite element equations. In A. K. Noor and W. D. Pilkey (Eds.), *State-of-the-Art Surveys on Finite Element Technology*, pp. 183–223. New York: The American Society of Mechanical Engineers.
- Riks, E. (1979). An incremental approach to the solution of snapping and buckling problems. *International J. Solids Structures* 15, 529–551.
- Saada, A. S. (1989). *Elasticity Theory and Applications*. New York: Pergamon Press.
- Sabir, A. B. and M. S. Djoudi (1995). Shallow shell finite element for the large deflection geometrically nonlinear analysis of shells and plates. *Thin-Walled Structures* 21(3), 253–267.
- Sabir, A. B. and A. C. Lock (1972). The application of finite elements to the large deflection geometrically non-linear behaviour of cylindrical shells. In C. A. Brebbia and H. Tottenham (Eds.), *Variational Methods in Engineering*, Chapter 7, pp. 66–75. UK: Southhampton Press.
- Sacco, E. and J. N. Reddy (1992). On first- and second-order moderate rotation theories of laminated plates. *International Journal for Numerical Methods in Engineering* 33, 1–17.
- Sanders, Jr., J. L. (1962). Nonlinear theories for thin shells. *Quarterly of Applied Mathematics* 21(1), 21–36.
- Schimmels, S. A. and A. N. Palazotto (1994, February). Nonlinear geometric and material behavior of shell structures with large strains. *Journal of Engineering Mechanics* 120(2), 320–345.
- Schweizerhof, K. and E. Ramm (1984). Displacement dependent pressure loads in nonlinear finite element analyses. *Computers & Structures* 18(6), 1099–1114.
- Silva, K. J. (1989). Finite element investigation of a composite cylindrical shell under transverse load with through thickness shear and snapping. Master's thesis, School of Engineering, Air Force Institute of Technology AU, Wright Patterson AFB, OH.
- Simo, J. C., D. D. Fox, and T. J. R. Hughes (1992, March). Formulations of finite elasticity with independent rotations. *Computer Methods in Applied Mechanics and Engineering* 95(2), 277–288.
- Simo, J. C., D. D. Fox, and M. S. Rifai (1989). Geometrically exact stress resultant shell models: Formulation and computational aspects of the nonlinear theory. In A. K. Noor, T. Belytschko, and J. C. Simo (Eds.), *Analytical and Computational Models of Shells*, pp. 161–190. New York: The American Society of Mechanical Engineers.
- Simo, J. C., D. D. Fox, and M. S. Rifai (1990). On a stress resultant geometrically exact shell model. part III. computational aspects of the nonlinear theory. *Computer Methods in Applied Mechanics and Engineering* 79(1), 21–70.
- Simo, J. C., M. S. Rifai, and D. D. Fox (1990). On a stress resultant geometrically exact shell model. part IV. variable thickness shells with through-the- thickness stretching. *Computer Methods in Applied Mechanics and Engineering* 81(1), 91–126.
- Simo, J. C., M. S. Rifai, and D. D. Fox (1992, March). On a stress resultant geometrically exact shell model. part VI. conserving algorithms for non-linear dynamics. *International Journal for Numerical Methods in Engineering* 34(1), 117–164.

- Simo, J. C. and N. Tarnow (1994). A new energy and momentum conserving algorithm for the non-linear dynamics of shells. *International Journal for Numerical Methods in Engineering* 37(15), 2527-2549.
- Sivakumaran, K. S. and C. Y. Chia (1985, September). Large-amplitude oscillations of unsymmetrically laminated anisotropic rectangular plates including shear, rotatory inertia, and transverse normal stress. *Journal of Applied Mechanics* 52(3), 536-542.
- Smith, R. A. (1991, September). *Higher-Order Thickness Expansions for Cylindrical Shells*. Ph. D. dissertation, School of Engineering, Air Force Institute of Technology AU, Wright-Patterson AFB, OH.
- Smith, R. A. and A. N. Palazotto (1993). Comparison of eight variations of a higher-order theory for cylindrical shells. *AIAA J.* 31(6), 1125-1132.
- Souchet, R. (1993, November). Concerning the polar decomposition of the deformation gradient. *International Journal of Engineering Science* 31(11), 1499.
- Stadter, J. T. and R. O. Weiss (1979, December). Analysis of contact through finite element gaps. *Computers & Structures* 10(6), 867-873.
- Strang, G. (1988). *Linear Algebra and Its Applications*. San Diego: Harcourt Brace Jovanovich.
- Surana, K. S. (1983). Geometrically nonlinear formulation for the curved shell elements. *International Journal for Numerical Methods in Engineering* 19, 581-615.
- Sve, C. and G. Herrmann (1974, September). Moving load on a laminated composite. *Journal of Applied Mechanics* 41(3), 663-667.
- Taylor, R. L., J. C. Simo, O. C. Zienkiewicz, and A. C. H. Chan (1986). The patch test—a condition for assessing FEM convergence. *International Journal for Numerical Methods in Engineering* 22(1), 39-62.
- Taylor Jr., W. W. (1990). Finite element investigation into the dynamic instability characteristics of laminated composite panels. Master's thesis, School of Engineering, Air Force Institute of Technology AU, Wright Patterson AFB, OH.
- Timoshenko, S. (1921). On the correction for shear of the differential equation for transverse vibrations of prismatic bars. *Philosophical Magazine* 41, 744-746.
- Timoshenko, S. (1922). On the transverse vibration of bars of uniform cross section. *Philosophical Magazine* 43, 125-131.
- Timoshenko, S. P. and S. Woinowski-Krieger (1959). *Theory of Plates and Shells*. New York: McGraw-Hill.
- Torvik, P. J. (1992). MECH 701 - Inelastic Material Behavior. Class Notes, Spring Quarter.
- Truesdell, C. and R. A. Toupin (1960). The classical field theories. In S. Flügge (Ed.), *Encyclopedia of Physics*, Volume 3/1. Berlin: Springer-Verlag.
- Tsai, C. T. and A. N. Palazotto (1990). A modified riks approach to composite shell snapping using a high order shear deformation theory. *Computers & Structures* 35(3), 221-226.
- Tsai, C. T. and A. N. Palazotto (1991a). Nonlinear and multiple snapping responses of cylindrical panels comparing displacement control and riks method. *Computers & Structures* 41(4), 605-610.
- Tsai, C. T. and A. N. Palazotto (1991b). On the finite element analysis of non-linear vibration for cylindrical shells with high-order shear deformation theory. *International Journal of Non-Linear Mechanics* 26(3/4), 379-388.

- Tsuchiya, M. (1992). Levy Measure with generalized polar decomposition and the associated SDE with jumps. *Stochastics and Stochastics Reports* 38(2), 95-118.
- Voyiadjis, G. Z. and G. Shi (1991). A refined two-dimensional theory for thick cylindrical shells. *International Journal of Solids and Structures* 27, 261-282.
- Wagner, W. (1990, May). A finite element model for non-linear shells of revolution with finite rotations. *International Journal for Numerical Methods in Engineering* 29(7), 1455-1471.
- Washizu, K. (1982). *Variational Methods in Elasticity and Plasticity* (Third ed.). Oxford: Pergamon Press.
- Weinstock, R. (1974). *Calculus of Variations with Applications to Physics and Engineering*. New York: Dover.
- Whitney, J. M. (1971, July). On the use of shell theory for determining stresses in composite cylinders. *Journal of Composite Materials* 5, 340-353.
- Whitney, J. M. (1987). *Structural Analysis of Laminated Anisotropic Plates*. Lancaster, PA: Technomic Publishing, Inc.
- Whitney, J. M. and N. J. Pagano (1970). Shear deformation in heterogeneous anisotropic plates. *Journal of Applied Mechanics* 37, 1031-1036.
- Whitney, J. M. and C.-T. Sun (1974, June). A refined theory for laminated anisotropic cylindrical shells. *Journal of Applied Mechanics* 41(2), 471-476.
- Wriggers, P. and F. Gruttmann (1993, June). Thin shells with finite rotations formulated in biot stresses: Theory and finite element formulation. *International Journal for Numerical Methods in Engineering* 36(12), 2049.
- Wu, B. and X. Du (1995). Finite element formulation of radial tires with variable constraint conditions. *Computers & Structures* 55(5), 871-875.
- Zeid, I. and J. Padovan (1981). Finite element modeling of rolling contact. *Computers & Structures* 14(1-2), 163-170.
- Zhang, A. and D. Redekop (1992). Surface loading of a thin-walled toroidal shell. *Computers & Structures* 43(6), 1019-1028.
- Zienkiewicz, O. C. (1977). *The Finite Element Method* (Third ed.). London: McGraw-Hill.
- Zukas, J. A. and J. R. Vinson (1971, June). Laminated transversely isotropic cylindrical shells. *Journal of Applied Mechanics* 38(2), 400-407.

Appendix A. Elements of $[\Psi]$

In this appendix, the nontrivial elements of the $[\Psi]$ matrix are presented. These terms were generated using *Mathematica*. Here, Ψ_{ij} is represented by $\Psi(i, j)$. All of these entries are ultimately described in terms of the global displacements u, v, w and the initial curvatures k_i^0 . As an example, The entries of $[\Psi]$, in their most basic form, are:

$$\begin{aligned}
 \Psi(1, 1) &= \cos(\gamma_{61}) e_{1,u} - (1 + e_1) \sin(\gamma_{61}) \gamma_{61,u} \\
 \Psi(1, 2) &= \cos(\gamma_{61}) e_{1,u,x} - (1 + e_1) \sin(\gamma_{61}) \gamma_{61,u,x} \\
 \Psi(1, 3) &= - \left((1 + e_1) \sin(\gamma_{61}) \gamma_{61,u,y} \right) \\
 \Psi(1, 7) &= \cos(\gamma_{61}) e_{1,v} - (1 + e_1) \sin(\gamma_{61}) \gamma_{61,v} \\
 \Psi(1, 8) &= \cos(\gamma_{61}) e_{1,v,x} - (1 + e_1) \sin(\gamma_{61}) \gamma_{61,v,x} \\
 \Psi(1, 9) &= - \left((1 + e_1) \sin(\gamma_{61}) \gamma_{61,v,y} \right) \\
 \Psi(1, 13) &= \cos(\gamma_{61}) e_{1,w} - (1 + e_1) \sin(\gamma_{61}) \gamma_{61,w} \\
 \Psi(1, 14) &= \cos(\gamma_{61}) e_{1,w,x} - (1 + e_1) \sin(\gamma_{61}) \gamma_{61,w,x} \\
 \Psi(1, 15) &= - \left((1 + e_1) \sin(\gamma_{61}) \gamma_{61,w,y} \right) \tag{A.1}
 \end{aligned}$$

$$\begin{aligned}
 \Psi(2, 1) &= \cos(\gamma_{62}) e_{2,u} - (1 + e_2) \sin(\gamma_{62}) \gamma_{62,u} \\
 \Psi(2, 2) &= - \left((1 + e_2) \sin(\gamma_{62}) \gamma_{62,u,x} \right) \\
 \Psi(2, 3) &= \cos(\gamma_{62}) e_{2,u,x} - (1 + e_2) \sin(\gamma_{62}) \gamma_{62,u,y} \\
 \Psi(2, 7) &= \cos(\gamma_{62}) e_{2,v} - (1 + e_2) \sin(\gamma_{62}) \gamma_{62,v} \\
 \Psi(2, 8) &= - \left((1 + e_2) \sin(\gamma_{62}) \gamma_{62,v,x} \right) \\
 \Psi(2, 9) &= \cos(\gamma_{62}) e_{2,v,x} - (1 + e_2) \sin(\gamma_{62}) \gamma_{62,v,y} \\
 \Psi(2, 13) &= \cos(\gamma_{62}) e_{2,w} - (1 + e_2) \sin(\gamma_{62}) \gamma_{62,w}
 \end{aligned}$$

$$\begin{aligned}
\Psi(2, 14) &= - \left((1 + e_2) \sin(\gamma_{62}) \gamma_{62,w,x} \right) \\
\Psi(2, 15) &= \cos(\gamma_{62}) e_{2,w,y} - (1 + e_2) \sin(\gamma_{62}) \gamma_{62,w,y}
\end{aligned} \tag{A.2}$$

$$\begin{aligned}
\Psi(3, 1) &= \sin(\gamma_{61}) e_{1,u} + \sin(\gamma_{62}) e_{2,u} + \cos(\gamma_{61}) (1 + e_1) \gamma_{61,u} + \cos(\gamma_{62}) (1 + e_2) \gamma_{62,u} \\
\Psi(3, 2) &= \sin(\gamma_{61}) e_{1,u,x} + \cos(\gamma_{61}) (1 + e_1) \gamma_{61,u,x} + \cos(\gamma_{62}) (1 + e_2) \gamma_{62,u,x} \\
\Psi(3, 3) &= \sin(\gamma_{62}) e_{2,u,x} + \cos(\gamma_{61}) (1 + e_1) \gamma_{61,u,y} + \cos(\gamma_{62}) (1 + e_2) \gamma_{62,u,y} \\
\Psi(3, 7) &= \sin(\gamma_{61}) e_{1,v} + \sin(\gamma_{62}) e_{2,v} + \cos(\gamma_{61}) (1 + e_1) \gamma_{61,v} + \cos(\gamma_{62}) (1 + e_2) \gamma_{62,v} \\
\Psi(3, 8) &= \sin(\gamma_{61}) e_{1,v,x} + \cos(\gamma_{61}) (1 + e_1) \gamma_{61,v,x} + \cos(\gamma_{62}) (1 + e_2) \gamma_{62,v,x} \\
\Psi(3, 9) &= \sin(\gamma_{62}) e_{2,v,x} + \cos(\gamma_{61}) (1 + e_1) \gamma_{61,v,y} + \cos(\gamma_{62}) (1 + e_2) \gamma_{62,v,y} \\
\Psi(3, 13) &= \sin(\gamma_{61}) e_{1,w} + \sin(\gamma_{62}) e_{2,w} + \cos(\gamma_{61}) (1 + e_1) \gamma_{61,w} + \cos(\gamma_{62}) (1 + e_2) \gamma_{62,w} \\
\Psi(3, 14) &= \sin(\gamma_{61}) e_{1,w,x} + \cos(\gamma_{61}) (1 + e_1) \gamma_{61,w,x} + \cos(\gamma_{62}) (1 + e_2) \gamma_{62,w,x} \\
\Psi(3, 15) &= \sin(\gamma_{62}) e_{2,w,y} + \cos(\gamma_{61}) (1 + e_1) \gamma_{61,w,y} + \cos(\gamma_{62}) (1 + e_2) \gamma_{62,w,y}
\end{aligned} \tag{A.3}$$

$$\begin{aligned}
\Psi(4, 1) &= k_{1,u} \\
\Psi(4, 2) &= k_{1,u,x} \\
\Psi(4, 3) &= k_{1,u,y} \\
\Psi(4, 4) &= k_{1,u,xx} \\
\Psi(4, 5) &= k_{1,u,xy} \\
\Psi(4, 7) &= k_{1,v} \\
\Psi(4, 8) &= k_{1,v,x} \\
\Psi(4, 9) &= k_{1,v,y} \\
\Psi(4, 10) &= k_{1,v,xx}
\end{aligned}$$

$$\begin{aligned}
\Psi(4, 11) &= k_{1,v,xy} \\
\Psi(4, 13) &= k_{1,w} \\
\Psi(4, 14) &= k_{1,w,x} \\
\Psi(4, 15) &= k_{1,w,y} \\
\Psi(4, 16) &= k_{1,w,xx} \\
\Psi(4, 17) &= k_{1,w,xy}
\end{aligned} \tag{A.4}$$

$$\begin{aligned}
\Psi(5, 1) &= k_{2,u} \\
\Psi(5, 2) &= k_{2,u,x} \\
\Psi(5, 3) &= k_{2,u,y} \\
\Psi(5, 5) &= k_{2,u,xy} \\
\Psi(5, 6) &= k_{2,u,yy} \\
\Psi(5, 7) &= k_{2,v} \\
\Psi(5, 8) &= k_{2,v,x} \\
\Psi(5, 9) &= k_{2,v,y} \\
\Psi(5, 11) &= k_{2,v,xy} \\
\Psi(5, 12) &= k_{2,v,yy} \\
\Psi(5, 13) &= k_{2,w} \\
\Psi(5, 14) &= k_{2,w,x} \\
\Psi(5, 15) &= k_{2,w,y} \\
\Psi(5, 17) &= k_{2,w,xy} \\
\Psi(5, 18) &= k_{2,w,yy}
\end{aligned} \tag{A.5}$$

$$\Psi (6, 1) = k_{6,u}$$

$$\Psi (6, 2) = k_{6,u,x}$$

$$\Psi (6, 3) = k_{6,u,y}$$

$$\Psi (6, 4) = k_{6,u,xx}$$

$$\Psi (6, 5) = k_{6,u,xy}$$

$$\Psi (6, 6) = k_{6,u,yy}$$

$$\Psi (6, 7) = k_{6,v}$$

$$\Psi (6, 8) = k_{6,v,x}$$

$$\Psi (6, 9) = k_{6,v,y}$$

$$\Psi (6, 10) = k_{6,v,xx}$$

$$\Psi (6, 11) = k_{6,v,xy}$$

$$\Psi (6, 12) = k_{6,v,yy}$$

$$\Psi (6, 13) = k_{6,w}$$

$$\Psi (6, 14) = k_{6,w,x}$$

$$\Psi (6, 15) = k_{6,w,y}$$

$$\Psi (6, 16) = k_{6,w,xx}$$

$$\Psi (6, 17) = k_{6,w,xy}$$

$$\Psi (6, 18) = k_{6,w,yy} \quad , \quad (A.6)$$

$$\Psi (7, 20) = \Psi (8, 21) = \Psi (9, 23) = \Psi (10, 24) = \Psi (11, 19) = \Psi (12, 22) = 1 \quad (A.7)$$

To express these elements in terms of the displacements and initial curvatures, they are written in a more mathematically tractable form as (Pai and Palazotto 1995a):

$$\begin{aligned}
\Psi(1, 2) &= C_{11}/C_0 \\
\Psi(1, 8) &= C_{12}/C_0 \\
\Psi(1, 14) &= C_{13}/C_0 \\
\Psi(1, 3) &= C_{14}/C_0 \\
\Psi(1, 9) &= C_{15}/C_0 \\
\Psi(1, 15) &= C_{16}/C_0 \\
\Psi(1, 1) &= (C_{12}k_5^0 - C_{13}k_1^0 + C_{15}k_4^0 - C_{16}k_{62}^0)/C_0 \\
\Psi(1, 7) &= -(C_{11}k_5^0 + C_{13}k_{61}^0 + C_{14}k_4^0 + C_{16}k_2^0)/C_0 \\
\Psi(1, 13) &= (C_{11}k_1^0 + C_{12}k_{61}^0 + C_{14}k_{62}^0 + C_{15}k_2^0)/C_0
\end{aligned} \tag{A.8}$$

$$\begin{aligned}
\Psi(2, 2) &= C_{21}/C_0 \\
\Psi(2, 8) &= C_{22}/C_0 \\
\Psi(2, 14) &= C_{23}/C_0 \\
\Psi(2, 3) &= C_{24}/C_0 \\
\Psi(2, 9) &= C_{25}/C_0 \\
\Psi(2, 15) &= C_{26}/C_0 \\
\Psi(2, 1) &= (C_{22}k_5^0 - C_{23}k_1^0 + C_{25}k_4^0 - C_{26}k_{62}^0)/C_0 \\
\Psi(2, 7) &= -(C_{21}k_5^0 + C_{23}k_{61}^0 + C_{24}k_4^0 + C_{26}k_2^0)/C_0 \\
\Psi(2, 13) &= (C_{21}k_1^0 + C_{22}k_{61}^0 + C_{24}k_{62}^0 + C_{25}k_2^0)/C_0
\end{aligned} \tag{A.9}$$

$$\Psi(3, 2) = 2C_{31}/C_0$$

$$\Psi(3, 8) = 2C_{32}/C_0$$

$$\Psi(3, 14) = 2C_{33}/C_0$$

$$\Psi(3, 3) = 2C_{34}/C_0$$

$$\Psi(3, 9) = 2C_{35}/C_0$$

$$\Psi(3, 15) = 2C_{36}/C_0$$

$$\Psi(3, 1) = 2(C_{32}k_5^0 - C_{33}k_1^0 + C_{35}k_4^0 - C_{36}k_{62}^0)/C_0$$

$$\Psi(3, 7) = -2(C_{31}k_5^0 + C_{33}k_{61}^0 + C_{34}k_4^0 + C_{36}k_2^0)/C_0$$

$$\Psi(3, 13) = 2(C_{31}k_1^0 + C_{32}k_{61}^0 + C_{34}k_{62}^0 + C_{35}k_2^0)/C_0 \quad (\text{A.10})$$

$$\Psi(4, 2) = C_{41} + C_3T_{32}k_4^0 - C_3T_{33}k_{62}^0 - C_4T_{32}k_5^0 + C_4T_{33}k_1^0$$

$$\Psi(4, 8) = C_{42} - C_3T_{31}k_4^0 - C_3T_{33}k_2^0 + C_4T_{31}k_5^0 + C_4T_{33}k_{61}^0$$

$$\Psi(4, 14) = C_{43} + C_3T_{31}k_{62}^0 + C_3T_{32}k_2^0 - C_4T_{31}k_1^0 - C_4T_{32}k_{61}^0$$

$$\Psi(4, 3) = C_{44}$$

$$\Psi(4, 9) = C_{45}$$

$$\Psi(4, 15) = C_{46}$$

$$\Psi(4, 1) = C_{42}k_5^0 - C_{43}k_1^0 + C_{45}k_4^0 - C_{46}k_{62}^0 + C_3T_{32}k_{4x}^0 - C_3T_{33}k_{62x}^0 - C_4T_{32}k_{5x}^0 +$$

$$C_4T_{33}k_{1x}^0$$

$$\Psi(4, 7) = -C_{41}k_5^0 - C_{43}k_{61}^0 - C_{44}k_4^0 - C_{46}k_2^0 - C_3T_{31}k_{4x}^0 - C_3T_{33}k_{2x}^0 + C_4T_{31}k_{5x}^0 +$$

$$C_4T_{33}k_{61x}^0$$

$$\Psi(4, 13) = C_{41}k_1^0 + C_{42}k_{61}^0 + C_{44}k_{62}^0 + C_{45}k_2^0 + C_3T_{31}k_{62x}^0 + C_3T_{32}k_{2x}^0 - C_4T_{31}k_{1x}^0 -$$

$$C_4T_{32}k_{61x}^0$$

$$\Psi(4, 5) = C_3T_{31}$$

$$\begin{aligned}
\Psi(4, 11) &= C_3 T_{32} \\
\Psi(4, 17) &= C_3 T_{33} \\
\Psi(4, 4) &= -C_4 T_{31} \\
\Psi(4, 10) &= -C_4 T_{32} \\
\Psi(4, 16) &= -C_4 T_{33}
\end{aligned} \tag{A.11}$$

$$\begin{aligned}
\Psi(5, 2) &= C_{51} \\
\Psi(5, 8) &= C_{52} \\
\Psi(5, 14) &= C_{53} \\
\Psi(5, 3) &= C_{54} - C_1 T_{32} k_4^0 + C_1 T_{33} k_{62}^0 + C_2 T_{32} k_5^0 - C_2 T_{33} k_1^0 \\
\Psi(5, 9) &= C_{55} + C_1 T_{31} k_4^0 + C_1 T_{33} k_2^0 - C_2 T_{31} k_5^0 - C_2 T_{33} k_{61}^0 \\
\Psi(5, 15) &= C_{56} - C_1 T_{31} k_{62}^0 - C_1 T_{32} k_2^0 + C_2 T_{31} k_1^0 + C_2 T_{32} k_{61}^0 \\
\Psi(5, 1) &= C_{52} k_5^0 - C_{53} k_1^0 + C_{55} k_4^0 - C_{56} k_{62}^0 - C_1 T_{32} k_{4y}^0 + C_1 T_{33} k_{62y}^0 + C_2 T_{32} k_{5y}^0 - \\
&\quad C_2 T_{33} k_{1y}^0 \\
\Psi(5, 7) &= -C_{51} k_5^0 - C_{53} k_{61}^0 - C_{54} k_4^0 - C_{56} k_2^0 + C_1 T_{31} k_{4y}^0 + C_1 T_{33} k_{2y}^0 - C_2 T_{31} k_{5y}^0 - \\
&\quad C_2 T_{33} k_{61y}^0 \\
\Psi(5, 13) &= C_{51} k_1^0 + C_{52} k_{61}^0 + C_{54} k_{62}^0 + C_{55} k_2^0 - C_1 T_{31} k_{62y}^0 - C_1 T_{32} k_{2y}^0 + C_2 T_{31} k_{1y}^0 + \\
&\quad C_2 T_{32} k_{61y}^0 \\
\Psi(5, 5) &= C_2 T_{31} \\
\Psi(5, 11) &= C_2 T_{32} \\
\Psi(5, 17) &= C_2 T_{33} \\
\Psi(5, 6) &= -C_1 T_{31} \\
\Psi(5, 12) &= -C_1 T_{32}
\end{aligned}$$

$$\Psi(5, 18) = -C_1 T_{33} \quad (\text{A.12})$$

$$\Psi(6, 2) = C_{61} - C_1 T_{32} k_4^0 + C_1 T_{33} k_{62}^0 + C_2 T_{32} k_5^0 - C_2 T_{33} k_1^0$$

$$\Psi(6, 8) = C_{62} + C_1 T_{31} k_4^0 + C_1 T_{33} k_2^0 - C_2 T_{31} k_5^0 - C_2 T_{33} k_{61}^0$$

$$\Psi(6, 14) = C_{63} - C_1 T_{31} k_{62}^0 - C_1 T_{32} k_2^0 + C_2 T_{31} k_1^0 + C_2 T_{32} k_{61}^0$$

$$\Psi(6, 3) = C_{64} + C_3 T_{32} k_4^0 - C_3 T_{33} k_{62}^0 - C_4 T_{32} k_5^0 + C_4 T_{33} k_1^0$$

$$\Psi(6, 9) = C_{65} - C_3 T_{31} k_4^0 - C_3 T_{33} k_2^0 + C_4 T_{31} k_5^0 + C_4 T_{33} k_{61}^0$$

$$\Psi(6, 15) = C_{66} + C_3 T_{31} k_{62}^0 + C_3 T_{32} k_2^0 - C_4 T_{31} k_1^0 - C_4 T_{32} k_{61}^0$$

$$\begin{aligned} \Psi(6, 1) = & C_{62} k_5^0 - C_{63} k_1^0 + C_{65} k_4^0 - C_{66} k_{62}^0 - C_1 T_{32} k_{4x}^0 + C_1 T_{33} k_{62x}^0 + C_2 T_{32} k_{5x}^0 \\ & - C_2 T_{33} k_{1x}^0 + C_3 T_{32} k_{4y}^0 - C_3 T_{33} k_{62y}^0 - C_4 T_{32} k_{5y}^0 + C_4 T_{33} k_{1y}^0 \end{aligned}$$

$$\begin{aligned} \Psi(6, 7) = & -C_{61} k_5^0 - C_{63} k_{61}^0 - C_{64} k_4^0 - C_{66} k_2^0 + C_1 T_{31} k_{4x}^0 + C_1 T_{33} k_{2x}^0 - C_2 T_{31} k_{5x}^0 \\ & - C_2 T_{33} k_{61x}^0 - C_3 T_{31} k_{4y}^0 - C_3 T_{33} k_{2y}^0 + C_4 T_{31} k_{5y}^0 + C_4 T_{33} k_{61y}^0 \end{aligned}$$

$$\begin{aligned} \Psi(6, 13) = & C_{61} k_1^0 + C_{62} k_{61}^0 + C_{64} k_{62}^0 + C_{65} k_2^0 - C_1 T_{31} k_{62x}^0 - C_1 T_{32} k_{2x}^0 + C_2 T_{31} k_{1x}^0 \\ & + C_2 T_{32} k_{61x}^0 + C_3 T_{31} k_{62y}^0 + C_3 T_{32} k_{2y}^0 - C_4 T_{31} k_{1y}^0 - C_4 T_{32} k_{61y}^0 \end{aligned}$$

$$\Psi(6, 5) = -C_1 T_{31} - C_4 T_{31}$$

$$\Psi(6, 11) = -C_1 T_{32} - C_4 T_{32}$$

$$\Psi(6, 17) = -C_1 T_{33} - C_4 T_{33}$$

$$\Psi(6, 6) = C_3 T_{31}$$

$$\Psi(6, 12) = C_3 T_{32}$$

$$\Psi(6, 18) = C_3 T_{33}$$

$$\Psi(6, 4) = C_2 T_{31}$$

$$\Psi(6, 10) = C_2 T_{32}$$

$$\Psi(6, 16) = C_2 T_{33} \quad (\text{A.13})$$

$$\Psi(7, 20) = \Psi(8, 21) = \Psi(9, 23) = \Psi(10, 24) = \Psi(11, 19) = \Psi(12, 22) = 1 \quad (\text{A.14})$$

where

$$\begin{aligned}
C_0 &\equiv (1 + e_1) \cos \gamma_{61} + (1 + e_2) \cos \gamma_{62} \\
C_{01} &\equiv \frac{\hat{T}_{21} - \sin \gamma_6 \hat{T}_{11}}{\cos \gamma_6} \\
C_{02} &\equiv \frac{\hat{T}_{22} - \sin \gamma_6 \hat{T}_{12}}{\cos \gamma_6} \\
C_{03} &\equiv \frac{\hat{T}_{23} - \sin \gamma_6 \hat{T}_{13}}{\cos \gamma_6} \\
C_{04} &\equiv \frac{\hat{T}_{11} - \sin \gamma_6 \hat{T}_{21}}{\cos \gamma_6} \\
C_{05} &\equiv \frac{\hat{T}_{12} - \sin \gamma_6 \hat{T}_{22}}{\cos \gamma_6} \\
C_{06} &\equiv \frac{\hat{T}_{13} - \sin \gamma_6 \hat{T}_{23}}{\cos \gamma_6} \\
C_1 &\equiv \frac{\cos \gamma_{61}}{\cos \gamma_6 (1 + e_2)} \\
C_2 &\equiv \frac{\sin \gamma_{62}}{\cos \gamma_6 (1 + e_1)} \\
C_3 &\equiv \frac{\sin \gamma_{61}}{\cos \gamma_6 (1 + e_2)} \\
C_4 &\equiv \frac{\cos \gamma_{62}}{\cos \gamma_6 (1 + e_1)}
\end{aligned} \quad (\text{A.15})$$

$$\begin{aligned}
C_{11} &\equiv (1 + e_1 + (1 + e_2) \cos \gamma_{62} \cos \gamma_{61}) \hat{T}_{11} - (1 + e_2) \sin \gamma_{61} \cos \gamma_{62} C_{01} \\
C_{12} &\equiv (1 + e_1 + (1 + e_2) \cos \gamma_{62} \cos \gamma_{61}) \hat{T}_{12} - (1 + e_2) \sin \gamma_{61} \cos \gamma_{62} C_{02} \\
C_{13} &\equiv (1 + e_1 + (1 + e_2) \cos \gamma_{62} \cos \gamma_{61}) \hat{T}_{13} - (1 + e_2) \sin \gamma_{61} \cos \gamma_{62} C_{03} \\
C_{14} &\equiv -(1 + e_1) \sin \gamma_{61} \sin \gamma_{62} \hat{T}_{21} - (1 + e_1) \sin \gamma_{61} \cos \gamma_{62} C_{04} \\
C_{15} &\equiv -(1 + e_1) \sin \gamma_{61} \sin \gamma_{62} \hat{T}_{22} - (1 + e_1) \sin \gamma_{61} \cos \gamma_{62} C_{05} \\
C_{16} &\equiv -(1 + e_1) \sin \gamma_{61} \sin \gamma_{62} \hat{T}_{23} - (1 + e_1) \sin \gamma_{61} \cos \gamma_{62} C_{06}
\end{aligned} \quad (\text{A.16})$$

$$\begin{aligned}
C_{21} &\equiv -(1+e_2) \sin \gamma_{61} \sin \gamma_{62} \hat{T}_{11} - (1+e_2) \sin \gamma_{62} \cos \gamma_{61} C_{01} \\
C_{22} &\equiv -(1+e_2) \sin \gamma_{61} \sin \gamma_{62} \hat{T}_{12} - (1+e_2) \sin \gamma_{62} \cos \gamma_{61} C_{02} \\
C_{23} &\equiv -(1+e_2) \sin \gamma_{61} \sin \gamma_{62} \hat{T}_{13} - (1+e_2) \sin \gamma_{62} \cos \gamma_{61} C_{03} \\
C_{24} &\equiv (1+e_2 + (1+e_1) \cos \gamma_{62} \cos \gamma_{61}) \hat{T}_{21} - (1+e_1) \sin \gamma_{62} \cos \gamma_{61} C_{04} \\
C_{25} &\equiv (1+e_2 + (1+e_1) \cos \gamma_{62} \cos \gamma_{61}) \hat{T}_{22} - (1+e_1) \sin \gamma_{62} \cos \gamma_{61} C_{05} \\
C_{26} &\equiv (1+e_2 + (1+e_1) \cos \gamma_{62} \cos \gamma_{61}) \hat{T}_{23} - (1+e_1) \sin \gamma_{62} \cos \gamma_{61} C_{06} \tag{A.17}
\end{aligned}$$

$$\begin{aligned}
C_{31} &\equiv (1+e_2) \sin \gamma_{61} \cos \gamma_{62} \hat{T}_{11} + (1+e_2) \cos \gamma_{61} \cos \gamma_{62} C_{01} \\
C_{32} &\equiv (1+e_2) \sin \gamma_{61} \cos \gamma_{62} \hat{T}_{12} + (1+e_2) \cos \gamma_{61} \cos \gamma_{62} C_{02} \\
C_{33} &\equiv (1+e_2) \sin \gamma_{61} \cos \gamma_{62} \hat{T}_{13} + (1+e_2) \cos \gamma_{61} \cos \gamma_{62} C_{03} \\
C_{34} &\equiv (1+e_1) \cos \gamma_{61} \sin \gamma_{62} \hat{T}_{21} + (1+e_1) \cos \gamma_{61} \cos \gamma_{62} C_{04} \\
C_{35} &\equiv (1+e_1) \cos \gamma_{61} \sin \gamma_{62} \hat{T}_{22} + (1+e_1) \cos \gamma_{61} \cos \gamma_{62} C_{05} \\
C_{36} &\equiv (1+e_1) \cos \gamma_{61} \sin \gamma_{62} \hat{T}_{23} + (1+e_1) \cos \gamma_{61} \cos \gamma_{62} C_{06} \tag{A.18}
\end{aligned}$$

$$\begin{aligned}
C_{41} &\equiv \frac{k_{61}}{2C_0} \left[2 \sin \gamma_{61} \hat{T}_{11} + ((1+e_1) \cos \gamma_{61} - (1+e_2) \cos \gamma_{62} + C_0) \frac{C_{01}}{1+e_1} \right] \\
&\quad - (C_4 T_{31})_x - k_5 C_2 T_{31} \\
C_{42} &\equiv \frac{k_{61}}{2C_0} \left[2 \sin \gamma_{61} \hat{T}_{12} + ((1+e_1) \cos \gamma_{61} - (1+e_2) \cos \gamma_{62} + C_0) \frac{C_{02}}{1+e_1} \right] \\
&\quad - (C_4 T_{32})_x - k_5 C_2 T_{32} \\
C_{43} &\equiv \frac{k_{61}}{2C_0} \left[2 \sin \gamma_{61} \hat{T}_{13} + ((1+e_1) \cos \gamma_{61} - (1+e_2) \cos \gamma_{62} + C_0) \frac{C_{03}}{1+e_1} \right] \\
&\quad - (C_4 T_{33})_x - k_5 C_2 T_{33} \\
C_{44} &\equiv \frac{k_{61}}{2C_0} \left[-2 \sin \gamma_{62} \hat{T}_{21} + ((1+e_1) \cos \gamma_{61} - (1+e_2) \cos \gamma_{62} - C_0) \frac{C_{04}}{1+e_2} \right] \\
&\quad + (C_3 T_{31})_x + k_5 C_1 T_{31}
\end{aligned}$$

$$\begin{aligned}
C_{45} &\equiv \frac{k_{61}}{2C_0} \left[-2 \sin \gamma_{62} \hat{T}_{22} + ((1+e_1) \cos \gamma_{61} - (1+e_2) \cos \gamma_{62} - C_0) \frac{C_{05}}{1+e_2} \right] \\
&\quad + (C_3 T_{32})_x + k_5 C_1 T_{32} \\
C_{46} &\equiv \frac{k_{61}}{2C_0} \left[-2 \sin \gamma_{62} \hat{T}_{23} + ((1+e_1) \cos \gamma_{61} - (1+e_2) \cos \gamma_{62} - C_0) \frac{C_{06}}{1+e_2} \right] \\
&\quad + (C_3 T_{33})_x + k_5 C_1 T_{33}
\end{aligned} \tag{A.19}$$

$$\begin{aligned}
C_{51} &\equiv -\frac{k_{62}}{2C_0} \left[2 \sin \gamma_{61} \hat{T}_{11} + ((1+e_1) \cos \gamma_{61} - (1+e_2) \cos \gamma_{62} + C_0) \frac{C_{01}}{1+e_1} \right] \\
&\quad + (C_2 T_{31})_y - k_4 C_4 T_{31} \\
C_{52} &\equiv -\frac{k_{62}}{2C_0} \left[2 \sin \gamma_{61} \hat{T}_{12} + ((1+e_1) \cos \gamma_{61} - (1+e_2) \cos \gamma_{62} + C_0) \frac{C_{02}}{1+e_1} \right] \\
&\quad + (C_2 T_{32})_y - k_4 C_4 T_{32} \\
C_{53} &\equiv -\frac{k_{62}}{2C_0} \left[2 \sin \gamma_{61} \hat{T}_{13} + ((1+e_1) \cos \gamma_{61} - (1+e_2) \cos \gamma_{62} + C_0) \frac{C_{03}}{1+e_1} \right] \\
&\quad + (C_2 T_{33})_y - k_4 C_4 T_{33} \\
C_{54} &\equiv -\frac{k_{62}}{2C_0} \left[-2 \sin \gamma_{62} \hat{T}_{21} + ((1+e_1) \cos \gamma_{61} - (1+e_2) \cos \gamma_{62} - C_0) \frac{C_{04}}{1+e_2} \right] \\
&\quad - (C_1 T_{31})_y + k_4 C_3 T_{31} \\
C_{55} &\equiv -\frac{k_{62}}{2C_0} \left[-2 \sin \gamma_{62} \hat{T}_{22} + ((1+e_1) \cos \gamma_{61} - (1+e_2) \cos \gamma_{62} - C_0) \frac{C_{05}}{1+e_2} \right] \\
&\quad - (C_1 T_{32})_y + k_4 C_3 T_{32} \\
C_{56} &\equiv -\frac{k_{62}}{2C_0} \left[-2 \sin \gamma_{62} \hat{T}_{23} + ((1+e_1) \cos \gamma_{61} - (1+e_2) \cos \gamma_{62} - C_0) \frac{C_{06}}{1+e_2} \right] \\
&\quad - (C_1 T_{33})_y + k_4 C_3 T_{33}
\end{aligned} \tag{A.20}$$

$$\begin{aligned}
C_{61} &\equiv \frac{k_2 - k_1}{2C_0} \left[2 \sin \gamma_{61} \hat{T}_{11} + ((1+e_1) \cos \gamma_{61} - (1+e_2) \cos \gamma_{62} + C_0) \frac{C_{01}}{1+e_1} \right] \\
&\quad + (C_2 T_{31})_x - (C_4 T_{31})_y - k_4 C_2 T_{31} - k_5 C_4 T_{31} \\
C_{62} &\equiv \frac{k_2 - k_1}{2C_0} \left[2 \sin \gamma_{61} \hat{T}_{12} + ((1+e_1) \cos \gamma_{61} - (1+e_2) \cos \gamma_{62} + C_0) \frac{C_{02}}{1+e_1} \right] \\
&\quad + (C_2 T_{32})_x - (C_4 T_{32})_y - k_4 C_2 T_{32} - k_5 C_4 T_{32}
\end{aligned}$$

$$\begin{aligned}
C_{63} &\equiv \frac{k_2 - k_1}{2C_0} \left[2 \sin \gamma_{61} \hat{T}_{13} + ((1 + e_1) \cos \gamma_{61} - (1 + e_2) \cos \gamma_{62} + C_0) \frac{C_{03}}{1 + e_1} \right] \\
&\quad + (C_2 T_{33})_x - (C_4 T_{33})_y - k_4 C_2 T_{33} - k_5 C_4 T_{33} \\
C_{64} &\equiv \frac{k_2 - k_1}{2C_0} \left[-2 \sin \gamma_{62} \hat{T}_{21} + ((1 + e_1) \cos \gamma_{61} - (1 + e_2) \cos \gamma_{62} - C_0) \frac{C_{04}}{1 + e_2} \right] \\
&\quad + (C_3 T_{31})_y - (C_1 T_{31})_x + k_4 C_1 T_{31} + k_5 C_3 T_{31} \\
C_{65} &\equiv \frac{k_2 - k_1}{2C_0} \left[-2 \sin \gamma_{62} \hat{T}_{22} + ((1 + e_1) \cos \gamma_{61} - (1 + e_2) \cos \gamma_{62} - C_0) \frac{C_{05}}{1 + e_2} \right] \\
&\quad + (C_3 T_{32})_y - (C_1 T_{32})_x + k_4 C_1 T_{32} + k_5 C_3 T_{32} \\
C_{66} &\equiv \frac{k_2 - k_1}{2C_0} \left[-2 \sin \gamma_{62} \hat{T}_{23} + ((1 + e_1) \cos \gamma_{61} - (1 + e_2) \cos \gamma_{62} - C_0) \frac{C_{06}}{1 + e_2} \right] \\
&\quad + (C_3 T_{33})_y - (C_1 T_{33})_x + k_4 C_1 T_{33} + k_5 C_3 T_{33}
\end{aligned} \tag{A.21}$$

Appendix B. Mathematica¹ Source Files

This appendix contains selected *Mathematica* source code used in the theoretical development and computational implementation of the current research.

B.1 Development of the Matrix $[\Phi]$

The matrix $[\Phi]$ of Eq (4.12) was developed using the following code.

```
Write[$Output,"Forming S-matrix..."]

S[1] = {{ 1, 0, 0, Z, 0, 0},
        { 0, 1, 0, 0, Z, 0},
        { G30, G31, G32, G33, G34, G35},
        { 0, 0, 1, 0, 0, Z}}

S[3]={{G14, 0, G15, 0,-RK05*G24, -RK05*G25},
      { 0, G24, 0, G25, RK04*G14, RK04*G15},
      {G36, G37, G38, G39, G51, G61},
      {G24, G14, G25, G15, G52, G62}}

S[4] = {{ G53, G63},
        { G54, G64}}

SBIG = Table[0,{6},{12}]

Do[ SBIG[[i,j]] = S[1][[i,j]], {i,4},{j,6} ]
Do[ SBIG[[i,j+6]] = S[3][[i,j]], {i,4},{j,6} ]
Do[ SBIG[[i+4,j+10]] = S[4][[i,j]], {i,2},{j,2} ]

Write[$Output,"Forming Q-matrix..."]

QMAT[1] = {{QB[1,1],QB[1,2],QB[1,3],QB[1,6]},
           {QB[1,2],QB[2,2],QB[2,3],QB[2,6]},
           {QB[1,3],QB[2,3],QB[3,3],QB[3,6]},
           {QB[1,6],QB[2,6],QB[3,6],QB[6,6]}}

QMAT[2] = {{QB[4,4],QB[4,5]},
           {QB[4,5],QB[5,5]}}

QBIG = Table[0,{6},{6}]
Do[ QBIG[[i,j]] = QMAT[1][[i,j]], {i,4},{j,4}]
Do[ QBIG[[i+4,j+4]] = QMAT[2][[i,j]], {i,2},{j,2}]

Write[$Output,"Forming PHIHAT..."]

PHIHAT = Transpose[SBIG].QBIG.SBIG;

Write[$Output,"Saving PHIHAT to 'phihat.out'..."]

Save["phihat.out",PHIHAT];

Write[$Output,"Writing fortran form to 'phihat.f'..."]

stmp = OpenWrite["phihat.f",FormatType->FortranForm]
```

¹ *Mathematica* is a registered trademark of Wolfram Research, Inc.

```
<<printphi.m
```

```
Write[$Output,"Done."]
```

This developed the elements of $[\hat{\Phi}]$, which was integrated using Gauss quadrature to yield $[\Phi]$.

B.2 Development of the Matrix $[\Psi]$

This 12×24 matrix of Eq (4.71) was developed using these input decks. First, the stretches e_1 and e_2 and their derivatives are developed.

```
xx1 = 1 + ux - v*k05 + w*k01;
xx2 = vx + u*k05 + w*k061;
xx3 = wx - u*k01 - v*k061;
xx4 = uy - v*k04 + w*k062;
xx5 = 1 + vy + u*k04 + w*k02;
xx6 = wy - u*k062 - v*k02;
e1 = Sqrt[xx1^2 + xx2^2 + xx3^2] - 1;
e2 = Sqrt[xx4^2 + xx5^2 + xx6^2] - 1;
evec = {e1,e2}
uvec = {u,ux,uy,uxx,uxy,uyy,v,vx,vy,vxx,vxy,vyy,w,wx,wy,wxw,wxy,wyy,
        g4,g4x,g4y,g5,g5x,g5y}

devec = Outer[D,evec,uvec]
devec2 = Outer[D,devec,uvec]

xx1=.;xx2=.;xx3=.;xx4=.;xx5=.;xx6=.;e1=.;e2=.

devec = devec /. Dispatch[{
1 + ux - v*k05 + w*k01 -> xx1,
vx + u*k05 + w*k061 -> xx2,
wx - u*k01 - v*k061 -> xx3,
uy - v*k04 + w*k062 -> xx4,
1 + vy + u*k04 + w*k02 -> xx5,
wy - u*k062 - v*k02 -> xx6}]

devec2 = devec2 /. Dispatch[{
1 + ux - v*k05 + w*k01 -> xx1,
vx + u*k05 + w*k061 -> xx2,
wx - u*k01 - v*k061 -> xx3,
uy - v*k04 + w*k062 -> xx4,
1 + vy + u*k04 + w*k02 -> xx5,
wy - u*k062 - v*k02 -> xx6}]

devec = devec //. {xx1^2 + xx2^2 + xx3^2 -> (1 + e1)^2,
xx4^2 + xx5^2 + xx6^2 -> (1 + e2)^2}

devec2 = devec2 //. {xx1^2 + xx2^2 + xx3^2 -> (1 + e1)^2,
xx4^2 + xx5^2 + xx6^2 -> (1 + e2)^2}

devec = PowerExpand[devec]
devec = devec /. Dispatch[{1/(1+e1) -> xx9,
1/(1+e1)^2 -> xx15,
1/(1+e2) -> 1/xx16,
1/(1+e2)^2 -> 1/xx17,
-2 k04 xx4 - 2 k02 xx6 -> xx8,
2 k062 xx4 + 2 k02 xx5 -> xx11,
2 k04 xx5 - 2 k062 xx6 -> xx12,
```

```

-2 k05 xx1 - 2 k061 xx3 -> xx13,
2 k01 xx1 + 2 k061 xx2 -> xx14}]

devec = Simplify[devec]

devec2 = PowerExpand[devec2]
devec2 = devec2 /. Dispatch[{1/(1+e1) -> xx9,
1/(1+e1)^3 -> xx10,
1/(1+e2) -> 1/xx7,
1/(1+e2)^3 -> 1/xx7^3,
-2 k04 xx4 - 2 k02 xx6 -> xx8,
2 k062 xx4 + 2 k02 xx5 -> xx11,
2 k04 xx5 - 2 k062 xx6 -> xx12,
-2 k05 xx1 - 2 k061 xx3 -> xx13,
2 k01 xx1 + 2 k061 xx2 -> xx14}]

devec2 = Simplify[devec2]

fort = OpenWrite["devec.f"]

Do[ Do[
If[ ToString[devec[[i,j]] ] == "0", 0,
WriteString[fort,"e(",ToString[i],",",ToString[j],") = ",
FortranForm[ devec[[i,j]] ], "\n" ] ],
{j,24} ], {i,2} ]

Close[fort]

```

The in-plane rotation angles and their derivatives are found using the following.

```

sg6 = e1ux[u,ux,v,vx,w,wx]*e2uy[u,uy,v,vy,w,wy] +
e1vx[u,ux,v,vx,w,wx]*e2vy[u,uy,v,vy,w,wy] +
e1wx[u,ux,v,vx,w,wx]*e2wy[u,uy,v,vy,w,wy];
xx9 = (1 + e1[u,ux,v,vx,w,wx])/(1 + e2[u,uy,v,vy,w,wy]);
cg6 = Sqrt[1 - sg6^2];
sg61 = 1/Sqrt[1 + (1/(sg6*((xx9) + cg6)))^2];
sg62 = 1/Sqrt[1 + (1/(sg6*((1/xx9) + cg6)))^2];
cg61 = 1/Sqrt[1 + (sg6*((xx9) + cg6))^2];
cg62 = 1/Sqrt[1 + (sg6*((1/xx9) + cg6))^2];

gamvec = {sg61,sg62}
uvec = {u,ux,uy,uxx,uxy,uyy,v,vx,vy,vxx,vxy,vyy,w,wx,wy,wxw,wyw,wyw,
gam4,gam4x,gam4y,gam5,gam5x,gam5y}

dvec = (1/cg61)*Outer[D,gamvec,uvec]

xx9 = .
dvec = dvec /. (1 + e1[u,ux,v,vx,w,wx])/(1 + e2[u,uy,v,vy,w,wy]) -> xx9
dvec = dvec /. (cg6 + ((1 + e2[u,uy,v,vy,w,wy])/(1 + e1[u,ux,v,vx,w,wx]))) ->
(cg6 + 1/xx9)

sg6 = .
dvec = dvec /. e1ux[u,ux,v,vx,w,wx]*e2uy[u,uy,v,vy,w,wy] +
e1vx[u,ux,v,vx,w,wx]*e2vy[u,uy,v,vy,w,wy] +
e1wx[u,ux,v,vx,w,wx]*e2wy[u,uy,v,vy,w,wy] -> sg6

cg6 = .
dvec = dvec //. {Sqrt[1 - sg6^2] -> cg6, 1/Sqrt[1 - sg6^2] -> 1/cg6}

dvec = dvec //. {1 + sg6^2/(cg6 + xx9)^2 -> xx18,
(cg6 + 1/xx9) -> xx19,
1 + xx19^2/sg6^2 -> xx20,

```

```

1 + (cg6 + xx9)^2/sg6^2 -> xx21}

dvec = dvec /. Dispatch[{1/(1+e1[u,ux,v,vx,w,wx]) -> xx9,
1/(1+e1[u,ux,v,vx,w,wx])^2 -> xx15,
1/(1+e2[u,uy,v,vy,w,wy]) -> 1/xx16,
1/(1+e2[u,uy,v,vy,w,wy])^2 -> 1/xx17}]

Format[e1ux[u,ux,v,vx,w,wx]=e1ux,FortranForm]
Format[e1vx[u,ux,v,vx,w,wx]=e1vx,FortranForm]
Format[e1wx[u,ux,v,vx,w,wx]=e1wx,FortranForm]
Format[e2uy[u,uy,v,vy,w,wy]=e2uy,FortranForm]
Format[e2vy[u,uy,v,vy,w,wy]=e2vy,FortranForm]
Format[e2wy[u,uy,v,vy,w,wy]=e2wy,FortranForm]
Format[Derivative[1,0,0,0,0,0][e1ux][u,ux,v,vx,w,wx]=e1uxu,FortranForm]
Format[Derivative[0,1,0,0,0,0][e1ux][u,ux,v,vx,w,wx]=e1uxux,FortranForm]
Format[Derivative[0,0,1,0,0,0][e1ux][u,ux,v,vx,w,wx]=e1vux,FortranForm]
Format[Derivative[0,0,0,1,0,0][e1ux][u,ux,v,vx,w,wx]=e1vxux,FortranForm]
Format[Derivative[0,0,0,0,1,0][e1ux][u,ux,v,vx,w,wx]=e1wux,FortranForm]
Format[Derivative[0,0,0,0,0,1][e1ux][u,ux,v,vx,w,wx]=e1wxux,FortranForm]
Format[Derivative[1,0,0,0,0,0][e1vx][u,ux,v,vx,w,wx]=e1vxu,FortranForm]
Format[Derivative[0,1,0,0,0,0][e1vx][u,ux,v,vx,w,wx]=e1vxux,FortranForm]
Format[Derivative[0,0,1,0,0,0][e1vx][u,ux,v,vx,w,wx]=e1vuxv,FortranForm]
Format[Derivative[0,0,0,1,0,0][e1vx][u,ux,v,vx,w,wx]=e1vxv,FortranForm]
Format[Derivative[0,0,0,0,1,0][e1vx][u,ux,v,vx,w,wx]=e1wvx,FortranForm]
Format[Derivative[0,0,0,0,0,1][e1vx][u,ux,v,vx,w,wx]=e1wxvx,FortranForm]
Format[Derivative[1,0,0,0,0,0][e1wx][u,ux,v,vx,w,wx]=e1wxu,FortranForm]
Format[Derivative[0,1,0,0,0,0][e1wx][u,ux,v,vx,w,wx]=e1wxux,FortranForm]
Format[Derivative[0,0,1,0,0,0][e1wx][u,ux,v,vx,w,wx]=e1wxv,FortranForm]
Format[Derivative[0,0,0,1,0,0][e1wx][u,ux,v,vx,w,wx]=e1wxvx,FortranForm]
Format[Derivative[0,0,0,0,1,0][e1wx][u,ux,v,vx,w,wx]=e1wxw,FortranForm]
Format[Derivative[0,0,0,0,0,1][e1wx][u,ux,v,vx,w,wx]=e1wxwx,FortranForm]
Format[Derivative[1,0,0,0,0,0][e2uy][u,uy,v,vy,w,wy]=e2uyu,FortranForm]
Format[Derivative[0,1,0,0,0,0][e2uy][u,uy,v,vy,w,wy]=e2uyuy,FortranForm]
Format[Derivative[0,0,1,0,0,0][e2uy][u,uy,v,vy,w,wy]=e2vuy,FortranForm]
Format[Derivative[0,0,0,1,0,0][e2uy][u,uy,v,vy,w,wy]=e2vyuy,FortranForm]
Format[Derivative[0,0,0,0,1,0][e2uy][u,uy,v,vy,w,wy]=e2wuy,FortranForm]
Format[Derivative[0,0,0,0,0,1][e2uy][u,uy,v,vy,w,wy]=e2wyuy,FortranForm]
Format[Derivative[1,0,0,0,0,0][e2vy][u,uy,v,vy,w,wy]=e2vyu,FortranForm]
Format[Derivative[0,1,0,0,0,0][e2vy][u,uy,v,vy,w,wy]=e2vyuy,FortranForm]
Format[Derivative[0,0,1,0,0,0][e2vy][u,uy,v,vy,w,wy]=e2vyvy,FortranForm]
Format[Derivative[0,0,0,1,0,0][e2vy][u,uy,v,vy,w,wy]=e2wvy,FortranForm]
Format[Derivative[0,0,0,0,1,0][e2vy][u,uy,v,vy,w,wy]=e2wyvy,FortranForm]
Format[Derivative[1,0,0,0,0,0][e2wy][u,uy,v,vy,w,wy]=e2wyu,FortranForm]
Format[Derivative[0,1,0,0,0,0][e2wy][u,uy,v,vy,w,wy]=e2wyuy,FortranForm]
Format[Derivative[0,0,1,0,0,0][e2wy][u,uy,v,vy,w,wy]=e2wyv,FortranForm]
Format[Derivative[0,0,0,1,0,0][e2wy][u,uy,v,vy,w,wy]=e2wyuy,FortranForm]
Format[Derivative[0,0,0,0,1,0][e2wy][u,uy,v,vy,w,wy]=e2wyw,FortranForm]
Format[Derivative[0,0,0,0,0,1][e2wy][u,uy,v,vy,w,wy]=e2wywy,FortranForm]
Format[e1[u,ux,v,vx,w,wx]=e1,FortranForm]
Format[e2[u,uy,v,vy,w,wy]=e2,FortranForm]
Format[Derivative[1,0,0,0,0,0][e1][u,ux,v,vx,w,wx]=e1u,FortranForm];
Format[Derivative[0,1,0,0,0,0][e1][u,ux,v,vx,w,wx]=e1ux,FortranForm];
Format[Derivative[0,0,1,0,0,0][e1][u,ux,v,vx,w,wx]=e1v,FortranForm];
Format[Derivative[0,0,0,1,0,0][e1][u,ux,v,vx,w,wx]=e1vx,FortranForm];
Format[Derivative[0,0,0,0,1,0][e1][u,ux,v,vx,w,wx]=e1w,FortranForm];
Format[Derivative[0,0,0,0,0,1][e1][u,ux,v,vx,w,wx]=e1wx,FortranForm];
Format[Derivative[1,0,0,0,0,0][e2][u,uy,v,vy,w,wy]=e2u,FortranForm];
Format[Derivative[0,1,0,0,0,0][e2][u,uy,v,vy,w,wy]=e2uy,FortranForm];
Format[Derivative[0,0,1,0,0,0][e2][u,uy,v,vy,w,wy]=e2v,FortranForm];
Format[Derivative[0,0,0,1,0,0][e2][u,uy,v,vy,w,wy]=e2y,FortranForm];
Format[Derivative[0,0,0,0,1,0][e2][u,uy,v,vy,w,wy]=e2w,FortranForm];
Format[Derivative[0,0,0,0,0,1][e2][u,uy,v,vy,w,wy]=e2wy,FortranForm];

dvec = dvec /. (1 + e1)/xx17 -> xx22

```



```

dvec = Simplify[dvec]

fort = OpenWrite["dvec.f"]

Do[ Do[
If[ ToString[dvec[[i,j]] ] == "0", 0,
WriteString[fort,"e(",ToString[i],",",ToString[j],") = ",
FortranForm[ dvec[[i,j]] ]," \n" ] ] ,
{j,24} ], {i,2} ]

Close[fort]

```

B.3 Development of Shear Warping Functions

The following code was used to develop the coefficient matrix and right-hand-side of the system of equations used to determine the layer-wise cubic shear warping functions.

```

Clear["@"]

SetOptions[$Output, FormatType -> FortranForm, PageWidth -> Infinity]

(* for layers NOT containing reference surface *)

g14[i_,z_] := c14[i]      + b14[i] z^3
g15[i_,z_] := c15[i] + z + b15[i] z^3
g24[i_,z_] := c24[i] + z + b24[i] z^3
g25[i_,z_] := c25[i]      + b25[i] z^3

g14z[i_,z_] :=      3 b14[i] z^2
g15z[i_,z_] := 1 + 3 b15[i] z^2
g24z[i_,z_] := 1 + 3 b24[i] z^2
g25z[i_,z_] :=      3 b25[i] z^2

(* for layers containing reference surface *)

g14[i_,z_] :=          a14[i] z^2 + b14[i] z^3
g15[i_,z_] :=          z + a15[i] z^2 + b15[i] z^3
g24[i_,z_] :=          z + a24[i] z^2 + b24[i] z^3
g25[i_,z_] :=          a25[i] z^2 + b25[i] z^3

g14z[i_,z_] :=      2 a14[i] z + 3 b14[i] z^2
g15z[i_,z_] := 1 + 2 a15[i] z + 3 b15[i] z^2
g24z[i_,z_] := 1 + 2 a24[i] z + 3 b24[i] z^2
g25z[i_,z_] :=      2 a25[i] z + 3 b25[i] z^2

(* In-plane displacements *)

u1[i_,z_] := g15[i,z] g5 + g14[i,z] g4
u2[i_,z_] := g25[i,z] g5 + g24[i,z] g4

(* Transverse shear strains *)

b13[i_,z_] := (g15z[i,z] - rk1d g15[i,z] - rk7d g25[i,z]) g5 +
              (g14z[i,z] - rk1d g14[i,z] - rk7d g24[i,z]) g4
b23[i_,z_] := (g25z[i,z] - rk8d g15[i,z] - rk2d g25[i,z]) g5 +
              (g24z[i,z] - rk8d g14[i,z] - rk2d g24[i,z]) g4

```

```

(* Transverse shear stresses *)

j23[i_,z_] := 2 qb[4,4][i] b23[i,z] + 2 qb[4,5][i] b13[i,z]
j13[i_,z_] := 2 qb[4,5][i] b23[i,z] + 2 qb[5,5][i] b13[i,z]

(* miscellanea *)

clist[i_] := {a14[i], a15[i], a24[i], a25[i],
              b14[i], b15[i], b24[i], b25[i],
              c14[i], c15[i], c24[i], c25[i]}
clist2[i_] := {a14[i], a15[i], a24[i], a25[i],
              b14[i], b15[i], b24[i], b25[i],
              c14[i], c15[i], c24[i], c25[i],
              a14[i+1], a15[i+1], a24[i+1], a25[i+1],
              b14[i+1], b15[i+1], b24[i+1], b25[i+1],
              c14[i+1], c15[i+1], c24[i+1], c25[i+1]}
dum4[expr_,i_] := (dum = Collect[expr,{g4,g5}];
                  coefg4 = Coefficient[dum,g4];
                  dum = Collect[coefg4,clist[i]])
dum5[expr_,i_] := (dum = Collect[expr,{g4,g5}];
                  coefg5 = Coefficient[dum,g5];
                  dum = Collect[coefg5,clist[i]])
dum42[expr_,i_] := (dum = Collect[expr,{g4,g5}];
                  coefg4 = Coefficient[dum,g4];
                  dum = Collect[coefg4,clist2[i]])
dum52[expr_,i_] := (dum = Collect[expr,{g4,g5}];
                  coefg5 = Coefficient[dum,g5];
                  dum = Collect[coefg5,clist2[i]])

(* Pagano's flat plate *)

(*
np = 3
Do[ Do[ a[i,j]=0, {j,10*np}], {i,10*np}]
Do[ rhs[i]=0, {i,10*np}]
rk1d=rk2d=rk7d=rk8d=0
z[1] = -1
z[2] = -1/3
z[3] = 1/3
z[4] = 1
g13 = 30000000000
g23 = (2/5) g13
j13[1,z_] := 2 g13 b13[1,z]
j13[2,z_] := 2 g23 b13[2,z]
j13[3,z_] := 2 g13 b13[3,z]
j23[1,z_] := 2 g23 b23[1,z]
j23[2,z_] := 2 g13 b23[2,z]
j23[3,z_] := 2 g23 b23[3,z]
*)

(*--- Case I: Bottom layer is NOT reference surface -----*)

(* Find coefficients for b23=0 at bottom surface *)

Clear["g*"]
Clear["a"]
Clear["rhs"]

g14[i_,z_] := c14[i] + b14[i] z^3
g15[i_,z_] := c15[i] + z + b15[i] z^3
g24[i_,z_] := c24[i] + z + b24[i] z^3
g25[i_,z_] := c25[i] + b25[i] z^3

g14z[i_,z_] := 3 b14[i] z^2
g15z[i_,z_] := 1 + 3 b15[i] z^2

```

```

g24z[i_,z_] := 1 + 3 b24[i] z^2
g25z[i_,z_] :=      3 b25[i] z^2

expr = b23[1,z[1]]

Do[ a[1,i] = Coefficient[dum4[expr,1],clist[1][[i]]], {i,12} ]
rhs[1] = (dum = dum4[expr,1];
          Do[ dum = dum - a[1,j] clist[1][[j]], {j,1,12} ];
          dum = -dum)

Do[ a[2,i] = Coefficient[dum5[expr,1],clist[1][[i]]], {i,12} ]
rhs[2] = (dum = dum5[expr,1];
          Do[ dum = dum - a[2,j] clist[1][[j]], {j,1,12} ];
          dum = -dum)

(* Find coefficients for b13=0 at bottom surface *)

expr = b13[1,z[1]]

Do[ a[3,i] = Coefficient[dum4[expr,1],clist[1][[i]]], {i,12} ]
rhs[3] = (dum = dum4[expr,1];
          Do[ dum = dum - a[3,j] clist[1][[j]], {j,1,12} ];
          dum = -dum)

Do[ a[4,i] = Coefficient[dum5[expr,1],clist[1][[i]]], {i,12} ]
rhs[4] = (dum = dum5[expr,1];
          Do[ dum = dum - a[4,j] clist[1][[j]], {j,1,12} ];
          dum = -dum)

$Output = OpenWrite["amat_greer.f"]
Print["Case I"]
Information[a]
Information[rhs]
Close["amat_greer.f"]

$Output = {OutputStream["stdout",1]}
SetOptions[$Output, FormatType -> OutputForm]

(*----- Case II: Bottom layer IS reference surface -----*)

(* Find coefficients for b23=0 at bottom surface *)

Clear["g*"]
Clear["a"]
Clear["rhs"]

g14[i_,z_] :=      a14[i] z^2 + b14[i] z^3
g15[i_,z_] :=      z + a15[i] z^2 + b15[i] z^3
g24[i_,z_] :=      z + a24[i] z^2 + b24[i] z^3
g25[i_,z_] :=      a25[i] z^2 + b25[i] z^3

g14z[i_,z_] :=      2 a14[i] z + 3 b14[i] z^2
g15z[i_,z_] :=      1 + 2 a15[i] z + 3 b15[i] z^2
g24z[i_,z_] :=      1 + 2 a24[i] z + 3 b24[i] z^2
g25z[i_,z_] :=      2 a25[i] z + 3 b25[i] z^2

expr = b23[1,z[1]]

Do[ a[1,i] = Coefficient[dum4[expr,1],clist[1][[i]]], {i,12} ]
rhs[1] = (dum = dum4[expr,1];
          Do[ dum = dum - a[1,j] clist[1][[j]], {j,1,12} ];
          dum = -dum)

Do[ a[2,i] = Coefficient[dum5[expr,1],clist[1][[i]]], {i,12} ]
rhs[2] = (dum = dum5[expr,1];

```

```

        Do[ dum = dum - a[2,j] clist[1][[j]], {j,1,12} ];
        dum = -dum)

(* Find coefficients for b13=0 at bottom surface *)

expr = b13[1,z[1]]

Do[ a[3,i] = Coefficient[dum4[expr,1],clist[1][[i]]], {i,12} ]
rhs[3] = (dum = dum4[expr,1];
        Do[ dum = dum - a[3,j] clist[1][[j]], {j,1,12} ];
        dum = -dum)

Do[ a[4,i] = Coefficient[dum5[expr,1],clist[1][[i]]], {i,12} ]
rhs[4] = (dum = dum5[expr,1];
        Do[ dum = dum - a[4,j] clist[1][[j]], {j,1,12} ];
        dum = -dum)

$Output = OpenAppend["amat_greer.f"]
Print["Case II"]
Information[a]
Information[rhs]
Close["amat_greer.f"]

$Output = {OutputStream["stdout",1]}
SetOptions[$Output, FormatType -> OutputForm]

(*----- Case VI: top layer is NOT reference surface-----*)

(* Find coefficients for b23=0 at top surface, z = z[np + 1] *)

Clear["g*"]
Clear["a"]
Clear["rhs"]

(* for polys NOT containing reference surface, a14 = a15 = a24 = a25 = 0 *)

a[5+12*(np-1),1+12*(np-1)] = 1;
rhs[5+12*(np-1)] = 0;

a[6+12*(np-1),2+12*(np-1)] = 1;
rhs[6+12*(np-1)] = 0;

a[7+12*(np-1),3+12*(np-1)] = 1;
rhs[7+12*(np-1)] = 0;

a[8+12*(np-1),4+12*(np-1)] = 1;
rhs[8+12*(np-1)] = 0;

g14[i_,z_] := c14[i] + b14[i] z^3
g15[i_,z_] := c15[i] + z + b15[i] z^3
g24[i_,z_] := c24[i] + z + b24[i] z^3
g25[i_,z_] := c25[i] + b25[i] z^3

g14z[i_,z_] := 3 b14[i] z^2
g15z[i_,z_] := 1 + 3 b15[i] z^2
g24z[i_,z_] := 1 + 3 b24[i] z^2
g25z[i_,z_] := 3 b25[i] z^2

expr = b23[np,z[np + 1]]

Do[ a[9+12*(np-1),i+12*(np-1)] = Coefficient[dum4[expr,np],clist[np][[i]]], {i,12} ]
rhs[9+12*(np-1)] = (dum = dum4[expr,np];
        Do[ dum = dum - a[9+12*(np-1),j+12*(np-1)] clist[np][[j]], {j,1,12} ];
        dum = -dum)

```

```

Do[ a[10+12*(np-1),i+12*(np-1)] = Coefficient[dum5[expr,np],clist[np][[i]]], {i,12} ]
rhs[10+12*(np-1)] = (dum = dum5[expr,np];
Do[ dum = dum - a[10+12*(np-1),j+12*(np-1)] clist[np][[j]], {j,1,12} ];
dum = -dum)

(* Find coefficients for b13=0 at top surface *)

expr = b13[np,z[np + 1]]

Do[ a[11+12*(np-1),i+12*(np-1)] = Coefficient[dum4[expr,np],clist[np][[i]]], {i,12} ]
rhs[11+12*(np-1)] = (dum = dum4[expr,np];
Do[ dum = dum - a[11+12*(np-1),j+12*(np-1)] clist[np][[j]], {j,1,12} ];
dum = -dum)

Do[ a[12+12*(np-1),i+12*(np-1)] = Coefficient[dum5[expr,np],clist[np][[i]]], {i,12} ]
rhs[12+12*(np-1)] = (dum = dum5[expr,np];
Do[ dum = dum - a[12+12*(np-1),j+12*(np-1)] clist[np][[j]], {j,1,12} ];
dum = -dum)

$Output = OpenAppend["amat_greer.f"]
Print["Case VI"]
Information[a]
Information[rhs]
Close["amat_greer.f"]

$Output = {OutputStream["stdout",1]}
SetOptions[$Output, FormatType -> OutputForm]

(*----- Case VII: top layer IS reference surface-----*)

(* Find coefficients for b23=0 at top surface, z = z[np + 1] *)

Clear["g*"]
Clear["a"]
Clear["rhs"]

(* for polys containing reference surface, c14 = c15 = c24 = c25 = 0 *)

a[5+12*(np-1),9+12*(np-1)] = 1;
rhs[5+12*(np-1)] = 0;

a[6+12*(np-1),10+12*(np-1)] = 1;
rhs[6+12*(np-1)] = 0;

a[7+12*(np-1),11+12*(np-1)] = 1;
rhs[7+12*(np-1)] = 0;

a[8+12*(np-1),12+12*(np-1)] = 1;
rhs[8+12*(np-1)] = 0;

g14[i_,z_] := a14[i] z^2 + b14[i] z^3
g15[i_,z_] := z + a15[i] z^2 + b15[i] z^3
g24[i_,z_] := z + a24[i] z^2 + b24[i] z^3
g25[i_,z_] := a25[i] z^2 + b25[i] z^3

g14z[i_,z_] := 2 a14[i] z + 3 b14[i] z^2
g15z[i_,z_] := 1 + 2 a15[i] z + 3 b15[i] z^2
g24z[i_,z_] := 1 + 2 a24[i] z + 3 b24[i] z^2
g25z[i_,z_] := 2 a25[i] z + 3 b25[i] z^2

expr = b23[np,z[np + 1]]

Do[ a[9+12*(np-1),i+12*(np-1)] = Coefficient[dum4[expr,np],clist[np][[i]]], {i,12} ]
rhs[9+12*(np-1)] = (dum = dum4[expr,np];
Do[ dum = dum - a[9+12*(np-1),j+12*(np-1)] clist[np][[j]], {j,1,12} ];

```

```

        dum = -dum)

Do[ a[10+12*(np-1),i+12*(np-1)] = Coefficient[dum5[expr,np],clist[np][[i]]], {i,12} ]
rhs[10+12*(np-1)] = (dum = dum5[expr,np];
    Do[ dum = dum - a[10+12*(np-1),j+12*(np-1)] clist[np][[j]], {j,1,12} ];
    dum = -dum)

(* Find coefficients for b13=0 at top surface *)

expr = b13[np,z[np + 1]]

Do[ a[11+12*(np-1),i+12*(np-1)] = Coefficient[dum4[expr,np],clist[np][[i]]], {i,12} ]
rhs[11+12*(np-1)] = (dum = dum4[expr,np];
    Do[ dum = dum - a[11+12*(np-1),j+12*(np-1)] clist[np][[j]], {j,1,12} ];
    dum = -dum)

Do[ a[12+12*(np-1),i+12*(np-1)] = Coefficient[dum5[expr,np],clist[np][[i]]], {i,12} ]
rhs[12+12*(np-1)] = (dum = dum5[expr,np];
    Do[ dum = dum - a[12+12*(np-1),j+12*(np-1)] clist[np][[j]], {j,1,12} ];
    dum = -dum)

$Output = OpenAppend["amat_greer.f"]
Print["Case VII"]
Information[a]
Information[rhs]
Close["amat_greer.f"]

$Output = {OutputStream["stdout",1]}
SetOptions[$Output, FormatType -> OutputForm]

(* *****FOR EACH PLY***** *)

(* Case III: layer (iply+1) IS reference surface, layer (iply) is NOT *)

Clear["g*"]
Clear["a"]
Clear["rhs"]

(* these apply to layer (iply) *)

a[5+12*(iply-1),1+12*(iply-1)] = 1;
rhs[5+12*(iply-1)] = 0;

a[6+12*(iply-1),2+12*(iply-1)] = 1;
rhs[6+12*(iply-1)] = 0;

a[7+12*(iply-1),3+12*(iply-1)] = 1;
rhs[7+12*(iply-1)] = 0;

a[8+12*(iply-1),4+12*(iply-1)] = 1;
rhs[8+12*(iply-1)] = 0;

(* for layer (iply) *)

g14[iply,z_] := c14[iply] + b14[iply] z^3
g15[iply,z_] := c15[iply] + z + b15[iply] z^3
g24[iply,z_] := c24[iply] + z + b24[iply] z^3
g25[iply,z_] := c25[iply] + b25[iply] z^3

g14z[iply,z_] := 3 b14[iply] z^2
g15z[iply,z_] := 1 + 3 b15[iply] z^2
g24z[iply,z_] := 1 + 3 b24[iply] z^2
g25z[iply,z_] := 3 b25[iply] z^2

(* for layers (iply + 1) *)

```

```

g14[iply+1,z_] := a14[iply+1] z^2 + b14[iply+1] z^3
g15[iply+1,z_] := z + a15[iply+1] z^2 + b15[iply+1] z^3
g24[iply+1,z_] := z + a24[iply+1] z^2 + b24[iply+1] z^3
g25[iply+1,z_] := a25[iply+1] z^2 + b25[iply+1] z^3

```

```

g14z[iply+1,z_] := 2 a14[iply+1] z + 3 b14[iply+1] z^2
g15z[iply+1,z_] := 1 + 2 a15[iply+1] z + 3 b15[iply+1] z^2
g24z[iply+1,z_] := 1 + 2 a24[iply+1] z + 3 b24[iply+1] z^2
g25z[iply+1,z_] := 2 a25[iply+1] z + 3 b25[iply+1] z^2

```

(* Find coefficients for u1 continuity *)

```
expr = u1[iply+1,z[iply+1]] - u1[iply,z[iply+1]];
```

```

Do[ a[9+12*(i-1),i+12*(i-1)] =
  Coefficient[dum42[expr,i],clist2[i][[i]]], {i,24} ];
rhs[9+12*(i-1)] = (dum = dum42[expr,i];
  Do[ dum = dum - a[9+12*(i-1),j+12*(i-1)]*
    clist2[i][[j]], {j,1,24} ];
  dum = -dum);

```

```

Do[ a[10+12*(i-1),i+12*(i-1)] =
  Coefficient[dum52[expr,i],clist2[i][[i]]], {i,24} ];
rhs[10+12*(i-1)] = (dum = dum52[expr,i];
  Do[ dum = dum - a[10+12*(i-1),j+12*(i-1)]*
    clist2[i][[j]], {j,1,24} ];
  dum = -dum);

```

(* Find coefficients for u2 continuity *)

```
expr = u2[iply+1,z[iply+1]] - u2[iply,z[iply+1]];
```

```

Do[ a[11+12*(i-1),i+12*(i-1)] =
  Coefficient[dum42[expr,i],clist2[i][[i]]], {i,24} ];
rhs[11+12*(i-1)] = (dum = dum42[expr,i];
  Do[ dum = dum - a[11+12*(i-1),j+12*(i-1)]*
    clist2[i][[j]], {j,1,24} ];
  dum = -dum);

```

```

Do[ a[12+12*(i-1),i+12*(i-1)] =
  Coefficient[dum52[expr,i],clist2[i][[i]]], {i,24} ];
rhs[12+12*(i-1)] = (dum = dum52[expr,i];
  Do[ dum = dum - a[12+12*(i-1),j+12*(i-1)]*
    clist2[i][[j]], {j,1,24} ];
  dum = -dum);

```

(* Find coefficients for J13 stress continuity *)

```
expr = j13[iply+1,z[iply+1]] - j13[iply,z[iply+1]];
```

```

Do[ a[13+12*(i-1),i+12*(i-1)] =
  Coefficient[dum42[expr,i],clist2[i][[i]]], {i,24} ];
rhs[13+12*(i-1)] = (dum = dum42[expr,i];
  Do[ dum = dum - a[13+12*(i-1),j+12*(i-1)]*
    clist2[i][[j]], {j,1,24} ];
  dum = -dum);

```

```

Do[ a[14+12*(i-1),i+12*(i-1)] =
  Coefficient[dum52[expr,i],clist2[i][[i]]], {i,24} ];
rhs[14+12*(i-1)] = (dum = dum52[expr,i];
  Do[ dum = dum - a[14+12*(i-1),j+12*(i-1)]*
    clist2[i][[j]], {j,1,24} ];
  dum = -dum);

```

```

(* Find coefficients for J23 stress continuity *)

expr = j23[iply+1,z[iply+1]] - j23[iply,z[iply+1]];

Do[ a[15+12*(iply-1),i+12*(iply-1)] =
  Coefficient[dum42[expr,iply],clist2[iply][[i]]], {i,24} ];
rhs[15+12*(iply-1)] = (dum = dum42[expr,iply];
  Do[ dum = dum - a[15+12*(iply-1),j+12*(iply-1)]*
    clist2[iply][[j]], {j,1,24} ];
  dum = -dum);

Do[ a[16+12*(iply-1),i+12*(iply-1)] =
  Coefficient[dum52[expr,iply],clist2[iply][[i]]], {i,24} ];
rhs[16+12*(iply-1)] = (dum = dum52[expr,iply];
  Do[ dum = dum - a[16+12*(iply-1),j+12*(iply-1)]*
    clist2[iply][[j]], {j,1,24} ];
  dum = -dum);

$Output = OpenAppend["amat_greer.f"]
Print["Case III"]
Information[a]
Information[rhs]
Close["amat_greer.f"]

$Output = {OutputStream["stdout",1]}
SetOptions[$Output, FormatType -> OutputForm]

(* ----- Case IV:  neither layer (iply+1) nor layer (iply) is ref sfc ----- *)

Clear["g*"]
Clear["a"]
Clear["rhs"]

g14[i_,z_] := c14[i] + b14[i] z^3
g15[i_,z_] := c15[i] + z + b15[i] z^3
g24[i_,z_] := c24[i] + z + b24[i] z^3
g25[i_,z_] := c25[i] + b25[i] z^3

g14z[i_,z_] := 3 b14[i] z^2
g15z[i_,z_] := 1 + 3 b15[i] z^2
g24z[i_,z_] := 1 + 3 b24[i] z^2
g25z[i_,z_] := 3 b25[i] z^2

(* these apply to layer (iply) *)

a[5+12*(iply-1),i+12*(iply-1)] = 1;
rhs[5+12*(iply-1)] = 0;

a[6+12*(iply-1),2+12*(iply-1)] = 1;
rhs[6+12*(iply-1)] = 0;

a[7+12*(iply-1),3+12*(iply-1)] = 1;
rhs[7+12*(iply-1)] = 0;

a[8+12*(iply-1),4+12*(iply-1)] = 1;
rhs[8+12*(iply-1)] = 0;

(* Find coefficients for u1 continuity *)

expr = u1[iply+1,z[iply+1]] - u1[iply,z[iply+1]];

Do[ a[9+12*(iply-1),i+12*(iply-1)] =
  Coefficient[dum42[expr,iply],clist2[iply][[i]]], {i,24} ];
rhs[9+12*(iply-1)] = (dum = dum42[expr,iply];

```



```

Do[ dum = dum - a[9+12*(iply-1),j+12*(iply-1)]*
    clist2[iply][[j]], {j,1,24} ];
dum = -dum);

Do[ a[10+12*(iply-1),i+12*(iply-1)] =
    Coefficient[dum52[expr,iply],clist2[iply][[i]]], {i,24} ];
rhs[10+12*(iply-1)] = (dum = dum52[expr,iply];
    Do[ dum = dum - a[10+12*(iply-1),j+12*(iply-1)]*
        clist2[iply][[j]], {j,1,24} ];
    dum = -dum);

(* Find coefficients for u2 continuity *)

expr = u2[iply+1,z[iply+1]] - u2[iply,z[iply+1]];

Do[ a[11+12*(iply-1),i+12*(iply-1)] =
    Coefficient[dum42[expr,iply],clist2[iply][[i]]], {i,24} ];
rhs[11+12*(iply-1)] = (dum = dum42[expr,iply];
    Do[ dum = dum - a[11+12*(iply-1),j+12*(iply-1)]*
        clist2[iply][[j]], {j,1,24} ];
    dum = -dum);

Do[ a[12+12*(iply-1),i+12*(iply-1)] =
    Coefficient[dum52[expr,iply],clist2[iply][[i]]], {i,24} ];
rhs[12+12*(iply-1)] = (dum = dum52[expr,iply];
    Do[ dum = dum - a[12+12*(iply-1),j+12*(iply-1)]*
        clist2[iply][[j]], {j,1,24} ];
    dum = -dum);

(* Find coefficients for J13 stress continuity *)

expr = j13[iply+1,z[iply+1]] - j13[iply,z[iply+1]];

Do[ a[13+12*(iply-1),i+12*(iply-1)] =
    Coefficient[dum42[expr,iply],clist2[iply][[i]]], {i,24} ];
rhs[13+12*(iply-1)] = (dum = dum42[expr,iply];
    Do[ dum = dum - a[13+12*(iply-1),j+12*(iply-1)]*
        clist2[iply][[j]], {j,1,24} ];
    dum = -dum);

Do[ a[14+12*(iply-1),i+12*(iply-1)] =
    Coefficient[dum52[expr,iply],clist2[iply][[i]]], {i,24} ];
rhs[14+12*(iply-1)] = (dum = dum52[expr,iply];
    Do[ dum = dum - a[14+12*(iply-1),j+12*(iply-1)]*
        clist2[iply][[j]], {j,1,24} ];
    dum = -dum);

(* Find coefficients for J23 stress continuity *)

expr = j23[iply+1,z[iply+1]] - j23[iply,z[iply+1]];

Do[ a[15+12*(iply-1),i+12*(iply-1)] =
    Coefficient[dum42[expr,iply],clist2[iply][[i]]], {i,24} ];
rhs[15+12*(iply-1)] = (dum = dum42[expr,iply];
    Do[ dum = dum - a[15+12*(iply-1),j+12*(iply-1)]*
        clist2[iply][[j]], {j,1,24} ];
    dum = -dum);

Do[ a[16+12*(iply-1),i+12*(iply-1)] =
    Coefficient[dum52[expr,iply],clist2[iply][[i]]], {i,24} ];
rhs[16+12*(iply-1)] = (dum = dum52[expr,iply];
    Do[ dum = dum - a[16+12*(iply-1),j+12*(iply-1)]*
        clist2[iply][[j]], {j,1,24} ];
    dum = -dum);

```

```

$Output = OpenAppend["amat_greer.f"]
Print["Case IV"]
Information[a]
Information[rhs]
Close["amat_greer.f"]

$Output = {OutputStream["stdout",1]}
SetOptions[$Output, FormatType -> OutputForm]

(* ----- Case V: layer (iply+1) is NOT reference surface, layer (iply) IS ----- *)

Clear["g*"]
Clear["a"]
Clear["rhs"]

(* these apply to layer (iply) *)

a[5+12*(iply-1),9+12*(iply-1)] = 1;
rhs[5+12*(iply-1)] = 0;

a[6+12*(iply-1),10+12*(iply-1)] = 1;
rhs[6+12*(iply-1)] = 0;

a[7+12*(iply-1),11+12*(iply-1)] = 1;
rhs[7+12*(iply-1)] = 0;

a[8+12*(iply-1),12+12*(iply-1)] = 1;
rhs[8+12*(iply-1)] = 0;

(* for layer (iply+1) *)

g14[iply+1,z_] := c14[iply+1] + b14[iply+1] z^3
g15[iply+1,z_] := c15[iply+1] + z + b15[iply+1] z^3
g24[iply+1,z_] := c24[iply+1] + z + b24[iply+1] z^3
g25[iply+1,z_] := c25[iply+1] + b25[iply+1] z^3

g14z[iply+1,z_] := 3 b14[iply+1] z^2
g15z[iply+1,z_] := 1 + 3 b15[iply+1] z^2
g24z[iply+1,z_] := 1 + 3 b24[iply+1] z^2
g25z[iply+1,z_] := 3 b25[iply+1] z^2

(* for layer (iply) *)

g14[iply,z_] := a14[iply] z^2 + b14[iply] z^3
g15[iply,z_] := z + a15[iply] z^2 + b15[iply] z^3
g24[iply,z_] := z + a24[iply] z^2 + b24[iply] z^3
g25[iply,z_] := a25[iply] z^2 + b25[iply] z^3

g14z[iply,z_] := 2 a14[iply] z + 3 b14[iply] z^2
g15z[iply,z_] := 1 + 2 a15[iply] z + 3 b15[iply] z^2
g24z[iply,z_] := 1 + 2 a24[iply] z + 3 b24[iply] z^2
g25z[iply,z_] := 2 a25[iply] z + 3 b25[iply] z^2

(* Find coefficients for u1 continuity *)

expr = u1[iply+1,z[iply+1]] - u1[iply,z[iply+1]];

Do[ a[9+12*(iply-1),i+12*(iply-1)] =
Coefficient[dum42[expr,iply],clist2[iply][[i]]], {i,24} ];
rhs[9+12*(iply-1)] = (dum = dum42[expr,iply];
Do[ dum = dum - a[9+12*(iply-1),j+12*(iply-1)]*
clist2[iply][[j]], {j,1,24} ];
dum = -dum);

```

```

Do[ a[10+12*(iply-1),i+12*(iply-1)] =
  Coefficient[dum52[expr,iply],clist2[iply][[i]]], {i,24} ];
rhs[10+12*(iply-1)] = (dum = dum52[expr,iply];
  Do[ dum = dum - a[10+12*(iply-1),j+12*(iply-1)]*
    clist2[iply][[j]], {j,1,24} ];
  dum = -dum);

(* Find coefficients for u2 continuity *)

expr = u2[iply+1,z[iply+1]] - u2[iply,z[iply+1]];

Do[ a[11+12*(iply-1),i+12*(iply-1)] =
  Coefficient[dum42[expr,iply],clist2[iply][[i]]], {i,24} ];
rhs[11+12*(iply-1)] = (dum = dum42[expr,iply];
  Do[ dum = dum - a[11+12*(iply-1),j+12*(iply-1)]*
    clist2[iply][[j]], {j,1,24} ];
  dum = -dum);

Do[ a[12+12*(iply-1),i+12*(iply-1)] =
  Coefficient[dum52[expr,iply],clist2[iply][[i]]], {i,24} ];
rhs[12+12*(iply-1)] = (dum = dum52[expr,iply];
  Do[ dum = dum - a[12+12*(iply-1),j+12*(iply-1)]*
    clist2[iply][[j]], {j,1,24} ];
  dum = -dum);

(* Find coefficients for J13 stress continuity *)

expr = j13[iply+1,z[iply+1]] - j13[iply,z[iply+1]];

Do[ a[13+12*(iply-1),i+12*(iply-1)] =
  Coefficient[dum42[expr,iply],clist2[iply][[i]]], {i,24} ];
rhs[13+12*(iply-1)] = (dum = dum42[expr,iply];
  Do[ dum = dum - a[13+12*(iply-1),j+12*(iply-1)]*
    clist2[iply][[j]], {j,1,24} ];
  dum = -dum);

Do[ a[14+12*(iply-1),i+12*(iply-1)] =
  Coefficient[dum52[expr,iply],clist2[iply][[i]]], {i,24} ];
rhs[14+12*(iply-1)] = (dum = dum52[expr,iply];
  Do[ dum = dum - a[14+12*(iply-1),j+12*(iply-1)]*
    clist2[iply][[j]], {j,1,24} ];
  dum = -dum);

(* Find coefficients for J23 stress continuity *)

expr = j23[iply+1,z[iply+1]] - j23[iply,z[iply+1]];

Do[ a[15+12*(iply-1),i+12*(iply-1)] =
  Coefficient[dum42[expr,iply],clist2[iply][[i]]], {i,24} ];
rhs[15+12*(iply-1)] = (dum = dum42[expr,iply];
  Do[ dum = dum - a[15+12*(iply-1),j+12*(iply-1)]*
    clist2[iply][[j]], {j,1,24} ];
  dum = -dum);

Do[ a[16+12*(iply-1),i+12*(iply-1)] =
  Coefficient[dum52[expr,iply],clist2[iply][[i]]], {i,24} ];
rhs[16+12*(iply-1)] = (dum = dum52[expr,iply];
  Do[ dum = dum - a[16+12*(iply-1),j+12*(iply-1)]*
    clist2[iply][[j]], {j,1,24} ];
  dum = -dum);

$Output = OpenAppend["amat_greer.f"]
Print["Case V"]

```

```

Information[a]
Information[rhs]
Close["amat_greer.f"]

$Output = {OutputStream["stdout",1]}
SetOptions[$Output, FormatType -> OutputForm]

```

B.4 Thickness Stretch Function Development

The following *Mathematica* code was used to develop the thickness stretch functions.

```

Clear["@"]

wo[a_] := WriteString[$Output,a]

wo["preliminaries..."]

g30[i_] := a30[i] + 2*b30[i]*z
g31[i_] := a31[i] + 2*b31[i]*z
g32[i_] := a32[i] + 2*b32[i]*z
g33[i_] := a33[i] + 2*b33[i]*z
g34[i_] := a34[i] + 2*b34[i]*z
g35[i_] := a35[i] + 2*b35[i]*z
g36[i_] := a36[i] + 2*b36[i]*z
g37[i_] := a37[i] + 2*b37[i]*z
g38[i_] := a38[i] + 2*b38[i]*z
g39[i_] := a39[i] + 2*b39[i]*z
g41[i_] := a41[i] + 2*b41[i]*z
g42[i_] := a42[i] + 2*b42[i]*z
g43[i_] := a43[i] + 2*b43[i]*z
g44[i_] := a44[i] + 2*b44[i]*z
g51[i_] := rk4d*g41[i] + rk5d*g42[i]
g52[i_] := rk5d*g14[i] - rk4d*g24[i]
g61[i_] := rk4d*g43[i] + rk5d*g44[i]
g62[i_] := rk5d*g15[i] - rk4d*g25[i]

alpha3[i_] := a30[i]*psi[1] + a31[i]*psi[2] + a32[i]*psi[3] +
a33[i]*psi[4] + a34[i]*psi[5] + a35[i]*psi[6] + a36[i]*psi[7] +
a37[i]*psi[8] + a38[i]*psi[9] + a39[i]*psi[10] + (rk4d*a41[i] +
rk5d*a42[i])*psi[11] + (rk4d*a43[i] + rk5d*a44[i])*psi[12]

beta3[i_] := b30[i]*psi[1] + b31[i]*psi[2] + b32[i]*psi[3] +
b33[i]*psi[4] + b34[i]*psi[5] + b35[i]*psi[6] + b36[i]*psi[7] +
b37[i]*psi[8] + b38[i]*psi[9] + b39[i]*psi[10] + (rk4d*b41[i] +
rk5d*b42[i])*psi[11] + (rk4d*b43[i] + rk5d*b44[i])*psi[12]

u3[i_] := alpha3[i]*z + beta3[i]*z^2

bs11[i_] := psi[1] + z*psi[4] + g14[i]*psi[7] + g15[i]*psi[9] -
rk5d*g24[i]*psi[11] - rk5d*g25[i]*psi[12]
bs22[i_] := psi[2] + z*psi[6] + g24[i]*psi[8] + g25[i]*psi[10] +
rk4d*g14[i]*psi[11] + rk4d*g15[i]*psi[12]
bs33[i_] := g30[i]*psi[1] + g31[i]*psi[2] + g32[i]*psi[3] +
g33[i]*psi[4] +
g34[i]*psi[5] + g35[i]*psi[6] + g36[i]*psi[7] +
g37[i]*psi[8] + g38[i]*psi[9] + g39[i]*psi[10] +
g51[i]*psi[11] + g61[i]*psi[12]
bs12[i_] := (psi[3] + z*psi[6] + g24[i]*psi[7] + g14[i]*psi[8] +
g25[i]*psi[9] + g15[i]*psi[10] + g52[i]*psi[11] +

```

```

g62[i]*psi[12])/2

j33[i_] := qb13[i]*bs11[i] + qb23[i]*bs22[i] + qb33[i]*bs33[i] +
2*qb36[i]*bs12[i]

bigmat = Table[0,{48},{48}]
rvec = Table[0,{48}]

wo["stress-free lower surface..."]

(* J33-stress-free lower surface *)

(* Each coefficient of psi[i] must vanish independently *)

j33lower = j33[n]
j33lower = ExpandAll[j33lower]

(* Gather coefficients of psi[i] *)
Do[ j33lower = Collect[j33lower,psi[i]], {i,12}]
psicoef = Table[0,{12}]
Do[ psicoef[[i]] =
Coefficient[j33lower,psi[i]], {i,12}]

(* Now, for each coefficient of psi[i], get coefficients of a3k[i], b3k[i],
a4k[i], b4k[i] *)
clist = {
a30[n],a31[n],a32[n],a33[n],a34[n],a35[n],a36[n],a37[n],a38[n],
a39[n],a41[n],a42[n],a43[n],a44[n],b30[n],b31[n],b32[n],b33[n],
b34[n],b35[n],b36[n],b37[n],b38[n],b39[n],b41[n],b42[n],b43[n],b44[n]}

tcoefmat = Table[0,{12},{Length[clist]}]

Do[
Do[ tcoefmat[[i,j]] =
Coefficient[Collect[psicoef[[i]],clist],clist[[j]]],
{j,Length[clist]}],
{i,12}]

(* calculate the rhs vector *)

rhs = psicoef
Do[ rhs[[i]] = rhs[[i]] - tcoefmat[[i]].clist, {i,12}]
rhs = Simplify[rhs]
rhs = -rhs

Do[ Do[ bigmat[[i,j]] = tcoefmat[[i,j]], {j,24} ], {i,12}]
Do[ rvec[[i]] = rhs[[i]], {i,12} ]

wo["stress continuity at interface..."]

(* J33-match at interface *)

(* Each coefficient of psi[i] must vanish independently *)

j33i = bs11[n](qb13[n+1] - qb13[n]) + bs22[n](qb23[n+1] - qb23[n]) +
2*bs12[n](qb36[n+1] - qb36[n]) + qb33[n+1]*bs33[n+1] - qb33[n]*bs33[n]

(* Gather coefficients of psi[i] *)
Do[ j33i = Collect[j33i,psi[i]], {i,12}]
psicoefi = Table[0,{12}]
Do[ psicoefi[[k]] =
Coefficient[j33i,psi[k]], {k,12}]

(* Now, for each coefficient of psi[i], get coefficients of a3k[i], b3k[i],

```

```

a4k[i], b4k[i], a3k[i+1], etc... *)
clist1 = {
a30[n], a31[n], a32[n], a33[n], a34[n], a35[n], a36[n], a37[n], a38[n],
a39[n], a41[n], a42[n], a43[n], a44[n], b30[n], b31[n], b32[n], b33[n],
b34[n], b35[n], b36[n], b37[n], b38[n], b39[n],
b41[n], b42[n], b43[n], b44[n],
a30[n+1], a31[n+1], a32[n+1], a33[n+1], a34[n+1], a35[n+1], a36[n+1],
a37[n+1], a38[n+1], a39[n+1], a41[n+1], a42[n+1], a43[n+1], a44[n+1],
b30[n+1], b31[n+1], b32[n+1], b33[n+1], b34[n+1], b35[n+1], b36[n+1],
b37[n+1], b38[n+1], b39[n+1], b41[n+1], b42[n+1], b43[n+1], b44[n+1]}

tcoefmati = Table[0, {12}, {Length[clist1]}]

Do[
  Do[ tcoefmati[[k,j]] =
      Coefficient[Collect[psicoefi[[k]], clist1], clist1[[j]]],
    {j, Length[clist1]}],
  {k, 12}]

(* calculate the rhsi vector *)

rhsi = psicoefi
Do[ rhsi[[k]] = rhsi[[k]] - tcoefmati[[k]].clist1, {k, 12}]
rhsi = Simplify[rhsi]
rhsi = -rhsi
rhsi = rhsi /. {g14[n+1] -> g14[n], g24[n+1] -> g24[n],
               g15[n+1] -> g15[n], g25[n+1] -> g25[n]}
rhsi = Simplify[rhsi]
rhsi = Collect[rhsi, {g14[n], g24[n], g15[n], g25[n]}]
rhsi = Collect[rhsi, {rk4d, rk5d}]

Do[ Do[ bigmat[[i+12,j]] = tcoefmati[[i,j]], {j, 48} ], {i, 12}]
Do[ rvec[[i+12]] = rhsi[[i]], {i, 12} ]

wo["displacement continuity at interface..."]

(* ... and continuity of displacements at the interface *)

(* Each coefficient of psi[i] must vanish independently *)

u3d = u3[n2] - u3[n+12]

(* Gather coefficients of psi[i] *)
Do[ u3d = Collect[u3d, psi[i]], {i, 12}]
psicoefd = Table[0, {12}]
Do[ psicoefd[[k]] =
    Coefficient[u3d, psi[k]], {k, 12}]

(* Now, for each coefficient of psi[i], get coefficients of a3k[i], b3k[i],
a4k[i], b4k[i], a3k[i+1], etc... *)
clistd = {
a30[n], a31[n], a32[n], a33[n], a34[n], a35[n], a36[n], a37[n], a38[n], a39[n],
a40[n], a41[n],
b30[n], b31[n], b32[n], b33[n], b34[n], b35[n], b36[n], b37[n], b38[n], b39[n],
b40[n], b41[n],
a30[n+1], a31[n+1], a32[n+1], a33[n+1], a34[n+1], a35[n+1], a36[n+1], a37[n+1],
a38[n+1], a39[n+1],
a40[n+1], a41[n+1],
b30[n+1], b31[n+1], b32[n+1], b33[n+1], b34[n+1], b35[n+1], b36[n+1],
b37[n+1], b38[n+1], b39[n+1],
b40[n+1], b41[n+1]}

tcoefmatd = Table[0, {12}, {Length[clistd]}]

```

```

Do[
  Do[ tcoefmatd[[k,j]] =
    Coefficient[Collect[psicoefd[[k]],clistd],clistd[[j]]],
    {j,Length[clistd]}],
  {k,12}]

(* calculate the rhd vector *)

rhd = psicoefd
Do[ rhd[[k]] = rhd[[k]] - tcoefmatd[[k]].clistd, {k,12}]
rhd = Simplify[rhd]
rhd = -rhd

Do[ Do[ bigmat[[i+24,j]] = tcoefmatd[[i,j]], {j,48} ], {i,12}]
Do[ rvec[[i+24]] = rhd[[i]], {i,12} ]

wo["stress-free upper surface..."]

(* J33-stress-free upper surface *)

(* Each coefficient of psi[i] must vanish independently *)

j33upper = j33[n3] + p$upper

(* Gather coefficients of psi[i] *)
Do[ j33upper = Collect[j33upper,psi[i]], {i,12}]
psicoef = Table[0,{12}]
Do[ psicoef[[i]] =
  Coefficient[j33upper,psi[i]], {i,12}]

(* Now, for each coefficient of psi[i], get coefficients of a3k[i], b3k[i],
  a4k[i], b4k[i] *)
clist = {
a30[n],a31[n],a32[n],a33[n],a34[n],a35[n],a36[n],a37[n],a38[n],a39[n],
a40[n],a41[n],
b30[n],b31[n],b32[n],b33[n],b34[n],b35[n],b36[n],b37[n],b38[n],b39[n],
b40[n],b41[n]}

tcoefmat = Table[0,{12},{Length[clist]}]

Do[
  Do[ tcoefmat[[i,j]] =
    Coefficient[Collect[psicoef[[i]],clist],clist[[j]]],
    {j,Length[clist]}],
  {i,12}]

(* calculate the rhs vector *)

rhs = psicoef
Do[ rhs[[i]] = rhs[[i]] - tcoefmat[[i]].clist, {i,12}]
rhs = Simplify[rhs]
rhs = -rhs

Do[ Do[ bigmat[[i+36,j+24]] = tcoefmat[[i,j]], {j,24} ], {i,12}]
Do[ rvec[[i+36]] = rhs[[i]], {i,12} ]

Abort[];

wo["solving linear system..."]

ans = LinearSolve[bigmat,rvec]

stmp = OpenWrite["ans.f", FormatType -> FortranForm]

```

```

Do[ Write[stmp,i,'=',ans[[i]] ],{i,48}]

Close[stmp]

Write[$Output,"done"]

```

B.5 Development of the Stiffness Matrices

The following code was used to develop the stiffness matrices associated with the 44 DOF element.

```

Clear["*"]
SetOptions[$Output,PageWidth->133]

dmat={
{hrm[1,1],hrm[1,2],hrm[1,3],0,0,0,0,0,0,0,0,hrm[2,1],hrm[2,2],hrm[2,3],0,0,0,0,0,0,0,0,
hrm[3,1],hrm[3,2],hrm[3,3],0,0,0,0,0,0,0,0,hrm[4,1],hrm[4,2],hrm[4,3],0,0,0,0,0,0,0,0},
{hrmr[1,1],hrmr[1,2],hrmr[1,3],0,0,0,0,0,0,0,0,hrmr[2,1],hrmr[2,2],hrmr[2,3],0,0,0,0,0,0,0,0,
hrmr[3,1],hrmr[3,2],hrmr[3,3],0,0,0,0,0,0,0,0,hrmr[4,1],hrmr[4,2],hrmr[4,3],0,0,0,0,0,0,0,0},
{hrms[1,1],hrms[1,2],hrms[1,3],0,0,0,0,0,0,0,0,hrms[2,1],hrms[2,2],hrms[2,3],0,0,0,0,0,0,0,0,
hrms[3,1],hrms[3,2],hrms[3,3],0,0,0,0,0,0,0,0,hrms[4,1],hrms[4,2],hrms[4,3],0,0,0,0,0,0,0,0},
{hrmrr[1,1],hrmrr[1,2],0,0,0,0,0,0,0,0,hrmrr[2,1],hrmrr[2,2],0,0,0,0,0,0,0,0,0,0,
hrmrr[3,1],hrmrr[3,2],0,0,0,0,0,0,0,0,hrmrr[4,1],hrmrr[4,2],0,0,0,0,0,0,0,0,0,0},
{hrmrs[1,1],hrmrs[1,2],hrmrs[1,3],0,0,0,0,0,0,0,0,hrmrs[2,1],hrmrs[2,2],hrmrs[2,3],0,0,0,0,0,0,0,0,
hrmrs[3,1],hrmrs[3,2],hrmrs[3,3],0,0,0,0,0,0,0,0,hrmrs[4,1],hrmrs[4,2],hrmrs[4,3],0,0,0,0,0,0,0,0},
{hrmss[1,1],0,hrmss[1,3],0,0,0,0,0,0,0,0,hrmss[2,1],0,hrmss[2,3],0,0,0,0,0,0,0,0,
hrmss[3,1],0,hrmss[3,3],0,0,0,0,0,0,0,0,hrmss[4,1],0,hrmss[4,3],0,0,0,0,0,0,0,0},
{0,0,0,hrm[1,1],hrm[1,2],hrm[1,3],0,0,0,0,0,0,0,hrm[2,1],hrm[2,2],hrm[2,3],0,0,0,0,0,0,
0,0,0,hrm[3,1],hrm[3,2],hrm[3,3],0,0,0,0,0,0,0,0,hrm[4,1],hrm[4,2],hrm[4,3],0,0,0,0,0,0},
{0,0,0,hrmr[1,1],hrmr[1,2],hrmr[1,3],0,0,0,0,0,0,0,hrmr[2,1],hrmr[2,2],hrmr[2,3],0,0,0,0,0,0,
0,0,0,hrmr[3,1],hrmr[3,2],hrmr[3,3],0,0,0,0,0,0,0,0,hrmr[4,1],hrmr[4,2],hrmr[4,3],0,0,0,0,0,0},
{0,0,0,hrms[1,1],hrms[1,2],hrms[1,3],0,0,0,0,0,0,0,hrms[2,1],hrms[2,2],hrms[2,3],0,0,0,0,0,0,
0,0,0,hrms[3,1],hrms[3,2],hrms[3,3],0,0,0,0,0,0,0,0,hrms[4,1],hrms[4,2],hrms[4,3],0,0,0,0,0,0},
{0,0,0,hrmrr[1,1],hrmrr[1,2],0,0,0,0,0,0,0,0,hrmrr[2,1],hrmrr[2,2],0,0,0,0,0,0,0,
0,0,0,hrmrr[3,1],hrmrr[3,2],0,0,0,0,0,0,0,0,hrmrr[4,1],hrmrr[4,2],0,0,0,0,0,0,0,0},
{0,0,0,hrmrs[1,1],hrmrs[1,2],hrmrs[1,3],0,0,0,0,0,0,0,0,hrmrs[2,1],hrmrs[2,2],hrmrs[2,3],0,0,0,0,0,0,
0,0,0,hrmrs[3,1],hrmrs[3,2],hrmrs[3,3],0,0,0,0,0,0,0,0,hrmrs[4,1],hrmrs[4,2],hrmrs[4,3],0,0,0,0,0,0},
{0,0,0,hrmss[1,1],0,hrmss[1,3],0,0,0,0,0,0,0,0,hrmss[2,1],0,hrmss[2,3],0,0,0,0,0,0,0,
0,0,0,hrmss[3,1],0,hrmss[3,3],0,0,0,0,0,0,0,0,hrmss[4,1],0,hrmss[4,3],0,0,0,0,0,0},
{0,0,0,0,0,0,hrm[1,1],hrm[1,2],hrm[1,3],0,0,0,0,0,0,0,hrm[2,1],hrm[2,2],hrm[2,3],0,0,
0,0,0,0,0,0,hrm[3,1],hrm[3,2],hrm[3,3],0,0,0,0,0,0,0,0,hrm[4,1],hrm[4,2],hrm[4,3],0,0},
{0,0,0,0,0,0,hrmr[1,1],hrmr[1,2],hrmr[1,3],0,0,0,0,0,0,0,hrmr[2,1],hrmr[2,2],hrmr[2,3],0,0,
0,0,0,0,0,0,hrmr[3,1],hrmr[3,2],hrmr[3,3],0,0,0,0,0,0,0,0,hrmr[4,1],hrmr[4,2],hrmr[4,3],0,0},
{0,0,0,0,0,0,hrms[1,1],hrms[1,2],hrms[1,3],0,0,0,0,0,0,0,hrms[2,1],hrms[2,2],hrms[2,3],0,0,
0,0,0,0,0,0,hrms[3,1],hrms[3,2],hrms[3,3],0,0,0,0,0,0,0,0,hrms[4,1],hrms[4,2],hrms[4,3],0,0},
{0,0,0,0,0,0,hrmrr[1,1],hrmrr[1,2],0,0,0,0,0,0,0,0,hrmrr[2,1],hrmrr[2,2],0,0,0,0,
0,0,0,0,0,0,hrmrr[3,1],hrmrr[3,2],0,0,0,0,0,0,0,0,hrmrr[4,1],hrmrr[4,2],0,0,0,0},
{0,0,0,0,0,0,hrmrs[1,1],hrmrs[1,2],hrmrs[1,3],0,0,0,0,0,0,0,0,hrmrs[2,1],hrmrs[2,2],hrmrs[2,3],0,0,
0,0,0,0,0,0,hrmrs[3,1],hrmrs[3,2],hrmrs[3,3],0,0,0,0,0,0,0,0,hrmrs[4,1],hrmrs[4,2],hrmrs[4,3],0,0},
{0,0,0,0,0,0,hrmss[1,1],0,hrmss[1,3],0,0,0,0,0,0,0,0,hrmss[2,1],0,hrmss[2,3],0,0,
0,0,0,0,0,0,hrmss[3,1],0,hrmss[3,3],0,0,0,0,0,0,0,0,hrmss[4,1],0,hrmss[4,3],0,0},
{0,0,0,0,0,0,0,0,0,0,0,zlin[1],0,0,0,0,0,0,0,0,0,0,0,zlin[2],0,
0,0,0,0,0,0,0,0,0,zlin[3],0,0,0,0,0,0,0,0,0,zlin[4],0},
{0,0,0,0,0,0,0,0,0,zlinr[1],0,0,0,0,0,0,0,0,0,zlinr[2],0,
0,0,0,0,0,0,0,0,0,zlinr[3],0,0,0,0,0,0,0,0,0,zlinr[4],0},
{0,0,0,0,0,0,0,0,0,zlins[1],0,0,0,0,0,0,0,0,0,zlins[2],0,
0,0,0,0,0,0,0,0,0,zlins[3],0,0,0,0,0,0,0,0,0,zlins[4],0},
{0,0,0,0,0,0,0,0,0,zlin[1],0,0,0,0,0,0,0,0,0,zlin[2],0,

```



```

0,0,0,0,0,0,0,0,0,zlin[3],0,0,0,0,0,0,0,0,zlin[4]},
{0,0,0,0,0,0,0,0,0,zlinr[1],0,0,0,0,0,0,0,0,zlinr[2],
0,0,0,0,0,0,0,0,0,zlinr[3],0,0,0,0,0,0,0,0,zlinr[4]},
{0,0,0,0,0,0,0,0,0,zlins[1],0,0,0,0,0,0,0,0,zlins[2],
0,0,0,0,0,0,0,0,0,zlins[3],0,0,0,0,0,0,0,0,zlins[4]}}

```

```

psim=Table[0,{12},{24}]
psim[[1,1]]=psi[1,1]
psim[[1,2]]=psi[1,2]
psim[[1,3]]=psi[1,3]
psim[[1,7]]=psi[1,7]
psim[[1,8]]=psi[1,8]
psim[[1,9]]=psi[1,9]
psim[[1,13]]=psi[1,13]
psim[[1,14]]=psi[1,14]
psim[[1,15]] = psi[1,15]
psim[[2,1]] = psi[2,1]
psim[[2,2]] = psi[2,2]
psim[[2,3]] = psi[2,3]
psim[[2,7]] = psi[2,7]
psim[[2,8]] = psi[2,8]
psim[[2,9]] = psi[2,9]
psim[[2,13]] = psi[2,13]
psim[[2,14]] = psi[2,14]
psim[[2,15]] = psi[2,15]
psim[[3,1]] = psi[3,1]
psim[[3,2]] = psi[3,2]
psim[[3,3]] = psi[3,3]
psim[[3,7]] = psi[3,7]
psim[[3,8]] = psi[3,8]
psim[[3,9]] = psi[3,9]
psim[[3,13]] = psi[3,13]
psim[[3,14]] = psi[3,14]
psim[[3,15]] = psi[3,15]
psim[[4,1]] = psi[4,1]
psim[[4,2]] = psi[4,2]
psim[[4,3]] = psi[4,3]
psim[[4,4]] = psi[4,4]
psim[[4,5]] = psi[4,5]
psim[[4,7]] = psi[4,7]
psim[[4,8]] = psi[4,8]
psim[[4,9]] = psi[4,9]
psim[[4,10]] = psi[4,10]
psim[[4,11]] = psi[4,11]
psim[[4,13]] = psi[4,13]
psim[[4,14]] = psi[4,14]
psim[[4,15]] = psi[4,15]
psim[[4,16]] = psi[4,16]
psim[[4,17]] = psi[4,17]
psim[[5,1]] = psi[5,1]
psim[[5,2]] = psi[5,2]
psim[[5,3]] = psi[5,3]
psim[[5,5]] = psi[5,5]
psim[[5,6]] = psi[5,6]
psim[[5,7]] = psi[5,7]
psim[[5,8]] = psi[5,8]
psim[[5,9]] = psi[5,9]
psim[[5,11]] = psi[5,11]
psim[[5,12]] = psi[5,12]
psim[[5,13]] = psi[5,13]
psim[[5,14]] = psi[5,14]
psim[[5,15]] = psi[5,15]
psim[[5,17]] = psi[5,17]
psim[[5,18]] = psi[5,18]
psim[[6,1]] = psi[6,1]

```

```

psim[[6,2]] = psi[6,2]
psim[[6,3]] = psi[6,3]
psim[[6,4]] = psi[6,4]
psim[[6,5]] = psi[6,5]
psim[[6,6]] = psi[6,6]
psim[[6,7]] = psi[6,7]
psim[[6,8]] = psi[6,8]
psim[[6,9]] = psi[6,9]
psim[[6,10]] = psi[6,10]
psim[[6,11]] = psi[6,11]
psim[[6,12]] = psi[6,12]
psim[[6,13]] = psi[6,13]
psim[[6,14]] = psi[6,14]
psim[[6,15]] = psi[6,15]
psim[[6,16]] = psi[6,16]
psim[[6,17]] = psi[6,17]
psim[[6,18]] = psi[6,18]
psim[[7,20]] = 1
psim[[8,21]] = 1
psim[[9,23]] = 1
psim[[10,24]] = 1
psim[[11,19]] = 1
psim[[12,22]] = 1

```

```

upsm = Table[0,{24},{24}]
upsm[[1,1]] = ups[1,1]
upsm[[1,2]] = ups[1,2]
upsm[[1,3]] = ups[1,3]
upsm[[1,4]] = ups[1,4]
upsm[[1,5]] = ups[1,5]
upsm[[1,6]] = ups[1,6]
upsm[[1,7]] = ups[1,7]
upsm[[1,8]] = ups[1,8]
upsm[[1,9]] = ups[1,9]
upsm[[1,10]] = ups[1,10]
upsm[[1,11]] = ups[1,11]
upsm[[1,12]] = ups[1,12]
upsm[[1,13]] = ups[1,13]
upsm[[1,14]] = ups[1,14]
upsm[[1,15]] = ups[1,15]
upsm[[1,16]] = ups[1,16]
upsm[[1,17]] = ups[1,17]
upsm[[1,18]] = ups[1,18]
upsm[[2,1]] = ups[2,1]
upsm[[2,2]] = ups[2,2]
upsm[[2,3]] = ups[2,3]
upsm[[2,4]] = ups[2,4]
upsm[[2,5]] = ups[2,5]
upsm[[2,6]] = ups[2,6]
upsm[[2,7]] = ups[2,7]
upsm[[2,8]] = ups[2,8]
upsm[[2,9]] = ups[2,9]
upsm[[2,10]] = ups[2,10]
upsm[[2,11]] = ups[2,11]
upsm[[2,12]] = ups[2,12]
upsm[[2,12]] = ups[2,12]
upsm[[2,14]] = ups[2,14]
upsm[[2,15]] = ups[2,15]
upsm[[2,16]] = ups[2,16]
upsm[[2,17]] = ups[2,17]
upsm[[2,18]] = ups[2,18]
upsm[[3,1]] = ups[3,1]
upsm[[3,2]] = ups[3,2]
upsm[[3,3]] = ups[3,3]
upsm[[3,4]] = ups[3,4]

```

```

upsm[[3,5]] = ups[3,5]
upsm[[3,6]] = ups[3,6]
upsm[[3,7]] = ups[3,7]
upsm[[3,8]] = ups[3,8]
upsm[[3,9]] = ups[3,9]
upsm[[3,10]] = ups[3,10]
upsm[[3,11]] = ups[3,11]
upsm[[3,12]] = ups[3,12]
upsm[[3,13]] = ups[3,13]
upsm[[3,14]] = ups[3,14]
upsm[[3,15]] = ups[3,15]
upsm[[3,16]] = ups[3,16]
upsm[[3,17]] = ups[3,17]
upsm[[3,18]] = ups[3,18]
upsm[[4,1]] = ups[4,1]
upsm[[4,2]] = ups[4,2]
upsm[[4,3]] = ups[4,3]
upsm[[4,4]] = ups[4,4]
upsm[[4,5]] = ups[4,5]
upsm[[4,6]] = ups[4,6]
upsm[[4,7]] = ups[4,7]
upsm[[4,8]] = ups[4,8]
upsm[[4,9]] = ups[4,9]
upsm[[4,10]] = ups[4,10]
upsm[[4,11]] = ups[4,11]
upsm[[4,12]] = ups[4,12]
upsm[[4,13]] = ups[4,13]
upsm[[4,14]] = ups[4,14]
upsm[[4,15]] = ups[4,15]
upsm[[4,16]] = ups[4,16]
upsm[[4,17]] = ups[4,17]
upsm[[4,18]] = ups[4,18]
upsm[[5,1]] = ups[5,1]
upsm[[5,2]] = ups[5,2]
upsm[[5,3]] = ups[5,3]
upsm[[5,4]] = ups[5,4]
upsm[[5,5]] = ups[5,5]
upsm[[5,6]] = ups[5,6]
upsm[[5,7]] = ups[5,7]
upsm[[5,8]] = ups[5,8]
upsm[[5,9]] = ups[5,9]
upsm[[5,10]] = ups[5,10]
upsm[[5,11]] = ups[5,11]
upsm[[5,12]] = ups[5,12]
upsm[[5,13]] = ups[5,13]
upsm[[5,14]] = ups[5,14]
upsm[[5,15]] = ups[5,15]
upsm[[5,16]] = ups[5,16]
upsm[[5,17]] = ups[5,17]
upsm[[5,18]] = ups[5,18]
upsm[[6,1]] = ups[6,1]
upsm[[6,2]] = ups[6,2]
upsm[[6,3]] = ups[6,3]
upsm[[6,4]] = ups[6,4]
upsm[[6,5]] = ups[6,5]
upsm[[6,6]] = ups[6,6]
upsm[[6,7]] = ups[6,7]
upsm[[6,8]] = ups[6,8]
upsm[[6,9]] = ups[6,9]
upsm[[6,10]] = ups[6,10]
upsm[[6,11]] = ups[6,11]
upsm[[6,12]] = ups[6,12]
upsm[[6,13]] = ups[6,13]
upsm[[6,14]] = ups[6,14]
upsm[[6,15]] = ups[6,15]

```

```

upsm[[6,16]] = ups[6,16]
upsm[[6,17]] = ups[6,17]
upsm[[6,18]] = ups[6,18]
upsm[[7,1]] = ups[7,1]
upsm[[7,2]] = ups[7,2]
upsm[[7,3]] = ups[7,3]
upsm[[7,4]] = ups[7,4]
upsm[[7,5]] = ups[7,5]
upsm[[7,6]] = ups[7,6]
upsm[[7,7]] = ups[7,7]
upsm[[7,8]] = ups[7,8]
upsm[[7,9]] = ups[7,9]
upsm[[7,10]] = ups[7,10]
upsm[[7,11]] = ups[7,11]
upsm[[7,12]] = ups[7,12]
upsm[[7,13]] = ups[7,13]
upsm[[7,14]] = ups[7,14]
upsm[[7,15]] = ups[7,15]
upsm[[7,16]] = ups[7,16]
upsm[[7,17]] = ups[7,17]
upsm[[7,18]] = ups[7,18]
upsm[[8,1]] = ups[8,1]
upsm[[8,2]] = ups[8,2]
upsm[[8,3]] = ups[8,3]
upsm[[8,4]] = ups[8,4]
upsm[[8,5]] = ups[8,5]
upsm[[8,6]] = ups[8,6]
upsm[[8,7]] = ups[8,7]
upsm[[8,8]] = ups[8,8]
upsm[[8,9]] = ups[8,9]
upsm[[8,10]] = ups[8,10]
upsm[[8,11]] = ups[8,11]
upsm[[8,12]] = ups[8,12]
upsm[[8,13]] = ups[8,13]
upsm[[8,14]] = ups[8,14]
upsm[[8,15]] = ups[8,15]
upsm[[8,16]] = ups[8,16]
upsm[[8,17]] = ups[8,17]
upsm[[8,18]] = ups[8,18]
upsm[[9,1]] = ups[9,1]
upsm[[9,2]] = ups[9,2]
upsm[[9,3]] = ups[9,3]
upsm[[9,4]] = ups[9,4]
upsm[[9,5]] = ups[9,5]
upsm[[9,6]] = ups[9,6]
upsm[[9,7]] = ups[9,7]
upsm[[9,8]] = ups[9,8]
upsm[[9,9]] = ups[9,9]
upsm[[9,10]] = ups[9,10]
upsm[[9,11]] = ups[9,11]
upsm[[9,12]] = ups[9,12]
upsm[[9,13]] = ups[9,13]
upsm[[9,14]] = ups[9,14]
upsm[[9,15]] = ups[9,15]
upsm[[9,16]] = ups[9,16]
upsm[[9,17]] = ups[9,17]
upsm[[9,18]] = ups[9,18]
upsm[[10,1]] = ups[10,1]
upsm[[10,2]] = ups[10,2]
upsm[[10,3]] = ups[10,3]
upsm[[10,4]] = ups[10,4]
upsm[[10,5]] = ups[10,5]
upsm[[10,6]] = ups[10,6]
upsm[[10,7]] = ups[10,7]
upsm[[10,8]] = ups[10,8]

```

```

upsm[[10,9]] = ups[10,9]
upsm[[10,10]] = ups[10,10]
upsm[[10,11]] = ups[10,11]
upsm[[10,12]] = ups[10,12]
upsm[[10,13]] = ups[10,13]
upsm[[10,14]] = ups[10,14]
upsm[[10,15]] = ups[10,15]
upsm[[10,16]] = ups[10,16]
upsm[[10,17]] = ups[10,17]
upsm[[10,18]] = ups[10,18]
upsm[[11,1]] = ups[11,1]
upsm[[11,2]] = ups[11,2]
upsm[[11,3]] = ups[11,3]
upsm[[11,4]] = ups[11,4]
upsm[[11,5]] = ups[11,5]
upsm[[11,6]] = ups[11,6]
upsm[[11,7]] = ups[11,7]
upsm[[11,8]] = ups[11,8]
upsm[[11,9]] = ups[11,9]
upsm[[11,10]] = ups[11,10]
upsm[[11,11]] = ups[11,11]
upsm[[11,12]] = ups[11,12]
upsm[[11,13]] = ups[11,13]
upsm[[11,14]] = ups[11,14]
upsm[[11,15]] = ups[11,15]
upsm[[11,16]] = ups[11,16]
upsm[[11,17]] = ups[11,17]
upsm[[11,18]] = ups[11,18]
upsm[[12,1]] = ups[12,1]
upsm[[12,2]] = ups[12,2]
upsm[[12,3]] = ups[12,3]
upsm[[12,4]] = ups[12,4]
upsm[[12,5]] = ups[12,5]
upsm[[12,6]] = ups[12,6]
upsm[[12,7]] = ups[12,7]
upsm[[12,8]] = ups[12,8]
upsm[[12,9]] = ups[12,9]
upsm[[12,10]] = ups[12,10]
upsm[[12,11]] = ups[12,11]
upsm[[12,12]] = ups[12,12]
upsm[[12,13]] = ups[12,13]
upsm[[12,14]] = ups[12,14]
upsm[[12,15]] = ups[12,15]
upsm[[12,16]] = ups[12,16]
upsm[[12,17]] = ups[12,17]
upsm[[12,18]] = ups[12,18]
upsm[[13,1]] = ups[13,1]
upsm[[13,2]] = ups[13,2]
upsm[[13,3]] = ups[13,3]
upsm[[13,4]] = ups[13,4]
upsm[[13,5]] = ups[13,5]
upsm[[13,6]] = ups[13,6]
upsm[[13,7]] = ups[13,7]
upsm[[13,8]] = ups[13,8]
upsm[[13,9]] = ups[13,9]
upsm[[13,10]] = ups[13,10]
upsm[[13,11]] = ups[13,11]
upsm[[13,12]] = ups[13,12]
upsm[[13,13]] = ups[13,13]
upsm[[13,14]] = ups[13,14]
upsm[[13,15]] = ups[13,15]
upsm[[13,16]] = ups[13,16]
upsm[[13,17]] = ups[13,17]
upsm[[13,18]] = ups[13,18]
upsm[[14,1]] = ups[14,1]

```

```

upsm[[14,2]] = ups[14,2]
upsm[[14,3]] = ups[14,3]
upsm[[14,4]] = ups[14,4]
upsm[[14,5]] = ups[14,5]
upsm[[14,6]] = ups[14,6]
upsm[[14,7]] = ups[14,7]
upsm[[14,8]] = ups[14,8]
upsm[[14,9]] = ups[14,9]
upsm[[14,10]] = ups[14,10]
upsm[[14,11]] = ups[14,11]
upsm[[14,12]] = ups[14,12]
upsm[[14,13]] = ups[14,13]
upsm[[14,14]] = ups[14,14]
upsm[[14,15]] = ups[14,15]
upsm[[14,16]] = ups[14,16]
upsm[[14,17]] = ups[14,17]
upsm[[14,18]] = ups[14,18]
upsm[[15,1]] = ups[15,1]
upsm[[15,2]] = ups[15,2]
upsm[[15,3]] = ups[15,3]
upsm[[15,4]] = ups[15,4]
upsm[[15,5]] = ups[15,5]
upsm[[15,6]] = ups[15,6]
upsm[[15,7]] = ups[15,7]
upsm[[15,8]] = ups[15,8]
upsm[[15,9]] = ups[15,9]
upsm[[15,10]] = ups[15,10]
upsm[[15,11]] = ups[15,11]
upsm[[15,12]] = ups[15,12]
upsm[[15,13]] = ups[15,13]
upsm[[15,14]] = ups[15,14]
upsm[[15,15]] = ups[15,15]
upsm[[15,16]] = ups[15,16]
upsm[[15,17]] = ups[15,17]
upsm[[15,18]] = ups[15,18]
upsm[[16,1]] = ups[16,1]
upsm[[16,2]] = ups[16,2]
upsm[[16,3]] = ups[16,3]
upsm[[16,4]] = ups[16,4]
upsm[[16,5]] = ups[16,5]
upsm[[16,6]] = ups[16,6]
upsm[[16,7]] = ups[16,7]
upsm[[16,8]] = ups[16,8]
upsm[[16,9]] = ups[16,9]
upsm[[16,10]] = ups[16,10]
upsm[[16,11]] = ups[16,11]
upsm[[16,12]] = ups[16,12]
upsm[[16,13]] = ups[16,13]
upsm[[16,14]] = ups[16,14]
upsm[[16,15]] = ups[16,15]
upsm[[16,16]] = ups[16,16]
upsm[[16,17]] = ups[16,17]
upsm[[16,18]] = ups[16,18]
upsm[[17,1]] = ups[17,1]
upsm[[17,2]] = ups[17,2]
upsm[[17,3]] = ups[17,3]
upsm[[17,4]] = ups[17,4]
upsm[[17,5]] = ups[17,5]
upsm[[17,6]] = ups[17,6]
upsm[[17,7]] = ups[17,7]
upsm[[17,8]] = ups[17,8]
upsm[[17,9]] = ups[17,9]
upsm[[17,10]] = ups[17,10]
upsm[[17,11]] = ups[17,11]
upsm[[17,12]] = ups[17,12]

```

```

upsm[[17,13]] = ups[17,13]
upsm[[17,14]] = ups[17,14]
upsm[[17,15]] = ups[17,15]
upsm[[17,16]] = ups[17,16]
upsm[[17,17]] = ups[17,17]
upsm[[17,18]] = ups[17,18]
upsm[[18,1]] = ups[18,1]
upsm[[18,2]] = ups[18,2]
upsm[[18,3]] = ups[18,3]
upsm[[18,4]] = ups[18,4]
upsm[[18,5]] = ups[18,5]
upsm[[18,6]] = ups[18,6]
upsm[[18,7]] = ups[18,7]
upsm[[18,8]] = ups[18,8]
upsm[[18,9]] = ups[18,9]
upsm[[18,10]] = ups[18,10]
upsm[[18,11]] = ups[18,11]
upsm[[18,12]] = ups[18,12]
upsm[[18,13]] = ups[18,13]
upsm[[18,14]] = ups[18,14]
upsm[[18,15]] = ups[18,15]
upsm[[18,16]] = ups[18,16]
upsm[[18,17]] = ups[18,17]
upsm[[18,18]] = ups[18,18]

eln = Transpose[dmatrix].Transpose[psim].phimat.psim.dmat
tanstif = Transpose[dmatrix].(Transpose[psim].phimat.psim + upsm).dmat

edvec = Array[eld,{44}]

uvec = dmat.edvec;
stmp2 = OpenWrite["uvec.out",FormatType->FortranForm]
Do[ Write[stmp2, "uvec(",i,") = ",uvec[[i]] ], {i,24}]
Close[stmp2];

stmp1 = OpenWrite["stiff.out",FormatType->FortranForm]

eleind = Transpose[psim].phimat.psim;
elem = Array[ele,{24,24}]
phimat = Array[phi,{12,12}]
stif = Transpose[dmatrix].elem.dmat
psiv = Array[psivec,{12}]
dum1 = phimat.psim;
Do[ Write[stmp1,"dum1(",i,") = ",dum1[[i]] ], {i,12}]
Clear["dum1"]
dum = Array[dum1,{12}]
dum2 = Transpose[psim].dum
Do[ Write[stmp1,"dum2(",i,") = ",dum2[[i]] ], {i,24}]
Clear["dum2"]
dum = Array[dum2,{24}]
elr = Transpose[dmatrix].dum
Do[ Write[stmp1,"elr(",i,") = ",elr[[i]] ], {i,44}]

stmp = OpenWrite["eqforce", FormatType -> FortranForm]

phimat = Array[phi,{12,12}]
tmp = phimat.psim
tmp1 = Array[dum1,{12,24}]
Do[ Do[ If[ ToString[tmp[[i,j]] ] == "0", 0,
Write[stmp,"dum1(",i,"",j,") = ",tmp[[i,j]] ], {j,24}], {i,12}]
Do[ Do[ If[ tmp[[i,j]] == 0, tmp1[[i,j]] = 0, 0], {j,24}], {i,12}]

tmp2 = Transpose[psim].tmp1
Do[ Do[ If[ ToString[tmp2[[i,j]] ] == "0", 0,
Write[stmp,"dum2(",i,"",j,") = ",tmp2[[i,j]] ], {j,24}], {i,24}]

```

```

tmp3 = Array[dum2,{24,24}]
Do[ Do[ If[ tmp2[[i,j]] == 0, tmp3[[i,j]] = 0, 0], {j,24}], {i,24} ]

tmp4 = Transpose[dmatrix].tmp3
Do[ Do[ If[ ToString[tmp4[[i,j]] ] == "0", 0,
Write[stmp,"dum3(",i,",",j,") = ",tmp4[[i,j]] ] ], {j,24}], {i,44}]
tmp5 = Array[dum3,{44,24}]
Do[ Do[ If[ tmp4[[i,j]] == 0, tmp5[[i,j]] = 0, 0], {j,24}], {i,44} ]

tmp6 = tmp5.dmatrix
Do[ Do[ If[ ToString[tmp6[[i,j]] ] == "0", 0,
Write[stmp,"zkint(",i,",",j,") = ",tmp6[[i,j]] ] ], {j,44}], {i,44}]

Close[stmp]
Close[stmp1]

```


Appendix C. The Computer Program

The program used for the current analysis, called *JAGS*, for 'Jaumann Analysis of General Shells', is written in FORTRAN. The vast majority of the code is devoted to developing the transformation matrix $[T]$ and the deformed curvatures k_i needed to update the stiffness matrices at each iteration of each displacement increment. Much of the code was generated with the help of *Mathematica*, the symbolic mathematics software of Wolfram Research, Inc. The need for using the software became apparent in attempting to form the expressions for the derivatives required to generate the $[\Psi]$ and $[\Upsilon]$ matrices of Eqns (4.71) and (4.104) respectively.

The code has been used to analyze isotropic and laminated flat plates and beams, cylindrical shells and arches, circular toroidal shells and toroidal shells of elliptical cross-section. Analyses for shells of multiple curvature (like the toroidal shell) are more computationally intensive, as even the undeformed curvatures change when moving along a coordinate curve. These curvatures are calculated and stored at the beginning of the analysis, but the undeformed curvatures must be calculated at each Gauss point during the stiffness matrix integration process for each iteration of each displacement increment. In all analyses, including flat plates, the deformed curvatures must be calculated at each Gauss point in order to generate the new warping/stretching functions at that point and the attendant constitutive array, $[\Phi]$, of Eq (4.12).

For most these analyses, the program was run on the SparcStation 20 workstation. Typical run times were on the order of five minutes to several hours depending on the application.

The size and structure of the program differ significantly from its AFIT predecessor, *ISHELL*. These differences are outlined in Table C.1. Note that while the source code is more than four times the length of its predecessor, the run time is only about twice as much (for the same mesh), indicating that *JAGS* is significantly more efficient in terms of speed versus size (on the Sparc platform) than *ISHELL*. But a *JAGS* analysis need not use as many elements as one using *ISHELL*,

Attribute	<i>JAGS</i> Code (1995)	<i>ISHELL</i> Code (1988/92)
Analysis Type	Jaumann (T.L. Corotational)	T.L. Green's Strain
Shell Geometries	Composite Plates, Cyl. Shells, Spherical Caps, Shells of Rev. w/arb. cross-sec, Shells with Twist	Composite Plates, Cyl. Shells, Spherical Caps
Lines of Code (approx.)	56,000	13,000
Number of Routines	118	41
Relative Execution Time (same number of elements)	1.0τ	0.55τ
Element	4-Noded, 44 DOF	8-Noded, 36 DOF
DOF Continuity	C^1 in all DOF except C^0 in transverse shears γ_4, γ_5	C^0 in all DOF except C^1 in transverse displacement w
Additional <i>JAGS</i> Features	<ul style="list-style-type: none"> • Variable element properties (number of plies, ply properties, angle(s) of plies, thickness of plies) • Strain Energy Calculations (total and by element) • Varying Curvature within Element (in y direction) • Includes Thickness Stretching 	

Table C.1 Differences in AFIT shell analysis codes

so, for a given problem, *JAGS* imposes only a modest penalty in speed. Note also that the new code handles a much broader range of problems.

C.1 Using the *JAGS* Program.

The input file for the program is defined as follows. Note that integer values begin with letters **i-n**, while real (double precision) values begin with **a-h**, **o-z**. Sample input files are provided in Appendix C.3.

- Card 1: **title**

The first line of the program is a title. It is printed on the first line of the output file, and may not exceed 133 characters.

- Card 2: **iel,nanal,imesh,nrestr,nstore,idebug,isymm**

The variable **iel** indicates the element type: 1 for plate or beam, 2 for circular cylindrical shell, 3 for circular torus, and 4 for a torus of spline cross section.

Variable **nanal** specifies whether analysis is linear (no iteration) or nonlinear: 0 for nonlinear,

1 for linear.

Setting **imesh=1** causes automated mesh generation. Alternate settings of this variable are not recommended.

If the file is being started from a previously generated restart file, set **nrestr** to 1. Otherwise, set it to 0. The restart file must be of the form *filename.rst*, where *filename* is the name of the input file.

If **nstore**≠0, the the displacement data for each converge increment of the nonlinear analysis is written to *filename.rst*.

Flag **idebug** is chiefly a debugging tool and should be left at 0.

Variable **isymm** denotes symmetry conditions for output to the post-processing file. It is not used, but should be set to 0.

- Card 3: **xjoined,yjoined,wupdate**

The first two variables of this card govern mesh connection and are logical variables. If the mesh is to be joined along the mesh ends corresponding to constant values of *x*, set **xjoined=.true.**

Similarly, **yjoined=.true.** will connect the mesh along the ends corresponding to constant values of *y*.

The variable **wupdate** determines whether the shear warping functions, and therefore the constitutive matrix, will be updated to use the current deformed curvatures (**wupdate=.true.**), or the undeformed curvatures **wupdate=.false.**

- Card 4: **intyp,ninc,imax,tol,nordr**

Variable **intyp=0** indicates load control for nonlinear incrementation, while **intyp=1** is used for displacement control. If **intyp=2**, the user has specified a contact problem. Note: the contact algorithm is set up for **iel=4**. Use of any other value will produce unpredictable results.

Variable **ninc** specifies the number of load or displacement increments.

A maximum of **imax** iterations will be performed in any one increment. The program halts if **imax** is reached.

The initial convergence criterion, in percent, is specified by **tol**. *JAGS* will increase this convergence tolerance if an increment fails to converge, notifying the user. Once the convergence tolerance is increased to 100% with failure to converge, the program halts. The order of Gauss integration used to integrate the stiffness equations is specified by **nordr**.

- If **nanal=0** and **intyp=1**, then

Card 4a: **table(i)**

This is the table of multipliers for the displacements specified on input. For example, if degree-of-freedom 27 is to be displaced 2 units in three displacement increments, its displacement would be specified as 2.0 (see Card 7b), and **table(i)** would be 0.333, 0.667, 1.0 .

- If **intyp=2**, then

Card 4b: **nrefnods**

This variable dictates the number of initial nodes in contact with a surface.

Card 4c: **nrefnod(i)** is the list of the **nrefnods** node numbers initially in contact.

Card 4c: **ncontinc,zmininc,zmaxinc,nchecks**

The number of contact displacement increments is specified by **ncontinc**, and the displacement magnitude in a given increment is bounded by **zmininc** and **zmaxinc**. If the distance to the closest node not yet in contact with the surface is between these two values, then that distance is used as the increment step size. The variable **nchecks** is the number of nodes to be checked for contact.

Card 4d: **nctact(i)**

This is the list of node numbers to be checked at each displacement increment.

- If **iel=1,2,3** then

Card 5: **nx,ny**

These variables indicate the number of elements in the x and y directions, respectively.

Card 5a: `dx(i)`

This is the table of the width of each of the `nx` elements.

Card 5b: `dy(i)`

This is the table of the width of each of the `ny` elements.

- If `iel=4` then

Card 5: `nx`

This is the number of elements along the x axis of the mesh.

Card 5a: `dx(i)`

This is a table of the width of each of the `nx` elements.

Card 5b: `nsnodes,yp(1),yp(nsnodes),unifrm`

The number of nodes used to define the spline cross section is `nsnodes`. *Note that this need not be the number of nodes in the mesh. It may be useful to use more points in defining the spline than are used in defining the mesh.*

The value of the slope of the spline at the first and last nodes is given by `yp(1)` and `yp(nsnodes)` respectively.

A spline of uniform tension is generated when `unifrm=.true.`, otherwise, the tension algorithm generates the spline tension at nodes.

- If `unifrm=.true.` then

Card 5c: `sigma(1)`

This variable indicates the value of the tension factor to be used.

Cards 5d: `idum,stheta(idum),srad(idum)`

For each of the `nsnodes`, these three values are read.

The variable **idum** is simply the entry number (1,2,3, etc.) and is not used (though the user may find it helpful in reading the input file).

Variables **stheta(i)** and **srad(i)** are the angle (in degrees and measured in accordance with Figure 3.5) and the radius to the point on the curve used for the spline.

Card 5e: **nynodes**

This variable specifies the number of nodes in the mesh in the *y* direction.

Cards 5f: **idum,ytheta(idum)**

These cards (one for each node) give the theta coordinate of each of the **nynodes** in the *y* direction. The radial coordinate is calculated using the tension spline generated by the **nsnodes** points on the curve. At least two points **nynods** must be used, and the first and last points must coincide with **stheta(1)** and **stheta(nsnodes)**. Any additional nodes must lie between these two points.

- Card 6: **ld**

The type of loading is specified by **ld**. If **ld=4**, then a uniform pressure load is assumed, otherwise, the loads specified in **vbsf** (Card 8b) are applied.

- Card 7: **nbdy1**

This specifies the number of nodes having displacement boundary conditions.

Cards 7a: **nbound(i,j)**

Each of these cards have twelve entries. The first is the node number, and the next eleven indicate whether the degree of freedom at that node is prescribed (=1) or free (=0). A node need only be listed if one or more of its degrees of freedom are prescribed. For example, if node 112 has degrees of freedom *u*, *v*, and *w* prescribed, its entry would look like

112,1,0,0,1,0,0,1,0,0,0,0

Card 7b: **vbdy(i)**

This vector contains an entry for each of the prescribed displacements from Cards 7a. (The example node would contribute 3 entries.)

- If $ld \neq 4$ then

Card 8: **nbsf**

This is the number of degrees of freedom having specified loads.

Card 8a: **ibsf(i)**

This is an array **nbsf** degree-of-freedom numbers with prescribed loads.

Card 8b: **vbsf(i)**

These are the loads associated with the degrees of freedom specified in **ibsf(i)**. Note that the order of the degree-of-freedom numbers must match the order of the prescribed loads.

- Card 9: **neconfs**

This is the number of element configurations. Element configurations differ if the elements have a different ply lay-up, different numbers of plies, different ply thicknesses, or different material properties.

- If **neconfs** > 1, then for properties 2 through **neconfs**,

Cards 9a: **iconf, ipeles**

The configuration number **iconf** ≥ 2 is followed by **ipeles**, which is the number of elements having configuration **iconf**.

- Cards 9b: **ielprop(i)**

These are the **ipeles** element numbers having properties **iconf**.

- For each of the **neconfs** configurations, beginning with the default configuration (configuration 1), read

Card 10a: **np(i)**

This is the number of plies in configuration **i**.

Then, for each of the **np(i)** plies, read

Cards 10b: **e11(i), e22(i), e33(i), v12(i), v23(i), v13(i), g12(i), g23(i), g13(i)**

Which are the material properties of the plies, from bottom to top.

Card 10c: **angl(i,j)**

For configuration **i**, read the **np(i)** angles of the plies, from bottom to top.

Card 10d: **zcoor(i,j)**

For configuration **i**, read the **np(i)+1** **z** coordinates of the ply interfaces. Care must be taken so that a ply interface does not lie on (or very close to) the reference (**z = 0**) surface.

- Card 11: **Curvatures**

This card is omitted for the flat plate or beam.

For **iel=2**, the cylindrical shell, the radius of the shell is input.

For **iel=3**, the circular torus, the major radius, the minor radius, and the offset (in degrees) from $y^2 = 0$ to the start of the mesh (see Figure 3.5) are input. For **iel=4**, the spline torus, the major radius of the torus is input.

- If **ld=4** then

Card 12: **pload,palign**

The pressure load for **ld=4** is given by **pload**. It's final value will be **pload*ninc**. The variable **palign** is a logical variable specifying whether the direction of the pressure vector will be changed to coincide with the surface normal as the object deforms. The direction is updated if **palign=.true.**

- Card 13: **nfor**

This variable specifies the number of nodal forces to be calculated at the end of each converged increment.

Card 13a: **ifor(i)**

This is an array of **nfor** degree-of-freedom numbers for the force calculation.

- Card 14: **nstres**

This variable specifies the number of elements for which to calculate stresses and strains at the end of each increment.

Card 14a: **npoints** This specifies the number of points in each layer through the thickness for the stress/strain calculations. Card 14b: **istres(i)**

This is an array of **nstres** element numbers for the stress/strain calculations.

C.2 Program Output

JAGS produces some or all of the following files, depending on the nature of the analysis:

1. *filename.out*: This is the general output file. It echoes the inputs, and gives displacement and strain energy results. A history of loading and some of the details of the numerical solution are also included.
2. *filename.xcp*: This is a plot file generated for tension spline problems. It allows the user to plot (using an x-y plotting program) the user-defined spline.
3. *filenamestrs.dat*: This is the stress output calculated at each gauss point on the elements requested in the input file by variables **nstrs** and **istres(i)**.
4. *filenamestrn.dat*: Same as above, but for strains.
5. *filename.m*: A plot file for MATLAB. For problems having constant undeformed curvatures, this file is generated. It generates plots for all warping/stretch functions simply by typing *filename* at the first MATLAB prompt.
6. *filename.unv*: A universal file for use by the I-DEAS program of SDRC. Used for post-processing.
7. *filename.crv*: A file detailing the undeformed curvatures calculated by the program for spline cross-section problems.

C.3 Sample Input Files

Below are some sample input files as used by the *JAGS* finite element code.

[illegible]

142.d9,9.8d9,9.8d9,0.3,0.345,0.3,6.d9,3.63d9,6.0d9
142.d9,9.8d9,9.8d9,0.3,0.345,0.3,6.d9,3.63d9,6.0d9
142.d9,9.8d9,9.8d9,0.3,0.345,0.3,6.d9,3.63d9,6.0d9
142.d9,9.8d9,9.8d9,0.3,0.345,0.3,6.d9,3.63d9,6.0d9
142.d9,9.8d9,9.8d9,0.3,0.345,0.3,6.d9,3.63d9,6.0d9
142.d9,9.8d9,9.8d9,0.3,0.345,0.3,6.d9,3.63d9,6.0d9
0.,90.,0.,90.,0.,90.,0.,90.,0.,90.,0.
-744.d-6,-620.d-6,-496.d-6,-372.d-6,-248.d-6,-124.d-6,
124.d-6,248.d-6,372.d-6,496.d-6,620.d-6,744.d-6
1
249
1
20
22

C.3.2 The Cylindrical Arch. This input file is used to analyze an isotropic deep arch

having asymmetric boundary conditions. Note that `wupdate=.false.`, indicating that the warping functions will be calculated using the undeformed curvatures throughout the analysis

```
p245, arch, surana, 1x16, same steps as Surana
2,0,1,0,3,0,0
.false.,.false.,.false.
1,2,80,1.d-4,4
10.,20.
1,16
25.4d-3
595.80264d-3,595.80264d-3,595.80264d-3,595.80264d-3,
595.80264d-3,595.80264d-3,595.80264d-3,595.80264d-3,
595.80264d-3,595.80264d-3,595.80264d-3,595.80264d-3,
595.80264d-3,595.80264d-3,595.80264d-3,595.80264d-3
0
19
1,1,1,1,1,0,1,1,1,1,1
2,1,1,1,1,0,1,1,1,1,1
4,1,0,1,0,1,0,0,1,0,0,1
6,1,0,1,0,1,0,0,1,0,0,1
8,1,0,1,0,1,0,0,1,0,0,1
10,1,0,1,0,1,0,0,1,0,0,1
12,1,0,1,0,1,0,0,1,0,0,1
14,1,0,1,0,1,0,0,1,0,0,1
16,1,0,1,0,1,0,0,1,0,0,1
18,1,0,1,0,1,0,1,1,0,0,1
20,1,0,1,0,1,0,0,1,0,0,1
22,1,0,1,0,1,0,0,1,0,0,1
24,1,0,1,0,1,0,0,1,0,0,1
26,1,0,1,0,1,0,0,1,0,0,1
28,1,0,1,0,1,0,0,1,0,0,1
30,1,0,1,0,1,0,0,1,0,0,1
32,1,0,1,0,1,0,0,1,0,0,1
33,1,1,1,1,1,0,1,1,0,0,1
34,1,1,1,1,1,0,1,1,0,0,1
0.,0.,0.,0.,0.,0.,0.,0.,0.,0.,
0.,0.,0.,0.,0.,0.,0.,0.,0.,0.,
0.,0.,0.,0.,0.,0.,0.,0.,0.,0.,
0.,0.,0.,0.,0.,0.,0.,0.,0.,0.,
0.,0.,0.,0.,0.,0.,0.,0.,0.,0.,
0.,0.,0.,0.,0.,0.,0.,0.,-25.4d-3,0.,
0.,0.,0.,0.,0.,0.,0.,0.,0.,0.,
0.,0.,0.,0.,0.,0.,0.,0.,0.,0.,
0.,0.,0.,0.,0.,0.,0.,0.,0.,0.,
0.,0.,0.,0.,0.,0.,0.,0.,0.,0.,
0.,0.
0
1
1
41.3688d9,41.3688d9,41.3688d9,0.33,0.33,0.33,
15.55218d9,15.55218d9,15.55218d9
0.
-12.7d-3,12.7d-3
2.54
1
194
0
```